FEASIBILITY OF USING FLY ASH AS A BINDER IN COARSE AND FINE AGGREGATES FOR BASES

By
Joakim G. Laguros
and
Petros Zenieris
Office of Research Administration
University of Oklahoma

Sponsored By
Oklahoma Department of Transportation
Research and Development Division

in cooperation with the
Federal Highway Administration

June, 1987

TECHNICAL REPORT STANDARD TITLE PAGE

1. REPORT NO.	2. GOVERNMENT ACCESSION NO.	3. RECIPIENT'S CATALOG NO.
FHWA/OK 86(8)		TE716.05 .A34 no. 86(8)

4. TITLE AND SUBTITLE	5. REPORT DATE
The Feasibility of Using Fly Ash as a Binder in Coarse and Fine Aggregates for Base Courses	June 1987
	6. PERFORMING ORGANIZATION CODE
7. AUTHOR(S) Joakim G. Laguros and Petros Zenieris	8. PERFORMING ORGANIZATION REPORT ORA 155-404
9. PERFORMING ORGANIZATION NAME AND ADDRESS The University of Oklahoma Norman, OK 73019	10. WORK UNIT NO. Proj. Agreement No.31
	11. CONTRACT OR GRANT NO. ODOT 83-03-2. Item2125
12. SPONSORING AGENCY NAME AND ADDRESS Oklahoma Department of Transportation Research and Development Division 200 N.E. 21st Oklahoma City, Oklahoma 73105	13. TYPE OF REPORT AND PERIOD COVERED
	14. SPONSORING AGENCY CODE

15. SUPPLEMENTARY NOTES

Done in cooperation with FHWA

16. ABSTRACT Aggregate-fly ash mixes consisting of fine aggregate bases (FAB), coarse aggregate bases (CAB) and Class C fly ash additions of 15, 25 and 35% were tested in compressive and flexural strength for curing periods of up to six months. X-ray diffraction (XRD) was employed to study the mineralogical composition of the mixes and identify the fly ash hydration products. Scanning electron microscopy (SEM) was used to verify the XRD findings and study the microstructural developments in the mixes.

The compressive strength of the mixes varied considerably during the first week of curing but exhibited better uniformity in later ages. The variation was attributed to the massive formation of ettringite. Later, when ettringite was transformed to monosulfoaluminate and the CAH, CASH and CSH hydration phases form, the strength of the mixes gained uniformity and magnitude. After a month's curing the mixes presented little resistance to flexural failure but in 90 days the flexural strength level was substantial. The mixes were characterized as stiff but structurally flexible and a flexural design approach was devised. SEM observations indicated packing and densification of the mix matrix with time, as the hydration products form skeletal matrices in the mixes, resulting in better strength. The study establishes the dual role of the fly ash as a filler and a chemical agent (binder).

17. KEY WORDS	18. DISTRIBUTION STATEMENT
aggregates, bases, fly ash SEM, strength, XRD	

19. SECURITY CLASSIF. (OF THIS REPORT)	20. SECURITY CLASSIF. (OF THIS PAGE)	21. NO. OF PAGES	22. PRICE
none	none	267	

FINAL REPORT

ODOT Study No. 83-03-2

ORA 155-404

THE FEASIBILITY OF USING FLY ASH AS A BINDER IN COARSE AND FINE AGGREGATES FOR BASE COURSES

Prepared by

Joakim G. Laguros, David Ross Boyd Professor
Petros Zenieris, Research Assistant
School of Civil Engineering and Environmental Science

Prepared in Cooperation with
The U.S. Department of Transportation
Federal Highway Administration

Submitted to

Research Division
OKLAHOMA DEPARTMENT OF TRANSPORTATION

From the

OFFICE OF RESEARCH ADMINISTRATION
UNIVERSITY OF OKLAHOMA
Norman, Oklahoma
June, 1987

DISCLAIMER

This publication was printed and issued by the Oklahoma Department of Transportation as authorized by Neal McCaleb, Director. One hundred twenty-five (125) copies have been prepared and distributed at a cost of $412.25.

The contents of this report reflect the views of the authors who are responsible for the facts and the accuracy of the data presented herein. The contents do not necessarily reflect the official views of the Oklahoma Department of Transportation or the Federal Highway Administration. This report does not constitute a standard, specification, or regulation. While equipment and contractor names are used in this report, it is not intended as an endorsement of any machine, contractor, or process.

SUMMARY

The purpose of this study was to investigate the feasibility of using high calcium content Class C fly ash as a binding agent in aggregates of fine and coarse gradation and to evaluate the performance of the resulting mixes when used as base courses for roadway construction. To address the problem in a manner to cover a range of aggregates - currently used in bituminous base construction - five different sources were sampled. This yielded five fine aggregate bases (FAB) and five coarse aggregates bases (CAB) which were mixed with 15, 25 and 35% fly ash to produce a total of 30 different mixes. Cylindrical specimens of the mixes were tested to determine their unconfined compressive strength. Small beams were manufactured for use in the flexural strength tests. The curing periods ranged from one to 180 days. In the course of characterizing, classifying and evaluating the raw materials and the mixes, various qualitative or quantitative engineering and physical tests and procedures were employed. Additionally, X-ray diffraction (XRD) was used to study the mineralogical composition of the mixes with emphasis on the crystal-

linity of the products, resulting from the fly ash hydration, particularly those possessing cementing potential. Scanning electron microscopical (SEM) observations were also employed to monitor the microstructural developments in the matrix of the mixes as a result of the unfolding of the hydration process.

In terms of compressive strength, there was a considerable variation during the first week of curing but in later ages the strength pattern became more uniform. The majority of the mixes exhibited peak strength values after 180 days of curing which became indicative of the general pattern of strength gain with time. On the other hand, the 28-day beams proved very weak, suggesting that a month's time is not enough for the mixes to acquire resistance to flexural failure. In 90 days the beams of the mixes performed well and gave substantial flexural strengths. Based on the data of this curing period a flexural design approach that treats the base course as a beam on an elastic foundation is proposed.

The addition of fly ash increases the density of FABs but decreases the density of CABs. From a strength perspective the 35% fly ash addition appears to be favorable to the long term strength (180 days) and only partially beneficial to the 90-day strength of the mixes, while the 25% fly ash addition favors the development of

early strength (28 days).

XRD analysis of the mixes indicates the formation of fly ash hydration products that belong to the following groups: $C\bar{A}\bar{S}H$, CAH, CASH, CSH. SEM observations verify the XRD findings and indicate a densification of the microstructural formations in time, as the hydration process progresses and its products attain higher and more massive crystallization, are grouped together and create matrices that support the loose individual particles in the mix. The strength increase with time is attributed to this phenomenon.

Finally, it is recommended that a better understanding of the behavior of the aggregate-fly ash mixes will be gained by extending this investigation to cover the study of laboratory compaction methods, durability studies, the determination of optimum base gradation for maximum utilization of the fly ash potential and, field implementation and evaluation of the promising mixes.

TABLE OF CONTENTS

Table of Contents (continued)

Table of Contents (continued)

LIST OF TABLES

List of Tables (continued)

List of Tables (continued)

List of Tables (continued)

LIST OF FIGURES

List of Figures (continued)

List of Figures (continued)

List of Figures (continued)

List of Figures (continued)

List of Figures (continued)

PREFACE

In cooperation with the Oklahoma Department of Transportation a research project was undertaken in 1982 by the University of Oklahoma Office of Research Administration to study the feasibility of using fly ash as a binding agent in coarse and fine aggregate mixes used as bases in Oklahoma highways.

During the course of this effort, which was conducted by the School of Civil Engineering and Environmental Science, reports were submitted quarterly, and the present constitutes the final report.

The opinions, findings and conclusions expressed in this publication are those of the authors and not necessarily those of the Oklahoma Department of Transportation.

ACKNOWLEDGEMENTS

This investigative study was supported by the Research Division of the Oklahoma Department of Transportation and the Federal Highway Administration under ODOT study 83-06-2 (ORA 155-404).

During the conduct of this study numerous meetings were held with representatives of the sponsoring agency and the authors are grateful for all the helpful suggestions and cooperation they received.

Thanks are also extended to Mr. Curtis J. Hayes, Research Division, ODOT for supplying the materials used in this study and for his support in general. The authors are also grateful for certain X-ray diffraction analyses and interpretations provided by Dr. T. Demirel, Professor of Civil Engineering and Mr. Scott S. Schlorholtz, Research Associate, at Iowa State University, Ames Iowa.

The assistance of Mr. Douglas Powell of the University of Oklahoma X-ray Diffraction Laboratory and Mr. William Chissoe of the University of Oklahoma Electron Microscopy Laboratory is well acknowledged.

CHAPTER I

INTRODUCTION

For many years fly ash has been used as an ingredient in Portland cement concrete and in building blocks, as a soil stabilizer in road construction and more recently as an admixture with aggregates to enhance their strength characteristics. Through most of this period, specification writers have considered fly ash as a pozzolanic material, that is, a material which by itself has no cementitious value but in the presence of moisture and calcium hydroxide forms compounds possessing cementitious properties. These pozzolanic fly ashes have been classified under ASTM C 618 as Class F fly ashes.

Over the past decade, however, another type of fly ash has gained prominence which contains less pozzolanic material but possesses cementitious properties of its own. The 1977 version of the ASTM C 618 specification recognized this type of fly ash and by adding a new classification, Class C, it differentiated between the two types.

Presently, the state of Oklahoma has an abundant

supply of high quality Class C fly ash. Its disposal, in the form of a usable product, found a market in PC concrete and the study which culminated in the final report presented to ODOT in 1984 further supported its value as an ingredient. The confidence gained from that study opened the avenue to investigate the feasibility of using fly ash as a binder in aggregate mixes - which conform to standard ODOT base specifications. Thus, fine aggregate (FAB) and coarse aggregate (CAB) mixes were included. Specifically, the study attempts to explain why these mixes show promise or why they are not workable.

A number of tests were conducted to determine the compactive characteristics to give maximum compressive strength for a range of fly ash contents; also, the beam strength of the various mixes and the effect of time of curing were studied. To identify the fly ash-aggregate reaction products and thus help interpret the results of these tests, X-ray diffraction analysis (XRD) and scanning electron microscopy (SEM) observations were employed.

CHAPTER II

LITERATURE REVIEW

2.1 Introduction

Fly ash, a by-product of coal combustion, is a pozzolanic material primarily known for its use in cement and concrete. For quite a long time it was believed that fly ash did not possess cementitious properties of its own. Recent studies (9,19,30) though, emphasize the importance of its physical and chemical characteristics as a key factor in determining the hydration profile in particular, and the engineering behavior of the material in general. In this chapter the production and classification of fly ash are presented, and the physical and chemical characteristics of the material are discussed in view of the latest developments. Also, an overview and examination of treated base courses is presented in this chapter.

2.2 Fly Ash Production

Coal fired power plants are the source of fly ash production. Finely ground coal is injected into the boiler and burned in a stream of steam and air. The res-

idue collected at the bottom of the boiler furnace is bottom ash or slag. Fly ash is that portion of the inorganic residue which is carried along in the air stream to a collector (9). Electrical precipitators are very often the collecting devices, although mechanical collectors or a combination of electrical and mechanical means may be encountered. Electrostatic precipitators are favored because of their collection efficiency (95% to 99%+); they can remove fly ash of all particle sizes (down to 2μm) from the gas stream, and they have minimum effect on the pollution of the environment (30). In general, fly ash constitutes about 70 to 80% of the solid wastes produced by the combustion of pulverized coal, the remaining 20 to 30% being bottom ash (dry-bottom boiler) or slag (wet-bottom boiler) (11,30).

The 1973 Arab oil embargo underlined dramatically the dependence of the United States on foreign oil and emphasized the need for energy sources other than oil. Soon it was Federal energy policy to urge the conversion of oil-fired power plants back to coal wherever possible. As a result, an ever increasing percentage of the nation's electricity is produced at plants using coal burning boilers, which in return, leads to an increase of coal consumption and production of coal ashes (27). Figure 2.1 depicts the coal consumption and ash production between the years 1966 and 1982. In 1983, the

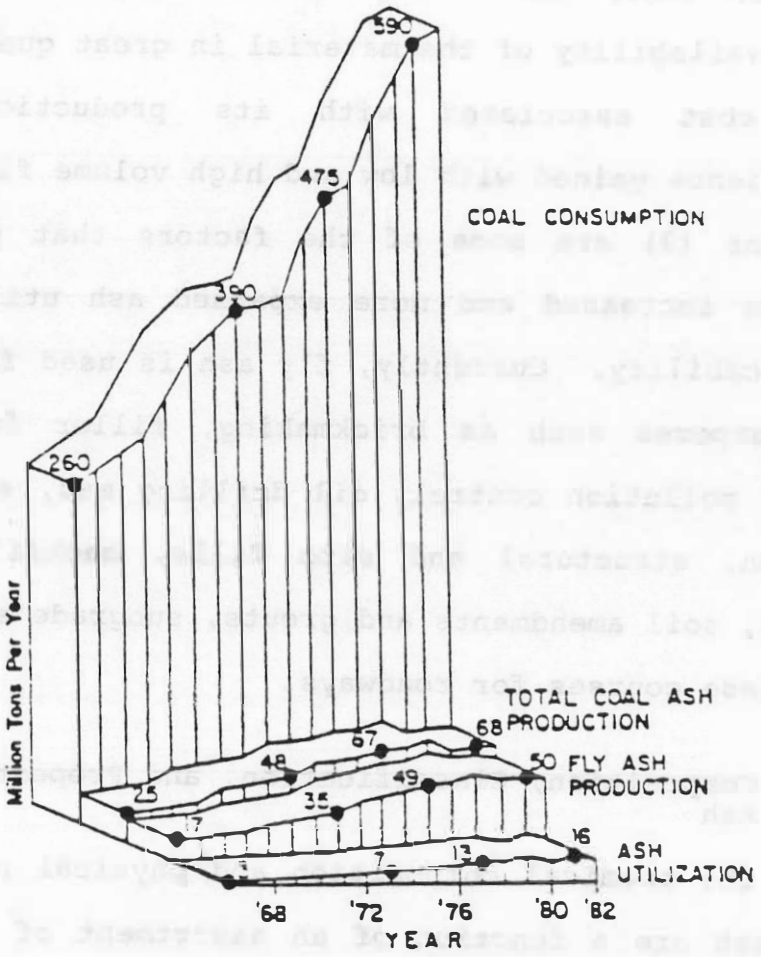

Figure 2.1 Coal consumption and ash generation by United States electric power stations (after Burnet et al., 1984)

electric utility companies in the United States burned 600.1 million tons of coal that resulted in the production of 52.4 million tons of fly ash and only 7.5 million tons was utilized (National Ash Association, 1984). By 1990, fly ash generation is forecast to reach 14.1 million tons, and is expected to keep increasing (28). The availability of the material in great quantities, the low cost associated with its production and the experience gained with low and high volume fly ash applications (3) are some of the factors that point toward future increased and more expanded ash utilization and applicability. Currently, fly ash is used for a variety of purposes such as brickmaking, filler for plastics, water pollution control, oil drilling mud, soil stabilization, structural and site fills, backfills, embankments, soil amendments and grouts, subgrade stabilization and base courses for roadways.

2.3 Composition, Classification, and Properties of Fly Ash

The chemical composition and physical properties of fly ash are a function of an assortment of factors, including the origin and rank of coal, the degree of pulverization and the processes of combustion, collection, handling and storage (30). Fly ash, being the inorganic residue of coal after combustion, is chemically directly related to the mineral components present in coal, which

can comprise 4 to 20 percent of the fuel material. The minerals most frequently found in fly ashes are primarily silica and alumina and secondary oxides of calcium, magnesium, iron and sulfur. Table 2.1 depicts the typical oxides and their amounts as major constituents of fly ash.

Considering the type of coal, fly ashes can be classified into two categories. Class F fly ash, of low calcium content, is commonly derived from bituminous and anthracite coals, and class C fly ash, of high calcium content, is associated with lignitic and subbituminous coals. Class C fly ash usually has more than 30% of calcium oxide and no less than 50% of SiO_2 + Al_2O_3 + Fe_2O_3, while class F fly ash contains no less than 70% of the combination of silicon, aluminum and iron oxides (9). The low calcium content fly ashes are mainly used as synthetic pozzolans, while the high calcium oxide content of Class C fly ash enriches it with self hardening properties in addition to the pozzolanic behavior (20). A pozzolan is

> "a siliceous or silicious aluminous material, which in itself possesses little or no cementitious value but which will, in finely divided form and in the presence of moisture, chemically react with calcium hydroxide at ordinary temperatures to form compounds containing cementitious properties" (ASTM, 1973).

From a physical point of view one of the most interesting

Table 2.1. TYPICAL COMPOSITION OF FLY ASH

Oxide Composition	Weight %
SiO_2	10-70
Al_2O_3	8-38
Fe_2O_3	2-50
CaO	0.5-30
MgO	0.3-9
Na_2O	0.1-8
K_2O	0.1-3
TiO_2	0.4-3.5
SO_3	0.1-30

(after Diamond, 1981)

features of fly ash is the spherical shape of the particles. The fine fly ash particles suspended in the air stream undergo melting and as liquid droplets assume spherical shapes. Upon rapid cooling they solidify preserving their spherical form. While some of the particles cool slowly enough to partially recrystallize, others remain amorphous (9). The diameter of the spherical particles ranges from 1 to 100 microns, with an average particle size of about 7 microns (16,23). Frequently though, irregularly shaped particles are observed and their presence can be attributed to incomplete melting, insufficiently high temperature, too short a time of exposure, poor burning of the coal, or the chemical composition of the coal particle (9). Figure 2.2 depicts a typical fly ash particle distribution. The vast majority of the fly ash particles are essentially solid. Occasionally however, thin walled hollow spherical particles are in evidence, and in some fly ashes their amount is quite substantial. The spherical particles are categorized as cenospheres if they are completely hollow thin walled particles, and plerospheres when they contain solid spheres. A fly ash specific gravity of 2.1 to 2.2 is a good indication that a substantial amount of cenospheres is present in the fly ash, while a specific gravity of 2.7 to 2.8 is not supportive of such an assumption (9).

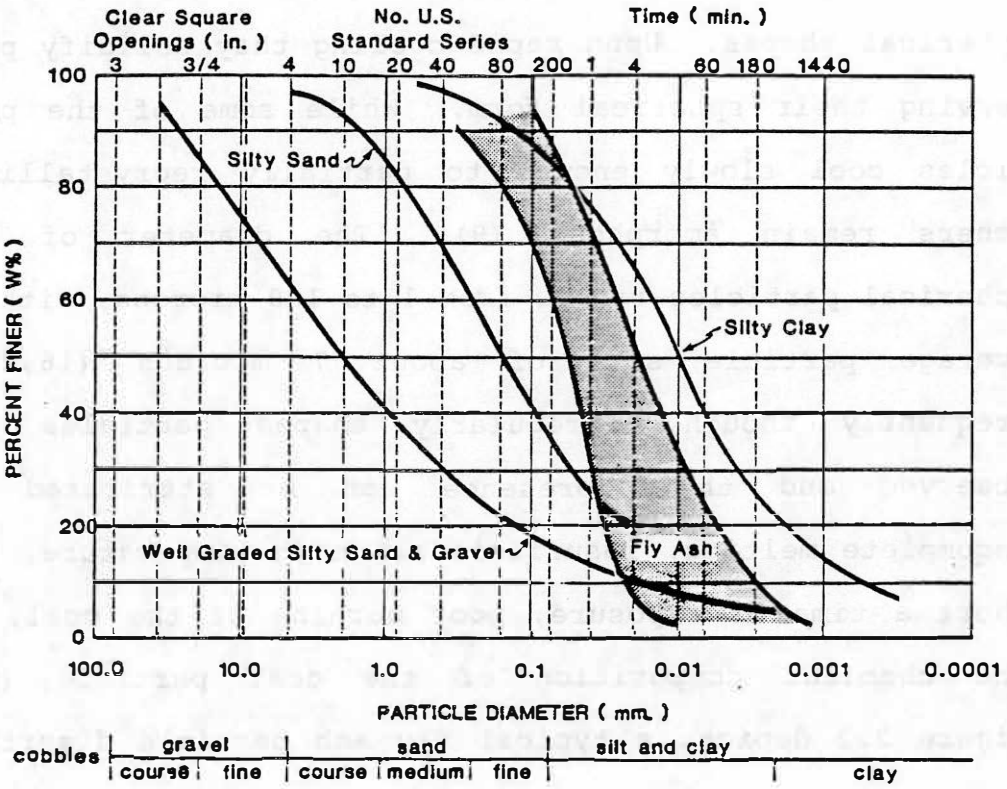

Figure 2.2 Typical fly ash particle distribution (after EPRI, 1986)

The physical characteristics and chemical properties of fly ash vary widely. The classification of fly ash into Class C and Class F (ASTM C 618) provides some accomodation for these variations, but there is still room for more detailed classification. For example, there are no provisions or specifications on the "free" or active calcium oxide (CaO) content of fly ash, which is of major importance. Further research possibly will determine the need of subcategorization.

2.4 Fly Ash Hydration

Fly ash, classified as a pozzolanic material, was believed by definition "to possess little or no cementitious value in itself." Studies on Class F fly ash (9,10) verify the non-cementitious behavior of the material. Nevertheless, a recent increase in the production of Class C fly ash has changed the picture, as considerable cementitious potential is attributed to this high calcium content fly ash (19).

Demirel et al. (10) found that fly ashes with cementitious properties contained significant amounts of tricalcium aluminate and calcium aluminum sulfate cements as well as anhydrite (19), and all the fly ashes so tested were high calcium, Class C fly ashes. Two inch cubes of fly ash paste, when tested after three days of curing, gave an average compressive strength of 2493 psi.

Laguros and Baker (19) report that Demirel explained the primary reaction mechanism of the cementitious Class C fly ashes as follows:

> "Aluminate hydrates appear to be the key reaction products in the case of this fly ash (Class C fly ash from Iowa). Oscillation diffraction analysis showed formation of ettringite in a period of 4 to 22 minutes, monosulfoaluminate formation in the period of 12 to 58 minutes, and anhydrite removal in the period of 10 to 61 minutes. This seems to represent a good example of Portland cement chemistry and can be rationalized that tricalcium aluminate is present in the fly ash (5.2 percent by weight) and is very reactive with water. Also present is an internal source of calcium sulfate in the form of anhydrite. Where hydration begins, the free calcium sulfate content of the paste is high and ettringite begins to form. As the sulfate content decreases, due to consumption by ettringite formation, monosulfoaluminate begins to form and continues to form, at the expense of ettringite formation, until the anhydrite is nearly exhausted. The precise reaction mechanism might be complicated due to the fact that the fly ash contained 2.3 percent calcium aluminum sulfate which might hydrate directly to ettringite."

Similarly, Diamond (9) reports

> "A considerable suite of cement minerals occurs in some high calcium fly ashes. C_3A is quite common, sometimes in appreciable quantities. Where C_3A is present along with anhydrite, the fly ash alone may generate significant amounts of ettringite, irrespective of the contribution from the portland cement. Calcium aluminum sulfate ($C_4A_3\bar{S}$) is also occasionally found in high calcium fly ash, but in smaller proportions.

2.5 Cement Treated Granular Bases

Cement treated granular base courses have been used successfully over the years with both rigid and flexible pavements. The addition of cement to granular bases increases their tensile and flexural strength, provides tight binding of the particles and waterproofing, while the relatively low strength and modulus of elasticity of the material enables it to adjust to the settlement of the underlying less flexible subgrade(26). The quantity and quality of the fines contained in the aggregates and the final compacted density are the factors that determine the required amount of cement. Typical values of cement content range between 2 and 6% by weight of the final compacted material, and unconfined compressive strengths in the order of 1000 to 2000 psi are not uncommon (39). The California Department of Transportation requires that the cement content for a Class A base is not to exceed 5% by weight of dry aggregate and a seven day minimum compressive strength 750 psi. For Class B bases the cement requirement is 2.5% maximum.

2.6 Lime-Fly-Ash-Aggregate Courses

Lime-fly-ash-aggregate (LFA) mixtures find application primarily in base and subbase courses for flexible pavements and subbases for rigid pavements. The lime requirements of LFA mixes are generally 3 to 10% by

weight, while the total lime plus fly ash percentage varies between 15 and 30. Lime to fly ash ratios of 1:2 to 1:4 are common, unless fly ash is used as fines and their lime-fines ratios of 1:4 to 1:7 are used (34). The aggregates are sands, gravels, crushed stone, and slag. Durability is the most important consideration in the performance of LFA materials (35), while several factors can influence the strength such as, properties of the materials, relative compacted density, curing temperature and time (33). Barenberg (5) states that the single most important factor governing the quality of LFA compositions is the compacted density.

> "A reduction of only five percent in the compacted density of a composition can result in a loss of 40 to 60 percent in the compressive strength of the composition. Furthermore, lime-fly-ash-aggregate compositions will develop little strength at densities less than approximately 85 percent of standard Proctor density. The gradation of a composition influences the density and thus, the strength of the composition" (33).

The effect of relative density on the compressive strength of LFA cores is shown in Figure 2.3. Core strengths of lime-fly-ash-aggregate compositions can range from 750 to 2500 psi after a few years of service (5). ASTM C 593 designates the procedures for evaluation of lime-fly ash-aggregate mixtures in the following ways.

- use of Proctor size specimens (diameter 4.0 in, height 4.5 in)

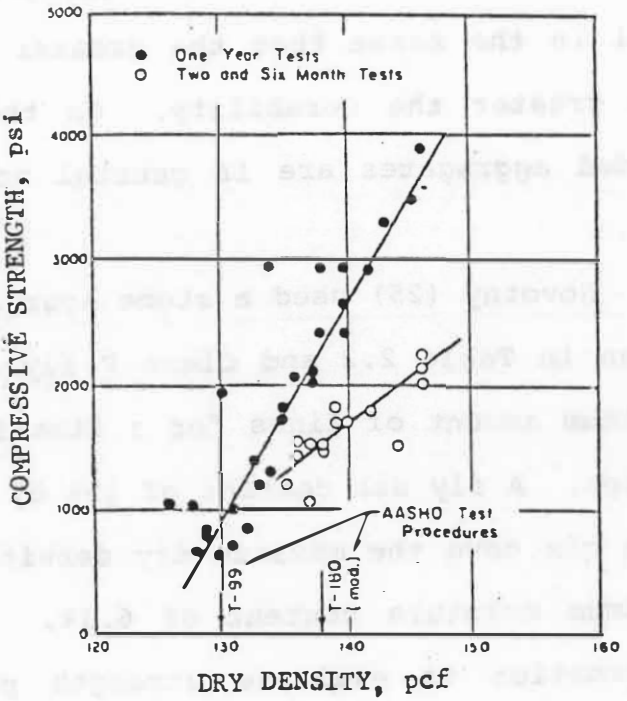

Figure 2.3 Effect of relative density on the compressive strengths of cores from lime-fly ash-aggregate mixtures (after Barenberg, 1967)

- compaction under modified conditions (10 lb rammer with 18 in drop)
- seven day curing at a temperature of 100°F
- minimum allowable compressive strength 400 psi

The content of fines in the aggregate mixtures is essential in the sense that the greater the amount of fines, the greater the durability. On the other hand, coarse graded aggregates are in general more mechanically stable.

Novotny (25) used a stone aggregate of the gradation given in Table 2.2 and Class F fly ash to determine the optimum amount of fines for a lime-fly ash-aggregate mix design. A fly ash content of 15% by weight, in an aggregate mix gave the maximum dry density of 138.7 pcf at an optimum moisture content of 6.1%. He, then, used this information to evaluate strength performance of mixes containing 15 percent by weight fine material (lime+ fly ash) and aggregate, cured at a temperature of 100°F. His findings are shown in Table 2.3.

Barenberg (4) experimenting with cement as an accelerator for lime-fly ash-aggregate mixes and even a complete replacement for lime reported that, using Class F fly ash and Type N lime, "The data suggest that for comparable mixes under comparable curing the cement-fly ash mixes develop compressive strengths between two and

Table 2.2 STONE AGGREGATE GRADATION

Sieve size	% passing
2 in	100
3/4 in	70-100
3/8 in	58-100
#4	45-80
#16	25-50
#100	6-20

(after Novotny, 1985)

Table 2.3 OPTIMUM MIX DESIGN

Mix	% by weight		Max. dry density	Mositure content	7-day strength
Lime	Fly Ash	Aggregate	pcf	%	psi
3.0	12.0	85	136.3	5.7	1815
3.5	11.5	85	138.1	6.1	1927
4.0	11.0	85	137.1	5.2	1453

(after Novotny, 1985)

three times greater than the comparable lime-fly ash-aggregates mixes. Selective data from Barenberg's work using gravel are given in Table 2.4.

2.7 Electron Microscopy

The need of magnifications of the order 5000X and upward for the study of microstructures associated with the hydration of Portland cement led researchers to use electron microscopy as early as 1938 (32). Currently, SEM is extensively used in the study of Portland cement hydration products, and in the last few years for the study of microstructures and products associated with the hydration of fly ash concrete and cement fly ash pastes.

Ghose and Pratt (13) used SEM to study the hydration reactions and the microstructural development in a cement-fly ash paste. Mohan and Taylor (24) analyzed pastes of tricalcium silicate with a fly ash of high glass content by TEM (transmission electron microscopy) to confirm earlier observations that partial replacement of tricalcium silicate by fly ash, accelerates reaction of the C_3S, reduces the content of $Ca(OH)_2$ and accelerates polymerization of the silicate ions. Diamond (9) used scanning electron micrographs to illustrate typical morphologies and characteristic types of fly ash particles and Grutzeck et al. (15), based on detailed SEM microstructural observations, proposed a phenomenological

Table 2.4 STRENGTH DEVELOPMENT OF CEMENT/LIME-FLY ASH-AGGREGATE MIXTURES

Mix Proportions, % by weight					7-day Strength (psi)
Cement	Lime	F Fly Ash	C Fly Ash	Aggregate	
0	2.5	10.0	0	87.5	980
0	3.0	10.0	0	87.0	1100
2.5	0	10.0	0	87.5	970
3.5	0	10.0	0	86.5	1270
4.5	0	10.0	0	85.5	1500
0	2.5	10.0	0	87.5	590
0	3.0	10.0	0	87.5	626
2.5	0	10.0	0	87.5	564
3.5	0	10.0	0	86.5	1355
4.5	0	10.0	0	85.5	1700
2.5	0	0	10.0	87.5	1516
3.0	0	0	12.0	85.0	1783

(after Barenberg, 1985)

model of fly ash hydration. Finally, Laguros and Baker (19) employed scanning electron microscopic observations to identify reaction products in concrete.

2.8 X-ray Diffraction

X-ray diffraction analysis has long been employed by chemists and engineers to study the development of the hydration products in cement and concrete and unravel the mechanism of stabilization in cement, lime, or fly ash stabilized soils. Laguros and Medhani (18), and Laguros and Keshawarz (20), used X-ray diffraction to study the hydration products of stabilized Oklahoma shales. An extensive X-ray investigation of fly ash concrete by Laguros and Baker (19) suggested that the early formation of the mineral ettringite and its conversion to monosulfoaluminate can be associated with the retardation in the hydration process of the class C fly ash PC concrete mixes. Lea and Desch (21) have published diffraction profiles of cement minerals. Scheetz et al. (31) analyzed an anthracite fly ash, a subbituminious fly ash, and a bituminous fly ash and they detected the crystalline phases presented in Table 2.5. X-ray diffraction provides a qualitative analytical tool for determining the degree of crystallization of the identified mineral but no safe quantitative correlations can be made unless X-ray fluorescence is employed.

Table 2.5 MINERALS IDENTIFIED IN FLY ASH SAMPLES BY X-RAY DIFFRACTION

Fly Ash	Mineral	JCPDF*	Comments
Anthracite	Quartz	5-490	major
	Mullite	15-776	major
	Magnetite	19-629	possibility
Subbituminous	Quartz	5-490	major
	Periclase	4-829	minor
	Anhydrite	6-226	trace
	Magnetite	19-629	minor
	Mullite	15-776	minor
	Brownmillerite	11-128	minor
	Alite	11-593	major
	Gehlenite	27-81	trace
	CO_3-apatite	19-272	possibility
	Calcium oxide	4-771	possibility
Bituminous	Quartz	5-490	major
	Mullite	15-776	major
	a-hematite	13-534	minor
	Periclase	4-829	trace
	Spinel	16-367	trace
	Magnetite	19-629	possibility

* Powder diffraction file number

CHAPTER III

MATERIALS AND SOURCES

3.1 Introduction

Fly ash, coarse aggregates, fine aggregates, screenings, and sands were the materials used in the project. All of them were provided by the Oklahoma Department of Transportation and stored in the laboratory. The aggregates and sands were delivered in open barrels and stored in covered containers while the fly ash came in sealed barrels in order to be protected from moisture intrusion.

3.2 Aggregate Sources

An initial survey and aggregate sampling from various parts of the state of Oklahoma indicated that a wide variation of individual, locally available, aggregates are used for roadway construction. In order to account for the indicated variations (especially in gradations characteristics) and to ensure an expanded regional representation as well as to serve the scope of the study for a general investigation - rather, than viewed as an isolated case-study - five sampling locations were selected. Therefores, the aggregates were obtained from

the asphalt plants located at the cities of Norman, Ponca City, Coweta, Tupelo and Fort Gibson, which cover virtually the eastern half of the state of Oklahoma. Their locations are presented in Figure 3.1. Also, Table 3.1 summarizes the 17 individual aggregates corresponding to the five locations and their respective sources, while the gradation characteristics of all the aggregates are presented in Table 3.2.

3.3 Coarse Aggregates

The coarse aggregates obtained for this project, their type and quarried source are included in Table 3.1. Of the coarse aggregates listed in the table, the coarse 3/4 in from Coweta and the coarse 3/4 in from Ft. Gibson were finally eliminated when it was found that their gradation characteristics would not contribute to the improvement of the designed blends.

All coarse aggregates were stored in covered 30 gallon containers allowed to maintain their natural moisture. To prepare coarse aggregates for mixing, adequate quantities of the stone were spread on a leveled surface and left to dry at room temperature for at least 48 hours. Prior to batching, the stone lot was reduced to a batch size sample using the quartering method which is in accordance with AASHTO Designation T 248-74.

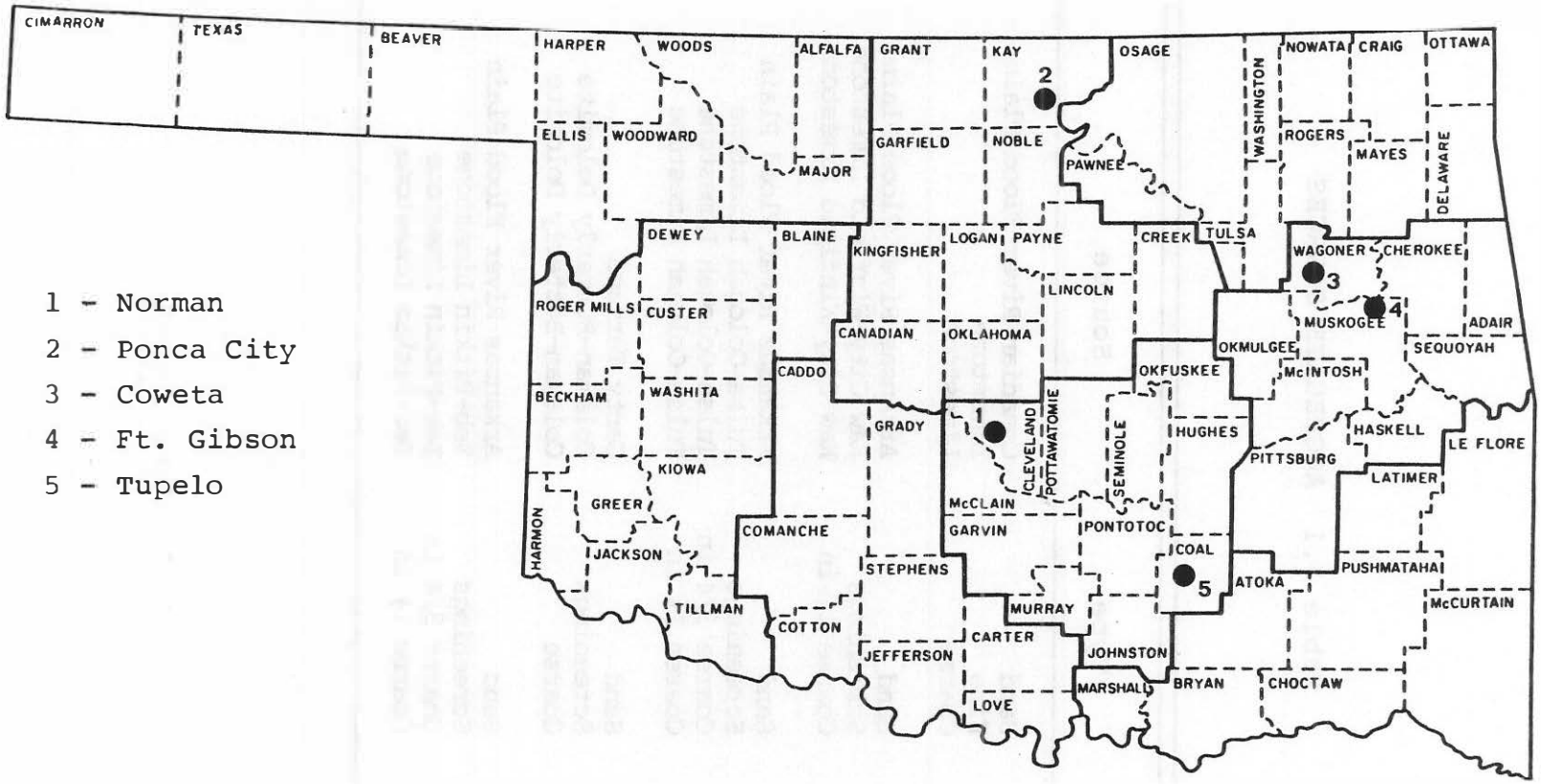

1 - Norman
2 - Ponca City
3 - Coweta
4 - Ft. Gibson
5 - Tupelo

Figure 3.1 Aggregate sources

Table 3.1 AGGREGATE SOURCES

Location	Type	Source
Norman	Sand	Canadian River Flood Plain
	Fine	Limestone
	Coarse	Limestone
Ponca City	Sand	Arkansas River Flood Plain
	Screenings	Kaw City-Winfield Limestone
	Coarse 1½ in	Kaw City-Winfield Limestone
Coweta	Sand	Arkansas River Flood Plain
	Screenings	Tulsa-Oologah Limestone
	Coarse 3/4 in	Tulsa-Oologah Limestone
	Coarse 1½in	Tulsa-Oologah Limestone
Tupelo	Sand	Gerty Terrace
	Screenings	Coleman-Butterly Dolomite
	Coarse	Coleman-Butterly Dolomite
Ft. Gibson	Sand	Arkansas River Flood Plain
	Screenings	Zeb-Pitkin Limestone
	Coarse 3/4 in	Zeb-Pitkin Limestone
	Coarse 1½ in	Zeb-Pitkin Limestone

Table 3.2 AGGREGATE GRADATIONS (% passing)

Sieve	Norman			Ponca City			Coweta			
Size or No.	Sand	Fine	Coarse	Sand	Screenings	Coarse (1½ in)	Sand	Screenings	Coarse (3/4 in)	Coarse (1½ in)
1½ in			100			100				100
1 in			95.1			96.8				97.6
3/4 in		100	46.7		100	63.7			100	59.6
3/8 in		93.8	1.6	100	99.2	2.9	100	100	30.3	3.1
#4		7.5	0.3	97.0	47.5	0.8	98.6	79.3	1.4	0.8
#10	100	0.9	0.3	88.6	8.9	0.7	86.1	41.7	0.6	0.7
#40	82.7	0.7	0.2	33.3	1.0	0.6	23.2	8.0	0.6	0.4
#200	1.0	0	0	3.3	0	0	0.6	0.5	0.1	0.1

(continued)

Table 3.2 AGGREGATE GRADATIONS (% passing) (continued)

Sieve	Tupelo			Ft. Gibson			
Size or No.	Sand	Screenings	Coarse	Sand	Screenings	Coarse (3/4 in)	Coarse (1½ in)
1½ in							100
1 in							96.4
3/4 in			100		100	100	58.6
3/8 in		100	67.2		94.7	53.2	5.7
#4	100	89.2	15.2	100	17.9	2.5	1.3
#10	99.9	44.1	3.3	99.9	1.7	1.0	0.8
#40	74.5	15.3	0.8	79.6	0.4	0.7	0.5
#200	3.5	5.0	0.2	1.9	0.1	0.3	0.1

3.4 Fine Aggregates and Screenings

The fine aggregate and the screenings used in the project are identified in Table 3.1, while their gradations are given in Table 3.2. The fine aggregates were stored and prepared for mixing in a manner identical to that of the coarse aggregates. The screenings, containing finer fractions, maintained higher amounts of moisture and were processed in a manner similar to that for the sands, as described in the following paragraph.

3.5 Sands

The five sands (Table 3.1) used in the project, were stored in 10 and 30 gallon covered containers preserving their natural moistures. Drying and sieving the entire volume of sand was considered impractical. Alternatively, the content of the particular container was thoroughly mixed by means of a shovel and a scoop to assure uniform moisture distribution throughout the sand mass. A representative 600 gram sample of the material was collected, weighed and oven dried to determine the moisture content of the sand in the container. Thus, it was possible to use the moist sand in the mix by making the appropriate adjustments in the mix design. Then, the oven dried sample was sieve analyzed to determine the gradation of the particular lot. All five sands were prepared and analyzed in the described manner which is in

accordance with ASTM Specification C 192-80. The gradations from different lots of the same sand were averaged on each sieve size to produce the typical sand gradations given in Table 3.2.

3.6 Fly Ash

The fly ash used in the study was collected from the Public Service Company power plant No. 88 at Oologah, Oklahoma and was classified as Class C fly ash (ASTM C 618)s. It was stored in 55 gallon drums lined with air tight plastic material and topped with a fitting hard cover. Table 3.3 presents the chemical and physical analyses of the fly ash.

Table 3.3 CHEMICAL AND PHYSICAL PROPERTIES OF CLASS C FLY ASH FROM OOLOGAH

CHEMICAL	
Oxides	Weight (% of Total)
$SiO_2+Al_2O_3+Fe_2O_3$	62.08
CaO	26.53
MgO	5.44
SO_3	2.00
Moisture Content	0.03
Loss on Ignition	0.23

PHYSICAL	
Test	Value
Specific Gravity	2.69
Variation from Avg., %	0.4
Variation, % Points from Avg.	1.9
Retained ons# 325, %	11.5
Water Requirement, % of Control	90.2
Pozz. Index (28 days), % of Control	110.0
Autoclave Soundness, % (40% FA)	+ 0.052

Analysis by Gifford Hill & Co., Inc., Ash Products Division; according to ASTM C 311 test procedure.

CHAPTER IV

EXPERIMENTAL METHODOLOGY AND TESTING

4.1 Introduction

The scope of this research was to investigate the feasibility of using fly ash as a binder (cementing agent) in aggregate mixes suitable for base construction in roadways. The determination of two variables was considered essential at the initial stage of the investigation, 1) the profile of the aggregate mixes to be evaluated, and 2) the range of the fly ash content to be used with the aggregate mixes.

The conventional bituminous roadway base course construction involves two types of aggregate bases: a fine and a coarse, the differences deriving from gradation characteristics. This practice was adopted for the study and it was decided that from each of the five aggregate sources a Fine Aggregate Base (FAB) and a Coarse Aggregate Base (CAB) should be designed. The Oklahoma Department of Transportation standard gradation specifications for bituminous base (ODOT 708.04) were adopted for the evaluation of the designed blends (Table 4.1).

A basic assumption was that all aggregate blends should be mixed with fly ash at optimum moisture content for maximum dry density with the expectation that the resulting maximum dry density will produce optimum compressive strength as implied from experience with LFA mixes (33).

In an effort to determine the range of fly ash contents to be used, mixes of aggregates with 15, 25 and 40% fly ash were evaluated. This exploratory work showed that aggregate mixes with 10% fly ash give very low strength while the 40% mixes set very rapidly and the introduction of a retarder would be necessary for their field application to be effective. Consequently, the fly ash additions were fixed at 15, 25 and 35%. The flow chart depicting the procedures and operations used is given in Figure 4.d.

4.2 Grain Size Analysis

Grain size distributions for the seven coarse aggregates, the fine aggregate, the five screenings and the five sands were performed in accordance with AASHTO Designation T 27-82. The sieve sizes selected were those specified by the standard gradation specifications used in this study and given in Table 4.1. As it can be deduced from the Table 3.2 the amount of the material finer than 0.075 mm (No. 200 sieve) was either very small

Table 4.1 ODOT STANDARD GRADATION SPECIFICATIONS

Sieve Size	FAB	CAB
1½ in		100
1 in	100	
3/4 in		60-100
1/2 in		
3/8 in		45-80
#4	75-100	35-65
#10	55-100	25-50
#40	25-85	10-35
#200	5-20	4-12

FAB = Fine Aggregate Base
CAB = Coarse Aggregate Base

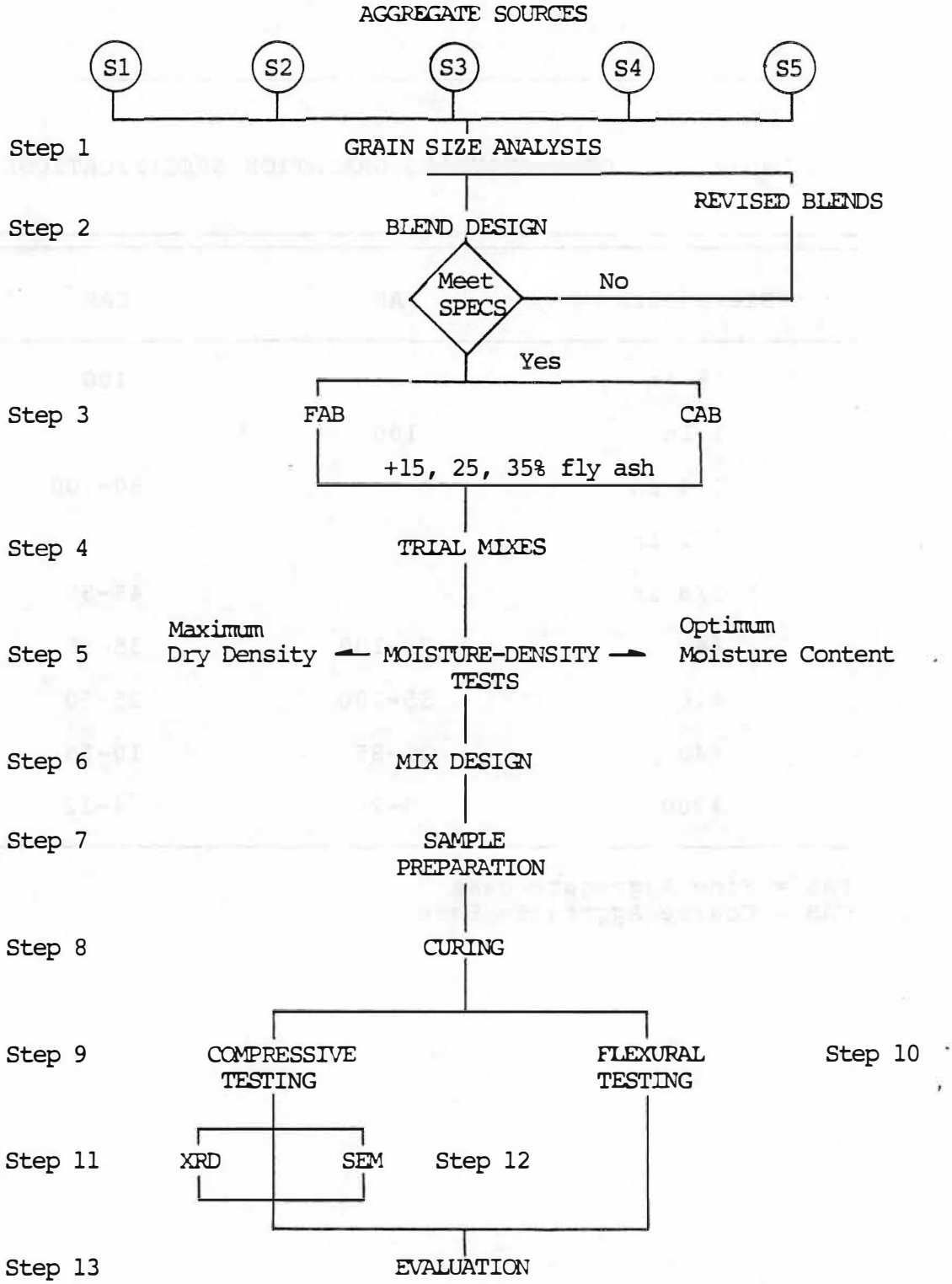

Figure 4.1 Activity flow chart of the study

or zero in all aggregates. The very small to zero amount of fines passing the No. 200 sieve plus the fact that the gradation specifications did not include finer than the No. 200 sieve requirements, deemed a further grain size analysis unnecessary.

4.3 Blend Design

The fine aggregate base (FAB) and the coarse aggregate base (CAB) blends for the five aggregate sources of the project were designed using a combination of two aggregate blending techniques, the mathematical method and the trial and error method. The standard gradation specifications of Table 4.1 were used as a guide and a reference in designing the blends. Special effort was expended to have the blend curves fall as close to the median of the specifications as permitted by the grain size distribution of the component aggregates. The mathematical method was used for the theoretical design of the desired blend and the trial and error method was employed for modifications until the optimum actual design was attained. The repetitive effort is shown in step 2 of the project activity chart of Figure 4.1 by the "revised blends" loop. In sequence the designed FABs and CABs were combined with 15, 25 and 35% fly ash to produce trial mixes for moisture-density evaluation (steps 3 and 4).

4.4 Moisture Density Tests

Moisture density relations were established with the use of standard Proctor apparatus and the tests were run in accordance with AASHTO Designation T 99-83. When the optimum conditions, i.e., maximum dry density and optimum water content for all the 30 mixes (5 FABs, 5 CABs, 3 fly ash percentages) were determined the study moved to step 6 of the activity chart, the mix design.

4.5 Mix Design

The mix design was done on a percent by weight basis. The percentages of the component aggregates totaled 100% of FAB or CAB; the percentage of fly ash in the mix is the weight of fly ash divided by the weight of the aggregates and the water content is the weight of the water used expressed as a percentage of the total weight of the solids. All references to contents or percentages of materials in this study are according to the aforementioned manner which was employed because of the convenience in calculations and adjustments it provides. The formula for the computation is:

$$[[xA_1 + yA_2 + zA_3] + aF] + bW = \text{Mix weight}$$

$$x + y + z = 100$$

$$a = \frac{F}{A_1+A_2+A_3} \times 100$$

$$b = \frac{W}{A_1+A_2+A_3+F} \times 100$$

where A_1, A_2, A_3 = weight of component aggregates

F = weight of fly ash

W = weight of water

x, y, z = % of component aggregates

a = % of fly ash

b = % of water

4.6 Batching Procedure

All mixes were prepared in plastic 15 quart pans. The volume of the pans provided adequate space for mixing enough material for two cylinders (D = 4 in, H = 4.5 in) or one beam (3 x 4 x 16 in) at a time. First, the component aggregates were weighed and placed in the pan where they were mixed by means of a large spoons then, fly ash was added and the whole mass was mixed to uniformity. Finally, the measured distilled water was added in small doses while the mixing was in progress. Mixing continued for five to ten minutes after the addition of all the materials and until a uniform mix was obtained.

4.7 Unconfined Compressive Strength

Standard Proctor size cylinders were manufactured for unconfined compressive strength testing. The mixes were compacted at optimum moisture content and maximum dry density in accordance with AASHTO Designation T 99-81. Because of the relatively rapid setting of the high calcium (CaO) content fly ash mixes and to avoid

prestress of the specimens when extracting them from the mold, it was found practical to use split type Proctor molds, thus eliminating the use of a hydraulic jack. The extracted cylinders - three per mix per curing period - were wrapped in plastic wrap to prevent moisture loss and were stored in humidifiers, at 70°F and 90% relative humidity for the specified curing periods. At the end of the curing periods samples were removed from the humidifier, unwrapped and tested for unconfined compressive strength as shown in Figure 4.2.

The Norman mixes were tested at the end of 1, 3, 7, 14, 28, 90 and 180 days curing time, thus obtaining the full spectrum of the strength gaining process with time. For the remaining four mixes, it was decided that the 28, 90, and 180 day strengths - 28 and 90 being the most critical - would be adequate to outline their compressive strength profiles. Table 4.2 lists the mixes and the curing periods. A total of 114 cylindrical specimens were manufactured and tested for compressive strength.

4.8 Flexural Strength

Most pavements utilizing lime, fly ash or cement treated bases are designed as flexible pavements using compressive strength criteria. However, properly cured treated bases can develop high values of modulus of elasticity which may cause the pavement to perform as a slab

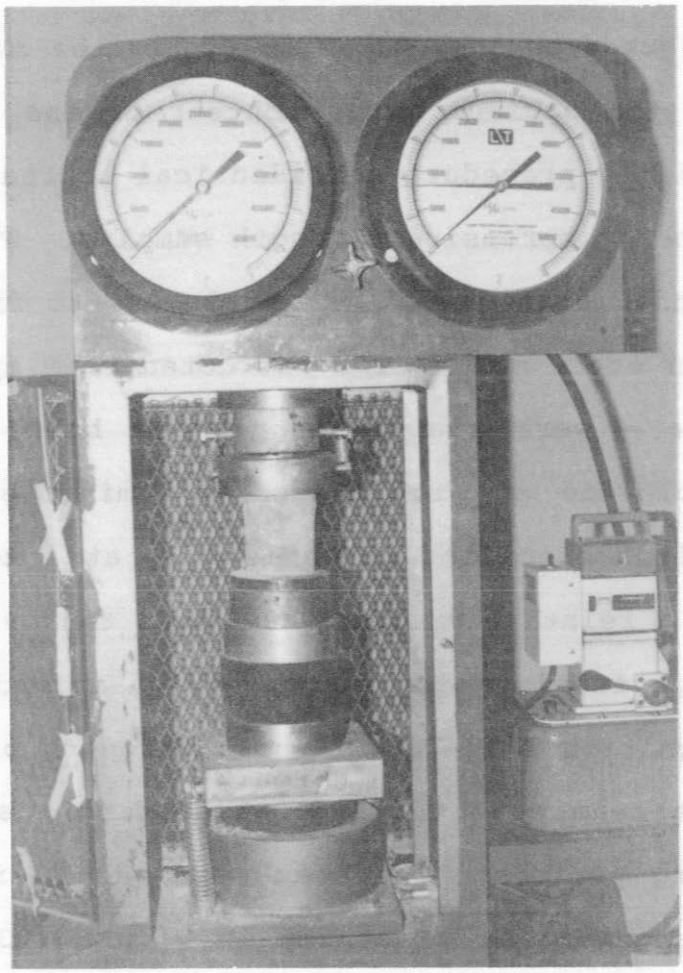

Figure 4.2 Compressive strength testing device

or beam rather than as flexible pavement (18). To account for such a possibility, beams of the mixes were manufactured to test their strength in bending. The beam specimens were prepared using precalculated amounts of fly ash, aggregates and water based on the maximum dry density and the optimum waterscontent of the particular mix. The mixing procedure was identical to that used for the unconfined compressive strength samples. The mix was compacted under static load in two layers to fill a 16 x 4 x 2-3/4 in steel mold. The extracted beam specimens - two per mix - were placed on plywood board and were wrapped in plastic wrap and placed in humidifiers to cure for the periods specified in Table 4.3, at a temperature of 70°F and a relative humidity not less than 90%.

Flexural testing was performed in accordance with AASHTO Designation T 97-76 (Flexural strength of concrete using single beam with third-point loading), at the end of the curing periods. The beam span was 15 in and the loading arrangement is presented in Figure 4.3. All of the beams tested failed in the middle one-third of the span where moment is maximum.

4.9 X-Ray Diffraction (XRD)

Portions of the broken cylinders subjected to compressive testing were collected and crushed with a hammer. The material passing through a 1/4 in U.S. stan-

Table 4.2 COMPRESSIVE STRENGTH CURING PERIODS

Aggregate Source	Blend Type	Curing Time, days
Norman	FAB	1-3-7-14-28-90-180
	CAB	1-3-7-14-28-90-180
Coweta	FAB	28-90-180
	CAB	28-90-180
Ponca City	FAB	28-90-180
	CAB	28-90-180
Tupelo	FAB	28-90-180
	CAB	28-90-180
Ft. Gibson	FAB	28-90-180
	CAB	28-90-180

Table 4.3 BEAM STRENGTH CURING PERIODS

Aggregate Source	Blend Type	Curing Time, days
Norman	FAB, CAB	28, 90, 180
Coweta, Ponca City, Tupelo, Ft. Gibson	FAB, CAB	28, 90

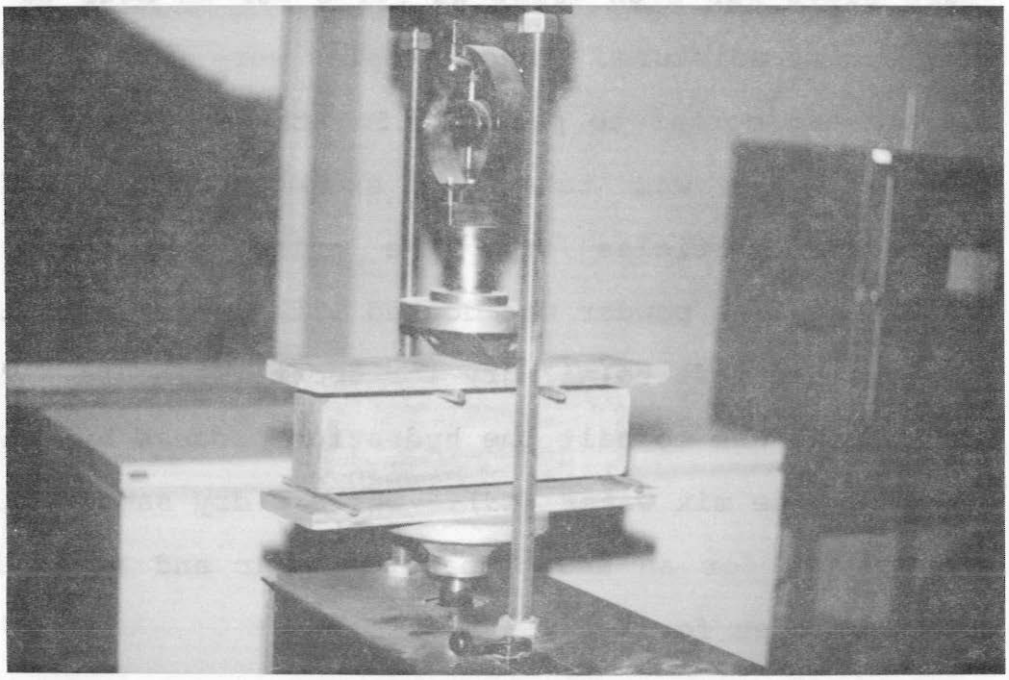

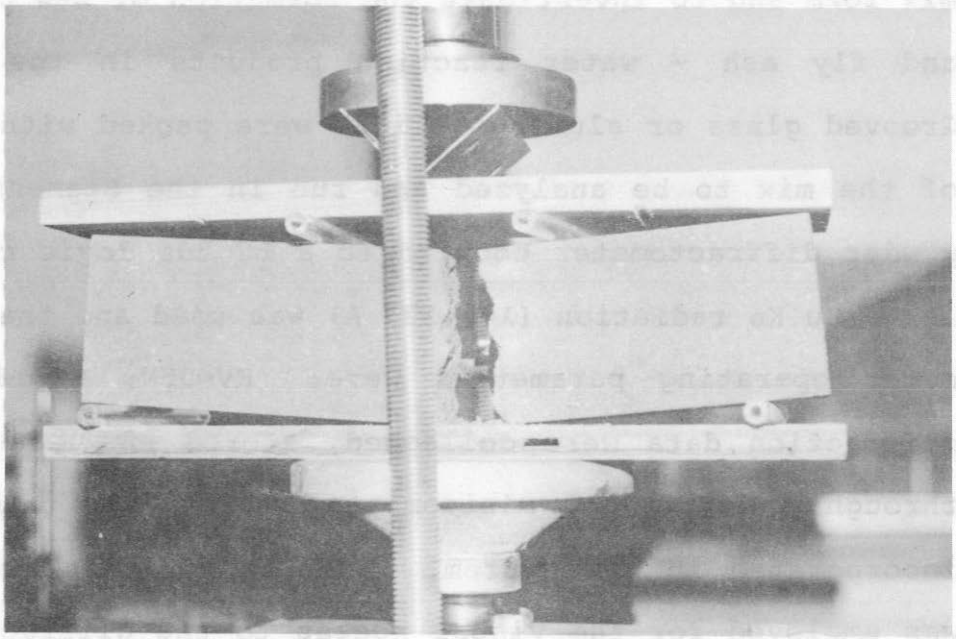

Figure 4.3 Beam loading arrangement and failure pattern

dard sieve was oven dried at 110°C for an hour to remove any excess moisture. These samples were then ground with pestle and mortar to pass a U.S. standard sieve No. 200. Special care was taken to exclude coarse and fine aggregate particles from the grinding process. The resulting fine powder was doused with large quantities of acetone and left to air dry for about two hours. The use of acetone was to halt the hydration process by evaporating the free mix water (19). The air dry sample was then oven dried for an additional one hour and saved in air tight bottles for X-ray analysis.

X-ray diffraction data in this study were used for the mineralogical analysis of fly ash in raw, paste and mix form and to investigate the formation of new crystals and fly ash - water reaction products in the mixes. Grooved glass or aluminum slides were packed with powder of the mix to be analyzed and run in the Siemens D 500 powder diffractometer coupled to a LC 500 logic controller. Cu Kα radiation (λ=1.537 Å) was used and the goniometer operating parameters were: KV=35V, MA=18. The diffraction data were collected, stored and manipulated through a PDP 11/23 minicomputer (256k RAM) which was incorporated in the system. A Tektronix color terminal was employed for the visual access to the diffractograms plotted by a Tektronix multicolor plotter. Analytical data were obtained through a Digital printer. The speci-

mens were scanned from 5°(2θ) to at least 50°(2θ) at a count time of two seconds and a step width of 0.05° (2θ). Finally, the diffractograms are presented divided into two regions; 20°(2θ) to 50° (2θ), where the major and strongest peaks occurred and the region between 5°(2θ) and 20°(2θ) where only a few weak peaks were observed.

4.10 Scanning Electron Microscopy (SEM)

To study the microstructural development in the mix matrix and to identify reaction products specially prepared specimens were microscopically examined by SEM. Broken portions of the failed compressive strength cylinders were reduced to dime size thin slices, carefully avoiding damage to the failure plane. As it was the case with XRD, the SEM specimens were oven dried at 110°C for one hour, then soaked in acetone and left to air dry for two hours and finally, oven dried again for an additional one hour to remove any excess water and halt the process of hydration. The dry specimens glued with rubber cement on aluminum stubs were coated with a thin layer (≅200 Å) of gold palladium to ensure surface conductivity. The coating unit was a Technics sputter coater operated under a vacuum of 110 millitor and using argon as ionizing gas. Immediately following coating, the specimen was placed in an ETEC electron microscope operating at 20 KV. Black and white exposures of the observations were taken using

self developing Polaroid 665 positive and negative film pack. Magnifications ranged from 400X to 10,000X but the majority of the exposures was at 3000X. On occasion, energy dispersive spectroscopy (EDS) was employed for the qualitative elemental analysis of selected specimensa It was performed by a γPGT energy dispersive spectroscope attached to the electron microscope and coupled with a computer/controller.

CHAPTER V

PRESENTATION AND DISCUSSION OF RESULTS

5.1 Introduction

The scope of this chapter is to characterize the fine aggregate bases and coarse aggregate bases mixed with Class C fly ash by examining the final products themselves but also by partially investigating the processes involved and the factors that contributed to the structural profile of the final product. Under this perspective the results reported in Chapter IV and related to standard engineering tests of grain size analysis, moisture-density relationships, unconfined compressive strength and flexural strength along with those produced by the blend design, the X-ray diffraction (XRD) and scanning electron microscopy (SEM), are presented and discussed in this chapter. Included is a flexural design approach involving the beam hypothesis. Correlations are attempted wherever suitable or appropriate.

5.2 Grain Size Analysis and Blend Design

The grain size distributions of the component aggregates have been presented in Table 4.2. A comparison be-

tween gradations of similar aggregates makes apparent the grain size variation of component aggregates from different sources with the possible exception of the coarse stone. In addition, an inspection of the percentages of material passing the No. 200 sieve (0.075 mm) indicates that all the available aggregates lack in fine fractions. On the other hand, the standard gradation specifications require a 5 to 20% of material passing sieve No. 200 for FAB, while the respective range for CAB is 4 to 12%. At this point it became obvious that the designed blends will be unable to meet the fine portion of the specifications (No. 200 sieve) because of lack of adequate fine material in the component aggregates. Two alternatives were considered as a solution to the problem at hand. One, the introduction of a fine aggregate available from another source with adequate fines to compensate for the lack in the original components and two, utilizing fly ash to partially act as a filler in order to close the gap. Exploratory SEM work verified the role of fly ash as a partial filler and alternate two was adopted. Later, more extensive SEM observations established the dual role of fly ash in this study as both a chemical agent and a filler.

With regard to the aforementioned consideration the blend design was focused on creating aggregate blends as close to the median of the specifications as the flexibi-

interesting to observe that for the FAB, increasing fly ash contents lead to higher values of dry density, while the reverse is true for CAB. In other words, with the FABs, the density of the mix is directly proportional to the fly ash content, but with the CABs, increasing the fly ash content seems to decrease the dry density. The observed density increase of the FAB mixes, containing increased fly ash amounts, supports the early hypothesis that fly ash - acting as a filler - will provide the missing fines, thus improving the uniformity of the mix and eventually the strength performance. The decrease in dry density associated with increased additions of fly ash in the CABs suggests that in these mixes the cementing potential of fly ash prevails over its role as a filler and it determines the strength outcome.

5.4 Unconfined Compressive Strength

The compressive strength results of all samples tested for the specified curing periods are presented in Appendix B, Tables B.1 to B.5. In Figures B.1 to B.10 (Appendix B) the average compressive strength of each blend is illustrated as a function of two variables: fly ash content and curing time.

5.4.1 Norman bases. As mentioned previously, the Norman mixes were cured for periods ranging from one day to six months, thus providing a complete strength

Table 5.1 AGGREGATE BLENDS (%)

Source	Aggregates	CAB	FAB	
Norman	Sand	35	78	
	Fine	35	22	
	Coarse	30	0	
Ponca City	Sand	37	90	
	Screenings	23	10	:scalped at 3/8 in
	Coarse 1½ in	40	0	
Coweta	Sand	30	100	
	Screenings	40	0	
	Coarse 1½ in	30	0	
Tupelo	Sand	25	60	
	Screenings	10	40	
	Coarse	65	0	
Ft. Gibson	Sand	40	80	
	Screenings	20	20	:scalped at 3/8 in
	Coarse 1½ in	40	0	

CABs= Coarse Aggregate Base
FAB = Fine Aggregate Base

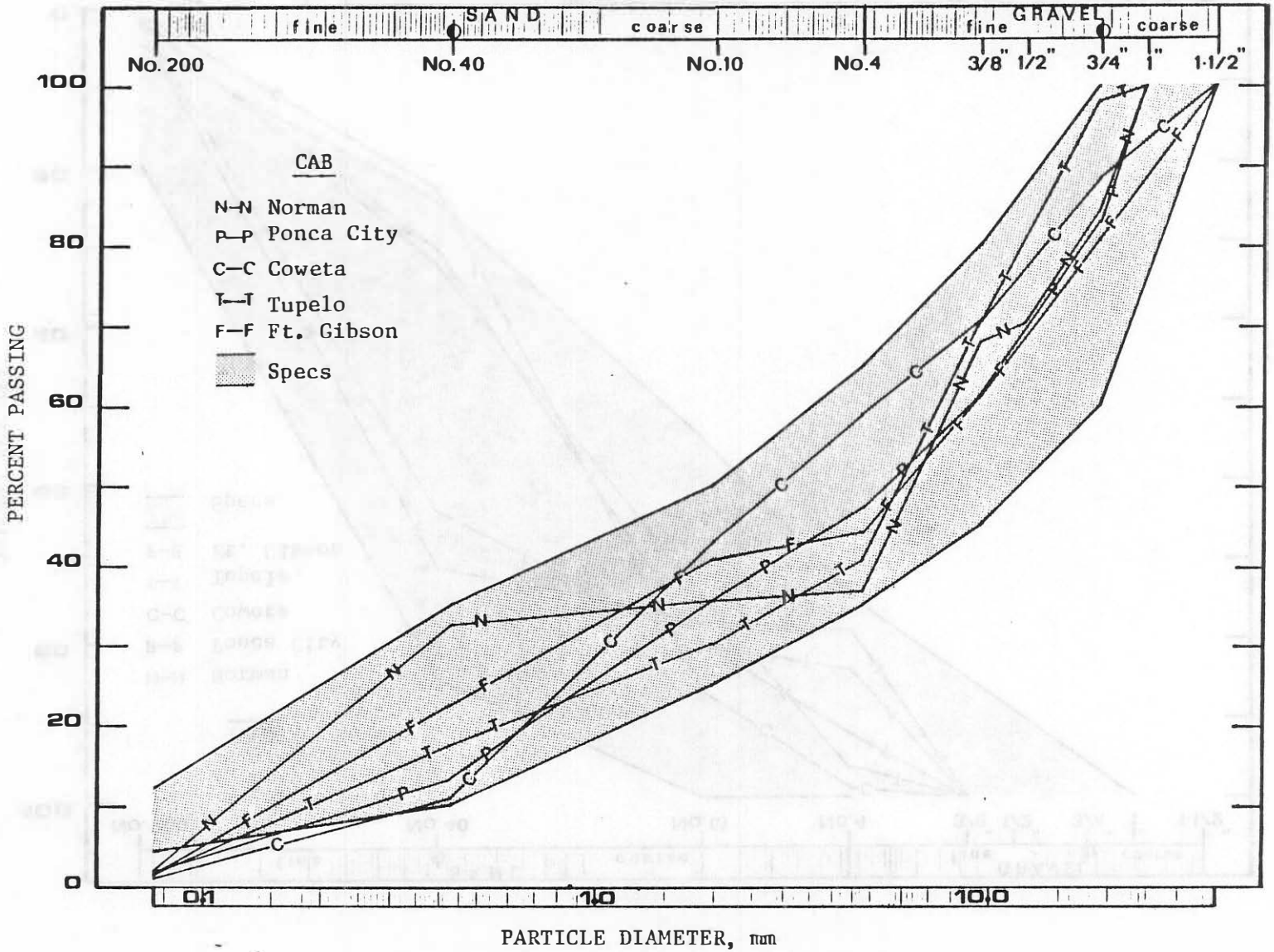

Figure 5.1 Coarse aggregate base (CAB) grain size distribution

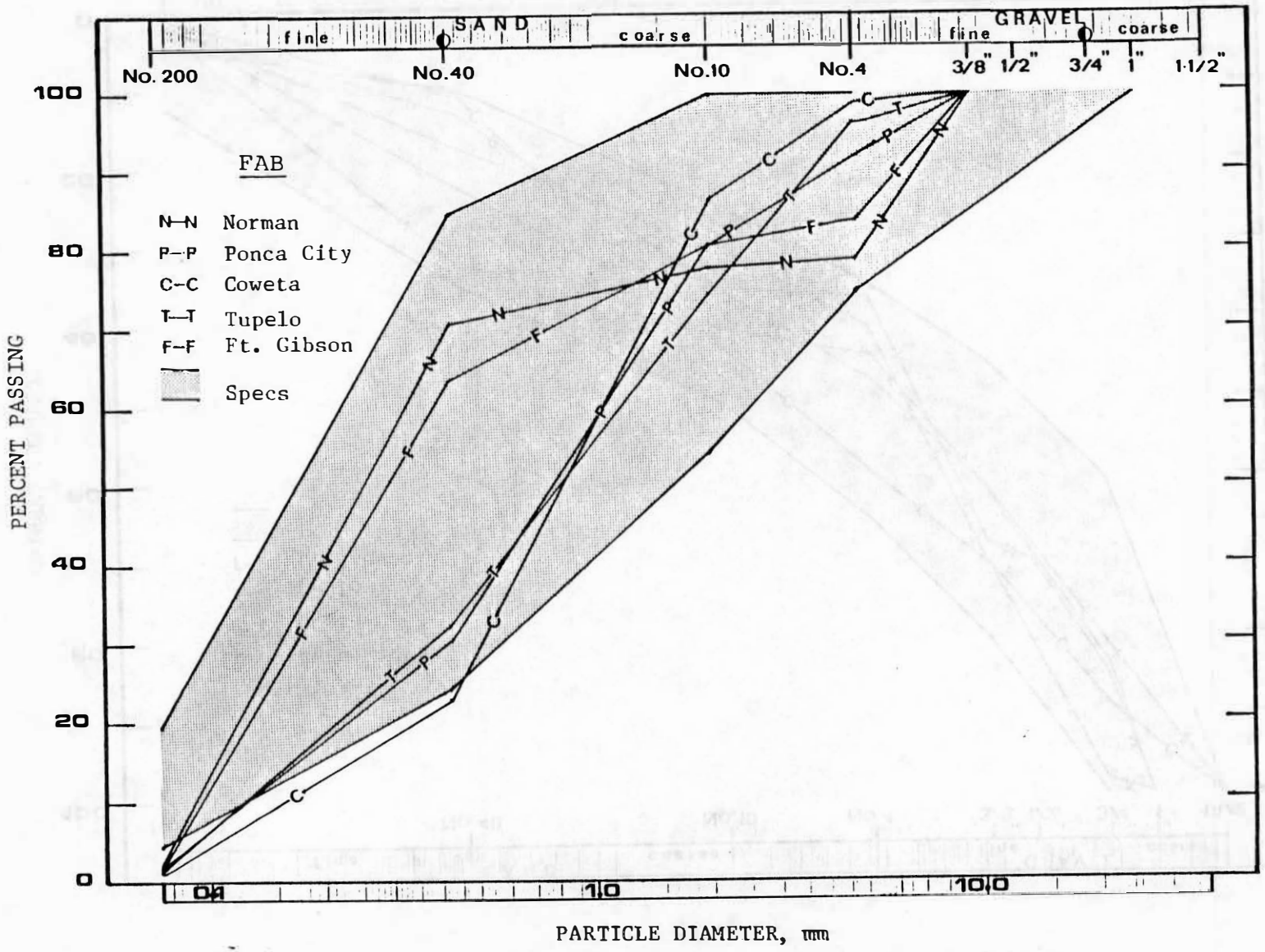

Figure 5.2 Fine aggregate base (FAB) grain size distribution

Table 5.2 MAXIMUM DRY DENSITY (pcf) - OPTIMUM MOISTURE CONTENT (%)

Mix Type	Norman		Ponca		Coweta		Tupelo		Ft. Gibson	
	γ_d	mc	γ_d	mc	γ_d	mc	γ_d	mc	γ_d	mc
FAB+15% f.a.	129.1	8.2	132.2	5.9	135.9	7.1	139.4	7.8	131.2	9.9
FAB+25% f.a.	133.2	5.1	133.8	5.8	140.3	5.2	142.7	5.5	130.2	5.3
FAB+35% f.a.	137.3	6.1	140.3	5.0	135.8	4.3	144.5	5.9	135.7	5.4
CAB+15% f.a.	146.8	5.0	145.1	5.9	145.6	6.1	140.0	8.6	140.5	6.0
CAB+25% f.a.	144.8	5.0	142.1	5.0	142.5	6.2	138.7	6.2	149.5	5.2
CAB+35% f.a.	143.0	6.2	137.5	4.8	139.2	6.4	137.5	5.0	146.1	5.8

f.a. = fly ash

γ_d = maximum dry density

mc = optimum moisture content

picture of the fly ash treated bases relative to the curing time. A close examination of the strength performance of these mixes, depicted in Figures 5.3 (FAB) and 5.4 (CAB), reveals some interesting and noteworthy patterns as well as some trends.

1. Both the FAB and the CAB appear to obtain their highest overall strength during the time interval between seven and 90 days. For the FAB, the highest strength (1348 psi) is recorded for a curing time of 28 days, while for the CAB the peak strength (1500 psi) occurs after 14 days of curing.
2. The strength performance ofsthe two bases after curing of seven days is surprisingly low, with the exception of the CAB + 15% fly ash mix which attains its maximum strength over the six month spectrum recorded strength of 711 psi.
3. With the Norman FAB, the one day strength is rather impressive, the leading fly ash content being 35%. FAB + 35% fly ash is the mix of the highest density. Then, strengths decline as as whole to reach their minimum values in seven days, with the exception of FAB + 15% fly ash which maintains a constant level of strength for curing times of 1, 3 and 7 days. The fly ash addition of 25% is the leading percentage

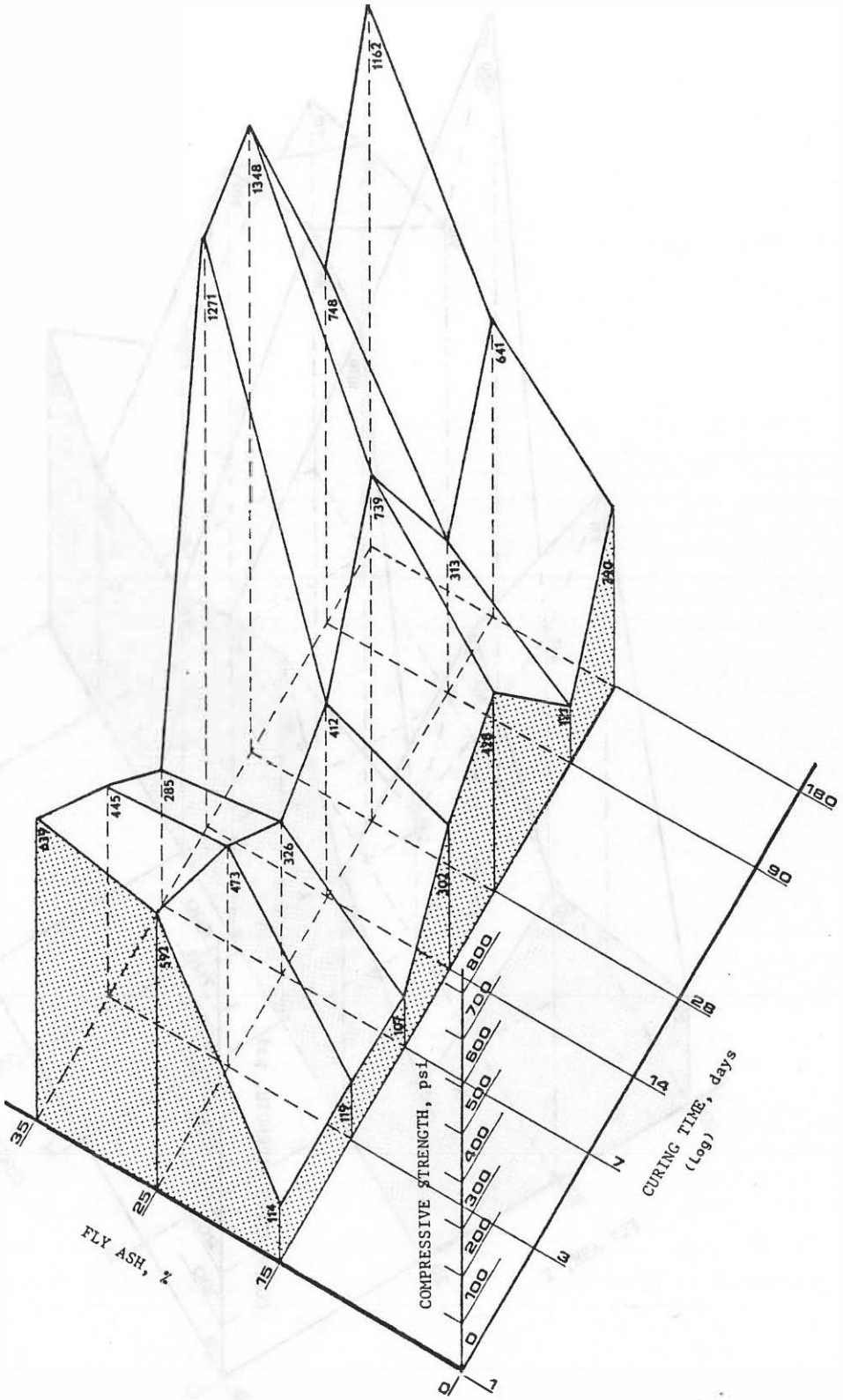

Figure 5.8 Compressive strength of Norman FAB mixes

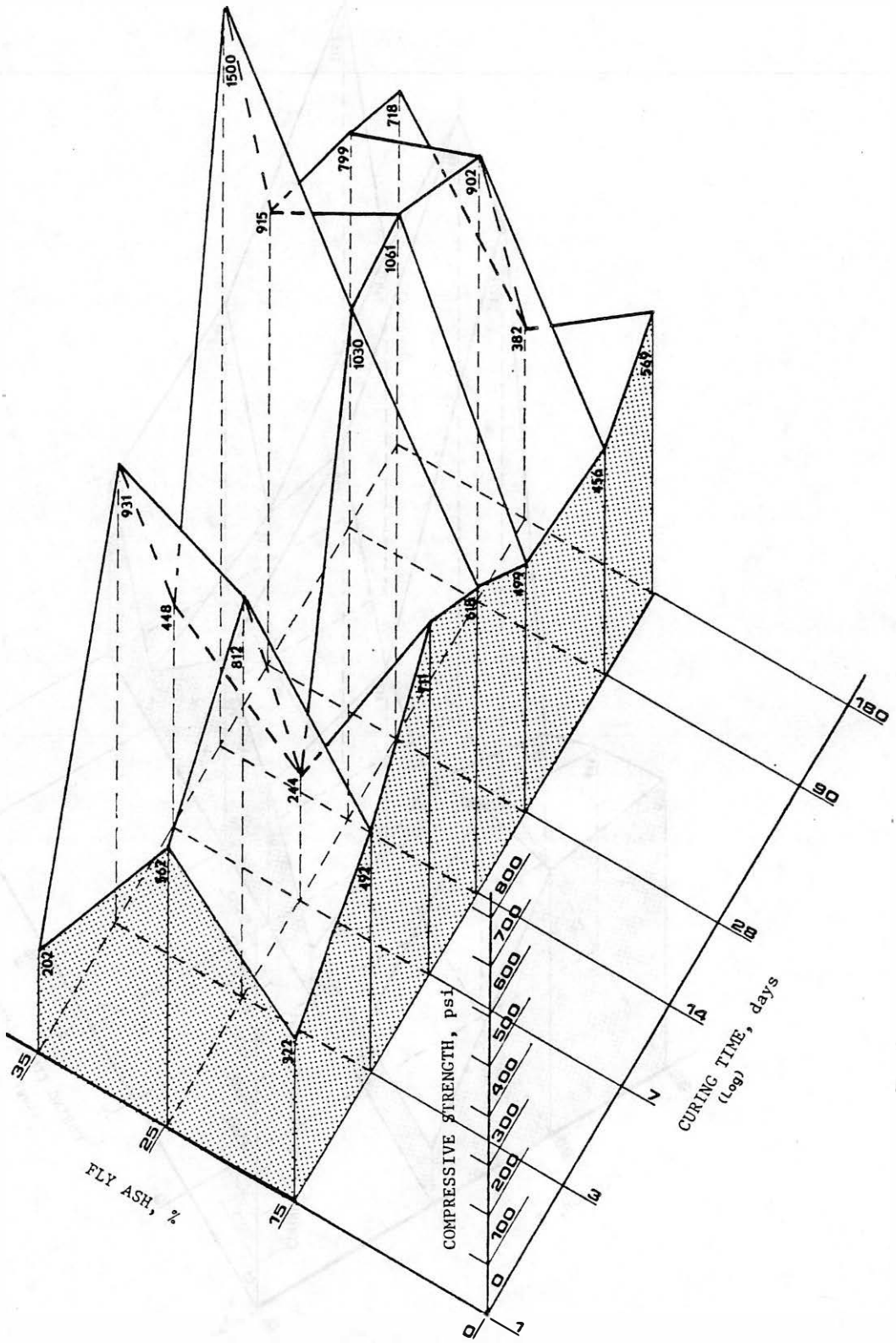

Figure 5.4 Compressive Strength of Norman CAB mixes

in terms of strength for the three and seven-day curing. After 14 days the pattern changes altogether, 35% fly ash content giving the mix by far the highest strength. The pattern as a whole reaches high performance in 28 days, drops rather sharply at 90 days and picks up again at 180 days.

4. For the Norman CAB the pattern observed is different than that of the FAB. For one day curing the 25% fly ash mix gives the best results. After three days of curing the strength values increase substantially and the highest strength is attained at 35% fly ash although the density is the lowest. In seven days the mix with the highest density (15% fly ash) reaches its maximum recorded strength, while the strengths of the other two mixes (25% and 35% fly ash) have declined considerably. After 14 days of curing the strength profile as a whole reaches its best overall performance, 35% fly ash content giving the peak strength. In 28 days the 25% fly ash mix attains its maximum strength (1061 psi); in 90 days the 25% fly ash is still the leading strength content but the overall strengths are lower and, finally, at 180 days strengths are rather

reduced with the 35% fly ash mix giving the highest value.

5.4.2 The other bases. The strength data of the Norman bases made it clear that there is a considerable variation in the strength of the mixes during the first seven days, and more uniform results are obtained in later ages. With this in mind and considering concrete practices, the remaining of the bases were tested for 28, 90 and 180 days curing times. Figures B.3 to B.10 (Appendix B) are the illustrations of their strength performance. The Coweta FAB and CAB graphs indicate fairly regular strength patterns showing an increase of strength with time. The Ponca City FAB shows small increases of strength with time after the 28th day and the CAB from the same source follows a similar pattern. The bases from Tupelo reach maximum strength in 180 days and the mix with 25% fly ash content continuously gives the highest strength, although the strength gaining rate between 90 and 180 days appears to be particularly slow. Finally, for Ft. Gibson, while the FAB shows an expected behavior, the CAB peaks in strength performance (1281 psi) in 28 days, to decline in 90 days and pick up again in 180 days.

A correlation of maximum strength and the corresponding time of curing is presented in Table 5.3. Earlier than 28 days Norman strength results were not taken

Table 5.3 MAXIMUM UNCONFINED COMPRESSIVE STRENGTH (psi) FOR ALL MIXES AT THE CURING TIME (days) INDICATED.

Mix Type	Norman		Ponca		Coweta		Tupelo		Ft. Gibson	
	σ_c	C.T.	σ_c	C.T.	σ_c	C.T.	σ_c	C.T.	σ_c	C.T.
FAB+15% f.a.	428.0	28	239.0	180	141.0	180	281.0	180	225.0	180
FAB+25% f.a.	739.0	28	822.0	180	348.0	180	573.0	180	716.0	180
FAB+35% f.a.	1348.0	28	848.0	180	515.0	180	281.0	180	955.0	180
CAB+15% f.a.	569.0	180	451.0	180	268.0	180	387.0	180	730.0	180
CAB+25% f.a.	1061.0	28	902.0	90,180	610.0	180	822.0	180	1281.0	28
CAB+35% f.a.	915.0	28	693.0	90	541.0	90	412.0	180	982.0	180

σ_c = unconfined compressive strength

C.T. = curing time

into account. The underlined strengths indicate the maximum overall strength of the particular blend. Thus, it can be observed that for all the CABs the prevailing fly ash addition in terms of strength performance is 25%, while for the FABs the respective percentage is 35%, at which maximum dry densities occur. The only exception is the Tupelo FAB, which gives better strength results with 25% fly ash.

5.5 Flexural Strength

Two beams per mix were tested at the end of 28 and 90 days to measure the flexural parameters and evaluate the behavior of the mixes in bending. A unique feature of the testing procedure was the sensitivity and flexural weakness of the 28-day cured beams. The majority of these beams would either crack during unwrapping and preparing the specimens for testing or fail upon application of very low load. Of the 60 beams prepared for testing after curing for 28 days only 10 presented resistance to two point loading, which represents a mere 17% of the total number of beams for this curing period. On the other hand, beams cured for 90 days did not indicate any testing difficulties and in this section their load-deflection patterns are presented, discussed and analyzed. The flexural parameters derived from the curves are the modulus of elastic rupture, the modulus of elas-

ticity and a new parameter is introduced - the modulus of plasticity - which describes the behavior of the mixes within the plastic range and could be used for plastic design if such criteria are used. Correlations of flexural and compressive strength are given as a ratio.

5.5.1 Load-deflection curves. The relationship between the load applied and the deflection of the beam is plotted and presented in Appendix C, Figures C.1 to C.10. Each graph contains the curves of the FAB or CAB mixed with 15, 25, and 35% fly ash; two graphs per aggregate source. The two beam specimens tested for each mix gave very similar load-deflection data for the majority of the mixes; so, the average value was plotted. When the data of the two specimens from the same mix varied by more than 10%, the pattern that was thought to best portray the mix, based on the laboratory experience of the particular mix, was chosen. Examination of the 30 curves corresponding to the equal number of mixes of this study reveals that any curve can be divided into three sections. The initial concave upward part of the curve, wherein the deflection increased exponentially for a moderate load increase, is attributed primarily to the nonhomogeneity of the mixes. This is followed by the linear elastic range of the curve which leads to the concave downward plastic range. The latter is quite extended with some curves. The characteristic loads

marking the limits of the three curve sections for all the mixes are given in Table 5.4. These loads are: (P_E), the load at which the concave upward first section ends and the elastic range starts; the load corresponding to the proportional limit (P_p), and the load at failure (P_F), or the end of the plastic range. For all practical purposes, the first section of the curve is not taken into account. To compensate, the straight line of the elastic range is extended to intersect the abscissa at a point which is taken as the origin of the deflection axis, and the deflection readings are corrected for the adjustment. The adjustments for all mixes are given in the tables of Appendix D and from this point on it is the adjusted deflection that is meant by any reference to deflection. With the incorporation of the first section into the second, the whole curve is simplified into two rangess the elastic and the plastic.

The amount of fly ash added and its effect on the flexural performance of the mixes does not appear to follow a general pattern. Rather, correlations of fly ash content and load-deflection response can be made fors the FAB and/or CAB of a particular mix. For instance, for both the Ponca City FAB and CAB blends (Figures C.3 and C.4) the mix with 25% fly ash requires the lowest load to induce the same deflection as those containing 15% and 35% fly ashs additionally, the 25% fly ash mix

Table 5.4 CRITICAL LOADS (lb) OF THE 90-DAY LOAD-DEFLECTION CURVES

Mix Type	Norman			Ponca			Coweta			Tupelo			Ft. Gibson		
	P_E	P_P	P_F	P_E	P_P	P_F	P_E	P_P	P_F	P_E	P_P	P_F	P_E	P_P	P_F
FAB + 15% f.a.	80	260	310	120	380	660	50	460	510	140	370	450	20	-	80
FAB + 25% f.a.	60	400	460	100	440	1350	140	450	710	140	360	640	100	450	550
FAB + 35% f.a.	120	300	650	120	360	540	140	440	550	140	420	700	80	300	680
CAB + 15% f.a.	20	470	480	100	410	640	100	400	730	140	350	670	140	485	780
CAB + 25% f.a.	40	250	390	80	315	930	80	430	750	125	330	860	200	400	750
CAB + 35% f.a.	30	250	390	100	320	660	100	400	700	50	320	730	80	485	885

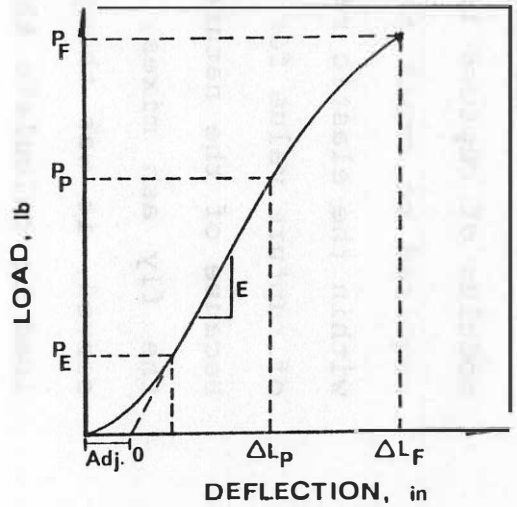

can withstand the highest load and undergo the maximum deflection before failure. For the Coweta FAB and CAB blends (Figures C.5 and C.6$ the 35% fly ash mixes require high loads, in order to deflect as much as their 15% and 25% fly ash counterparts. It is also interesting to observe that the three Ft. Gibson CAB mixes (Figure C.10) present a pivot point at which all three undergo the same deflection under the same load.

5.5.2 Modulus of elastic rupture (MER)s The modulus of rupture is the flexural stress under the load required to crack the beam (18) and is applicable only within the elastic range of the mixes. A typical modulus of rupture value for medium strength concrete is 450 psi. Because of the nature of the load-deflection patterns of the fly ash mixes, where wide plastic ranges are observed, it was thought unrealistic to use the breaking load to calculate the modulus of rupture. Instead, the modulus of elastic rupture was adopted, which is the highest flexural stress within the elastic range corresponding to the load at the proportional limit, where actual failure originates. The modulus of elastic ruptures is given as:

$$MERs = \frac{MC}{I} = \frac{PL}{bd^2} \qquad (5.1)$$

can withstand the highest load and undergo the maximum deflection before failure. For the Coweta FAB and CAB blends (Figures C.5 and C.6) the 35% fly ash mixes require high loads, in order to deflect as much as their 15% and 25% fly ash counterparts. It is also interesting to observe that the three Fts Gibson CAB mixes (Figure C.10) present a pivot point at which all three undergo the same deflection under the same load.

5.5.2 Modulus of elastic rupture (MER)s The modulus of rupture is the flexural stress under the load required to crack the beam (18) and is applicable only within the elastic range of the mixes. A typical modulus of rupture value for medium strength concrete is 450 psi. Because of the nature of the load-deflection patterns of the fly ash mixes, where wide plastic ranges are observed, it was thought unrealistic to use the breaking load to calculate the modulus of rupture. Instead, the modulus of elastic rupture was adopted, which is the highest flexural stress within the elastic range corresponding to the load at the proportional limit, where actual failure originates. The modulus of elastic ruptures is given as:

$$MER_s = \frac{MC}{I} = \frac{PL}{bd^2} \qquad (5.1)$$

where, MER = modulus of elastic rupture, psi

M = moment in middle one-third span, in-lb

C = distance from neutral axis to extreme fiber, in

I = moment of inertia, in^4

P = load, lb

L = span length, in

b = beam width, in

d = beam depth, in

The values for the modulus of elastic rupture for the 90-day beams - two beams per mix - are reported in Table 5.5 and the average MER for each mix is calculated. Figures 5.5 and 5.6 illustrate the MER values of the FABs and CABs respectively, with respect to the fly ash percentage. With the FABs (Figure 5.5) it is the 25% fly ash content that predominately produces high moduli of elastic rupture. An interesting feature of these graphs is the similarity of the MER - fly ash content patterns between FAB and CAB for the mixes of Tupelo and Cowetas For the Norman and Fts Gibson mixes comparing the FAB to the CAB curves their concave portions are reversed, indicating that the fly ash content which gives the highest modulus of elastic rupture with the FAB produces the lowest MER with the CAB.

The average MER and compressive strength values for each mix were used to compute the ratios of flexural to

Table 5.5 MODULUS OF ELASTIC RUPTURE (psi) - BEAMS CURED FOR 90 DAYS

Mix Type	Norman	Ponca	Coweta	Tupelo	Ft. Gibson
FAB +	60.9	118.8	134.4	115.6	25.0
15%	81.3	-	143.9	118.8	-
fly ash	Avg. 71.1	Avg.118.8	Avg.139.1	Avg.117.2	Avg.25.0
FAB +	125.0	137.5	140.6	112.5	146.9
25%	-	150.0	140.6	112.5	140.6
fly ash	Avg.125.0	Avg.143.8	Avg.140.6	Avg.112.5	Avg.143.7
FAB +	93.8	112.5	134.4	131.3	106.3
35%	-	-	137.5	137.5	93.8
fly ash	Avg. 93.8	Avg.112.5	Avg.136.0	Avg.134.4	Avg.100.0
CABs+	146.9	128.1	140.6	109.4	151.6
15%	125.0	128.1	125.0	106.3	143.7
fly ash	Avg.136.0	Avg.128.1	Avg.132.8	Avg.107.8	Avg.147.6
CAB +	78.1	98.4	134.4	100.0	125.0
25%	-	137.5	137.5	103.1	131.3
fly ash	Avg.78.1	Avg.118.0	Avg.136.0	Avg.101.6	Avg.128.1
CAB +	78.1	100.0	125.0	100.0	150.0
35%	110.1	100.0	128.1	125.0	151.6
fly ash	Avg.96.1	Avg.100.0	Avg.126.6	Avg.122.5	Avg.150.8

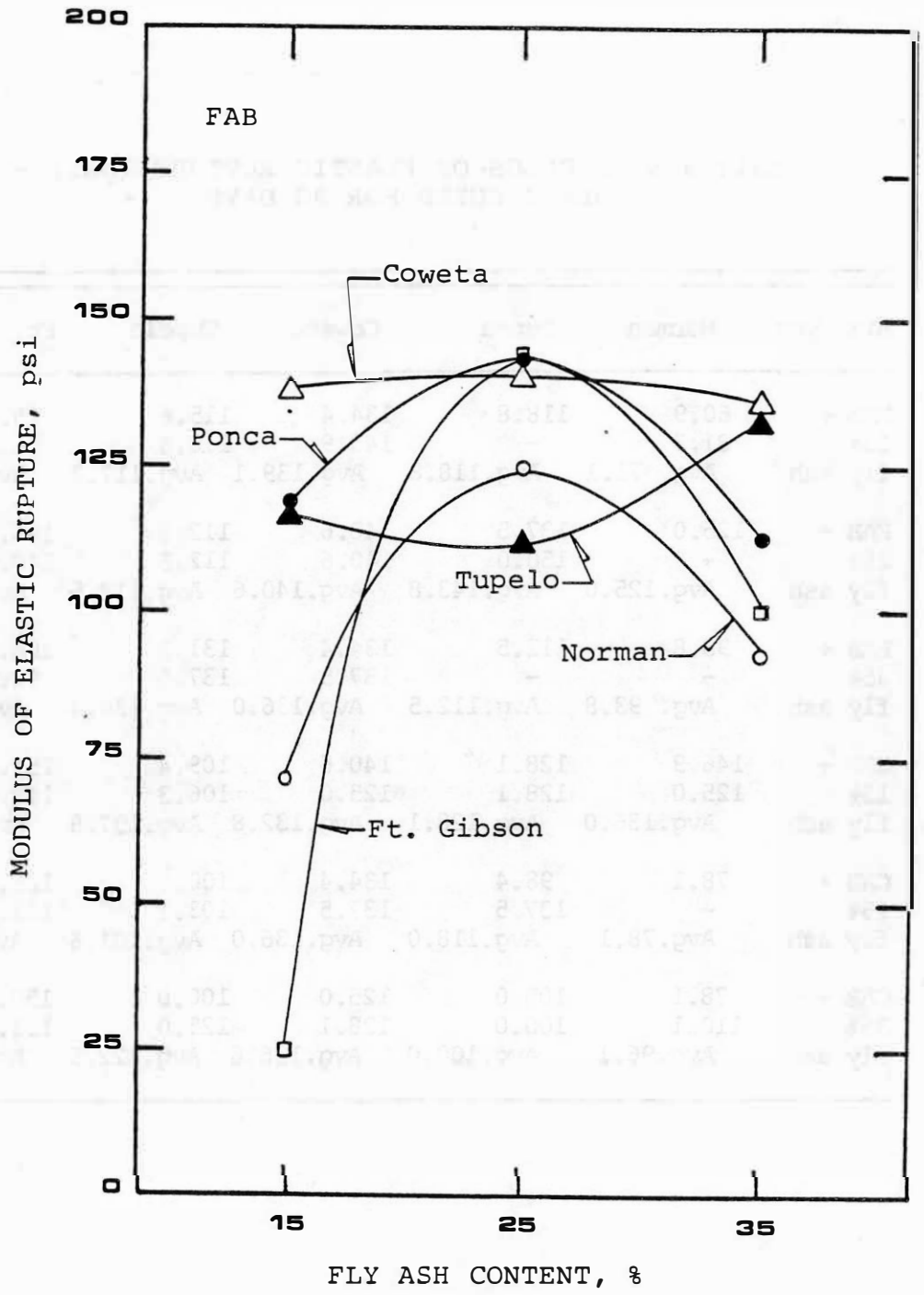

Figure 5.5 Effect of fly ash additions on the MER of the FABs

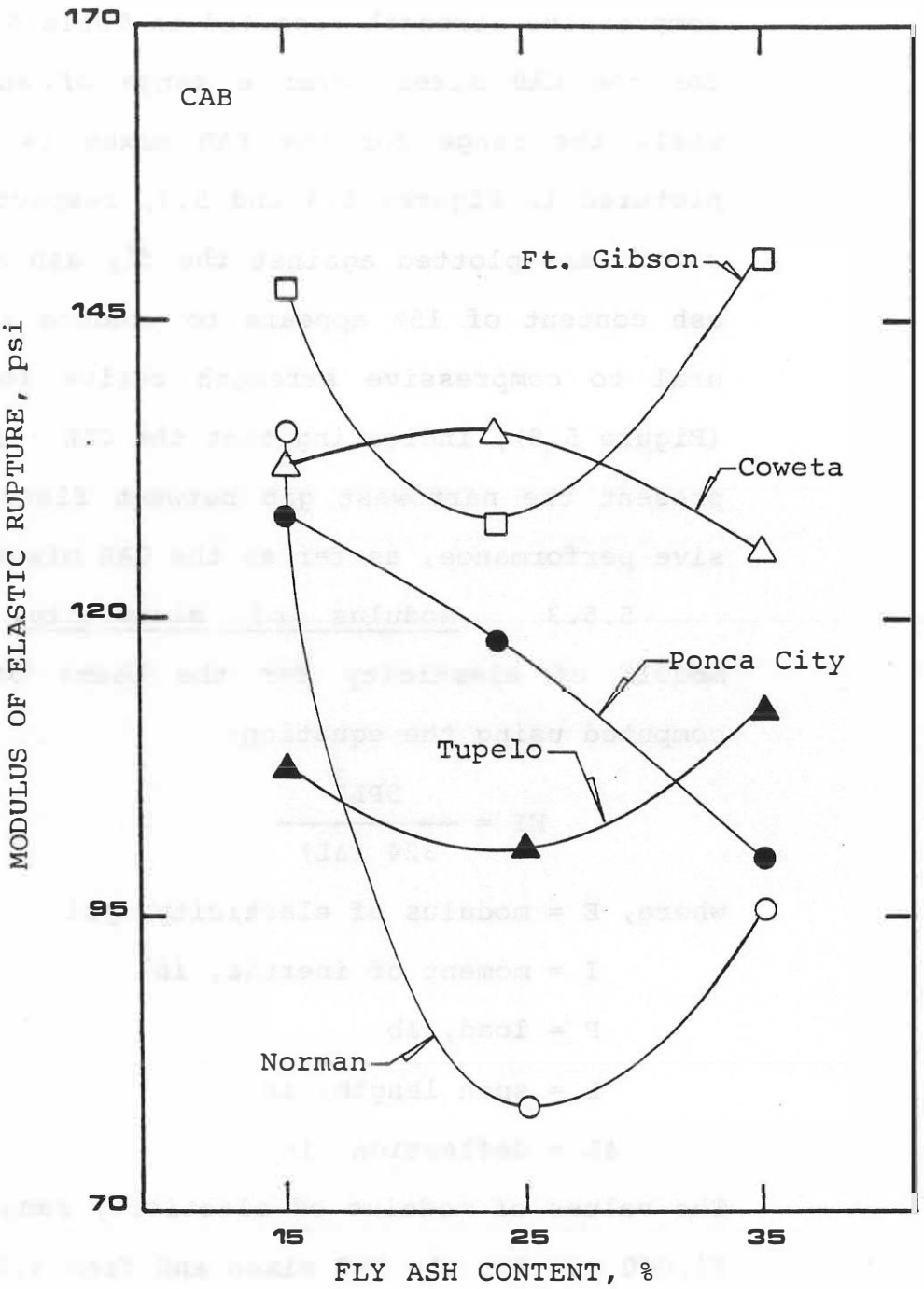

Figure 5.6 Effect of fly ash additions on the MER of the CABs

compressive strength reported in Table 5.6. These ratios for the CAB mixes cover a range of approximately 0.50 while the range for the FAB mixes is wider, as it is pictured in Figures 5.8 and 5.7, respectively, where the ratios are plotted against the fly ash additions. A fly ash content of 15% appears to produce the highest flexural to compressive strength ratios for the CAB mixes (Figure 5.8), indicating that the CABs+ 15% fly ash mixes present the narrowest gap between flexural and compressive performance, as far as the CAB mixes are concerned.

5.5.3 Modulus of elasticity. The flexural moduli of elasticity for the beams of each mix were computed using the equation:

$$EI = \frac{5PL^3}{324\ (\Delta L)} \qquad (5.2)$$

where, E = modulus of elasticity, psi

I = moment of inertia, in^4

P = load, lb

L = span length, in

ΔL = deflection, in

The values of modulus of elasticity ranged from 4,000 to 51,000 psi for the FAB mixes and from 4,500 to 54,500 psi for the CAB mixes. These values are presented in the tables in Appendix D, along with other flexural parameters.

Table 5.6 RATIOS OF FLEXURAL TO COMPRESSIVE STRENGTH FOR CURING TIME OF 90 DAYS

Mix Type	Norman	Ponca	Coweta	Tupelo	Ft. Gibson
FAB + 15% fly ash	0.59	0.53	1.55	0.42	0.17
FAB + 25% fly ash	0.40	0.19	0.78	0.30	0.26
FAB + 35% fly ash	0.13	0.14	0.32	0.37	0.16
CABs+ 15% fly ash	0.30	0.30	0.53	0.35	0.25
CAB + 25% fly ash	0.09	0.13	0.43	0.13	0.15
CABs+ 35% fly ash	0.12	0.14	0.23	0.32	0.23

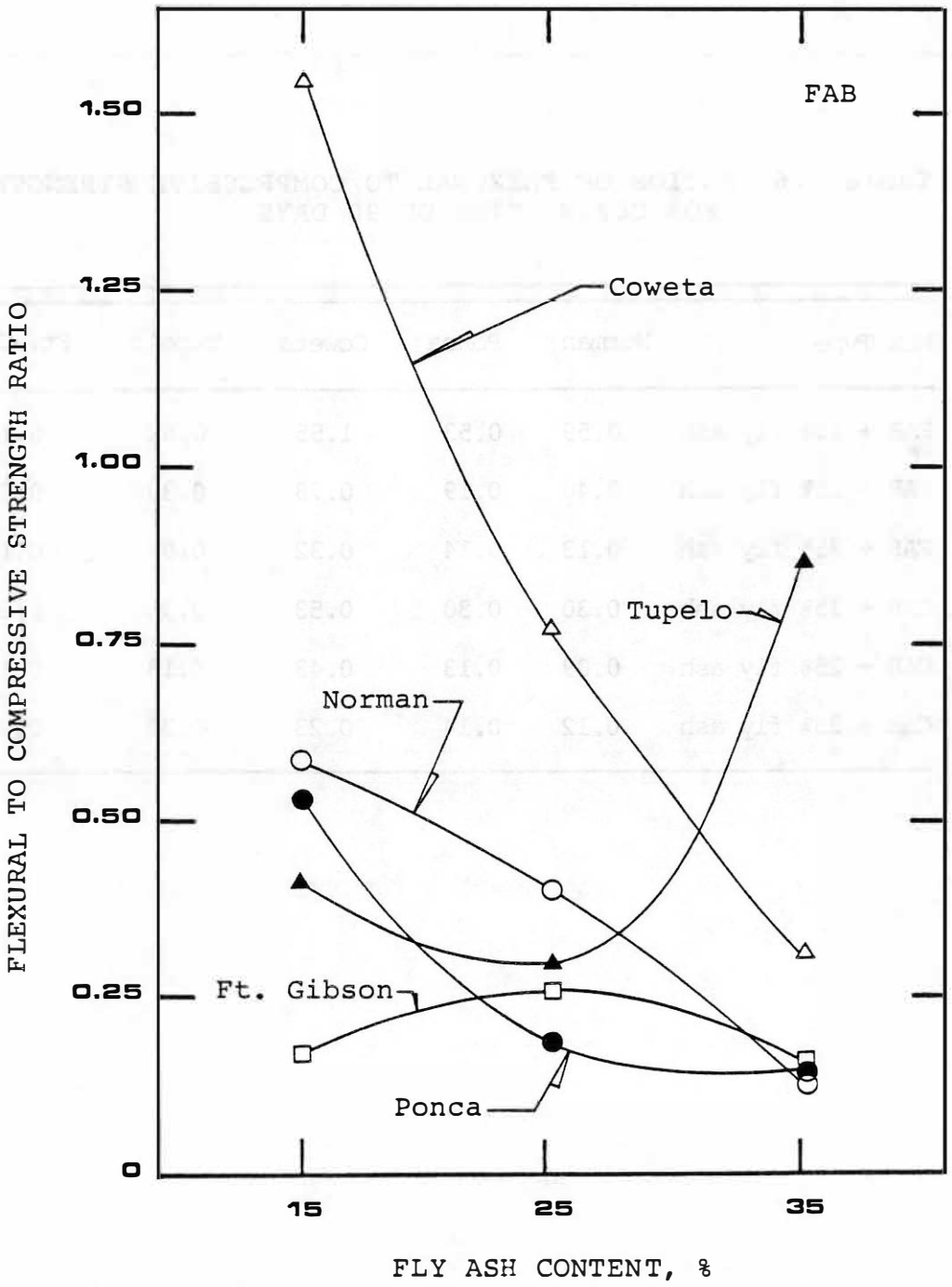

Figure 5.7 Effect of fly ash content on the flexural to compressive strength ratios of the FABs

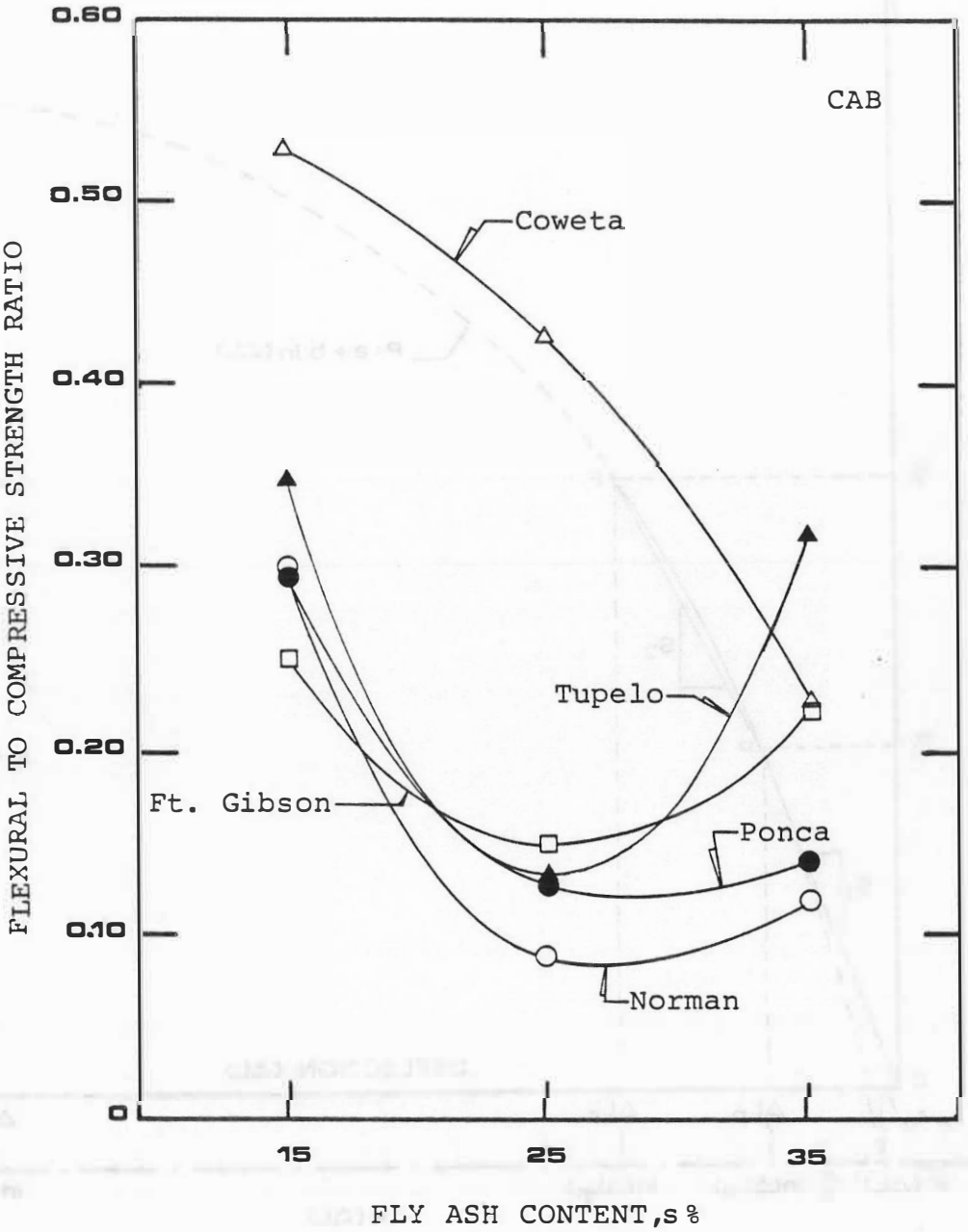

Figure 5.8 Effect of fly ash content on the flexural to compressive strength ratios of the CABs

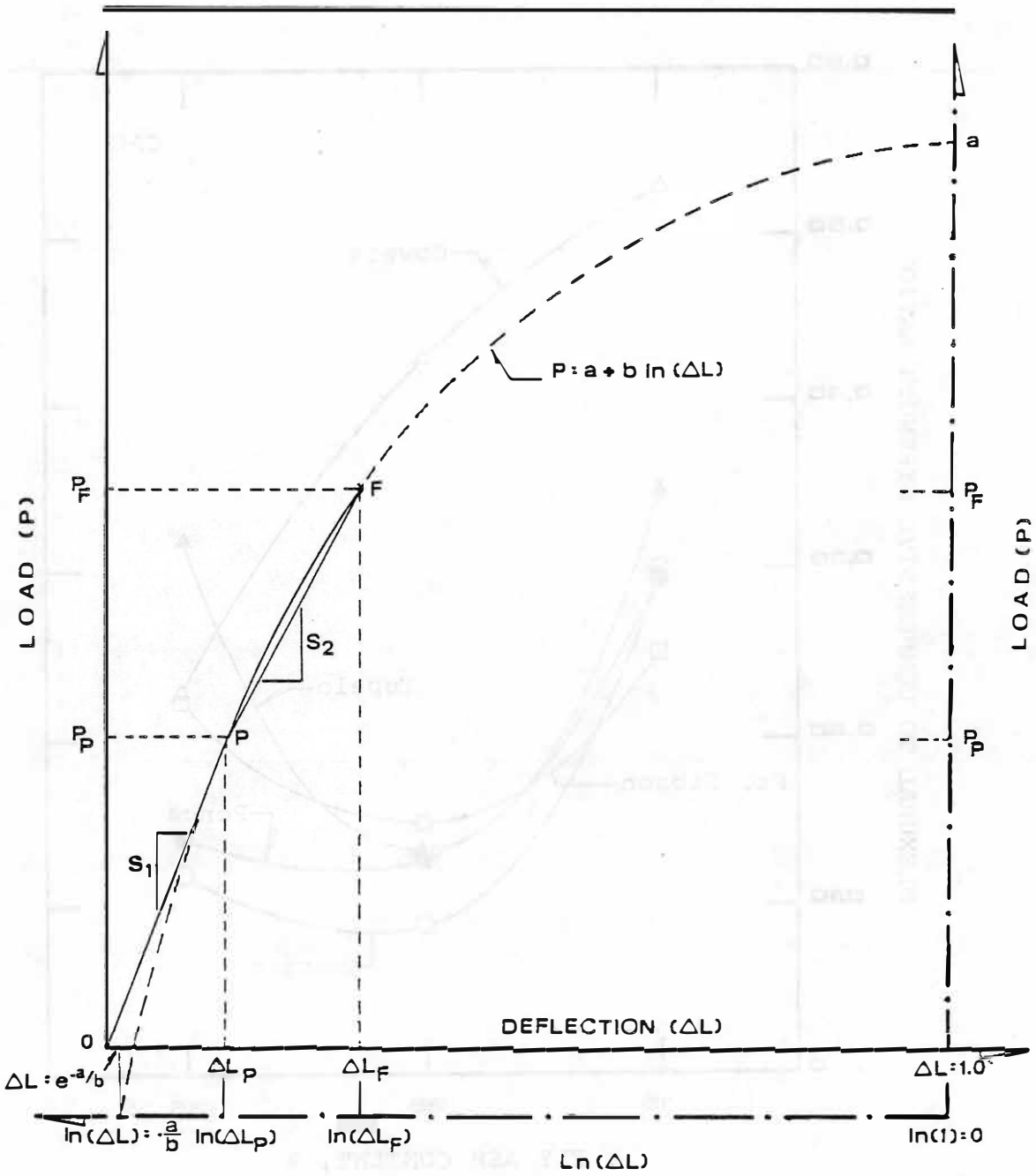

Figure 5.9 Typical aggregate-fly ash load-deflection curve with the plastic region fitting a logarithmic curve

LEGEND TO FIGURE 5.9

Curve Sections:

OPs= elastic range

PFs= plastic range

= a logarithmic curve in the P-ΔL coordinate system

= a straight line in the P-Ln(ΔL) coordinate system intersecting at P = a and ln(ΔL) = -a/b, or $\Delta L = e^{-a/b}$

Slopes:

Slope of elastic range:

$$S_1 = P_{ps}/\Delta L_P$$

Slope of plastic range with respect to the P-Ln(ΔL) coordinate system:

$$S_2 = b$$

Slope of plastic range with respect to the P-ΔL coordinate system:

$$S_2 = \frac{a}{1-e^{-a/b}}$$

Transition slope from P-Ln(ΔL) back to the P-ΔL coordinate systems

$$t = b \cdot \frac{(1-e^{-a/b})}{a}$$

5.5.4 Modulus of plasticity. A typical load-deflection curve of the fly ash mixes is depicted in Figure 5.9, consisting of two sections; the adjusted elastic region expressed by the modulus of elasticity (E) and the curved plastic region extended from the load corresponding to the proportional limit (P_p) to the load at failure (P_F). It was found through regression analysis that the data of the plastic range of all mixes form a logarithmic curve with satisfactory regression coefficients, ranging from 0.95 to 1.00. Therefore, the load at any point in between the proportional and failure loads can be expressed in terms of an equation containing the natural logarithm of the corresponding deflection. The general equation has the form $P = a + b \ln (\Delta L)$, where P = load (lb) and ΔL = deflection (in). These equations for all the mixes of the study along with the regression coefficients and other flexural data are reported in the tables in Appendix D. Where no equation is reported, the mix had either very limited or no plastic region. With this relation at hand, the curved plastic range becomes a straight line, if the deflectionso between the proportional deflection (ΔL_p) and the deflection at failure (ΔL_F) are plotted in terms of their natural logarithms (Figure 5.9). The slope of this line relates to the modulus of plasticity (E_p), which can be calculated from the following relationship:

$$E_p I = \frac{5\ (P_F - P_P)\ L^3}{324\ [\ln\ (\Delta L_F / \Delta L_P)]\, t} \qquad (5.3)$$

where

$$t = \frac{b\ (1-e^{-a/b})}{a} \quad : \text{transition slope, in}$$

a,b = parameters of the logarithmic equation

E_p = modulus of plasticity, psi

P_{Ps} = load at proportional limit, lb

P_{Fs} = load at failure, lb

L = span length, in

ΔL_F = deflection at failure, in

ΔL_{Ps} = deflection of proportional limit, in

It is obvious that the modulus of plasticity can be computed from any two loads within the plastic range and the natural logarithms of their corresponding deflections. The values for the modulus of plasticity of the 30 mixes are presented in Appendix D, Tables D.1 to D.5.

The modulus of elasticity describes the behavior of a mix within the elastic range, while the modulus of plasticity portrays the mix in the plastic range. For reasons of comparison the ratios of E_p/E were calculated for all the mixes and they are reported in Appendix D. The closer the E_p/E ratio is to one, the more "elastically plastic" is the plastic range of the mix. Low ratios values indicate large deformations for proportionally

small load increases within the plastic range.

As mentioned previously, the beam size used in the project was 3 x 4 x 16 inches. For a span length of 15 inches and load at the proportional limit equations 5.4 and 5.2 become:

$$MER = 0.3125\ P_P \tag{5.4}$$

$$E = 3.255\ \frac{P_P}{\Delta L_P} \tag{5.5}$$

and equation 5.3 assumes the form:

$$E_P = 3.255\ \frac{P_F^2 - P_P^2}{[\ln\ (\Delta L_F/\Delta L_P)]\ t} \tag{5.6}$$

But at the proportional limit, borderpoint between the elastic and plastic regions, both equations 5.5 and 5.6 hold true. Therefore, by solving each equation for P_P and equating the two, the modulus of plasticity can be expressed in terms of the modulus of elasticity:

$$E(\Delta L_P) = 3.255\ P_F^2 - E_P\ [\ln\ (\Delta L_F/\Delta L_P)]\ t$$

and $$E_P = \frac{3.255\ P_F^2 - E\ (\Delta L_P)}{[\ln\ (\Delta L_F/\Delta L_P)]\ t} \tag{5.7}$$

Solving equation 5.5 for P_P and substituting in 5.4; we get:

$$MER = 0.096\ E\ (\Delta L_P) \tag{5.8}$$

or $E\ (\Delta L_P) = \frac{MER}{0.096}$, which substituted in Equation 5.7 expresses the modulus of plasticity as a function of

the modulus of elastic rupture:

$$E_P = \frac{0.0125\ P_F - MER}{0.096\ \ln\ (\Delta L_F/\Delta L_P)} \tag{5.9}$$

Additionally, another way of computing the ratio E_P/E from the conditions at the proportional limit and theo formulation of the plastic region, is the following:

$$\frac{E_P}{E} = \frac{3.0255\ \dfrac{P_F - P_P}{[\ln\ (\Delta L_F/\Delta L_P)]\ t}}{3.0255\ \dfrac{P_P}{\Delta L_P}}$$

$$= \frac{(P_F - P_P)\ \Delta L_P}{P_P\ [\ln\ (\Delta L_F/\Delta L_P)]\ t}$$

$$= \frac{\Delta L_P}{P_P} \cdot \frac{P_F - P_P}{\ln\ (\Delta L_F/\Delta L_P)} \cdot \frac{1}{t}$$

$$= (S_1)^{-1} \cdot b \cdot (t)^{-1}$$

$$= (S_1)^{-1} \cdot b \cdot \frac{a}{b\ (1-e^{-a/b})}$$

$$= (S_1)^{-1}\ S_2$$

and finally

$$\frac{E_P}{E} = \frac{\Delta L_P}{P_P^o} \cdot \frac{a}{(1 - e^{-a/b})} \tag{5.10}$$

Given the ratio E_p/E and Equation 5.5 the moduli of elasticity and plasticity can be computed. The values for the ratios E_p/E and the moduli of plasticity of all the mixes are presented in tabular form in Appendix D.

In Figures 5.10 and 5.11 the E_p/E ratios of the FABs and the CABs are plotted with respect to the fly ash additions in the mixes. The FAB + 15% fly ash mixes (except the Ponca City FAB) did not yield substantial plastic regions, thus, the modulus of plasticity was not calculated and the relation between the elastic and plastic moduli could be not established. The remaining FAB + 15% fly ash mixes either had very limited plastic regions or they failed in bending at the end of the elastic range exhibiting brittle behavior. In contrast with the FABs, the CABs with 15% fly ash yielded substantial plastic regions with the exception of the Norman CABs. In both graphs the Norman mixes give the highest ratio values by a great margin, which is attributed to their relatively low values of modulus of elasticity. The mixes from Ponca City and Ft. Gibson appear to maintain their E_p/E-fly ash percentage patterns both for the fine to the coarse gradation. Finally, with the exception of the Norman mixes, the ratio values for the FABs ranged from 0.07 to 0.26, while for the CABs the range was 0.07 to 0.24. These ratio values help locate the modulus of plasticity within the region of

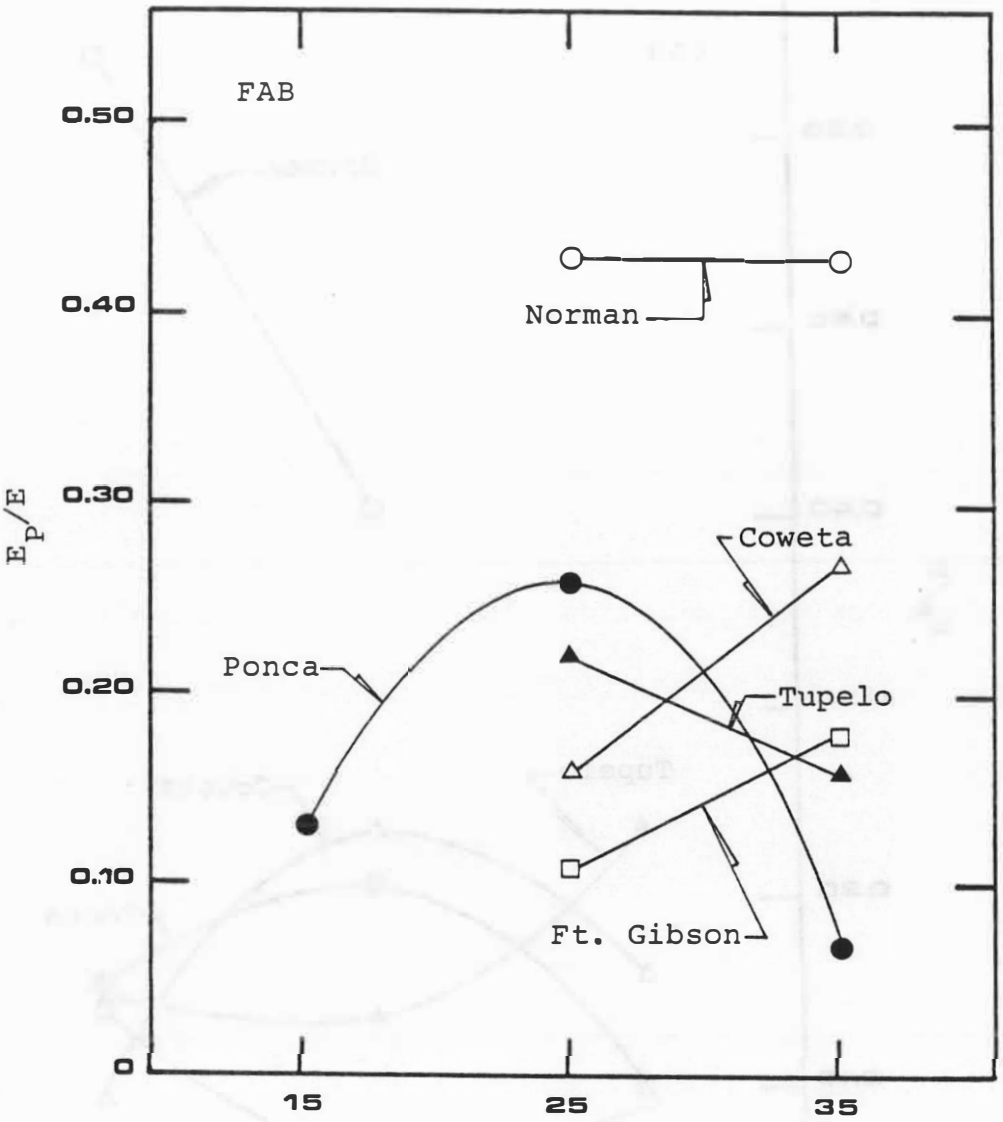

Figure 5.10 Relationships between fly ash content in the FABs and the ratio of the moduli of plasticity to elasticity

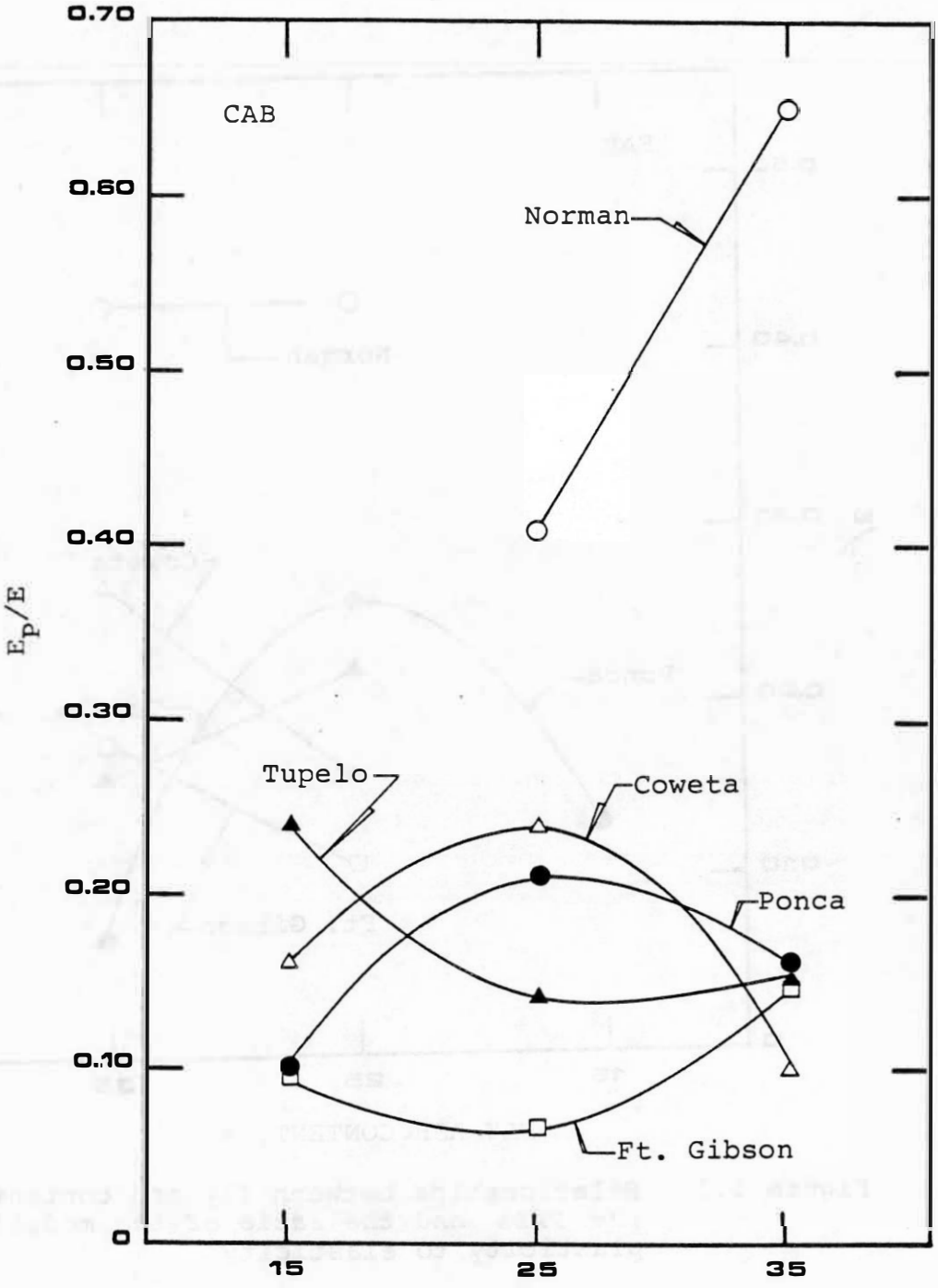

Figure 5.11 Relationships between fly ash content in the CABs and the moduli ratio of plasticity to elasticity

3,400 to 7,100 psi, the mean being 5,000 psi.

5.6 Application of Beam Analogy to Bases

The compressive strength approach for the design of bases has been used for many years, with the main objective being to minimize subgrade distress and pavement deflections. The experimental data of aggregate-fly ash mixes, and specifically the flexural moduli of elasticity, indicate that base courses made of these mixes are stiff enough to be considered as beams or slabs but, as shown later in this section, not stiff enough to be classified as rigid members. Considering the much lower values of modulus of elasticity of the underlying subbase or subgrade material, the base can be viewed as a continuous footing on an elastic foundation. Laguros (1964), in a study of lime stabilized soils, suggested that soil-lime and soil-cement base pavement components could be analyzed by a deflection beam method, following the traditional Winkler model (17).

5.6.1 Beam rigidity and the Winkler model. The conventional analysis of continuous footings, where the concept of a rigid footing is used, results in a nonuniform soil pressure distribution against the base of the footing. To acquire uniformity in the soil pressure distribution a very flexible footing is required. Borowicka's (1938) and Vesic's (1961) works established

rigidity criteria for the footing to be analyzed. According to these for

$\lambda L < 0.8$	the footing is rigid
$0.8 < \lambda L < 3$	the footing is intermediate
$3 < \lambda L$	the footing is flexible

where

$$\lambda L = \sqrt[4]{\frac{K_s' L^4}{4EI}} \quad \text{or} \quad \lambda = \sqrt[4]{\frac{K_s'}{4EI}} \qquad (5.11)$$

$k_s' = k_s B$, psi

L = footing length, ft

B = footing width, ft

E = flexural modulus of elasticity, psi

I = moment of inertia, in^4

k_s = modulus of subgrade reaction, pci

The characteristics of a rigid member are high bending moments and relatively small and uniform deflections while for an intermediate member bending and deflection values are intermediate. A flexible member is characterized by very large bending moments and deflections in the immediate locality of the appliedo loads and small values elsewhere (36).

The Winkler model treats the continuous footing as an infinite beam and the soil as a bed of springs, requiring the solution of the basic differential equation

$$EI \frac{d^4y}{dx^4} = - k_s' y$$

general solution of which is

$$y = e^{\lambda x} (A \cos \lambda x + B \sin \lambda x) + e^{-\lambda x} (C \cos \lambda x + D \sin \lambda x)$$

where,

A, B, C, Dsare integration constants

x is the distance from the load to any section

and the remaining parameters are as defined in Eq. 5.11. In practical problems though where beams have finite length the theoretical solution is quite laborious and time consuming. Hetenyi (1946) developed equations for the case of a finite beam loaded with a concentrated load P at a distance (a$ from the left end of the beam for the computation of deflection, bending moment and shear at a distance (x) measured from the left end. If x > a, then (a) is replaced by (b) in the equations and (x) is measured from the right end (Figure 5.12$.

The equations are as follows$

Deflection $$y = \frac{P\lambda}{k_s'} A \qquad (5.12\$$

Bending moment $$M = \frac{P}{2\lambda} B \qquad (5.13)$$

Shear $$V = PC \qquad (5.14)$$

where,

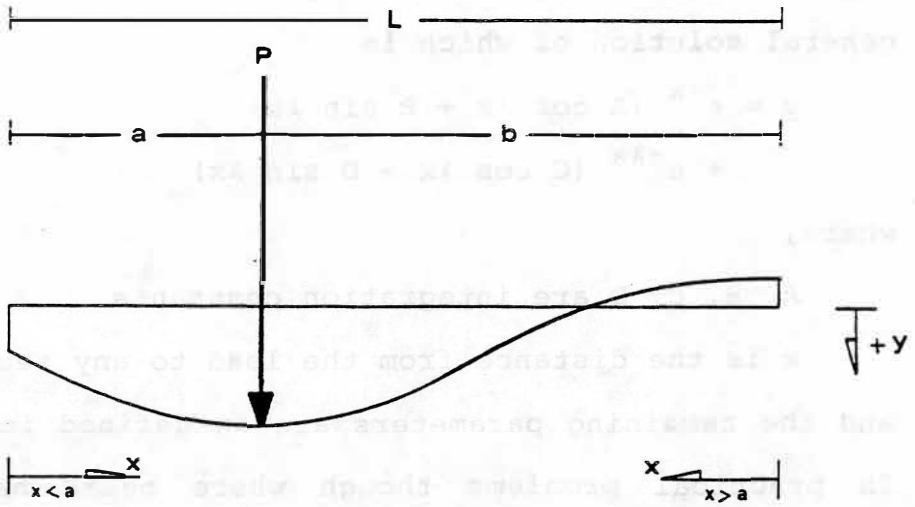

Figure 5.12 Depiction of the Hetenyi solution

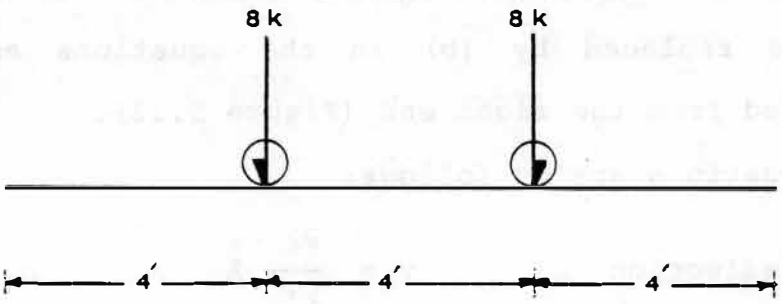

Figure 5.13 Loading arrangement on the base beam

$$A = \{\alpha_2 \cosh \lambda x \cos \lambda x (\sinh \lambda L \cos \lambda a \cosh \lambda b - \sin \lambda L \cosh \lambda a \cos \lambda b) + (\cosh \lambda x \sin \lambda x + \sinh \lambda x \cosh \lambda x)[(\sin \lambda a \cosh \lambda b - \cos \lambda a \sinh \lambda b) + \sin \lambda L (\sinh \lambda a \cos \lambda b - \cosh \lambda a \sin \lambda b)]\}/(\sinh^2 \lambda L - \sin^2 \lambda L) \quad (5.15)$$

$$B = \{\alpha_2 \sinh \lambda x \sin \lambda x (\sin \lambda L \cos \lambda a \cosh \lambda b - \sin \lambda L \cosh \lambda a \cos \lambda b) + (\cosh \lambda x \sin \lambda x - \sinh \lambda x \cos \lambda x) * [\sinh \lambda L (\sin \lambda a \cosh \lambda b - \cos \lambda a \sinh \lambda b) + \sin \lambda L (\sinh \lambda a \cos \lambda b - \cos \lambda a \sin \lambda b)]\}/ (\sinh^2 \lambda L - \sin^2 \lambda L) \quad (5.16)$$

$$C = \{(\cosh \lambda x \sin \lambda x \alpha_0 + \sinh \lambda x \cos \lambda x) * (\sinh \lambda L \cos \lambda a \cosh \lambda b - \sin \lambda L \cosh \lambda a \cos \lambda b) + \sinh \lambda x \sin \lambda x [\sinh \lambda L (\sin \lambda a \cosh \lambda b - \cos \lambda a \sinh \lambda b) + \sin \lambda L (\sinh \lambda a \cos \lambda b - \cosh \lambda a \sin \lambda b)]\alpha_0\}/(\sinh^2 \lambda L - \sin^2 \lambda L) \quad (5.17)$$

The advantage of this solution is that it can be easily programmed into a computer or even a programmable calculator and give results in a very reasonable amount of time.

5.6.2 Application of the finite beam approach.

For the application of the Winkler concept in the design of a pavement, whose base course consists of an aggregate-fly ash mixo the subbase or subgrade constitutes the elastic foundation characterized by its modulus

of subgrade reaction (k_s). The base infinite beam is made up of independent beams of unit width, length being equal to the width of the pavement and the height equal to the thickness of the base course. A single independent beam can be analyzed for the loads under consideration using the Hetenyi solution to the Winkler model.

The design vehicle is taken as an axle load of 16 kips and for a 12 foot pavement lane the loading arrangement is depicted in Figure 5.13. The deflection, bending moment and shear due to one 8-kip load can be computed at any point along the 12 foot base beams No additional calculations are required for the second 8-kip load because of the symmetry of the loading arrangement. Then, the effect of the two loads on the beam can be superimposed. In case the beam is found to be flexible ($\lambda L > 3$) the maximum deflection moment and shear occur under the loads or very close to these and thus the calculations are simplified. It also should be noted that this loading arrangement resembles the laboratory procedure where the 15 inch span beam of aggregate-fly ash mix is loaded with two equal loads at third points tos determine the flexural parameters of the mixes. Two illustrative examples of aggregate-fly ash base course design analysis and evaluation, using the Winkler concept, are presented belows

Problem 1. A pavement structure is to be built with a base of Ponca City FAB + 25% fly ash mix. The subgrade consists of clayey silty sand of K_{ss} = 175 pci. The design vehicle axle load is 16 kips. Analyze the base course deflection under the given loading (Figure 5.14) and determine the thickness (t) required to support it, using the Winkler concept.

Solution. For purposes of simplicity the surface layer is not taken into account and the loads are considered acting directly onto the base. The beam has a unit width B = 1 ft and is analyzed for the left 8-kip load. The modulus of subgrade reaction (k_s) is 175 pci.

$$K'_s = K_s B = 175(12) = 2{,}100 \text{ psi}$$

(I) Analysis

Trial thickness: t = 8 in

$$I = \frac{1}{12} B(t)^3 = \frac{1}{12} (12)\ (8)^3 = 512.0 \text{ in}^4$$

$$\lambda = \sqrt[4]{\frac{k'_s}{4EI}} = \sqrt[4]{\frac{2{,}100}{4(27{,}000)(512)}} = 0.078502 \text{ in}^{-1}$$

$$= 0.942025 \text{ ft}^{-1}$$

λL_s = (0.942025) (12) = 11.3 > 3

The base beam is very flexible and the maximum values of deflection, bending moment and shear occur directly below the load. Using Equations 5.12 to 5.17, the calculated

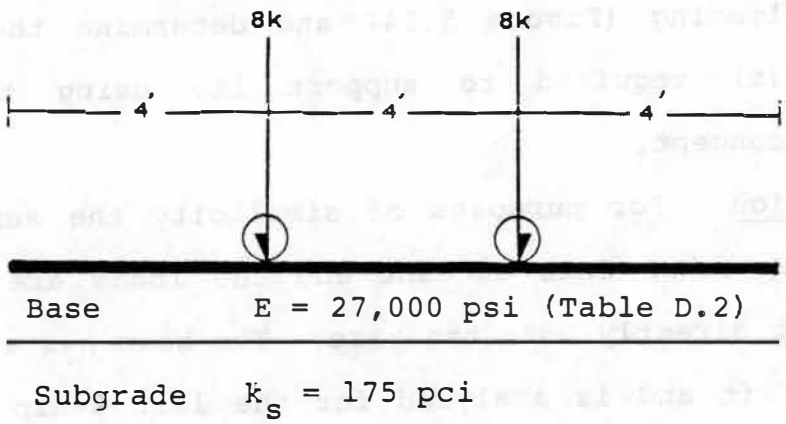

Figure 5.14 Loads on the pavement of problem 1

deflection, moment and shear at the ends and the middle of the beam and also under the loads are tabulated in Table 5.7. The distance is measured from the left end, while (x) is measured from the left if $x < a = 4$ ft and from the right end when $x > a$. Also, included are the conditions to the immediate left ($V = P/2$) and immediate right ($V = -P/2$) of the applied load. With the results of Table 5.7 the y, M and V curves of the base are presented in Figure 5.15. Considering the second 8-kip load, the symmetry of loading and applying the principle of superposition:

Points D_1 and D_5: $y = -0.011 + (-0.0001) = -0.0111$ in

$M = 0$

$V = 0$

Points D_2 and D_4: $y = 0.150 + (-0.005) = 0.145$ in

$M = 25,462 + (-132) = 25,330$ in-lb

$V = -4,000 + 74 = -3,926$ lb

Point D_3: $y = 2(0.015) = 0.030$ in

$M = 2(-4,876) = -9,752$ in-lb

$V = 2(-188) = -376$ lb

It is obvious that the effect of superposition is negligible for the points $D_2 = 4$ ft and $D_4 = 8$ ft where the loads are applied and the maximum values occur (flexible case) and of little significance for the middle point D_3. Therefore, by calculating the conditions under one load only and transferring them to the other, the maximum

Table 5.7 COMPUTATIONS FOR BASE THICKNESS t = 8 in

Distance (ft)	x (ft)	a (ft)	b (ft)	A	B	C	Deflection, y (in)	Moment, M (in-lb)	Shear, V (lb)
0	0	4	8	-0.0374	0.0000	0.0000	-0.011	0	0
4	4	4	8	0.5004	0.4997	0.5000	0.150	25,462	4,000
4	8	8	4	0.5004	0.4997	-0.5000	0.150	25,462	-4,000
6	6	8	4	0.0488	-0.0957	-0.0235	0.015	-4,876	-188
8	4	8	4	-0.0161	-0.0026	0.0093	-0.005	-132	74
12	0	8	4	-0.0005	0.0000	0.0000	-0.0001	0	0

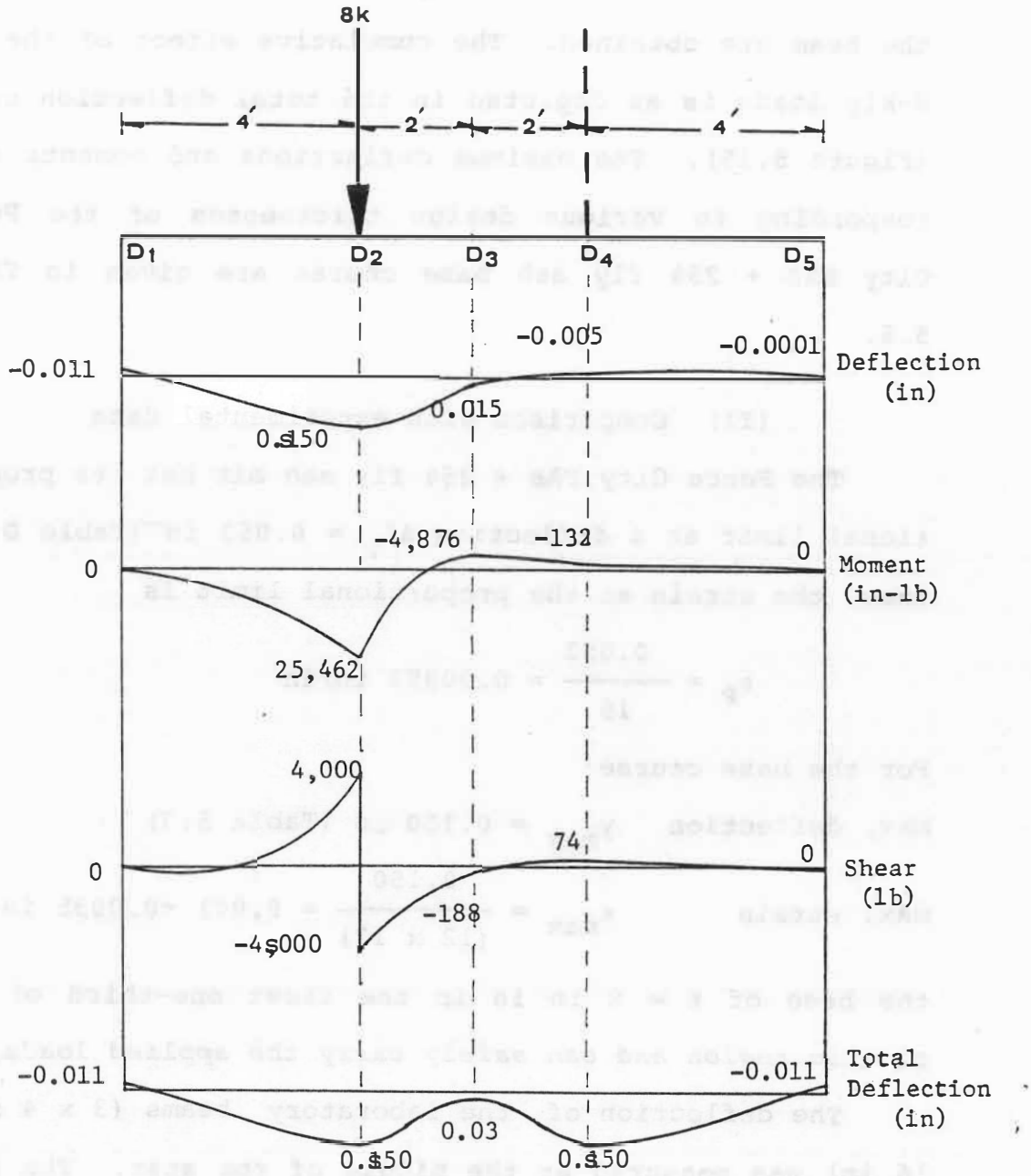

Figure 5.15 Deflection, moment and shear due to the 8-kip load

values of deflection, bending moment and shear acting on the beam are obtained. The cumulative effect of the two 8-kip loads is as depicted in the total deflection curve (Figure 5.15). The maximum deflections and moments corresponding to various design thicknesses of the Ponca City FAB + 25% fly ash base course are given in Table 5.8.

(II) Comparison with experimental data

The Ponca City FAB + 25% fly ash mix has its proportional limit at a deflection $\Delta L_{Ps} = 0.053$ in (Table D.2), thus, the strain at the proportional limit is

$$\varepsilon_p = \frac{0.053}{15} = 0.00353 \text{ in/in}$$

For the base course:

max. deflection $y_{max} = 0.150$ in (Table 5.7)

max. strain $\varepsilon_{max} = \frac{0.150}{(12 \times 12)} = 0.0001 < 0.0035$ in/in

the base of t = 8 in is in the first one-third of its elastic region and can safely carry the applied loads.

The deflection of the laboratory beams (3 x 4 x 16 in) was measured at the middle of the span. The calculated deflection for the base beam at the middle point is $Y_M = 0.03$ in. The corresponding strain $\varepsilon_{Ms} = 0.03/144 = 0.0002 << 0.0035$ in/in, indicating that the base beam is much safer. Furthermore, the base course

Table 5.8 MAXIMUM DEFLECTIONS AND MOMENTS FOR VARIOUS BASE THICKNESSES

Thickness, t (in)	λ (in^{-1})	λL	Deflection, y (in)	Moment, M (in-lb)	FS
12	0.057918	8.34	0.113	34,537	4.50
10	0.066405	9.56	0.127	30,066	4.01
8	0.078502	11.30	0.150	25,462	3.39
6	0.097406	14.03	0.186	20,540	2.74
4	0.132024	19.01	0.252	15,149	2.02
2	0.222038	31.97	0.423	9,007	1.20

reaches its proportional limit (end of its elastic region) when it undergoes a strain of ε_p = 0.00353 in/in, which corresponds to a proportional deflection (y_p)

$$y_p = (0.00353)\ (144) = 0.509 \text{ in}$$

and this is the limit of the elastic behavior of the base. The ratio of y_p/y_{max} can be used as a factor of safety for selecting the thickness of the base for a particular mix. The closer FS (i.e., y_p/y_{max}) is to 1.0 the closer the base beam is to its proportional limit. When FS < 1.0 the base course material has entered its plastic range. The factors of safety for various thicknesses of the Ponca City FAB + 25% fly ash base course are given in the last column of Table 5.8.

(III) Selection of base thickness

The data given in Table 5.8 indicate that even for a base thickness of 2 inches the factor of safety is 1.2. Nevertheless, because the Winkler method does not adjust easily to changes of the moment of inertia I (influenced by t) and in the absence of field deflection data, the choice of a rather high factor of safety is deemedo reasonable in order to compensate for unaccounted factors. For example, if FS = 3.39 it is considered adequate; hence, the base course will have a thickness of 8 inches.

Problem 2. The pavement in problem 1 following years of service experienced much heavier loads than considered during the design phase. The maximum deflection observed was 1.d0 inches. Evaluate the condition of the pavement and suggest measures to be taken in order to prevent excessive distress which may lead to failure.

Solution. The deflection of the base at the proportional limit is $y_p = 0.509 < 1.10$ in, thus the base is well into its plastic range. Failure occurs at a strain of 0.25/15 = 0.01667 in/in (Table D.2), thus,

$$\frac{y_F}{144} = 0.01677 \text{ in/in} \quad \rightarrow \quad y_F = 2.40 \text{ in}$$

The load corresponding to the proportional limit is (Eq. 5.11)

$$P_P = \frac{y_P k_s^{\circ}}{\lambda A} \qquad A = 0.5004 \text{ (Table 5.}\sigma\text{)}$$

$$P_P = \frac{(0.509)\ (2100)}{(0.078502)\ (0.5004)} = 27,\!\text{d}11 \text{ lb}$$

The experimental data of the Ponca City FAB + 25% fly ash mix (Table D.2) showed that the plastic region of the mixo can be expressed through the equation

$$P = a + b \ln (\Delta L)$$

where, ao= 210.93 and b = 606.669. On the premise that the base course consisting of the same material follows a logarithmic curve similar to the one for the experimental

beams, the higher magnitude of loads and deflections will modify the above equation into the following form:

$$P' = a' + b' \ln (y)$$

where the parameters (a's) and (b's) are multiples of (a) and (b) respectively, hence

$$P' = a' + b' \ln (y) = ka + kb \ln (y)$$

$$= k [a + b \ln (y)]$$

and $$k = \frac{P'}{a + b \ln (y)} = \frac{P'}{2110.93 + 606.69 \ln (y)}$$

but, at the proportional limit

$$k = \frac{27,211}{2110.93 + 606.69 \ln (0.509)} = 15.99 \cong 16$$

$$a' = 16a = 16 (2110.93) = 33,774.88$$

$$b' = 16b = 16 (606.69) = 9,707.04$$

Therefore, the equation expressing the plastic range of the base is

$$P' = 33,774.88 + 9,707.04 \ln (y) \qquad (5.18)$$

Substituting y = 1.10 in in the equation, we get a corresponding load P' = 34.7 kips and this is the load on the pavement that caused the current deflection of 1.10 in. The deflection at failure is 2.40 in. Solving Eq. 5.18 for this value we get P'_F = 42.2 kips, which is the load at which the pavement will fail.

Under no condition should the pavement be loaded close to 34.7 kips (current load level). Because of its

very sensitive condition it would be a good practice to limit the allowable load not to exceed the original design load (8 kips). Finally, record the deflection of the pavement regularly and reevaluate.

5.3 X-ray Diffraction

X-ray diffraction analysis was employed in this project to determine the mineralogical composition of raw fly ash and to study the reaction products in fly ash pastes and the mixes. Initially, diffractograms of the 28-day Norman mixes were inspected for fly ash-water reaction products and the possible formation of new crystalline compounds. Examination of these diffractograms verified the assumption that the aggregates used are quite inert and the formation of new minerals is due to the hydration of fly ash. At this point it was thought advisable to obtain diffraction data for the particular fly ash used in the study (Oologah, Oklahoma) in raw and paste form. The investigation was intended to shed light onto the development of the hydration products with time, pinpoint new formations and use the collected data as a guide and reference to evaluate the diffraction patterns of the aggregate-fly ash mixes. When diffractograms of the 28-day Coweta mixes appeared to follow a pattern, both in shape and chemical products similar to the Norman mixes it became

obvious that X-ray diffraction analysis of mixes from the other sources would not significantly improve the overall diffraction profile of the mixes. Additionally, XRDs of Norman and Coweta mixes for 90-days and certain of the Tupelo and Ft. Gibson mixes for 90-day were analyzed. A list of the pastes and mixes analyzed by X-ray diffraction is given in Table 5.9.

The diffractograms are presented in Appendix E (Figures E.1 and E.22). All the fly ash paste diffraction curves are presented together (Figures E.3 and E.4) for purposes of comparison. For the same reason the three curves of a FAB or CAB of a particular source corresponding to the three fly ash additions (15, 25, 35%) for a specific curing period are presented together. In all cases the bottom curve is drawn with the actual relative intensity. The remaining curves have been elevated by a 10% relative intensity for better depiction. Thus, in a three curve figure the actual relative intensity of the second curve is the graph reading minus 10%, while for the top curve it is the graph reading minus 20%. Incorporated in Appendix E are the crystalline data of fly ash in raw and paste form (Tables E.1 to E.6) along with the full range of the Coweta 90-days mixes and a few selected 28-day mixes (Tables E.7 to E.14). To reduce the large volume of analytical data in these tables, recordings of relative

Table 5.9 LIST OF X-RAY DIFFRACTIONS

Source	Mix Type	Fly Ash Content (%)	Curing Time (days)
	Raw Fly Ash	-	-
	Fly Ash Pastes	-	1-7-21-30-360
Norman	FABs CAB	15,25,35	28-90
Coweta	FAB, CAB	15,25,35	28-90
Tupelo	FAB, CAB	25	90
Ft. Gibson	FAB, CAB	25	90

intensity lower than 5% (corresponding to very weak peaks and often part of the "background noise") were omitted. Finally, a list of the X-ray diffractions is given in Table 5.9 and the identified minerals are presented in Table 5.10 where the three strongest lines are given in terms of d-spacing and relative intensity ($\lambda s = 2d \sin \theta$). The symbols assigned to the minerals are used to identify the peaks of the particular crystals on the diffractograms. The PDF number corresponds to the JCPDS powder diffraction file number. In this section the cement chemist's nomenclature is often used for reference to the chemical composition of the mineral compounds.

5.7.1 The stability of ettringite. Ettringite ($C_3A.3C\bar{S}.H_{32}$) is a hydration product of Portland cement, where addition of sulfate (usually gypsum) changes the course of reaction of C_3A (hexagonal plate phase) giving priority to the formation of thin prisms or rods of ettringite. After the sulfate is exhausted, further hydration of C_3A leads to decomposition of ettringite and the formation of hexagonal plates of monosulphate - C_4AH_{13} solid solution (32). A similar pattern has beens observed in fly ash hydration, but instead of gypsum the sulphate source is anhydrite.

As mentioned earlier the drying temperature of the majority of the X-ray diffraction specimens was 110°C with the exception of the 21-day fly ash paste and the

Table 5.10 MINERALS IDENTIFIED BY X-RAY DIFFRACTION

Mineral Name	Chemical Formula	Symbol	d-spacings (relative intensity) Å %			PDF Number
Dicalcium Silicate (C_2S)	$2CaO.SiO_2$	D	2.783(100)	2.79 (97)	2.745 (93)	33-302
Tricalcium Aluminate (C_3A)	$3CaO.Al_2O_3$	T	2.70 (100)	1.91 (36)	1.56 (27)	8-5
Calcite (Calcium Carbonate)	$CaCO_3$	C	3.04 (100)	2.29 (18)	2.10 (18)	5-586
Portlandite (Calcium Hydroxide)	$Ca(OH)_2$	Pt	2.628(100)	4.90 (74)	1.927 (42)	4-733
Ettringite ($C_3A.3C\bar{S}.H_{32}$)	$3CaO.Al_2O_3.3CaSO_4.32H_2O$	E	9.73 (100)	5.61 (80)	3.88 (50)	9-414
Monosulfoaluminate ($C_3A.C\bar{S}.H_{13}$)	$3CaO.Al_2O_3.CaSO_4.13H_2O$	Ms	8.92 (100)	2.87 (70)	4.46 (60)	11-179
Quartz	SiO_2	Q	3.34 (100)	4.26 (35)	1.82 (17)	33-1161
Periclase	MgO	P	2.106(100)	1.489(52)	0.942 (17)	4-829
Anhydrite	$CaSO_4$	A	3.49 (100)	2.85 (30)	2.33 (20)	6-226
Lime	CaO	L	2.406(100)	1.701(45)	2.778 (34)	4-777
Calcium Aluminum Oxide Sulfate ($C_3A_3\bar{S}$)	$3CaO.3Al_2O_3.CaSO_4$	X	3.75 (100)	2.65 (30)	2.17 (25)	16-440
Microline	$KAlSi_3O_8$	Mc	3.25 (100)	4.21 (50)	3.29 (48)	22-687
Gismondine (CAS_2H_4)	$CaO.2SiO_2.Al_2O_3.4H_2O$	G	3.34 (100)	4.27 (35)	3.19 (18)	20-452
Calcium Aluminate Oxide Hydrate (C_4AH_{19})	$4CaO.Al_2O_3.19H_2O$	Z	10.80 (100)	2.785(100)	2.492 (100)	14-631
Straetlingite (C_2ASH_8)	$2CaO.SiO_2.Al_2O_3.8H_2O$	S	12.50 (100)	4.18 (70)	6.27 (40)	29-285
Dolomite	$(MgCaFe)\ CO_3$	Dm	2.886(100)	2.191(30)	1.78 930)	*

* (32)

90-day mixes from Tupelo and Ft. Gibson, which were dried to 50ôC. The 21-day fly ash paste diffractogram (Figure E.3 and E.4) presents distinct and rather strong peaks of ettringite compared to the remaining paste ages. The observation contradicted that ettringite is formed in the very early stages of the hydration process and thus, should be strongly detected in the one or seven-day pastes, raising questions about the effect the 110°C temperature had on the crystal structure of the mineral compound. The literature appears to be hazy and rather uncertain about the lower limit of ettringite stability, with a number of studies (13, 21, 32) reporting that ettringite is stable up to 100°-110°C, or 90°C, or 50°C, before it loseso water and decomposes to monosulfoaluminate. To resolve the case, a sample of ettringite was oven dried for three hours at 110°C and diffracted; the structure of ettringite had been destroyed leaving behind weak peaks of $CaSO_4.15H_2O$. Furthermore, to investigate the effect of the 110°C drying temperature on the mineral in question in the mixes, a sample of Coweta FAB + 35% fly ash cured for 28 days was placed in the oven at 110°C for three hours. The sample was removed from the oven and after cooling to room temperature it was diffracted. Not only the ettringite, but also the monosulfoaluminate structure had been destroyed. Monosulfoaluminate is supposed to be stable up to 190ôC (21).

Then, the sample was allowed to sit at room temperature and humidity for one day and it was diffracted again to see if the process was reversible; it was not. The three diffraction curves are shown in Figure 5.16. The lower curve, where the peaks of ettringite and monosulfoaluminate occur, is the X-ray diffraction of a sample dried with the method used in this research - one hour oven drying to 110°C; two hours to ambient temperature; one hour to 110°C. The fact that ettringite and monosulfoaluminate are still detectable in the mixes after a total of two hours at 110°C is attributed to the uneven exposure to this destabilizing temperature. Nevertheless, it is reasonable to assume that in the diffractometer recordings of ettringite and monosulfoaluminate the intensities gave a reduced picture of the actual degree of crystallization of the two hydration products.

5.7.2 Raw fly ash and pastes. The minerals, as identified in every individual paste or mix, are given by the integrated intensity (cps) of their strongest identifiable line and the relative intensity (%) in the tabless of Appendix F. In powder fly ash (Figure E.2 and Table F.1) the strongest peak was that of α-quartz (3.34 Å) followed by the peak of C_3A (2.70 Å), periclase (2.106 Å), anhydrite (3.49 Å), CaO (2.406 Å)s, calcium aluminum oxide sulfate (3.75 Å)ş dicalcium silicate

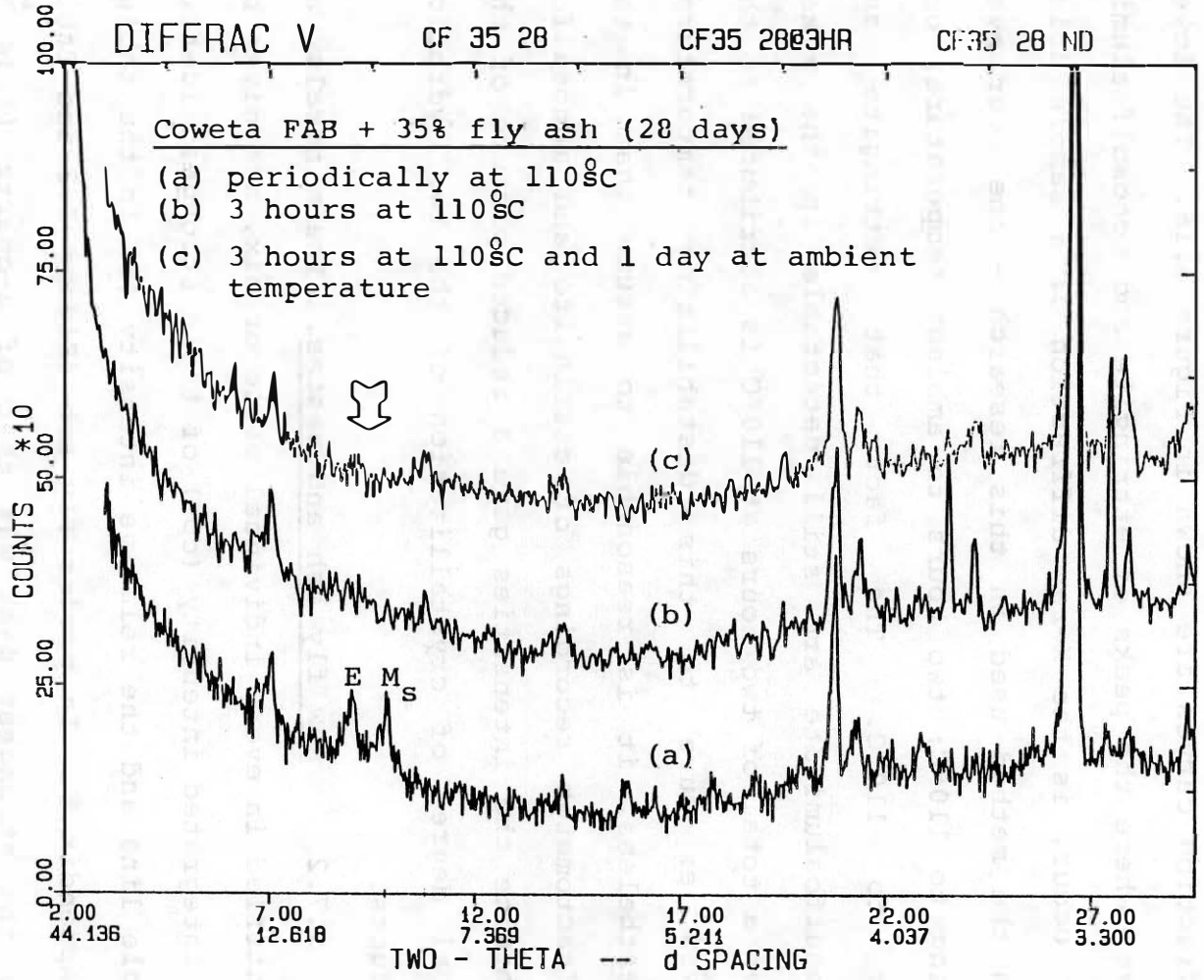

Figure 5.16 Effect of temperature on ettringite and monosulfoaluminate

(2.783 Å) and a trace of microcline (3.25Å). CaO, C_3A and anhydrite are the activators in this Class C fly ash. The amorphous halo is quite distinct around the 32° (2θ) region of the diffraction chart indicating the high calcium content of the glass. Figure 5.17 is a Van der Graff elemental analysis of the fly ash. The elements detected are identified on the corresponding peaks. Aluminum is not included as the aluminum sample holder in this process was thought to be the source of the metal peak.

The diffraction patterns of the fly ash pastes are presented are divided into two regions: 5 to 20 two theta degrees (Figure E.3) and 20 to 50 two theta degrees (Figure E.4). An inspection of Figure E.4 indicates that the amorphous halo in the region between the major quartz peak at 26.60° (3.34 Å) and the major C_3A peak at 33.40° (2.70Å) subsides with time as the calcium is consumed in the hydration process. The major peaks of C_3A and MgO (periclase) show a slow decline with time; yet they maintain considerable crystallinity after one year. On the other hand, in Figure E.3 and for the region of 6.00°(2θ) to 12.00 (2θ), the one-month paste presents a "hill", sign of the formation of calcium aluminum hydrates (CAH). The "hill" levels off in a year leaving the peak of C_4AH_{13} clearly visible. The minerals identified in the fly ash pastes are given in Table F.1 and their

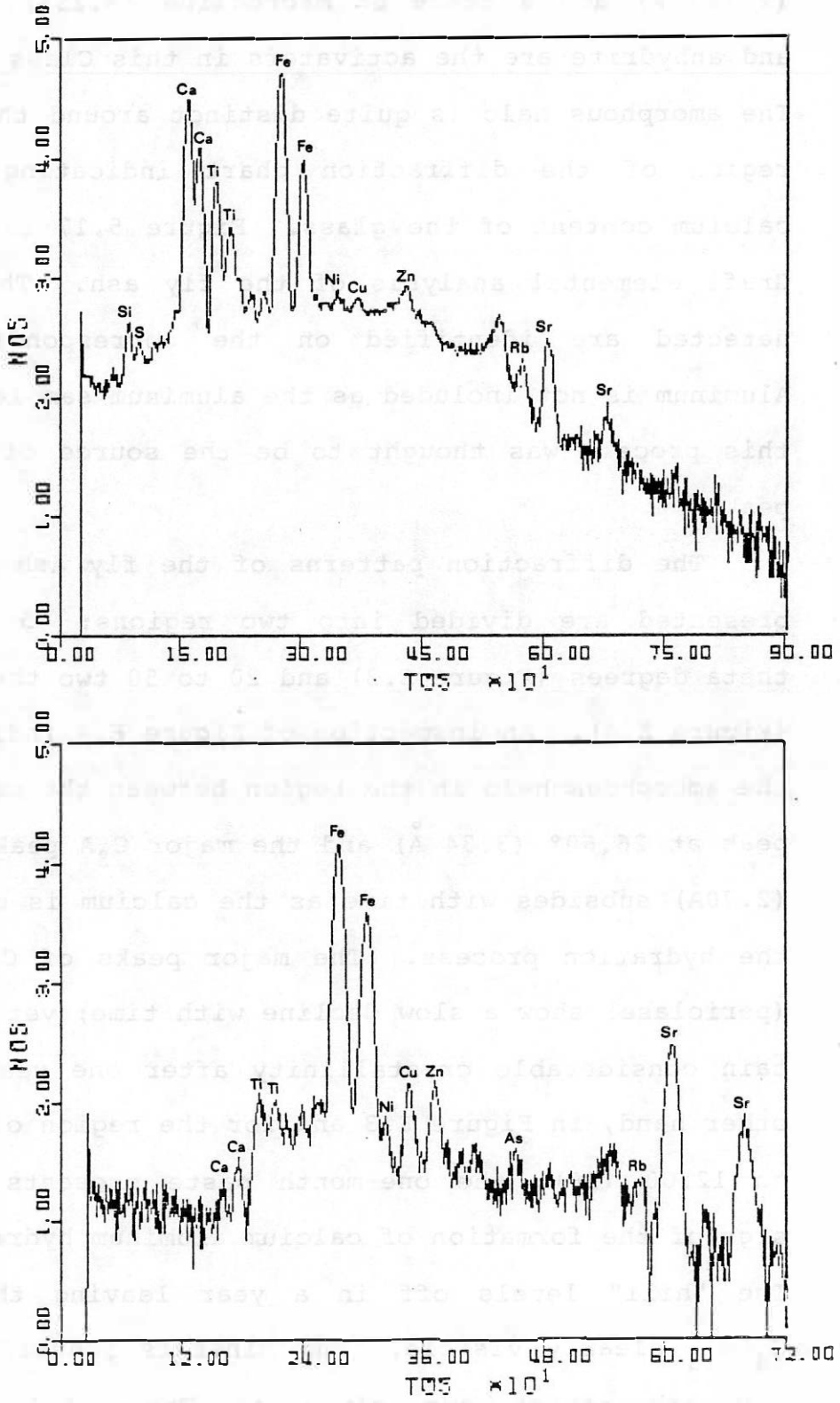

Figure 5.d7 Elemental analysis of raw fly ash

examination and comparison suggests the following trends:

1. The hydration products are primarily calcium aluminum sulfate hydrates ($C\bar{A}\bar{S}H$), then calcium aluminum silica hydrates (CASH) and calcium aluminum hydrates (CAH). The $C\bar{A}\bar{S}H$ mineral compounds are ettringite and monosulfoaluminate while the CASH minerals are straetlingite and gismondine. From the CAH group C_2AH_8 and a trace of C_3AH_6 were found present in the one-month paste, while C_4AH_{13}, C_3AH_6, C_4AH_{19} and a trace of C_2AH_8 were detected in the one-year paste.
2. Tobermorite type formations (CSH) were not identified in appreciable intensities. Nevertheless, calcium silicate hydrates of types I and II - CSH and C_2SH_2 - were detected in the one-month paste, with intensities of 29.8 (4%) and 38.0 (6%) cps, respectively. CSH I is the poorly crystalline hydrate that can easily pass undetected. The fact that dicalcium silicate (C_2S) was found in raw fly ash and is present in all the pastes, including the one-year paste where a trace of it was detected, makes it obvious that it is the C_2S hydration that produced the CSH minerals. C_2S is known from cement chemistry to hydrate slowly and be responsible for the late (after 28 days) strength developed in concrete. The dicalcium silicate hydration reaction is evolving beyond one year.

3. C_3A, which hydrates very quickly causing the "flash set" of fly ash, is believed to produce the two hexagonal plate hydrates of the CAH group.

$$2\ C_3A + 21\ H \rightarrow C_2AH_8 + C_4AH_{13}$$

$$C_3A + CH + 12\ H \rightarrow C_4AH_{13}$$

C_4AH_{13} can also result from the decomposition of ettringite. Only a trace of the latter appears present in the one-month paste, where the two CAH phases were first detected. With time and as the temperature increases due to the heat of hydration, a third member of the group, which is crystallized in the cubic system, is formed from the other two.

$$C_2AH_8 + C_4AH_{13} \rightarrow 2\ C_3AH_6 + 9\ H$$

The cubic calcium aluminum hydrate is stable in contact with saturated solutions of calcium hydroxide (CH).

4. Portlandite (CH), present in the pastes of up to one month indicates quite an irregular pattern; only a trace has been detected in the 21-day paste and it reappears in one month. Its presence in the one-day paste is partly attributed to the direct hydration of free lime in fly ash - CaO has been consumed after the first day - and partly to the reaction of C_4AH_{13} with the anhydrite in fly ash and water to produce ettringite.

$$C_4AH_{13} + 3C\bar{S} + 20\ H \rightarrow C_3A.3C\bar{S}.H_{32} + CH$$

In seven days the intensity of the sulfate source (anhydrite) has declined considerably and in 21 days is not detected. Ettringite on the other hand reaches its highest intensity (79.5 cps) in 21 days and only a trace of it appears in the one-month paste. The pattern suggests that CH is used up in the reaction to form C_4AH_{13} which in return reacts with anhydrite to form ettringite. Around the 21st day, when the supply of sulfate has been exhausted, no more ettringite is formed. At the same time C_4AH_{13} keeps forming from CH and the slowly hydrating C_3A. In the absence of anhydrite, ettringite enters reaction with C_4AH_{13} to form monosulfoaluminates

$$C_3A.3C\bar{S}.H_{32} + 2C_4AH_{13} \rightarrow 3[C_3A.C\bar{S}.H_{12}] + 2CH + 2OH$$

This reaction and the hydration of C_2S are believed to be the sources of portlandite detected in the one-month paste. This scenario is supported by the fact that monosulfoaluminate is a hexagonal plate phase and in one month the intensity increases to 103.0 cps. Later, the monosulfoaluminate dissolves in the C_4AH_{19} solid phase. C_4AH_{19} was identified in the one-year paste.

5. The calcium aluminum oxide sulfate ($C_4A_3\bar{S}$) present in raw fly ash is assumed to hydrate directly to monosulfoaluminate and be consumed in the time

interval between seven and 21 days.

6. Straetlingite (C_2ASH_8) is first identified in the 21-day paste and is also present in the one-month and one-year pastes. This compound is an early indication that the fly ash is reacting to form cementitious products. The hydration products detected in the one-month paste verify the fact. Additionally, gismondine (CAS_2H_4) identified in the one-year paste alone at an appreciable intensity could be a result of straetlingite's dehydration and loss of Ca ions in time instead of an independently occurring mineral product. The presence of gismondine in the pastes of earlier ages (i.e. one-month) should not altogether be excluded as some of its major peaks fall very close to the strongest quartz lines - the predominant mineral in the pastes - making its identification rather difficult if the mineral is not well crystallized.

7. Finally, the presence of calcite ($CaCO_3$) in the paste diffractograms is believed to be a product of the effect the atmospheric CO_2 had on the calcium contents of the pastes during the grinding and drying process.

5.7.3 The mixes. The Norman and Coweta mixes and some selected Ft. Gibson and Tupelo mixes yielded the XRD given in Appendix E. The corresponding mineralogical

and intensity information is given in the tables in Appendix F.

Unlike the fly ash paste, wherein the majority of the minerals were represented by peaks of appreciable intensities, the mixes featured relatively weak peaks making the identification of the hydration products a tedious and laborious exercise. Nevertheless, the findings from the paste XRD analyses proved to be of major assistance in pinpointing weak or partially overlapping peaks. It can be observed that the mixes with the higher fly ash content (35%) are more chemically active, as it was expected, than their counterparts containing lower amounts of fly ash. The mixes presented a lower degree of chemical activity than the pastes, but it should be kept in mind that the pastes were hydrated in the presence of excessive water while in the mixes the water content was the optimum amount under which the mix will give the maximum dry density. At one point, it was speculated that excessive water might prove beneficial for the overall performance of the mix. A Norman FAB with 35% fly ash was prepared with water almost twice the amount required for optimum. The SEM indicated more massive formations of hydration products, but seven-day strength was much lower than its counterpart mixed at optimum moisture content. Another factor to be considered is the relatively small amount of active material (fly

ash) in the matrix of the mix as compared with the matrix of the pastes consisting of 100% fly ash. These and the XRD data from tables F.2 to F.6 lead to the formulation of the following characteristic trends for the fly ash mixes:

1. Quartz low (SiO_2) and calcite ($CaCO_3$) are by far the predominant minerals in the mixes. Fly ash and the sand used in the mixes are the sources of quartz. Calcite is one aggregate compound that intruded the XRD samples when the mix material was crushed and ground to powder form. Its amount is probably exaggerated due to carbonation during the grinding and drying process.
2. Dolomite, detected in almost all the mixes, is another aggregate compound. An evidence of this comes from the mixes of Tupelo, where the aggregates used were of high dolomitic content. XRD (Table F.6) of the two Tupelo mixes present strong lines of dolomite.
3. Dicalcium silicate is identified in some of the mixes, while tricalcium aluminate and periclase area present in all of them.
4. With the exception of quartz, calcite and partly dolomite, periclase and tricalcium aluminate the remaining peaks are relatively weak indicating a low degree of crystallization, which complicated the

identification of the mineral compounds.

5. For the Norman 28-day mixes, out of the three cylinders per mix tested for unconfined compressive strengths, the ones with the higher and lower strengths were diffracted. It was interesting to observe that for two specimens of the same mix the one with the higher intensity of calcite gave the lower strengths.

6. In some of the mixes, weak peaks of $CaSO_4.15H_2O$ were detected suggesting the partial decomposition of ettringite due to the 110°C drying temperatures.

7. The peaks in the region between 3.34 Å and 3.04 Å d-spacing - the major quartz and calcite peaks, respectively - are normally interpreted as feldspar minerals either from the aggregates or from the sand. In this study microcline and gismondine were identified within this regions. X-ray analysis of the Norman and Coweta sands depicted peaks of microcline and a trace of gismondine. On the other hands, the one year fly ash paste suggests that gismondine is a product of the hydration process. The mineral presents somewhat higher intensities in the 90-day mixes as compared with its peaks in the 28-day diffractograms. It could then be assumed that its presence in the 28-day mixes is partly due to the sand component while in 90-days the gismon-

dine detected has been formed primarily through hydration and disintegration of the glass phase.

8. Tobermorite formations (CSH) were not identified but their presence suspected in some mixeso This was not unexpected, considering their low intensities detected in the one-month paste. If they form - and they do as it will be shown in the SEM section - they are too poorly crystallized to present distinct detectable XRD patterns.

9. From the CAH group only C_4AH_{19} was detected in the 28 and 90-day mixes. C_4AH_{19} is the result of dissolution of the monosulfoaluminate compound. The diffraction data indicate that C_4AH_{19} assumes better crystallinity in the 90-day mixes, as compared to those of the 28-day. In the high fly ash content Norman mixes, the 28-day curing presents only traces of ettringite and the 90-day curing reflects low amounts of the mineral.

10. It should be noted that ettringite is also detected in the Norman FAB+ 25% fly ash which was cured for nine months (Table F.3). Monosulfoaluminate followso a similar pattern in the Norman mixes. With the Coweta mixes, ettringite and monosulfoaluminate appear present in both the 28 and 90 day XRDs, but not in all the mixes. In the Ft. Gibson mixes both ettringite and the monosulfoaluminate are present,

while with the Tupelo mixes (Table F.6) the two sulfate compounds were detected only in the CAB+ 25% mix.

11. Portlandite (Calcium hydroxide) was not identified in any of the mixes, suggesting that it has either been consumed earlier than 28 days or its generation from the conversion of ettringite to monosulfoaluminate, and its subsequent reaction with C_3A to produce C_4AH_{13}, leaves very little crystalline $Ca(OH)_2$ for X-ray detection.

12. In some of the mixes, even for 90 days, CaO and $CaSO_4$ have been detected, but not with absolute certainty as ettringite has severe line overlaps with these compounds. Should we accept the presence of the two compounds the following speculations are in order, a) the fly ash at hand, in this case, is a "hard burned" ash, where CaO and $CaSO_4$ are not very reactive with water and b) $CaSO_4$ may result from further dehydration of $CaSO_4.15H_2O$ or the final conversion of the monosulfoaluminate to C_4AH_{19}. The hydration of the pastes, where excessive water wass available, does not indicate such patterns. On the other hand, the 90-day mixes had very little, if any, available water.

13. Calcium aluminum oxide sulfate ($C_4A_3\bar{S}$) is found in the 90-day Norman and Coweta mixes. In the pastes

it does not appear beyond seven days of curing as it is assumed to be hydrated to monosulfoaluminate directly. In the mixes its hydration is either very slow or it does not occur. The fact that in 28 days $C_4A_3\bar{S}$ appears much less crystallized than in 90 days introduces an additional complexity.

14. Finally, XRD analysis was done on a qualitative basis and no quantitative conclusions could safely be drawn from it.

5.8 Scanning Electron Microscopy

SEM was employed in this investigation to study the microstructural changes and developments with time in the matrix of the fly ash mixes and to visually examine the resulting hydration products. The XRD analyses indicated that the aggregates are quite inert and the chemical activity in the mixes is due to the hydration of the fly ash. The hydration products are almost identical regardless of the type or the mix source; depending on the amount of fly ash present in the mix their degree of their formation varies. With this in mind, it was thought adequate to thoroughly examine the mixes from one source only, thus obtaining the general SEM pattern for all the mixes. The Coweta mixes were selected for SEM observation because of the availability of full scale XRD data that would assist SEM identifications and

correlations. The Coweta FAB and CAB with 15% fly ash content were not scanned because of the relatively low activity they indicated compared to the mixes containing higher amounts of fly ash. Samples of the Coweta mixes with 25 and 35% fly ash additions cured for 28, 90 and 180 days were prepared for SEM observations in the manner described in Section 4.10. The micrographs of these mixes are presented in this section.

5.8.1 Fly ash powder and paste. Figure 5.18 is a micrograph of powder fly ash as received, wherein spherical particles of various sizes can be observed. It should be noted that very few amorphous particles, usually associated with the partial burning of pulverized coal, were found in the fly ash used in this study. The fly ash spherulites indicate a relatively smooth and glassy texture. To obtain additional information fly ash paste cured for seven and 60 days was scanned. The seven day paste SEM featured very few needle-like crystals and some irregular crystal formations around and among reacted fly ash particles. A great number of the fly ash particles were either very little reacted or unreacted, which may be indicative of the dual role of fly ash as a reactive chemical compound and a filler. The lack of a great number of needle-like crystals or rods of ettringite in the seven day paste suggests that the hydration process evolves faster in the pastes than in

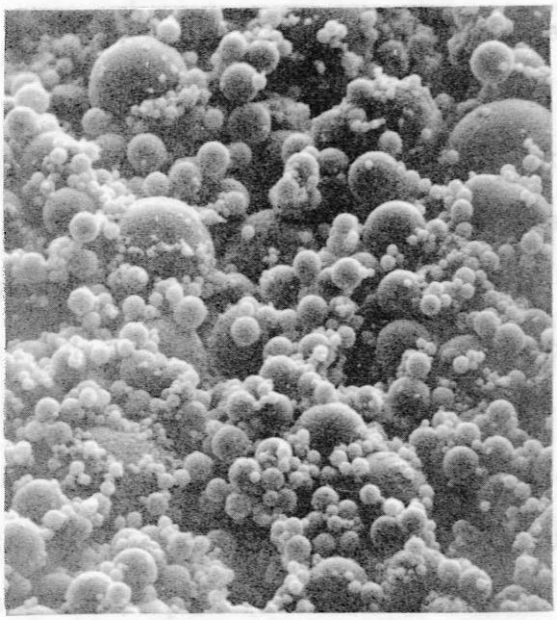

10 μm 1000X

Figure 5.18 Raw fly ash

the mixes where ettringite persists being present even in later ages. A similar trend was also evident following the XRD analysisa The irregular crystals observed in the seven day paste are believed to be a combination of the monosulfoaluminate (produced at the expense of ettringite) and calcium aluminum hydrates (CAH)a

In Appendix G (Figure G.1) the micrographs of the 60-day paste are presented. In this sample no needle-like crystals were observed but the fly ash particles have been reacted in a higher number and degree than in the seven day paste. Figure G.1a depicts the hydration rim of a fly ash particle which has been "pulled out." A great number of smaller spherical particles are held together by a matrix of crystalsa A narrow X-ray beam focused on a group of these crystals produced the EDS of Figure G.2. The Ca, Si and Al peaks suggest that the crystals are either CASH or a combination of CAH and CSH. In Figure G.1b part of the hydration rim of the fly ash sphere has been pulled out and traces of the hydration crystals are evident on the surface of the glassa A unique feature of the 60 day paste is depicted in Figurea G.1c. It looks like a plerosphere where the embodied smaller spheres have reacted and expanded to change the shape of the outer cella The phenomenon was observed at least at three specific localities in this particular pastea

5.8.2 Excessive water in mixes. It was mentioned in the XRD section that a sample of Norman FAB + 35% fly ash was mixed with excessive water to study the effect the additional moisture had on the chemical and strength behavior of the mix. This mix had a water:fly ash ratio of 0.4 while the corresponding ratio of the mix with the optimum amount of water (producing maximum dry density) was 0.2. Samples of the excessively moist mix were scanned in one day (Figure G.3), three days (Figure G.4), seven days (Figure G.5) and 28 days Figure G.6). The one day SEMs indicate the massive formation of ettringite needles which have grown more massive, thicker and longer in seven days, and they start grouping together to form monosulfate- C_4AH_{13} bundles. Also, seven-day cured specimens appear to have some fibrous CSH I. The ribbon-like chain of particles (Figure G.5c) is thought to be calcium hydroxide. In 28 days the grouping is more evident and even longer formations are observed (Figure G.6b). At places, groups of hexagonal plates have been formed as depicted in Figure G.6c, where two grains of sand have been bound together by reacted fly ash spherulites and hexagonal crystals; this is characteristic of the C_2AH_8, C_4AH_{13} and monosulfoaluminate phases.

On the other hand, the 28-day micrographs of the mix with water:fly ash ratio of 0.2 (optimum moisture

content) do not indicate the presence of ettringite, but only extensive formation of the hexagonal phase (Figure G.07). Additionally, the fly ash particles appear to be more reacted. The pattern of development suggests that the excessive water promotes the formation of ettringite for an extended period of time, which in turn, causes the slowing down of the C_3A hydration and the formation of the hexagonal phase. If this is true, it is no wonder that the seven-day compressive strength of the rich in water (and ettringite) mix was much lower than the corresponding strength of the same mix with optimum water content. The contribution of ettringite, per se, to strength performance is known to be either neutral or negative, depending on the degree of its presence and crystallization.

5.8.3 The 28-day mixes. The SEM observation of the Coweta mixes with fly ash addition of 25 and 35% and cured for 28 days are presented here. The Coweta FAB + 25% fly ash are shown in Figure 5.019, and as it has been depicted in the micrographs (c), the hydration products for this particular mix are primarily needle-like and rod-like crystals. In micrograph (a) a growth of peculiarly arranged crystals appears on the top of a partially reacted fly ash particle. The crystal growth, which suggests a hexagonal phase, has been magnified in micrograph (b) and its EDS (Figure 5.020) indicates the

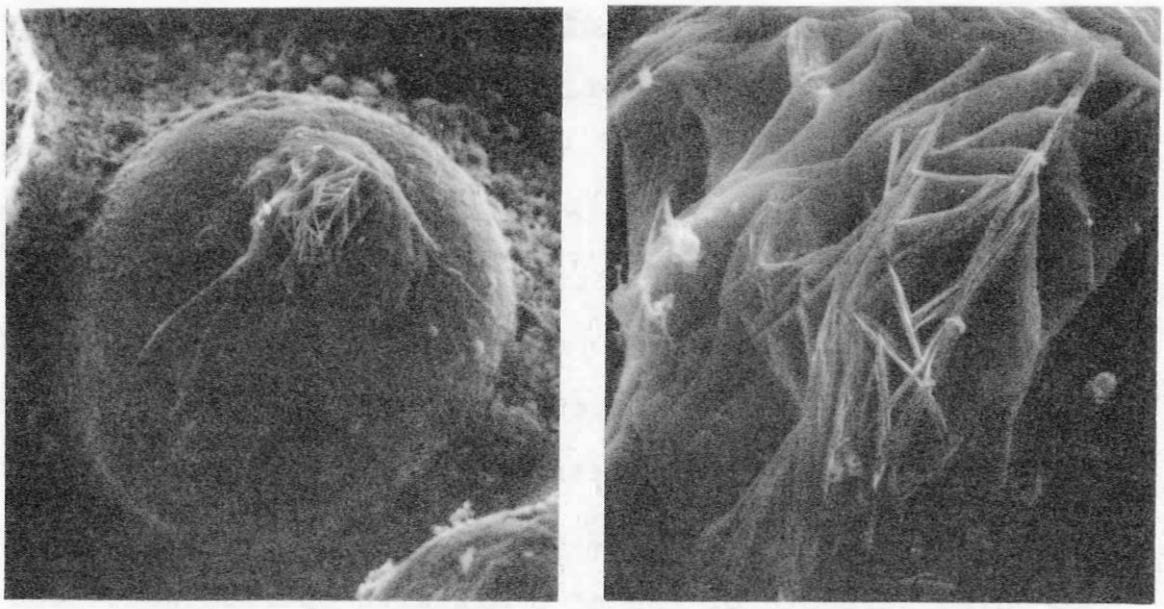

10 µm 1000X (a) 1 µm 5000X (b)

Reacted fly ash particle with crystal growth

Monosulfoaluminate Crystals

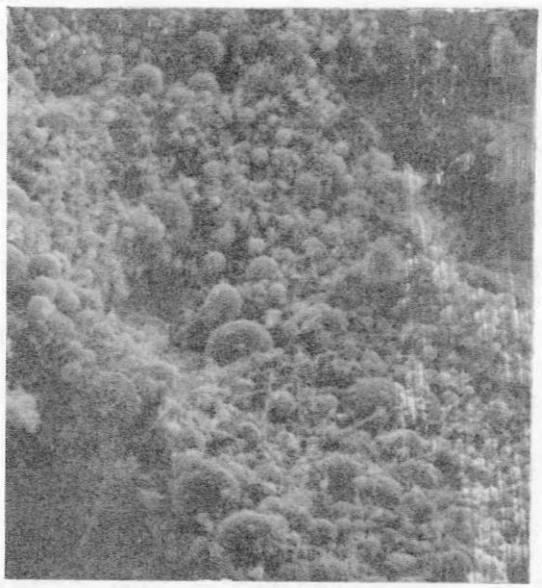

10 µm 1000X (c)

Figure 5.19 Coweta FAB + 25% fly ash at 28 days

presence of calcium, aluminum, silicon, and sulfur, denoting the presence of monosulfoaluminate produced from ettringite.

The Coweta FAB + 35% fly ash follows a similar pattern with the exception that the needle-like formations are less extensive. An interesting feature of the SEM from this mix is the group of flakes in Figure 5.21a. Part of the growth has been magnified in Figure 5.21b for a closer observation. The group of flakes shows a tendency towards the formation of hexagonal plates. Also, the group is on the failure plane and has been partially damaged. The EDS of this crystal formation (Figure 5.22) detected the presence of Ca, Al, Si, and S, indicating that the group is a formation of monosulfoaluminate at an early stage.

The micrographs for the Coweta CABs are presented in Figure 5.23. The matrix of these mixes was more compact than in the FABs and ettringite appeared present in lower quantities. Figure 5.23 a is a micrograph of the Coweta CAB +25% fly ash and depicts the hydration rim of a reacted plerosphere. The wall of the spherical cavity indicates a rather continuous paste matrix that embodies and holds together smaller fly ash particles. The fly ash particle within the cavity has been reacted and fibers of CSH I are radiating from it, indicating that the hydration of C_2S has taken place and it is manifested

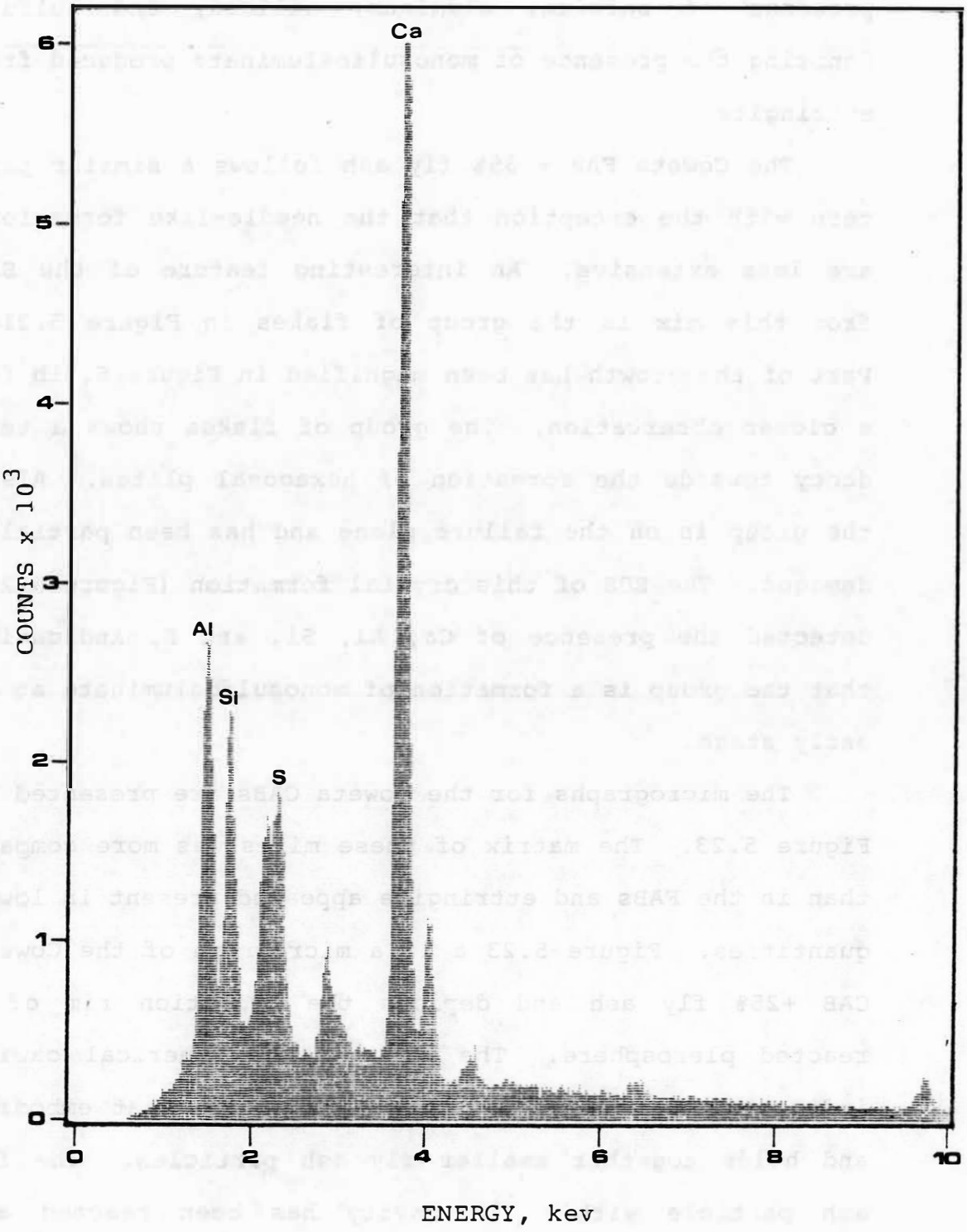

Figure 5.20 EDS of the crystals in Figure 5.d9b

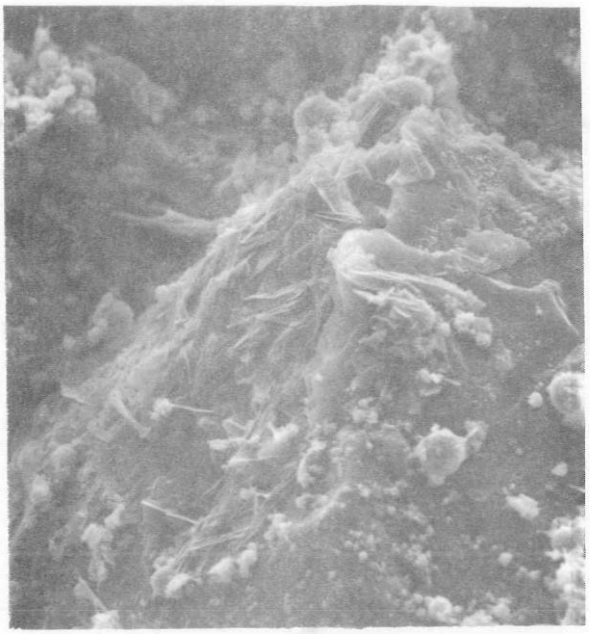

Flaky crystals

10 µm 1000X (a)

1 µm 3000X (b)

Figure 5.21 Coweta FAB + 35% fly ash at 28 days

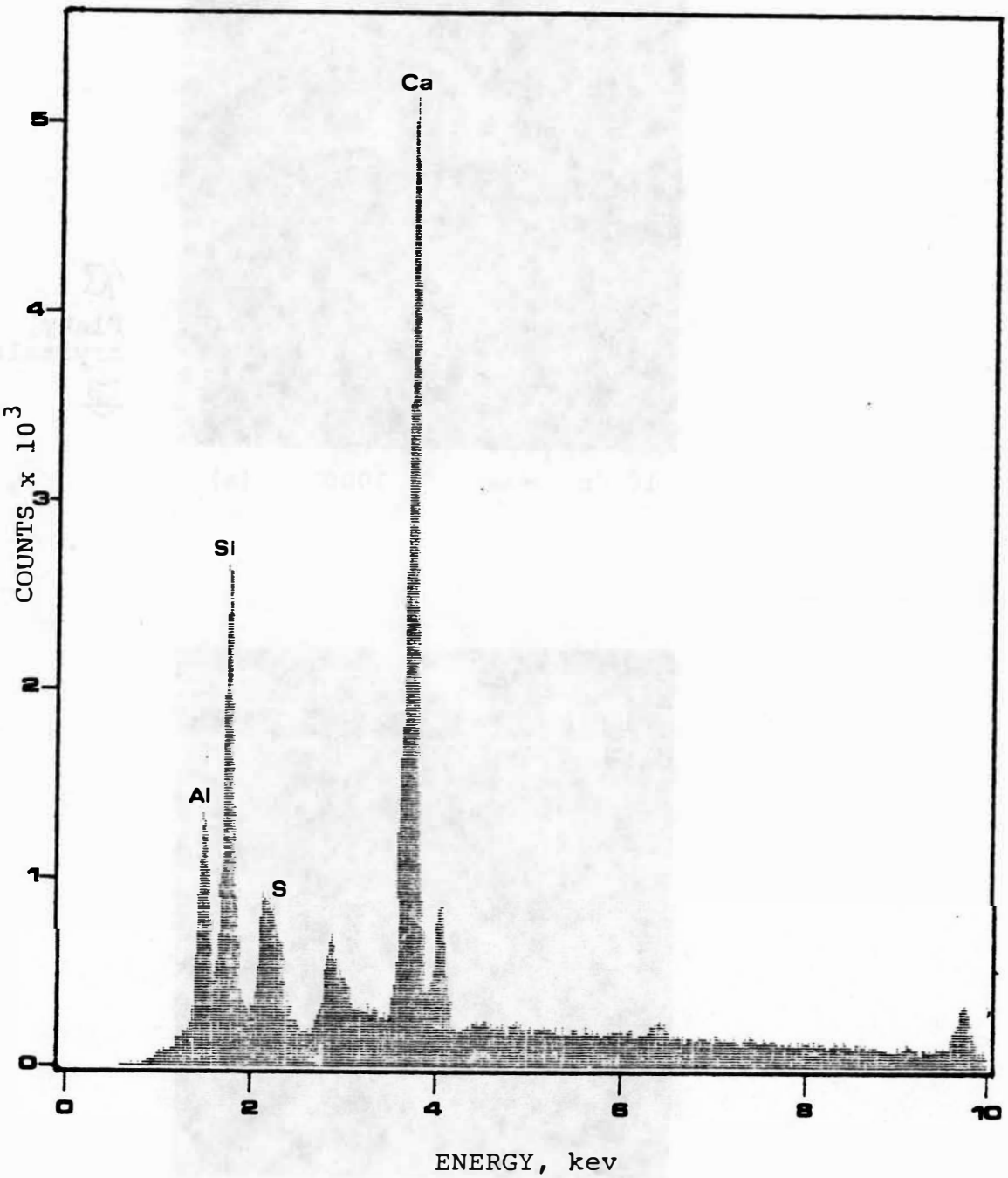

Figure 5.22 EDS of the crystals in Figure 5.21

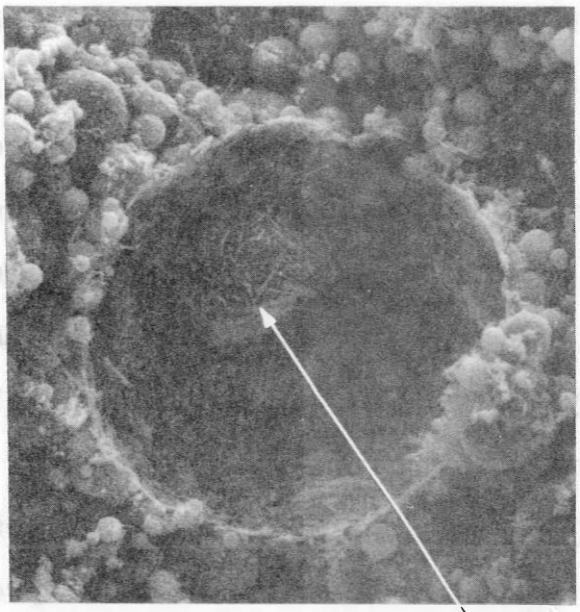

1 µm 2000X (a)

Fibers of CSH I radiating from particle within the hydration rim of a plerosphere

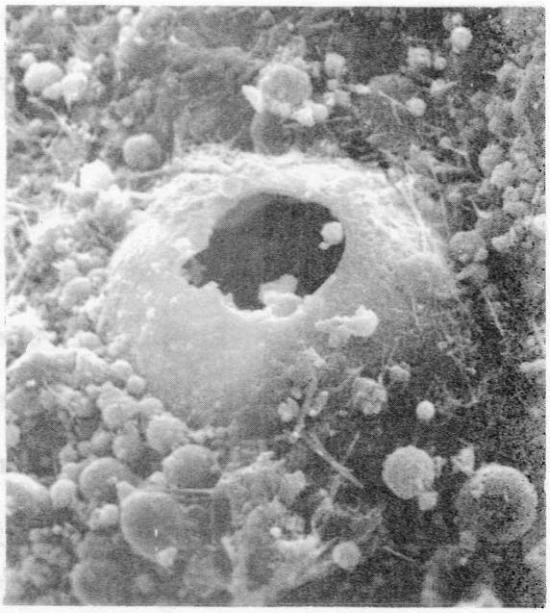

10 µm 1500X (b)

Cenosphere

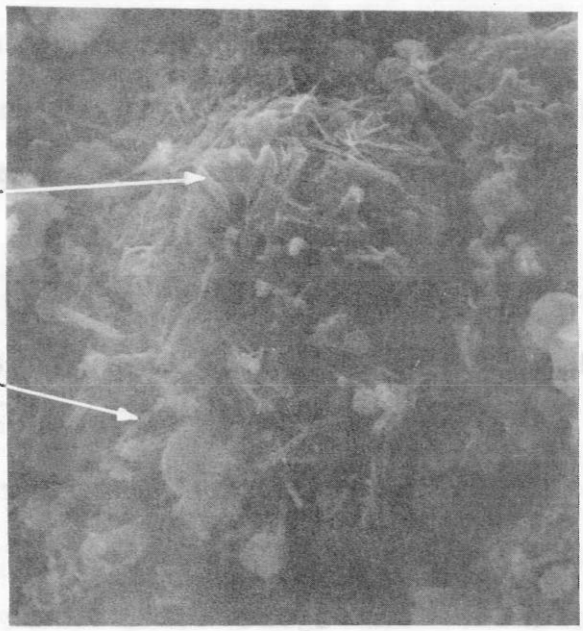

1 µm 3000X (c)

Figure 5.23 Coweta CABo+ 25 (a) and 35% (b,c) fly ash at 28 days

in the micrograph (28-day curing). Figure 5.23b depicts a partially reacted cenosphere observed in the Coweta CAB + 35% fly ash mix. Also from the same mix is micrograph (c) which shows a fly ash spherical particle with rod shaped crystals (ettringite) radiating from the lower half of the sphere and a growth of crystals on the upper half. The shape of the irregular crystals suggests the formation of CSH II (honeycomb calcium silicate hydrate); an additional indication that C_2S is active.

5.8.4 The 90-day mixes. The SEMs of the Coweta mixes with 25 and 35% fly ash, cured for 90 days are presented herein. The micrograph (a) in Figure 5.24 is typical of the pattern observed in the Coweta FAB + 25% fly ash, where fly ash particles were tightly packed on a matrix of paste. The thick rods shown on the micrograph emerging from the matrix were evident throughout the sample. An EDS of a group of these crystals presented a high peak of calcium and a little iron, which is usually present in all the energy dispersion spectrographs of the mixes. Also weak peaks of silicon and aluminum are present, but with such a narrow X-ray detection they could have been picked up from the neighboring matrix. The possibility that the rods are AF_t or AF_m crystals should not be excluded. In Figure 5.24b a fly ash particle is covered by a net of spiny CSH I and possibly some ettringite.

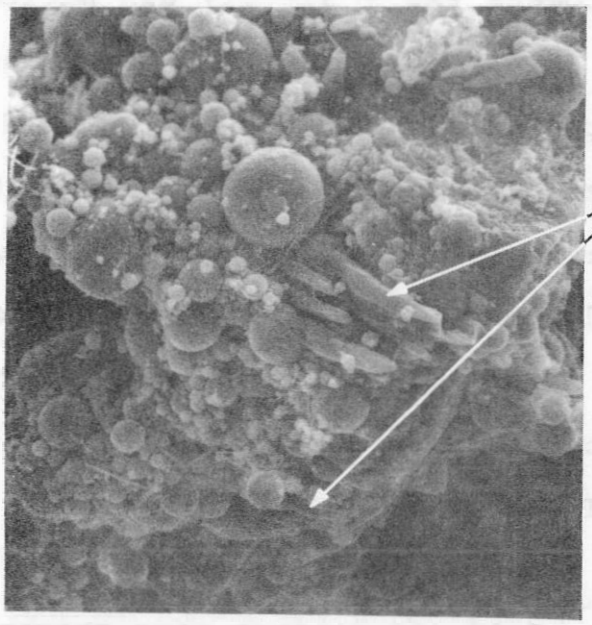

10 µm 1000X (a)

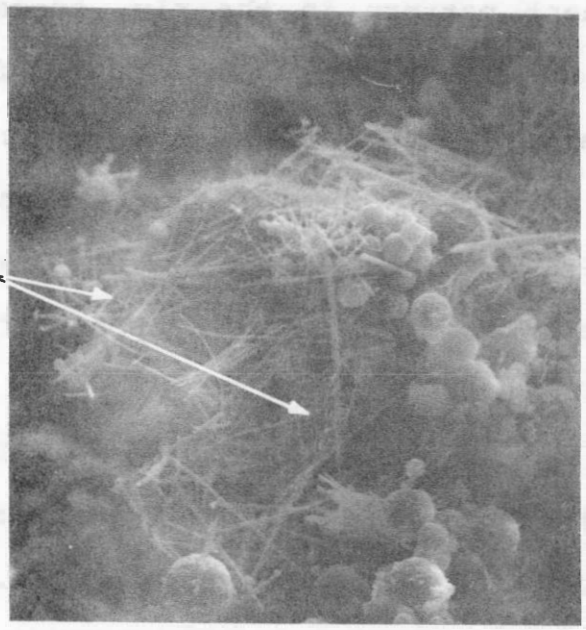

10 µm 1500X (b)

Figure 5.24 Coweta FAB + 25% fly ash at 90 days

The Coweta FAB + 35% fly ash micrographs are given in Figure 5.25. Micrograph (a) shows an arrangement of fly ash spherulites which appear partially reacted. The particle at the lower right corner of this picture has been magnified in micrograph (b) showing a heavily reacted fly ash particle. The hydration products have formed a multi-layer coating over the particle and although partially broken appear to be of the hexagonal phase. In Figure 5.25c a reacted plerosphere is depicted.

Figure 5.26 illustrates some characteristics of the Coweta CABs+ 25% fly ash mix. The network of spiny and needle-like crystals as observed in micrograph (a) was the prominent pattern in the mix, suggesting CSH I and possibly some ettringite. The group of flakes surrounded by the network has been magnified in micrograph (b) revealing an aggregation of thin hexagonal plates resembling C_4AH_{13} crystals. In micrograph (c) the hydration coating has been partially chipped off revealing the underlying fly ash particle.

Finally, for the Coweta 90-day mixes, the picture of Figure 5.27 represents the predominant matrix as it was observed in the Cowetas+ 35% fly ash mix. The "rolled up sheet" crystals evident in the micrograph were observed only in this particular mix of all the mixes scanned. They are believed to be crystals of CSH I and so are the

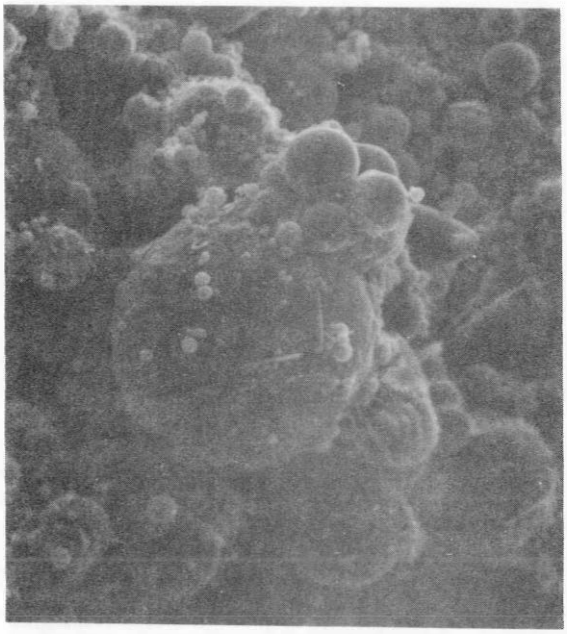

10 μm 1000X (a)

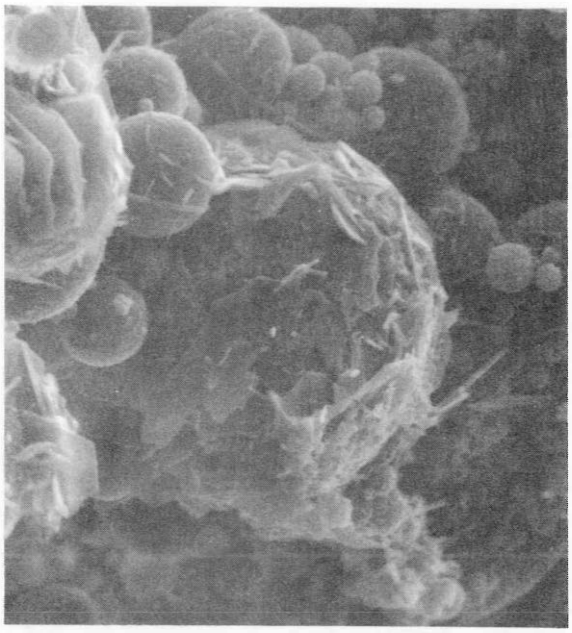

1 μm 3000X (b)

Multilayer coating of hydration crystals on fly ash particle

Reacted plerosphere

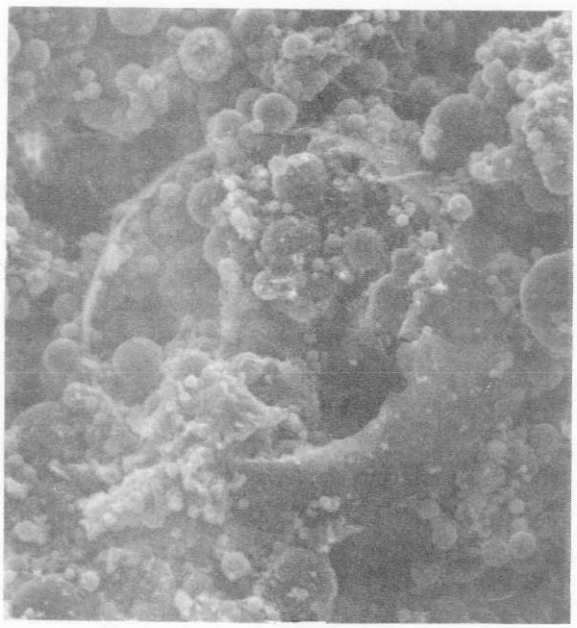

10 μm 1000X (c)

Figure 5.25 Coweta FAB + 35% fly ash at 90 days

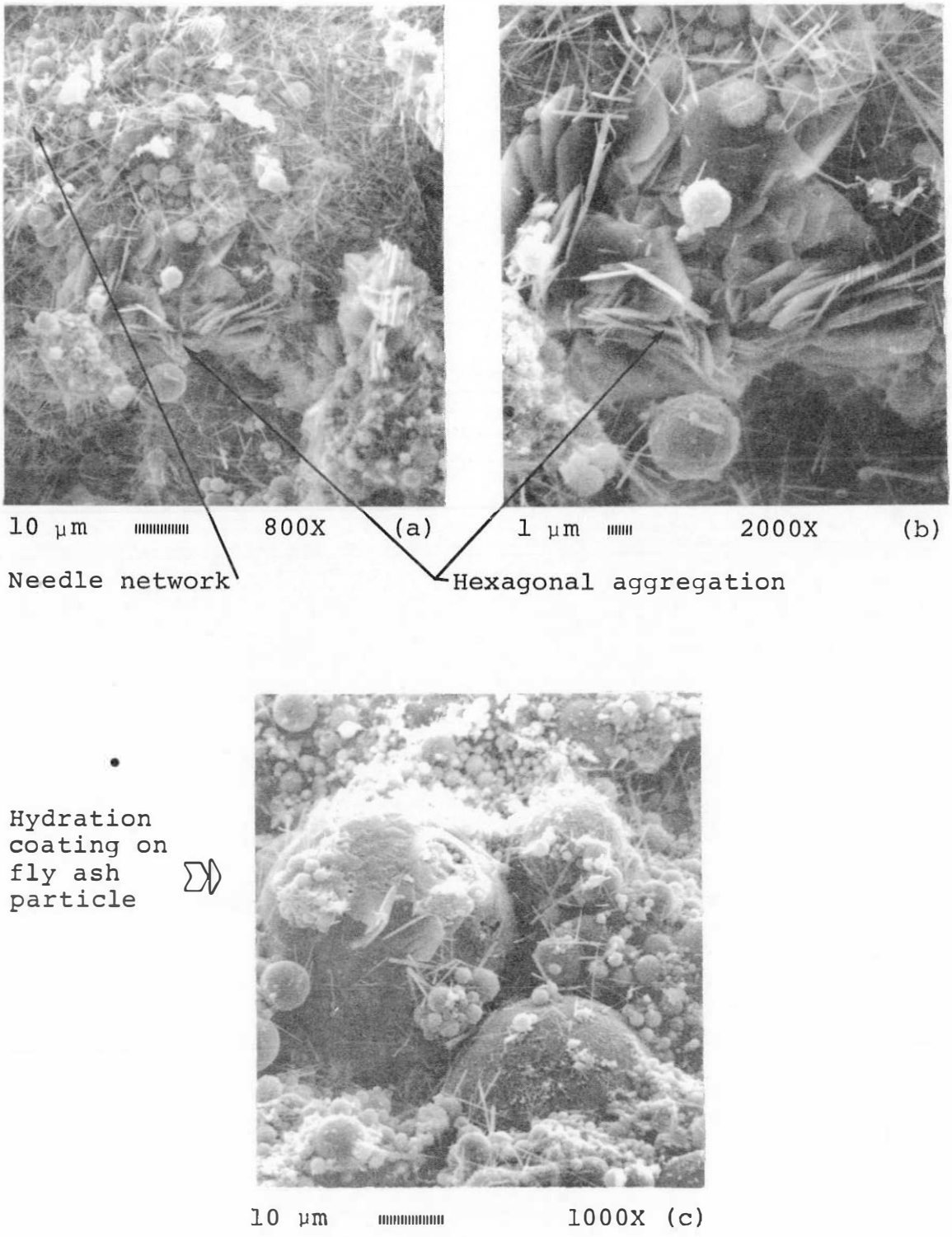

Figure 5.26 Coweta CABs+ 25% fly ash at 90 days

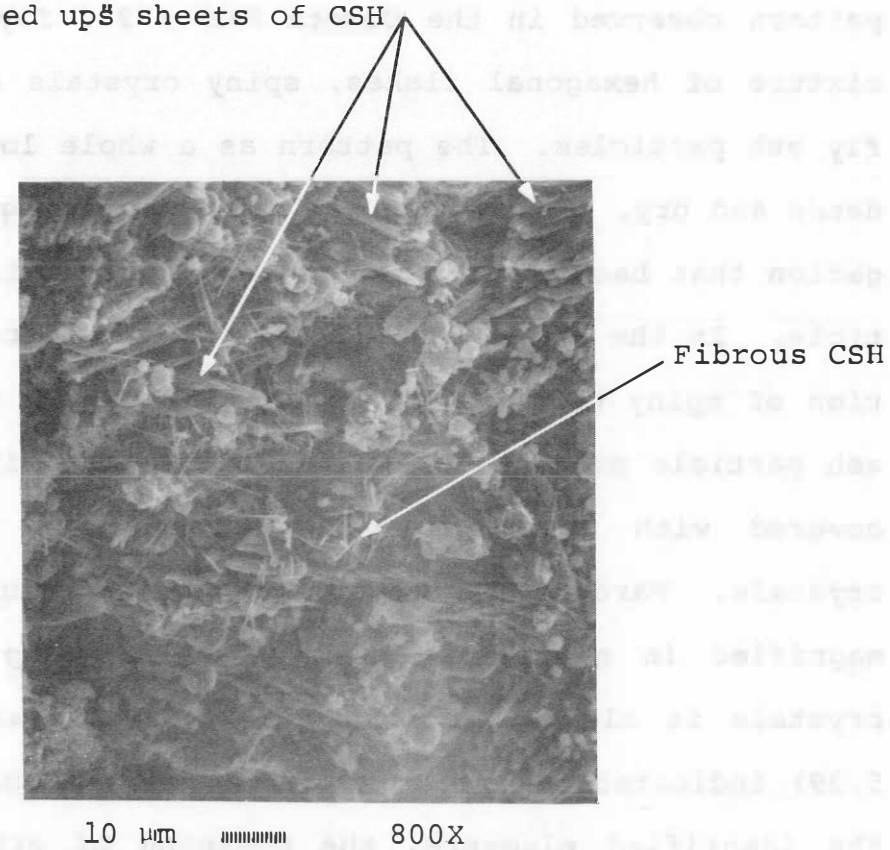

Figure 5.27 Coweta CABs+ 35% fly ash at 90 days

spiny crystals evident in the micrograph.

5.8.5 The 180-day mixes. Three of the Coweta mixes (FAB + 25% fly ash and CABs+ 25, 35% fly ash) were electronically scanned and their SEMs are presented in this section. As indicated in Figure 5.28c the general pattern observed in the Coweta FAB + 25% fly ash was a mixture of hexagonal flakes, spiny crystals and reacted fly ash particles. The pattern as a whole looked rather dense and dry. Micrograph (a) depicts a hexagonal aggregation that has totally covered a spherical fly ash particle. In the upper left half side of the scan a formation of spiny CSH I crystals is visible. A reacted fly ash particle presents a leached surface and is partially covered with hexagonal phase plates and needle-like crystals. Part of the surface of this particle has been magnified in micrograph (b), where a group of needle crystals is clearly visible. EDS of this area (Figure 5.29) indicated the presence of Ca, Al, Si and S. Given the identified elements, the presence of ettringite is presumed although it would not be assumed present at such a late age. Additionally, because of the low density of the needle formation mineral, elements might have been picked up from the reacted surface of the glass.

A micrograph of the Coweta CABs+ 25% fly ash mix is depicted in Figure 5.30a. The curved needles were evident throughout this sample suggesting CSH of type I.

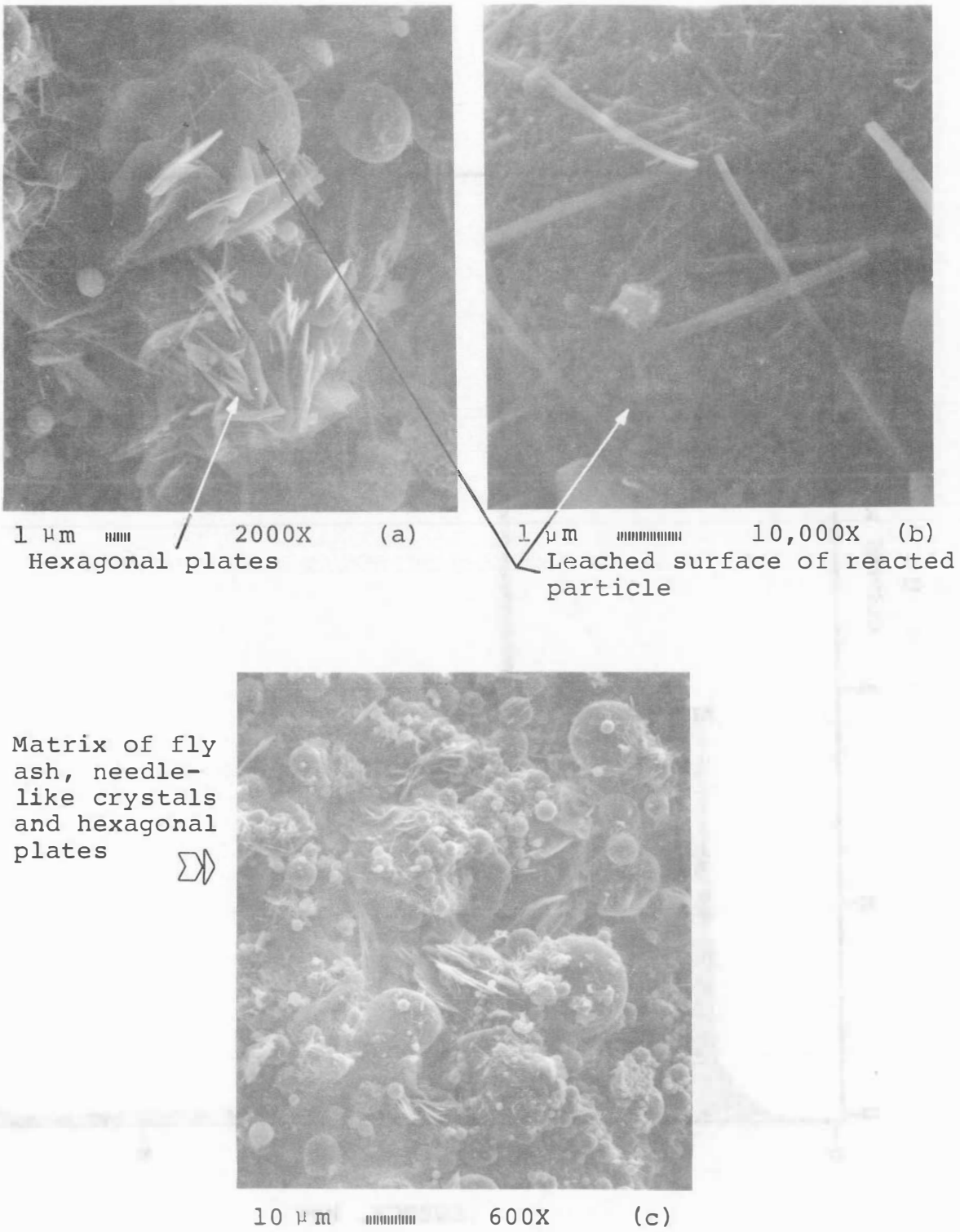

Figure 5.28 Coweta FAB + 25% fly ash at 180 days

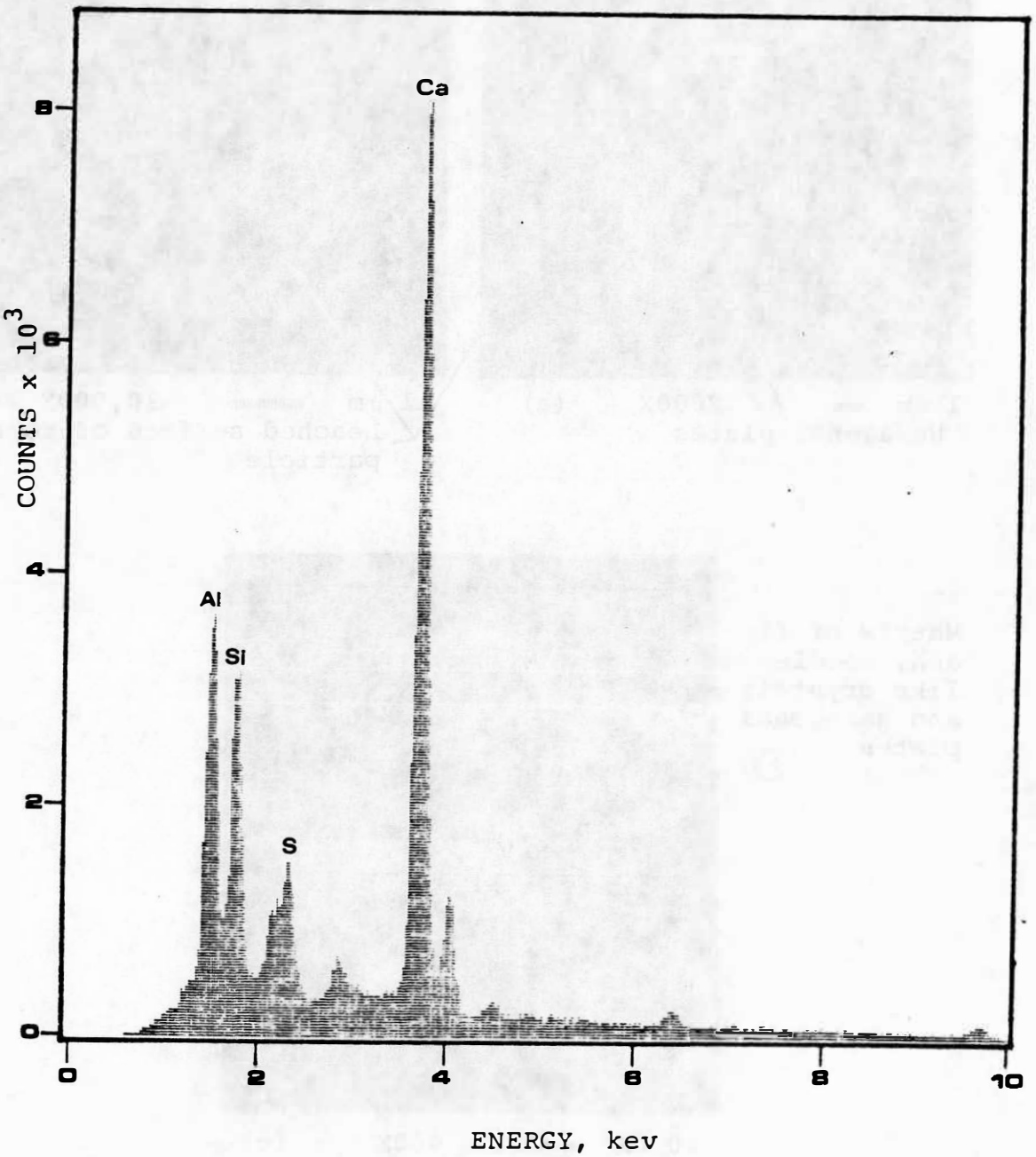

Figure 5.29 EDS of the needles in Figure 5.28b

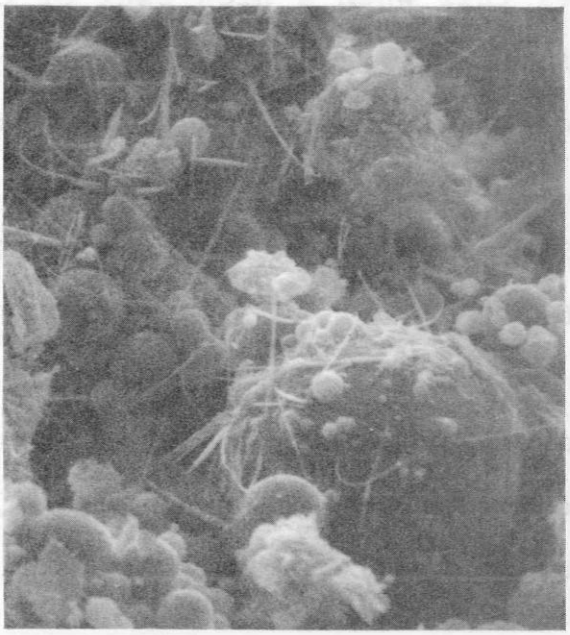

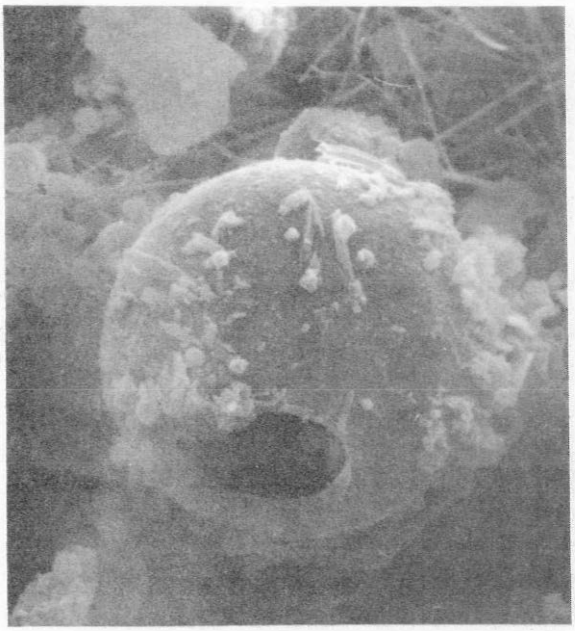

Figure 5.30 Coweta CAB + 25% (a) and 35% (b) fly ash at 180 days

EDS verified this when a high peak of Ca and a lower of Si were detected. Finally, micrograph (b) shows a reacted (consumed) cenosphere as it was detected in the Coweta CABs+ 35% fly ash. EDS of this fly ash particle (Figure 5.31) presents two high peaks of Si and Al and a low peak of Ca.

It is concluded, therefore, that the SEM observations supported, illustrated and at places clarified the chemical behavior profile of the mixes, as it was outlined by the detailed XRD analysis.

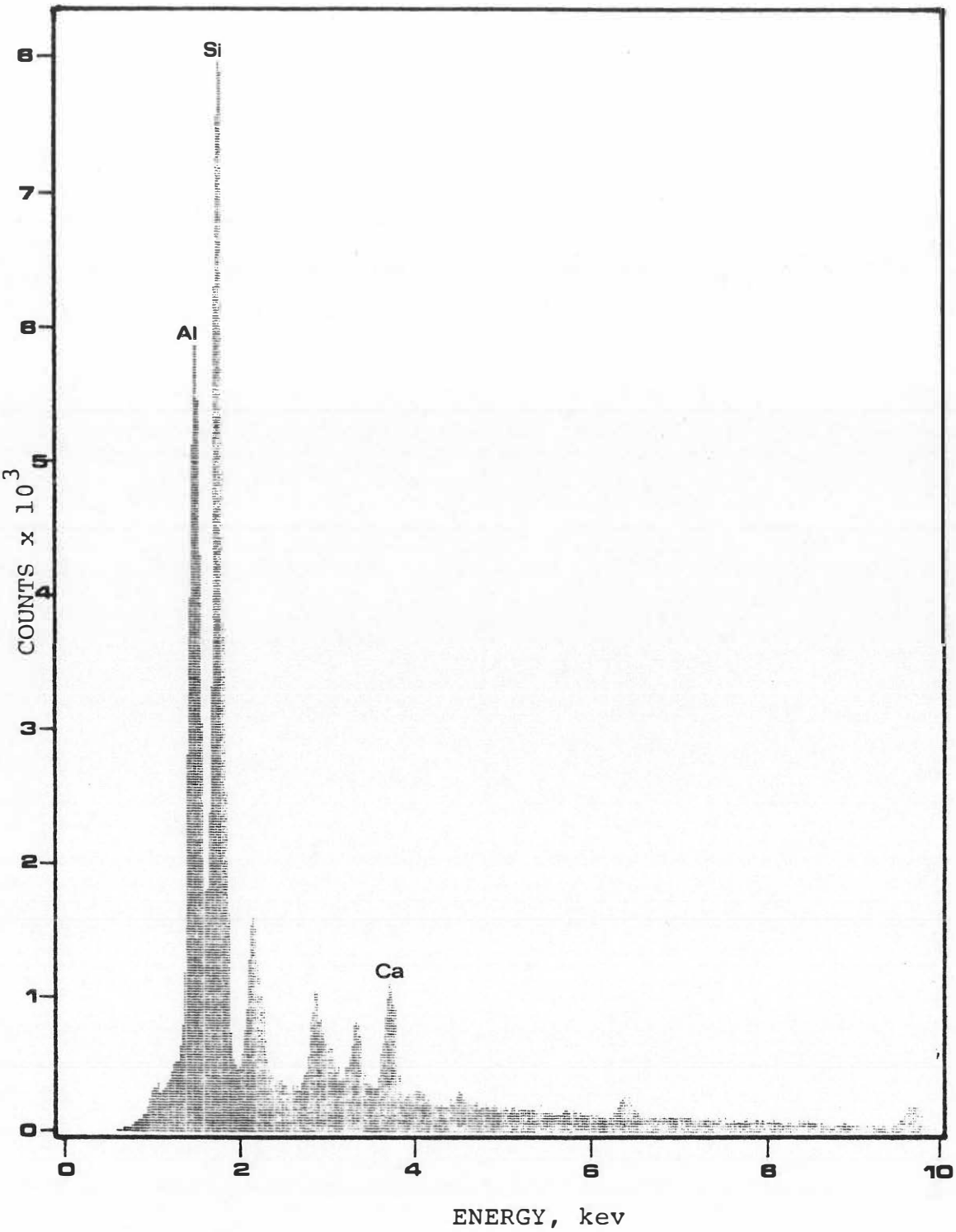

Figure 5.31 EDS of the cenosphere in Figure 5.30b

CHAPTER VI

FIELD IMPLEMENTATION

6.1 Introduction

This section discusses the major factors to be considered in the field application of the fly ash-aggregate mixes. Based on the laboratory experience gained in this study and information provided in Ref. 12 (Chapter 7) techniques for handling, mixing and spreading of the materials are suggested. Nevertheless, these suggestions and recommendations are tentative and may be modified as feedback is received from the actual field application experience.

6.2 Design Criteria

The single requirement specified in the state-of-the-art for stabilized fly ash base or subbase courses is that the mix be durable. The thickness design methods applicable to these courses is based on unconfined compressive strength and is the most practical method to measure durability. On the other hand, the present study brought forth the notion that the flexural properties of the cured mixes are of major importance and the blend

gradation along with the fly ash content are crucial factors contributing to the overall engineering evaluation of the mixes.

6.2.1 Optimum gradation. The data indicate that the more uniform the aggregate blend gradation, the more beneficial the addition of fly ash becomes to the dry density and unconfined compressive strength of the resulting mix. Using this perspective, the center points or median points of the ODOT standard gradation specifications for fine aggregate base and coarse aggregate base, which depict gradations of a well graded sand and a well graded gravel, respectively, are suggested as the targeted blend gradations for the design of fine or coarse blend. The percentages passing each sieve for the two centerlines are given in Table 6.1.

It should be emphasized that the design blends follow closely the gradations specified in Table 6.1, especially the No. 40 and Nos 200 sieves which reflect the amount of fines in the blend. If the blend lacks in fines, it is recommended that an additional source of fines be utilized to bring the percentages passing the No. 40 and No. 200 sieve to the specified levels. If this is not possible, increased amounts of fly ash will be required to close the gap at the No. 200 sieve. In this case, fly ash will be acting as a filler and its percentage will be recorded and added to the fly ash

Table 6.1 CENTERLINE OF ODOT STANDARD GRADATION SPECIFICATIONS (% Passing)

Sieve Size or No.	FAB	CAB
1 in		100
3/4 in		80
3/8 in	100	62.5
#4	87.5	50
#10	77.5	37.5
#40	55	22.5
#200	13	8

FAB = Fine Aggregate Base

CAB = Coarse Aggregate Base

amount required for the mix. The sum of the two amounts will constitute the total amount of fly ash to be used with the base mix. It should be noted that for a typical fly ash 60 to 90% of its particles are finer than the No. 200 sieve and almost 100% finer than the No. 60 sieve, so its effect as a filler will be manifested primarily on the No. 200 sieve of the blend.

6.2.2 Optimum fly ash content. The majority of the FABs in this study exhibited maximum dry density and maximum unconfined compressive strength when mixed with 35% fly ash but maximum flexural resistance (MER) occurred when fly ash was limited to 25%. In order to balance and enhance both the compressive and flexural properties of the FAB mix and given that the FAB gradation is following very closely the gradations specified in Table 6.1, the use of 30% fly ash is recommended as the optimum. Nevertheless, if the design blend deviates from the specified amount by more than 3% at sieves No. 40 and especially at No. 200, then 35% fly ash addition should be used.

With the CABs the maximum dry density occurring at 15% fly ash addition did not prove to be a crucial factor for strength criteria. For the majority of the coarse mixes maximum unconfined compressive strength was attained with 25% fly ash while the flexural resistance varied with the blend gradations; the less uniform the blends, the

smaller the amount of fly ash required to give the higher higher MER values. Thus, assuming that the CAB blend follows closely the specified gradation in Table 6.d, 25% fly ash is recommended as the optimum for the coarse mixes. Additional fly ash can be used if the blend lacks in fines and its amount can be determined as described in Section 6.2.1, but the total fly ash content of the coarse mix should not exceed 30%.

6.2.3 Strength requirements. The compressive strength of the fly ash-aggregate mixes attained uniform trends after 28 days of curing. Therefore, it is recommended that the 42-day strength (6 weeks) be used to establish minimum compressive strength requirements. If enough time is not available, an accelerated curing period of 14 days at 100% relative humidity and temperature of 140°F (60°C) can be used as an approximation of the condition the mixture is expected to attain at the end of the 42-day cure at 70±3°F (21±2°C). However, there is the possibility that certain pozzolanic reactions occurring at higher temperatures might not occur at lower temperatures.

The promising mixes should have a minimum unconfined compressive strength of 400 psi after 42 days of curing. Although the laboratory specimens did not exhibit any cracking, the EPRI experience considers it advisable to establish a maximum 42-day unconfined compressive

strength of 800 psi in order to minimize the cracking possibilities.

The laboratory specimens for unconfined compressive strength should have a length to diameter ratio of 2:1. For the FAB mixes 8 in high, 4 in diameter cylinders are considered suitable but for the CAB mixes it is recommended that 10 in high, 5 in diameter or 12 in high, 6 in diameter cylinders be used.

The flexural strength of the mixes need not be specified, but if the base thickness design is based on flexural parameters, as proposed in this report, these parameters should be obtained from beams cured in the laboratory for 90 days, when the resistance of the mixes in bending is apparent.

6.2.4 Thickness design. The thickness design of the base course carried out with the conventional method will be based on the 42-day unconfined compressive strength of the mix or, considering the flexibility of the mixes, the flexural approach can be employed as described in detail in Section 5.6. To simplify and assist in the analysis of the fly ash-aggregate base a program was written for the programmable calculator HP 41C, 41CV, or 41CX. The program is presented in Appendix H. Given the width of the pavement, the flexural modulus of elasticity of the base, the subgrade reaction, a wheel load and a trial base thickness, the program calculates

the rigidity of the base course together with its deflection, bending moment and shear force at any chosen point across the pavement in less than two minutes. It can be rerun for a second load (axle configuration). By superposition the total effect on the base is calculated and, in turn, the base design thickness determined. Thus, a quick analysis may be accomplished under a variety of wheel configurations and loading arrangements.

Such an analysis is presented at the end of Appendix H where the pavement of Problem 1 in Section 5.6.2 is studied under various loading arrangements. The axle loads used are 16 and 18 kips and the spacing between the wheels is 5 and 6 feet, respectively. The base thickness is taken as 8 inches. In each case the effect of every individual load is computed at the crucial points along the base. Employing the program and applying the principle of superposition the total effect of the axle is calculated. In Case III, where a vehicle is parked at the very edge of the pavement while another is passing by, the factor of safety is 0.75 which is less than 1, indicating that the base has failed elastically and therefore a thickness larger than 8 inches is required to sustain the specific loads. However, considering that the surface course will provide added support in carrying the loads, that point loads are used instead of tire contact pressures which will result in reduced deflec-

tions, that the outside 12-foot lane extends to the right and the shoulder to the left of the pavement, the deflections at the extremities will tend to be substantially reduced and the base course may still be stressed within its elastic range. For example, if the base is extended beyond the inside lane to include a two foot shoulder where parking is not allowed, even with the extreme loading of Case III the deflection of the base at the edge of the pavement will be only 0.156 inches as compared to the 0.600 inches. The analysis could also include the second lane for a more detailed base evaluation.

Finally, treated subgrades which have higher values of subgrade reaction and lead to the reduction of base thickness constitute an additional variable that can be included in the analysis. Thereafter, alternatives for optimum design will emanate from an economic analysis.

6.3 Materials Handling and Application

Fly ash aggregate bases combine the advantages of cost effectiveness and utilization of a product, namely fly ash, which would normally be discarded. Admittedly, the rapid setting of fly ash is a serious draw back. In order to maximize the overall engineering performance, minimize the cost and achieve optimum results it is necessary that the handling and application procedures be

suitably adjusted to the properties of the mixes.

For subgrade preparation the course must be crowned, graded and compacted to the design requirements before the base is constructedo It is essential that the subgrade surface be moist, but not wet, so that moisture is not absorbed from the base course, which should be maintained at optimum moisture conditions.

6.3.d Mixing procedures. Thorough mixing is extremely important in order for the fly ash-aggregate base to acquire strength and durability. Equally important are the quantity control, especially for fly ash and water, and the uniformity of the mixture. For the aforementioned reasons the mix-in-place method is considered unsuitable for the fly ash-aggregate mixes, primarily because of its tendency towards poor uniformity of the mix; therefore, it is recommended that this method be avoided. Another factor against the use of the mix-in-place method is the flash set of fly ash which occurs within 7-20 minutes, depending on the amount of fly ash used. A set retardant would prolong the handling time, but not without adding to the cost and lowering the strength of the mix. On the other hand, central mixing methods provide for a high degree of quality control and with the right coordination the mixes can be applied and compacted before the fly ash sets. An on-site batch plant (very similar to concrete) can be used. Batching

should be done on a weight basis and aggregates must be adequately moist so they do not absorb any of the mixing water. Fly ash can be introduced in the mix dry. It is recommended that concrete-type drum trucks be used to haul the base mix to the application site while mixing is in progress. When the mix leaves the batch plant, it should have 1/2 to 3/4 of the required amount of water, depending on the distance to be traveled. If the application site is less than three minutes away, use 3/4 of water, if it is more than three minutes away, use 1/2 water. In case of longer distances less water should be premixed and its amount can be determined by trial, allowing for final mixing, application and compaction time before the mix sets. At the job site the final amount of water is added from the 100 gallon tank of the truck and the base mixture should be thoroughly mixed for an additional two to three minutes before it is placed on the road. This two-stage mixing (preliminary and final) is suggested in order to ensure a uniform composition and also a slow down of the hydration process, which is attained by limiting the amount of water during thes preliminary stage.

6.3.2 Applying and compacting the base mix.

Time and uniformity, as crucial factors in this procedure, dictate the choice of an asphalt paver as the most effective applicator. The base mix is unloaded from

the drum truck onto the paver and placed or laid on the road. Following immediately behind the paver, the compaction equipment compacts the layer to the design thickness. The three units (drum truck, paver, compactor) form a train that moves at a speed of about three miles per hour. The uncompacted thickness must be such that when the layer is compacted to the design thickness, 100% of the maximum dry density, as determined in the laboratory, has been achieved. Field checks of the compacted density and the optimum moisture content can be done quickly with a nuclear device. If the base has a water content below optimum, additional water must be spread over it to bring it to the optimum. In case of rain, the base application should stop and if the moisture content exceeds the optimum by more than two percent or if the partially uncompacted layers are not compacted fully within 30 minutes, the layer must be removed and replaced. Also, if more than 30 minutes elapse between adjacent passes, it is recommended that a construction joint be formed along the edge of the previous pass. Construction joints should also be formed at the edge of each day's construction.

It is best that the base course be applied in a one lift thickness, but if the compacted thickness is in excess of 8 inches the base must be constructed in multiple layers, with each compacted layer being not less than 4 inches after compaction. If the upper layer is

not constructed (placed) immediately, the lower layer must be allowed to cure for a period of 14 days before the upper layer application.

With the FABs, the 10-ton pneumatic-tired rollers or vibrating rollers of 1 to 1.5 tons dead weight are suggested for efficient compaction, but the CABs might require larger vibratory rollers with heavier dead weights. In the case of vibratory compaction, the roller speed should not exceed three miles per hour.

Finally, base application should not be attempted if the ambient temperature is below 40°F (4°C). It is recommended that application procedures be terminated two months in advance of the first frost, thus allowing time for the base mix to cure properly.

6.3.3 Curing the base. Once the base course has been constructed and finished free of all loose and foreign material, a seal coat or paving course must be applied within 30 minutes. If for some reason this is not feasible, the surfaces of the base should be sprayed with water at regular intervals so that optimum moisture is maintained at all times until surfacing. The bituminous surfacing or a bituminous seal coat of the RS-1 type can be applied (0.15 to 0.30 gallons per yds^2) to prevent evaporation or protect the base from excessive moisture intrusion. The base should be cured before opening the road to traffic. This curing period is 14

days for construction traffic, 1.5 months for light traffic and 2.5 months for heavy traffic. Shoulders with a minimum width of two feet are highly recommended.

6.3.4 Monitoring. Quality control is very essential during the construction phase and strict compliance with specifications is required. Post construction monitoring will provide valuable data to help understand the field behavior of the fly ash-aggregate mixes. After comparison with the laboratory data, improved design procedure and techniques may evolve. A tentative monitoring schedule is suggested in Table 6.2 as being compatible with and complimentary to the laboratory tests.

Table 6.2 MONITORING SCHEDULE

Test	Curing Time (after construction), days								
	3	7	14	28	42	90	180	1 yr	2 yrs
Compressive strength (core samples)	x	x	x	x	x	x	x	x	x
Deflection (Dynaflect or Benkelman beam)					x	x	x	x	x
Leaching			x	x	x	x	x	x	x
Traffic count					x	x	x	x	x
Pavement Condition Survey (cracking, Rutting, etc.)					x	x	x	x	x
XRD, SEM					x	x	x	x	x

CHAPTER VII

CONCLUSIONS AND RECOMMENDATIONS

7.1 Conclusions

Based on the laboratory data presented in Chapter V and with the assistance of observations made during the course of the study the following conclusions have been drawns

1. The aggregates sampled from the five different locations are currently used for bituminous base construction. They produced blends with distinct gradation characteristics that display some variations.
2. All aggregate blends lack adequate fines to meet the lower end of the standard gradation specifications (No. 200 sieve)s. This is due to the component aggregates lacking adequate material passing the No. 200 sieve.
3. For the Ponca City, Coweta, and Tupelo FABs, a higher percentage of material passing the No. 40 sieve would substantially improve the blends, thus, contributing to better mixes and improved

performances

4. Fly ash contents of 10% or lower produced weak specimens. Fly ash in excess of 35% could result in better strength performance but the extremely rapid setting prohibits its use.
5. Increased fly ash contents lead to an increase of the maximum dry densities of the FAB mixes, but to a decrease of the maximum dry density for the CAB.
6. In general, the CAB mixes featured higher dry densities than the FAB mixes.
7. The considerable variation in strength of the mixes during the first seven days of curing is associated with the massive formation of ettringite in the early stage of the hydration process. The relative strength uniformity obtained with prolonged curing is attributed to the following features: conversion of ettringite to monosulfoaluminate, which later dissolves to the solid CAH phases; the C_2S hydration (CSH) and the appearance of the CASH phases
8. For the FABs, the 35% fly ash addition gives, in general, higher strengths and higher maximum dry densities. With the CABs it is the 25% fly ash content that performs better in terms of strength. The use of fly ash in excess of 35% with the coarse bases is unlikely to give better performance as both the filling and cementing potentials of fly ash

have been exhausted at around a 25% content. With regard to the FABs, excessive fly ash is likely to enhance the cementing effect and, therefore, improve the strength level.

9. The majority of the mixes attained maximum overall compressive strength after 180 days of curing, indicative of the general pattern of strength gaining with time.
10. Careful examination of the cylindrical specimens and beams for various mixes, and for curing periods varying from 28 days to 14 months, do not reveal any shrinkage in any direction whatsoever.
11. The optimum amount of fly ash in terms of strength varies with the aggregate source rather than the blend type. Nevertheless, the 35% fly ash content in FABs gives the higher strengths in 90 and 180 days with the exception of the Tupelo FAB. In terms of the 180 day strength, the CABs reach their higher strength when mixed with 35% fly ash, except for the Coweta CAB.
12. The massive premature failure and sensitivity of the 28-day beams suggests that a month's time is too early to expect aggregate fly ash mixes to acquire resistance to flexural failure.
13. The 90-day beams performed well and gave substantial flexural strengths (MER)s. With the FABs it is the

25% fly ash addition that, in general gives the higher MER values. With the CABs the pattern is rather inconsistent.

14. In terms of the ratio of flexural to compressive strength, FABs presented higher values than the CABs indicating that the gap between flexural and compressive performance is wider with the latter. The ratio values for the FABs ranged from 0.13 to 1.55 and for the CABs from 0.12 to 0.53.

15. The majority of the 90-day beams presented load-deflection curves with plastic regions resembling those of the plastics. With some mixes the plastic region is quite extended. The plastic range can fit a logarithmic curve of the form $P = a + b \ln (\Delta L)$, where P = load, ΔL = deflection and a,b parameters. Thus, the plastic regions of the mixes were formulated logarithmically and a new parameter was introduced (modulus of plasticity) which describes the behavior of the mix in the plastic region.

16. The ratio of modulus of plasticity (E_p) to the flexural modulus of elasticity (E) correlates the elastic and plastic regions of a load-deflection curve. The closer the ratio is to one, the slower the rate of permanent deformation of the mix when it is in the plastic range. The ratio values for the FABs ranged from 0.07 to 0.26 and the CABs from

0.07 to 0.24.

17. The flexural moduli of elasticity (E) of the aggregate-fly ash mixes are adequate to classify the base courses as stiff but from a structural perspective they are still flexible. Considering the underlying more flexible subgrade, the base course can be viewed as a beam on an elastic foundation. Based on this and the availability of flexural data, a flexural design approach was proposed using the Winkler model.
18. XRD analysis indicated that the aggregates are quite inert and the formation of new crystals in the mixes is due to the hydration of fly ash.
19. Diffractograms of pastes from the fly ash used in the study and cured for various times revealed the formation of calcium aluminum sulphate hydrates ($C\bar{A}S\bar{H}$)o, calcium aluminum hydrates (CAH)o, calcium aluminum silicate hydrates (CASH) and calcium silicate hydrates (CSH) as a result of the fly ash hydration. These phases were also detected in the actual mixes but at a lower degree of crystallization.
20. Water in excess of the optimum amount required to produce maximum dry density in a trial mix was found to promote the formation of ettringite and delay its transformation to monosulfoaluminate. The seven-day

strength of the mix rich in water was much lower than the corresponding mix with optimum water content.

21. The XRD analysis and SEM observations of pastes and mixes suggests that the hydration process in the mixes unfolds at a slower rate than in the fly ash pastes.

22. SEM observations with the assistance of energy disperssive spectroscopy verified and helped clarify the XRD findings.

23. Examination of the SEM photos indicate that, in addition to the presence of some paste and the crystal formation, resulting from fly ash water reaction, some fly ash is available in a partially reacted or unreacted form. It is safe, then, to assume that fly ash partially acts as a filler rather than as a chemical compound and its total potential is not brought into play.

24. Comparison of the SEM photos of the 28, 90 and 180 days indicate that the mix matrix "densifies" with time as the hydration products, especially theo hexagonal phases and CSH, gain better crystallinity and form aggregations, paste or networks (of needle-like crystals) that support, embody or enclose the partially reacted or unreacted fly ash spherulites. An overview of the XRD analysis

suggests a similar trend as the minerals possessing cementing potential are found present in higher intensities with the mixes cured for 90 days as compared to their 28 day counterparts. On the other hand, compressive strength generally improves with time, while the flexural strength jumps drastically from an exceptionally low value in 28 days to a very satisfactory level in 90 days. With regard to the aforementioned observations it is reasonable to attribute the strength improvement of the mixes in time to the better and more massive crystallization of the hydration products of fly ash which are grouped together to form a variety of supporting matrices.

7.2 Recommendations

Based on the conclusions formulated above and considering the positive aspects of this study the following recommendations appear to be in order.

1. Further more detailed investigation on the determination of the optimum base gradation and aggregate physical properties that will utilize both the filling and cementing potential of fly ash at a maximum degree.
2. Field implementation monitoring and evaluation of the promising mixes of this study based on strength criteria.

3. Thorough examination of the behavior of the mixes for the time interval between 28 and 90 days curinga Also, study of the long term performance of the mixes.
4. Study of the durability of aggregate-fly ash mixes exposed to the alternate wetting and drying cyclesa
5. Study methods of laboratory compaction which are similar to bituminous base preparationsa
6. The development of design specifications and minimum requirements for the practical application of the mixes. The minimum allowable compressive strength requirement should be based on the performance of the mix at ages later than 28 days, when the mixes produce more uniform results. It is recommended that the 42-day strength is used for this purpose. As the flexural potential of the mixes appears well manifested after 90 days of curing the flexural parameters should be determined from data of this curing age.
7. Additives, such as aluminum sulfates and other organic compounds, tend to retard the hydration process which in effect allows time for the chemical reaction to take place and prevents the undesirable effect of rapid setting. These retardants should be tested, especially, for mixes containing fly ash at or in excess of 35%.

REFERENCES

1. American Association of State Highway and Transportation Officials (AASHTO), Part II, 12th Edition, 1982.

2. American Society for Testing and Materials, "Book of ASTM Standards," 1984.

3. Bahor, M.P., Patelunas, G.M., "Existing High Volume Ash Demonstration Projects in the United States," Proceedings, Seventh International Ash Utilization, Symposium and Exposition, National Ash Association, 1985, pp. 11-18.

4. Barenberg, E.J., "Lime-Fly Ash-Aggregate Mixtures," U.S. Department of Interior, Bureau of Mines, Information Circular 8348, 1967, pp. 37-39.

5. Barenberg, E.J., "Utilization of Ash in Stabilized Base Construction," U.S. Department of Interior, Bureau of Mines, Information Circular 8640, 1974, pp. 180-196.

6. Barenberg, E.J., "Cement Fly Ash Mixes for Pavements," Proceedings, Seventh International Ash Utilization, Symposium and Exposition, National Ash Association, 1985, pp. 57-66.

7. Bowles, J.E., "Foundation Analysis and Design," Second edition, McGraw-Hill, New York, 1977.

8. Chu, Y.T., "Engineering Behavior of Pavement Materials. State of the Art," U.S. Army Engineering Waterways Experiment Station, Final Report No. FAA-RD-77-37, WES TR S-77-9, 1977.

9. Diamond, S., "The Characterization of Fly Ashes," Proceedings, Effects of Fly Ash Incorporation in Cement and Concrete, Symposium N, Material Research Society, 1981, pp. 12-23.

10. Demirel, T., Pitt, J.M., Mings, M.L., Schlorholtz, S.M., "Characterization of Fly Ash for use in Concrete-Interim Report," Iowa State University, 1982.

11. Dvorak, A.J., Lewis, B.G., et al., "Impacts of Coal Fired Power Plants on Fish, Wildlife and Their Habitats," Division of Environmental Impact Studies, Argone National Laboratory FWS/OBS-78/29, 1978, pp. 1-240.

12. Electric Power Research Institute (EPRI), "Fly Ash Design Manual for Road and Site Applications," Volume 1, Dry or Conditioned Placement, Interim Report, Project 2422-2, 1986.

13. Ghose A., Pratt, P.L., "Studies of the Hydration Reactions and Microstructure of Cement-Fly Ash Pastes," Proceedings, Effects of Fly Ash Incorporation in Cement and Concrete, Symposium N, Material Research Society, 1981, pp. 82-91.

14. Ghosh, S.N., "Advances in Cement Technology," Critical Reviews and Case Studies on Manufacturing, Quality Control, Optimization and Use," Pergamon Press, New York, 1983.

15. Grutzeck, M.W., Roy, D.M., Scheetz, B.E., "Hydration Mechanisms of High Lime Fly Ash in Portland Cement Composites," Proceedings, Effects of Fly Ash Incorporation in Cement and Concrete, Symposium N, Material Research Society, 1981, pp. 92-101.

16. Hect, N.L., Duval, D.S., "Characterization and Utilization of Municipal and Utility Sludges and Ashes; Vol. III-Utility Coal Ash," National Environmental Research Center Report, EPA, May 1975.

17. Laguros, J.G., "Lime Stabilized Soil Properties and the Beam Action Hypothesis," paper presented in the 43rd Annual Meeting of the Highway Research Board, Washington D.C., 1964.

18. Laguros, J.G. and Medhani, R., "Stabilization of Oklahoma Shales, Field Implementation Phases," Final Report ODOT 79-09-2 (Item 2185), ORA 158-867, University of Oklahoma, 1984.

19. Laguros, J.G., Baker, M., "Fly Ash Concrete: A Study of the Reaction Products Using X-ray Diffraction and SEM," Report No. ODOT 82-01-2, ORA 155-088, University of Oklahoma, August 1984.

20. Laguros, J.G. and Keshawarz, M.S., "Field Stabilization of Ponca City Shale," Report No. ORA 158-867, University of Oklahoma, 1985.

21. Lea, F.M., Desch, C.H., "The Chemistry of Cement and Concrete," Chemical Publishing Company, Inc., Third Edition, 1970.

22. McCormac, J.C., "Design of Reinforced Concrete," Harper and Row, Publishers, New York, 1978.

23. Meyers, J.F., Pichumain, R., Kapples, B.S., "Fly Ash as a Construction Material for Highways," Federal Highway Administration, FHWA-IP-76-16, June 1976.

24. Mohan, K., Taylor, H.F.W., "Pastes of Tricalcium Silicate with Fly Ash-Analytical Electron Microscopy, Trimethyl Simulation and Other Studies," Proceedings, Effects of Fly Ash Incorporation in Cement and Concrete, Symposium N, Material Research Society, 1981, pp. 54-59.

25. Novotny, S.J., "Fly Ash/Lime/Aggregate Roadway Base Course for Keystone Steam Generating Station Ash Haul Road," Proceedings, Seventh International Ash Utilization, Symposium and Exposition, National Ash Association, 1985, pp. 859-867.

26. Oglesby, C.H., Hicks, R.G., "Highway Engineering," John Wiley and Sons Inc., Fourth Edition, 1982, pp. 648.

27. Parks, P.W., "Progress Through Cooperation," Proceedings, Seventh International Ash Utilization, Symposium and Exposition, National Ash Association, 1985, pp. 6-10.

28. Parks, D.J., Boyd, R. Jr., Marchetti, J., "Forecasted Ash Utilization in Commercial Markets: An Econometric Analysis," Proceedings, Seventh International Ash Utilization, Symposium and Exposition, National Ash Association, 1985, pp. 151-160.

29. Portland Cement Association, "Thickness Design for Concrete Pavements," PCA, Skokie, Illinois, 1972, pp. 4.

30. Ravina, D., "Production and Collection of Fly Ash for Use in Concrete," Proceedings, Effects of Fly Ash Incorporation in Cement and Concrete, Symposium N, Material Research Society, 1981, pp. 2-11.

31. Scheetz, B.E., Strickler, D.W., Grutzeck, M.W., Roy, D.M., "Physical and Chemical Behavior of Selectively Etched Fly Ashes," Proceedings, Effects of Fly Ash Incorporation in Cement and Concrete, Symposium N, Material Research Society, 1981, pp. 24-33.

32. Taylor, H.F.W., "The Chemistry of Cements," Academic Press, London and New York, 1964.

33. Thornton, S.I., Parker, D.G., "Fly Ash as Fill and Base Material in Arkansas Highways," Federal Highway Administration, Technical Report, PB-250 480, October 1975.

34. Townsend, F.C., Donaghe, R.T., "Investigation of Accelerated Curing of Soil-Lime and Lime-Fly Ash-Aggregate Mixtures," U.S. Army Engineering Waterways Experiment Station, Technical Report, 1976.

35. Transportation Research Board, "Lime-Fly Ash Stabilized Base and Subbases," U.S. Department of Commerce, Technical Report PB-259 432, October 1976.

36. Winterkorn, H.F. and Fang, H.Y., "Foundation Engineering Handbook," Van Nostrand Reinhold Co., New York, 1975.

37. Word, J.E. and Green, W.B., "Current Interpretation of Stability Measurements on Two Experimental Projects in Maryland," Highway Research Board, Bulletin No. 282, 1961.

38. Yang, N.C., "New Paving Concept for Newark Airport," Civil Engineering Magazine, ASCE, 1970.

39. Yoder, E.J., Witczak, M.W., "Principles of Pavement Design," John Wiley and Sons, Inc., Second Edition, New York, 1975.

APPENDIX A

MOISTURE DENSITY RELATIONSHIPS

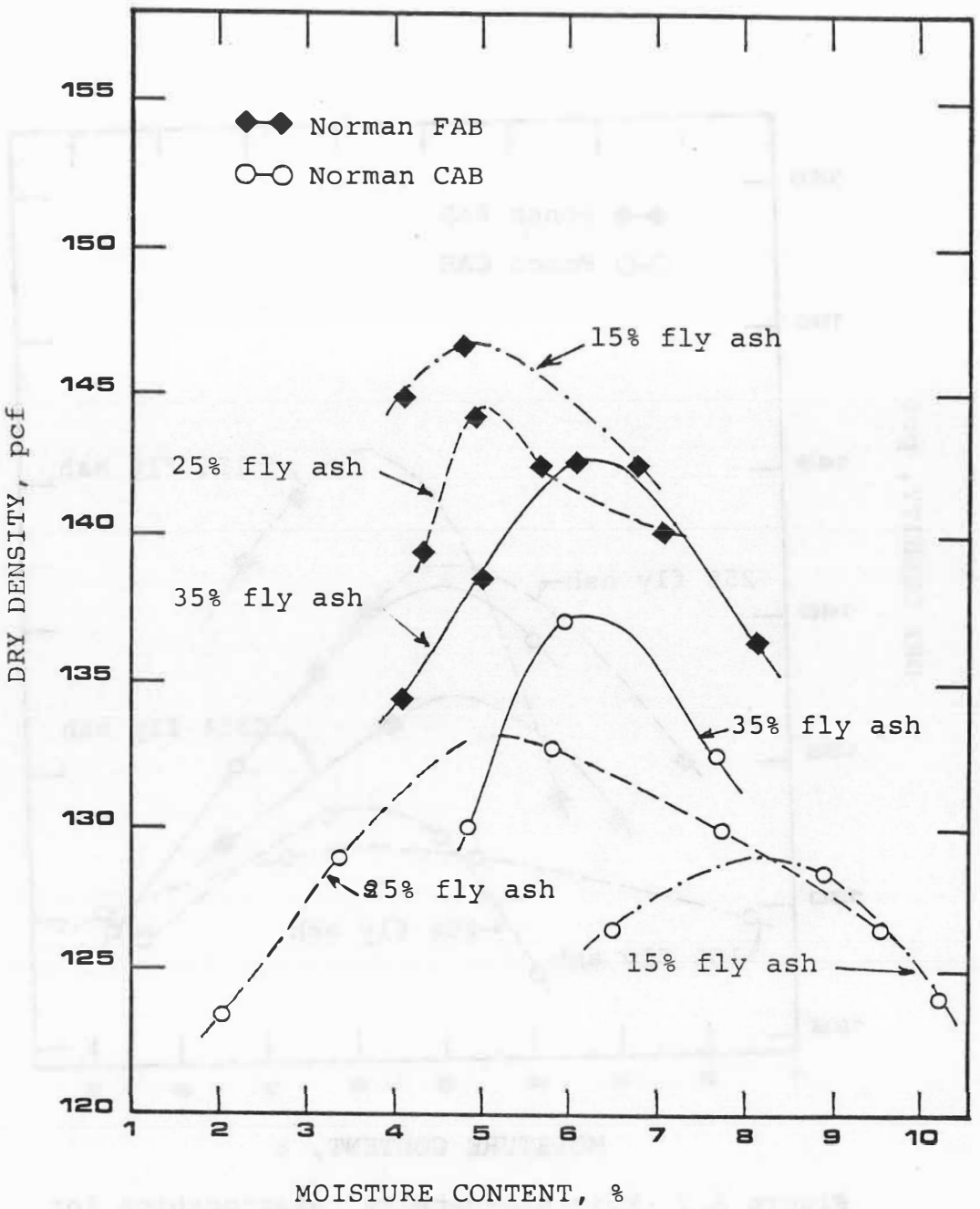

Figure A.3 Moisture-density relationships for Norman mixes

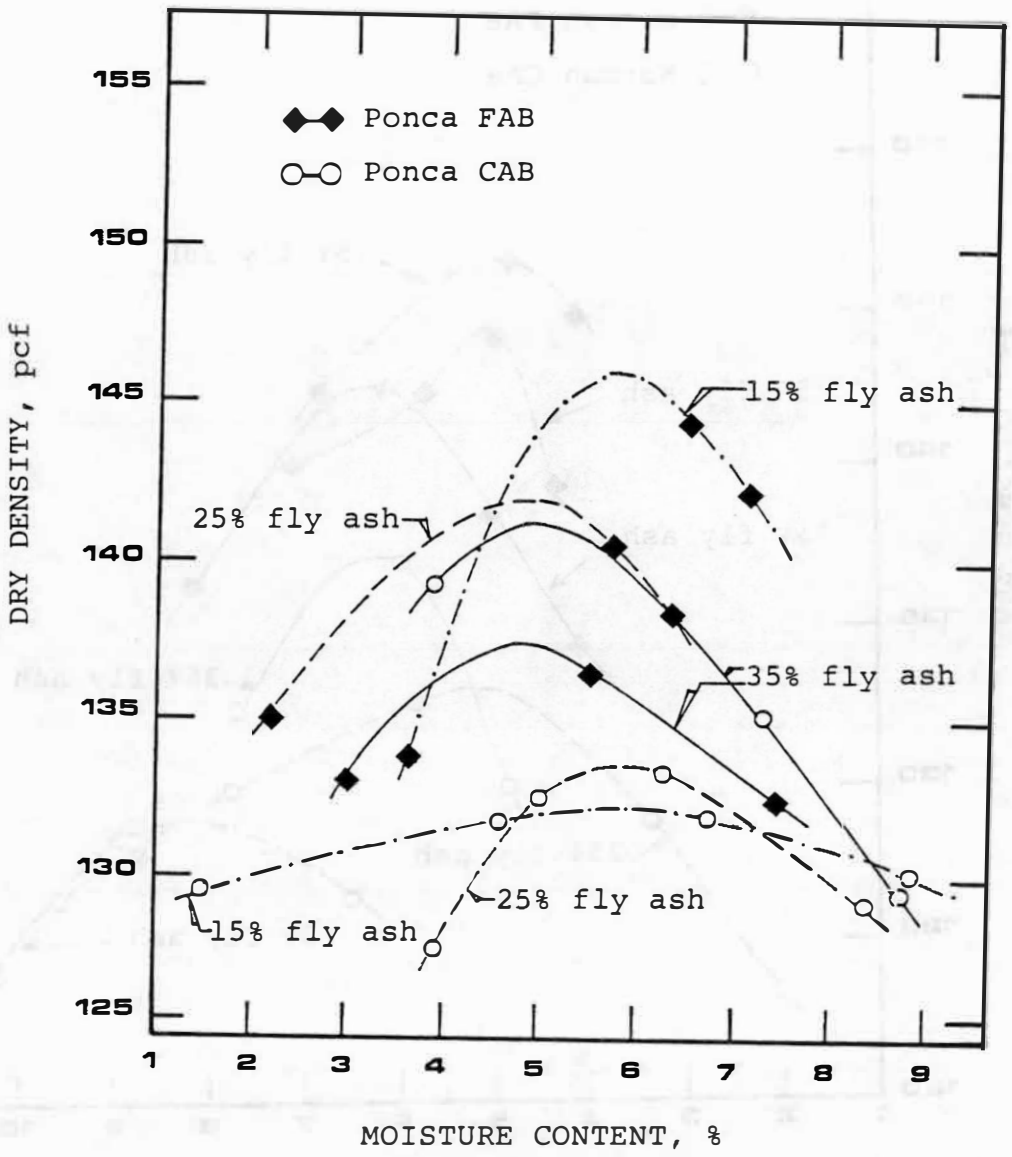

Figure A.2 Moisture-density relationships for Ponca City mixes

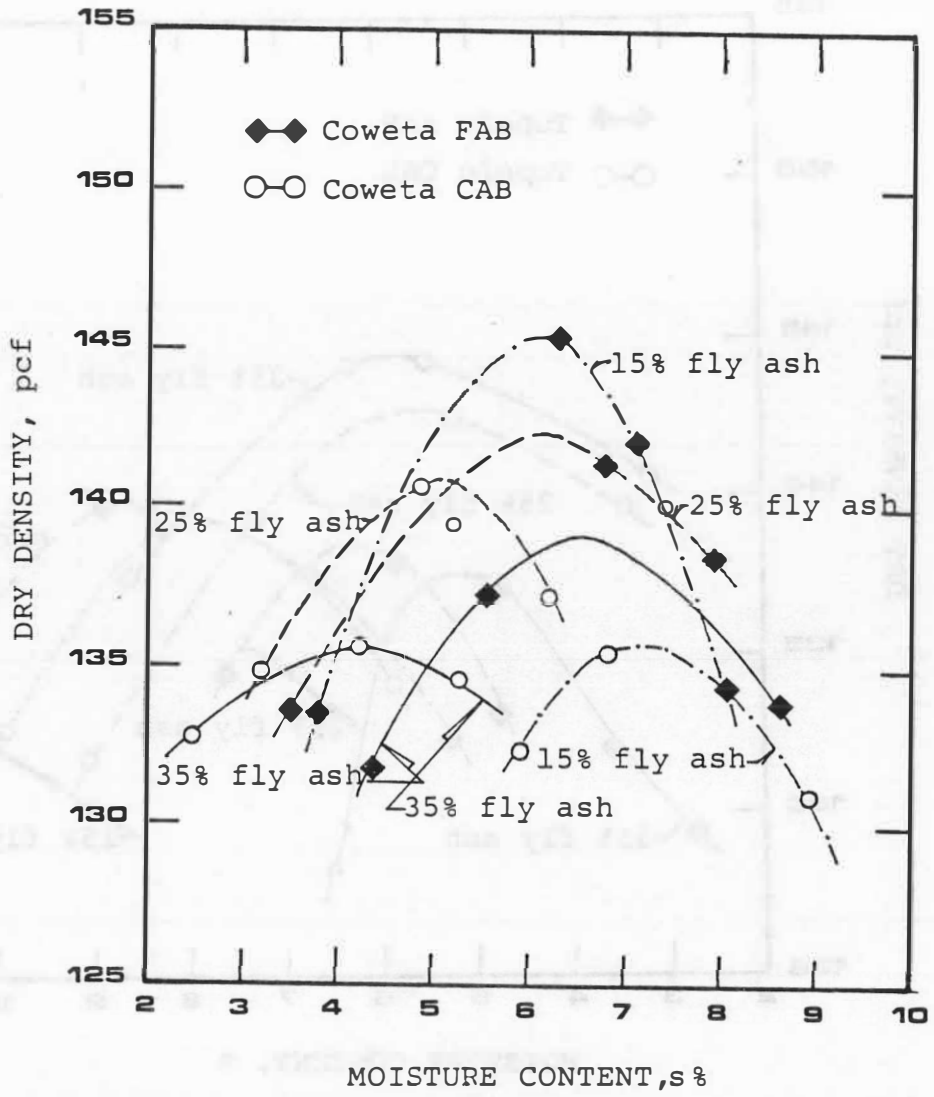

Figure A.3 Moisture-density relationships for Coweta mixes

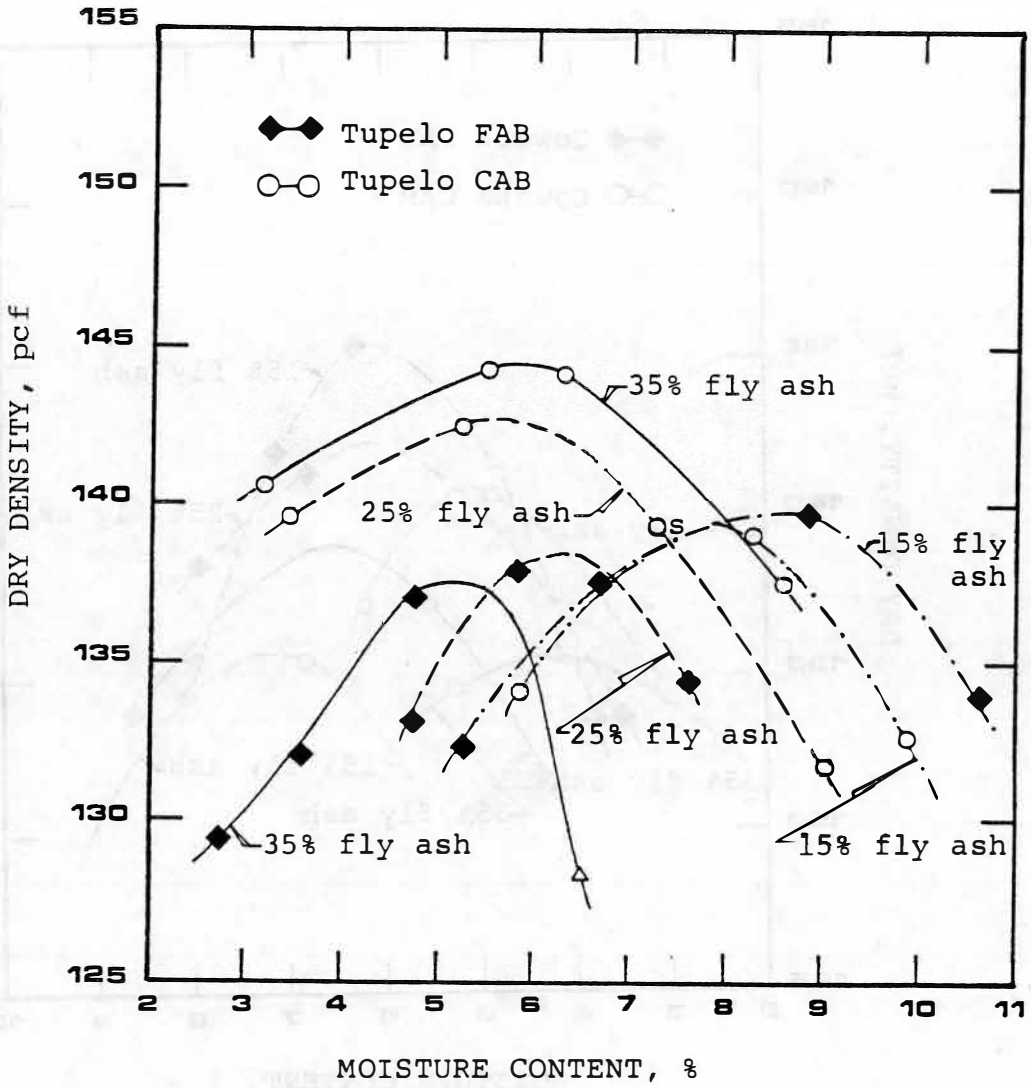

Figure A.4 Moisture-density relationships for Tupelo mixes

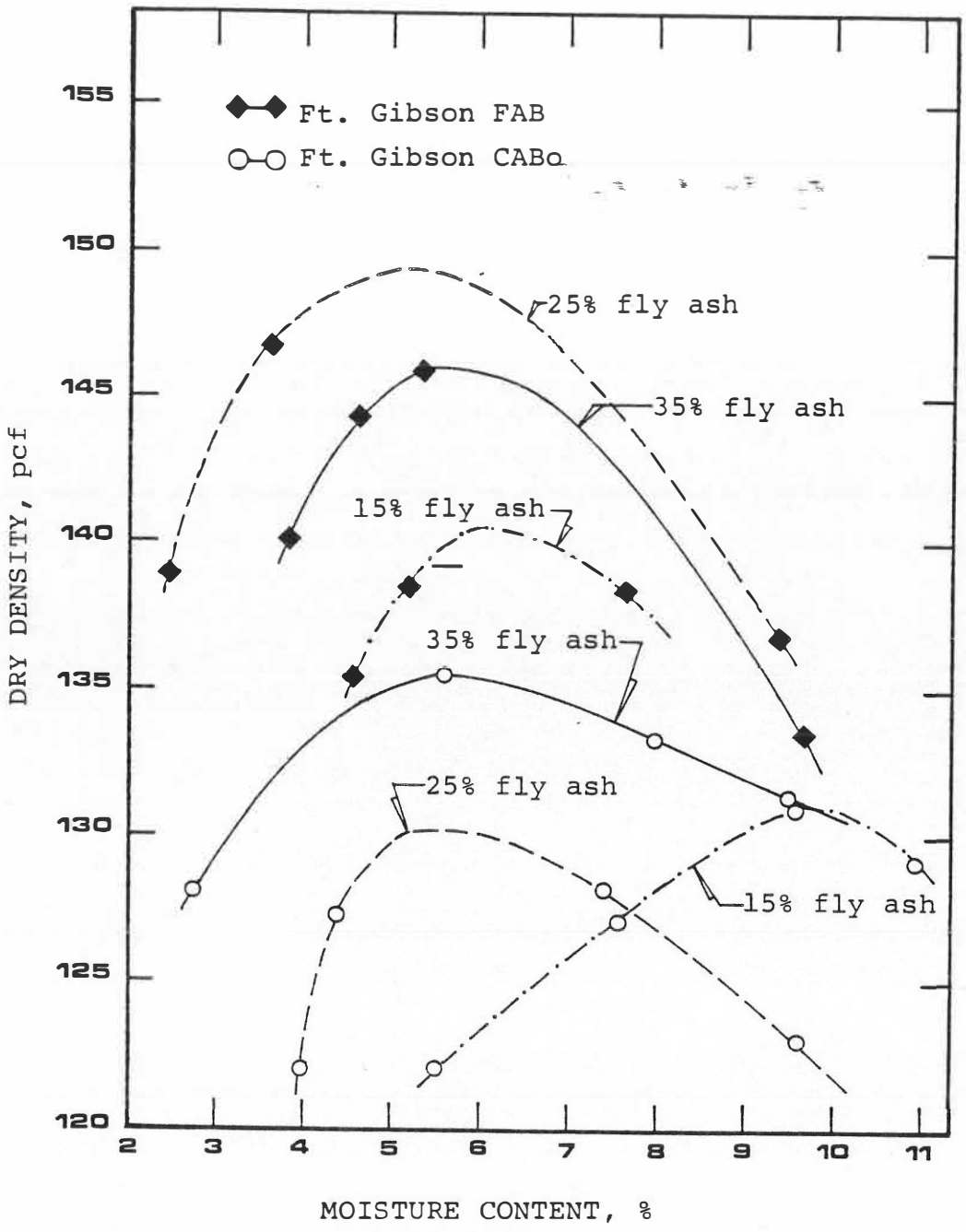

Figure A.5 Moisture-density relationships for Ft. Gibson mixes

APPENDIX B

UNCONFINED COMPRESSIVE STRENGTH

Table B.1 COMPRESSIVE STRENGTH (psi) FOR NORMAN BLENDS

Type of Mix	Moisture Content (%)	Curing Time, days						
		1	3	7	14	28	90	180
FAB +	8.2	143.2	95.5	119.4	-	354.9	114.0	397.9
15%	8.2	119.4	122.5	87.5	278.5	509.3	-	382.0
fly ash	8.2	111.4	138.5	114.6	326.3	421.8	127.3	-
		Avg. 114.1	Avg. 118.8	Avg. 107.2	Avg. 302.4	Avg. 428.7	Avg. 120.7	Avg.389.9
FAB +	5.1	676.4	622.3	417.0	254.6	1336.9	350.2	580.9
25%	5.1	795.8	461.5	385.2	278.5	442.5	238.7	700.3
fly ash	5.1	302.4	334.2	175.1	702.7	437.7	350.2	-
		Avg. 591.5	Avg. 472.7	Avg. 325.8	Avg. 411.9	Avg. 739.0	Avg. 313.0	Avg.640.6
FAB +	6.1	978.8	601.6	374.0	1408.5	1655.2	318.3	684.4
35%	6.1	477.5	376.4	278.5	1400.5	1392.6	652.5	1639.0
fly ash	6.1	461.5	358.1	202.1	1002.7	994.7	1273.2	-
		Avg. 639.2	Avg. 445.4	Avg. 285.1	Avg. 1270	Avg. 1347.5	Avg. 748.0	Avg.1161.8
CAB +	5.0	302.4	493.4	740.1	604.8[d]	461.5	573.0	525.2
15%	5.0	406.6	575.3	596.8	612.7[d]	517.3	445.6	728.1
fly ash	5.0	259.4	405.8	795.8	636.6[d]	517.3	350.1	452.6
		Avg. 322.8	Avg. 491.5	Avg. 710.9	Avg. 618.3	Avg. 498.7	Avg. 456.2	Avg. 569.0
CAB +	5.0	743.3	835.6	175.1	1464.2	970.8	1145.9	334.2
25%	5.0	536.4	994.7	318.3	847.5	1416.5	1018.6	557.1
fly ash	5.0	405.8	604.8	238.7	779.9	795.8	541.1	254.6
		Avg. 561.8	Avg. 811.7	Avg. 244.2	Avg. 1030.5	Avg. 1061.1	Avg. 901.9	Avg. 382.0
CAB +	6.2	286.5[a]	1320.9	384.2	1241.4	596.8	875.4	732.1
35%	6.2	151.2[a]	843.5	511.3	-	1233.5	724.2	708.2
fly ash	6.2	167.1[a]	628.7	-	1758.7	915.1	795.8	716.2
		Avg. 201.6	Avg. 931.0	Avg. 447.8	Avg. 1500.0	Avg. 915.2	Avg. 798.5	Avg. 718.8

a - air cured specimens

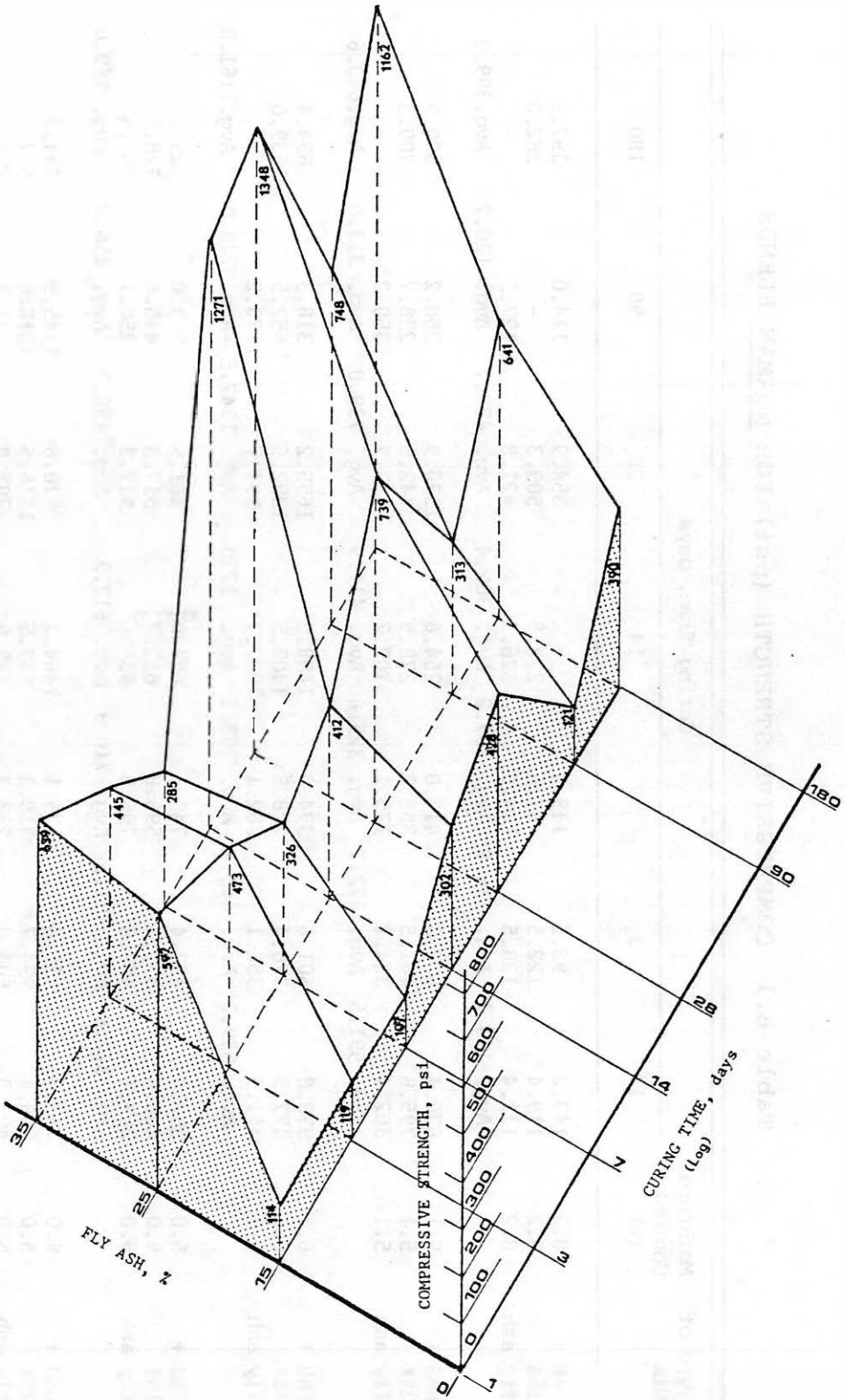

Figure 3.1 Compressive strength of Norman FAB mixes

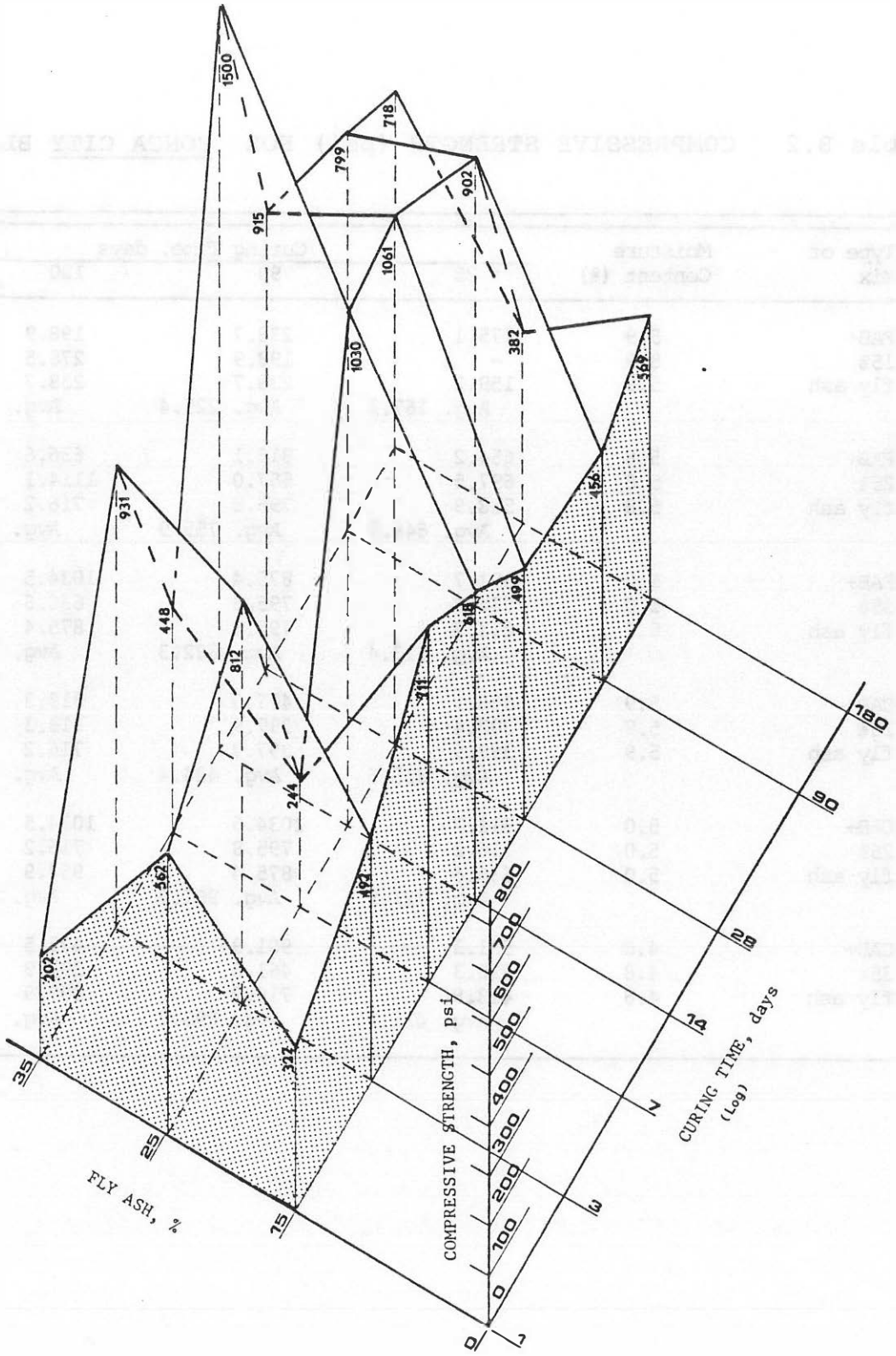

Figure B.2 Compressive strength of Norman CAB mixes

Table B.2 COMPRESSIVE STRENGTH (psi) FOR PONCA CITY BLENDS

Type of Mix	Moisture Content (%)	Curing Time, days		
		28	90	180
FAB+ 15% fly ash	5.9	175.1	238.7	198.9
	5.9	-	198.9	278.5
	5.9	159.2	238.7	238.7
		Avg. 167.2	Avg. 225.4	Avg. 238.7
FAB+ 25% fly ash	5.8	654.2	915.1	636.6
	5.8	697.5	557.0	1114.1
	5.8	558.9	795.8	716.2
		Avg. 646.9	Avg. 755.9	Avg. 822.3
FAB+ 35% fly ash	5.0	591.7	875.4	1034.5
	5.0	634.8	795.8	636.6
	5.0	613.7	795.8	875.4
		Avg. 613.4	Avg. 822.3	Avg. 848.8
CAB+ 15% fly ash	5.9	366.1	477.5	318.3
	5.9	302.4	397.9	318.3
	5.9	397.9	397.9	716.2
		Avg. 355.5	Avg. 424.4	Avg. 450.9
CAB+ 25% fly ash	5.0	811.7	1034.5	1034.5
	5.0	716.2	795.8	716.2
	5.0	636.6	875.4	954.9
		Avg. 721.5	Avg. 901.9	Avg. 901.9
CAB+ 35% fly ash	4.8	501.3	901.9	477.5
	4.8	318.3	461.6	397.9
	4.8	413.8	716.2	397.9
		Avg. 411.1	Avg. 693.2	Avg. 424.4

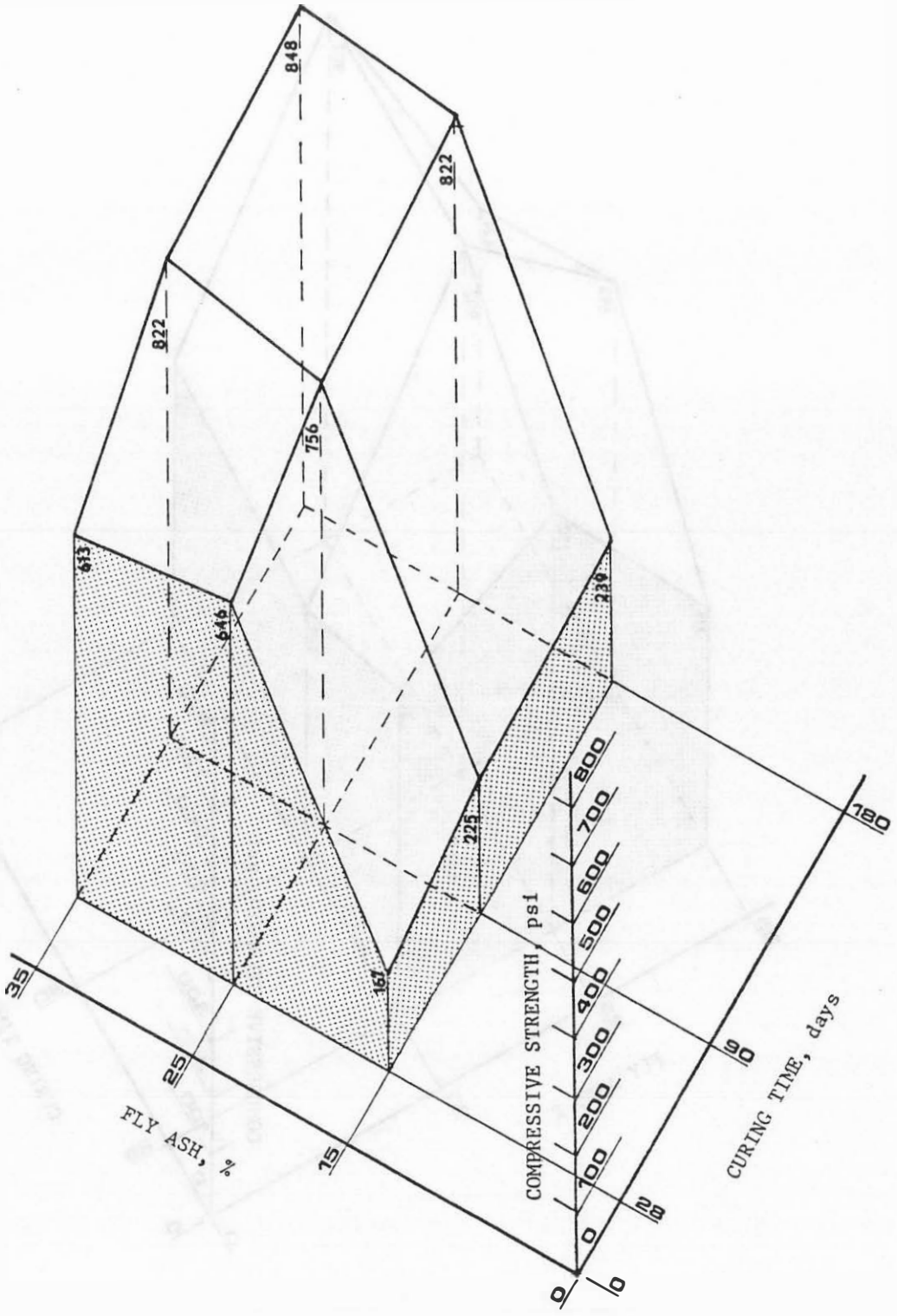

Figure B.3 Compressive strength of Ponca City FAB mixes

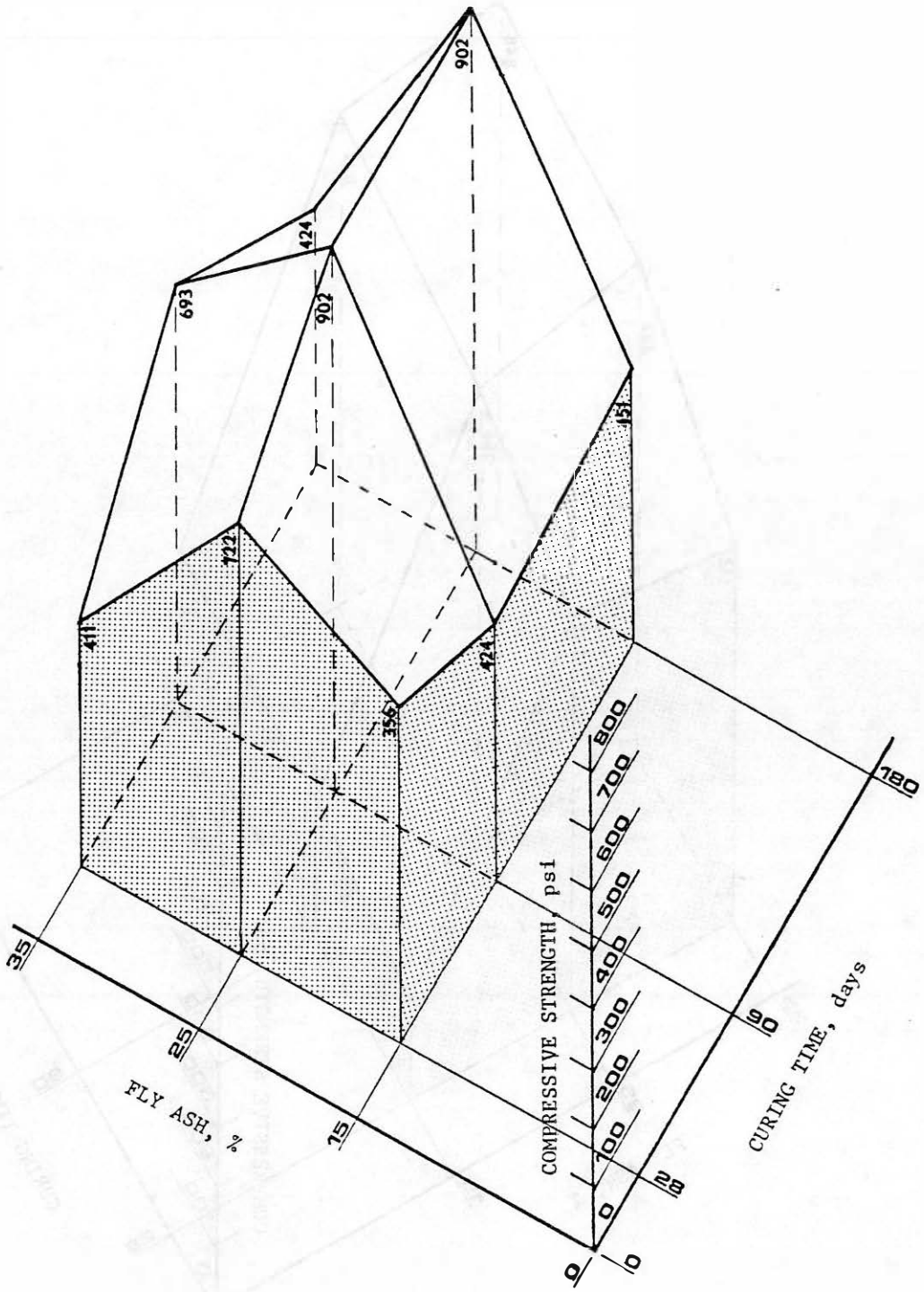

Figure B.4 Compressive strength of Ponca City CAB mixes

Table B.3 COMPRESSIVE STRENGTH (psi) FOR COWETA BLENDS

Type of Mix	Moisture Content (%)	Curing Time, days 28	90	180
FAB+	7.1	31.8	127.0	159.2
15%	7.1	55.7	95.0	143.2
fly ash	7.1	95.5	48.0	119.4
		Avg. 61.0	Avg. 90.0	Avg. 140.6
FAB+	5.2	95.5	191.0	318.3
25%	5.2	95.5	207.0	326.3
fly ash	5.2	111.4	143.0	397.9
		Avg. 100.8	Avg. 180.0	Avg. 347.6
FAB+	4.3	334.2	509.0	477.5
35%	4.3	381.9	286.0	509.3
fly ash	4.3	413.8	493.0	557.0
		Avg. 376.6	Avg. 429.0	Avg. 514.6
CAB+	6.1	286.5	318.3	270.6
15%	6.1	175.1	191.0	214.9
fly ash	6.1	191.0	238.7	318.3
		Avg. 217.5	Avg. 249.3	Avg. 267.9
CAB+	6.2	318.3	334.2	397.9
25%	6.2	206.9	270.6	795.8
fly ash	6.2	254.6	350.1	636.6
		Avg. 259.9	Avg. 318.3	Avg.610.1
CAB+	6.4	397.9	668.5	636.6
35%	6.4	238.7	477.5	797.9
fly ash	6.4	286.5	477.5	557.0
		Avg. 307.7	Avg. 541.2	Avg. 530.5

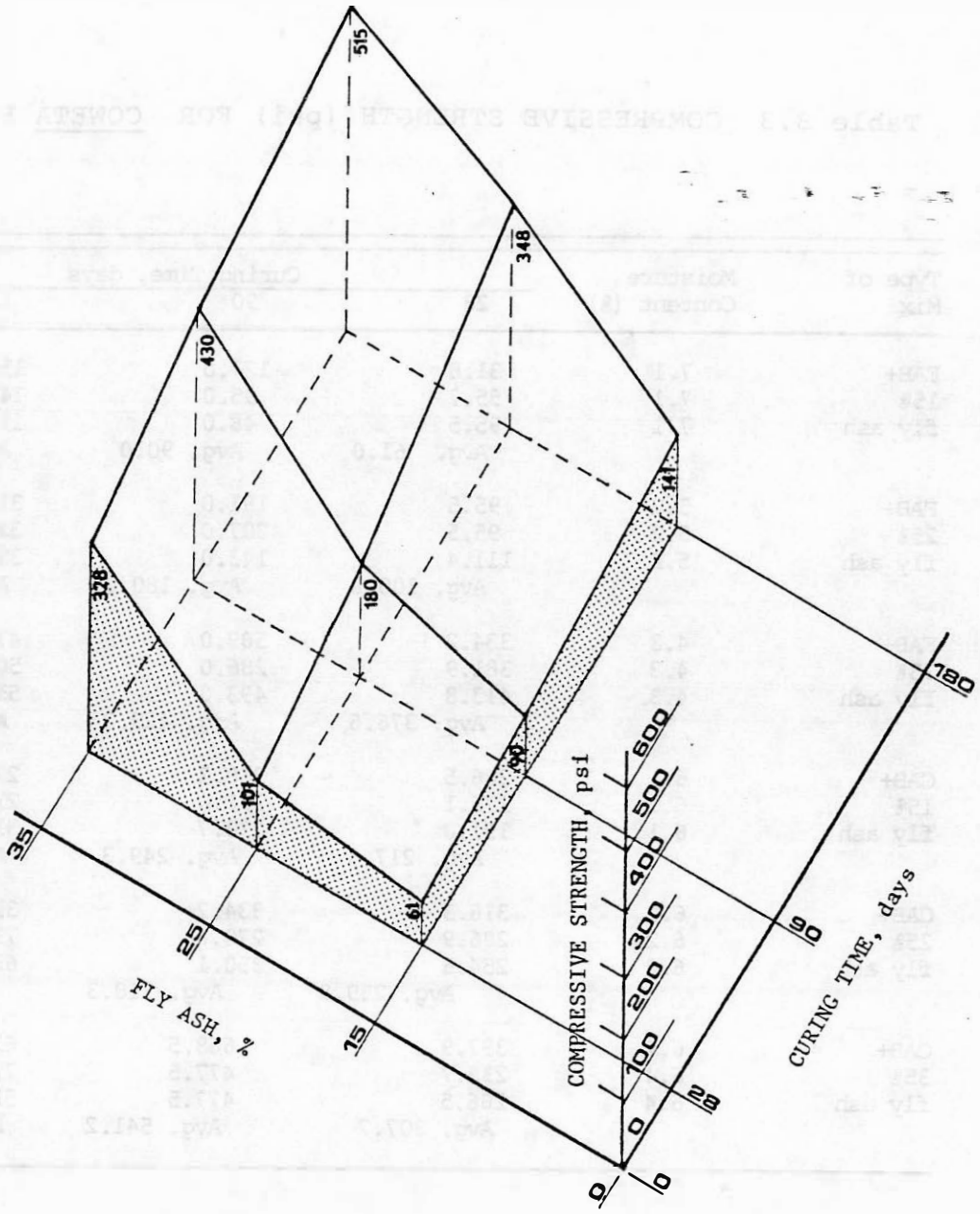

Figure B.5 Compressive strength of Coweta FAB mixes

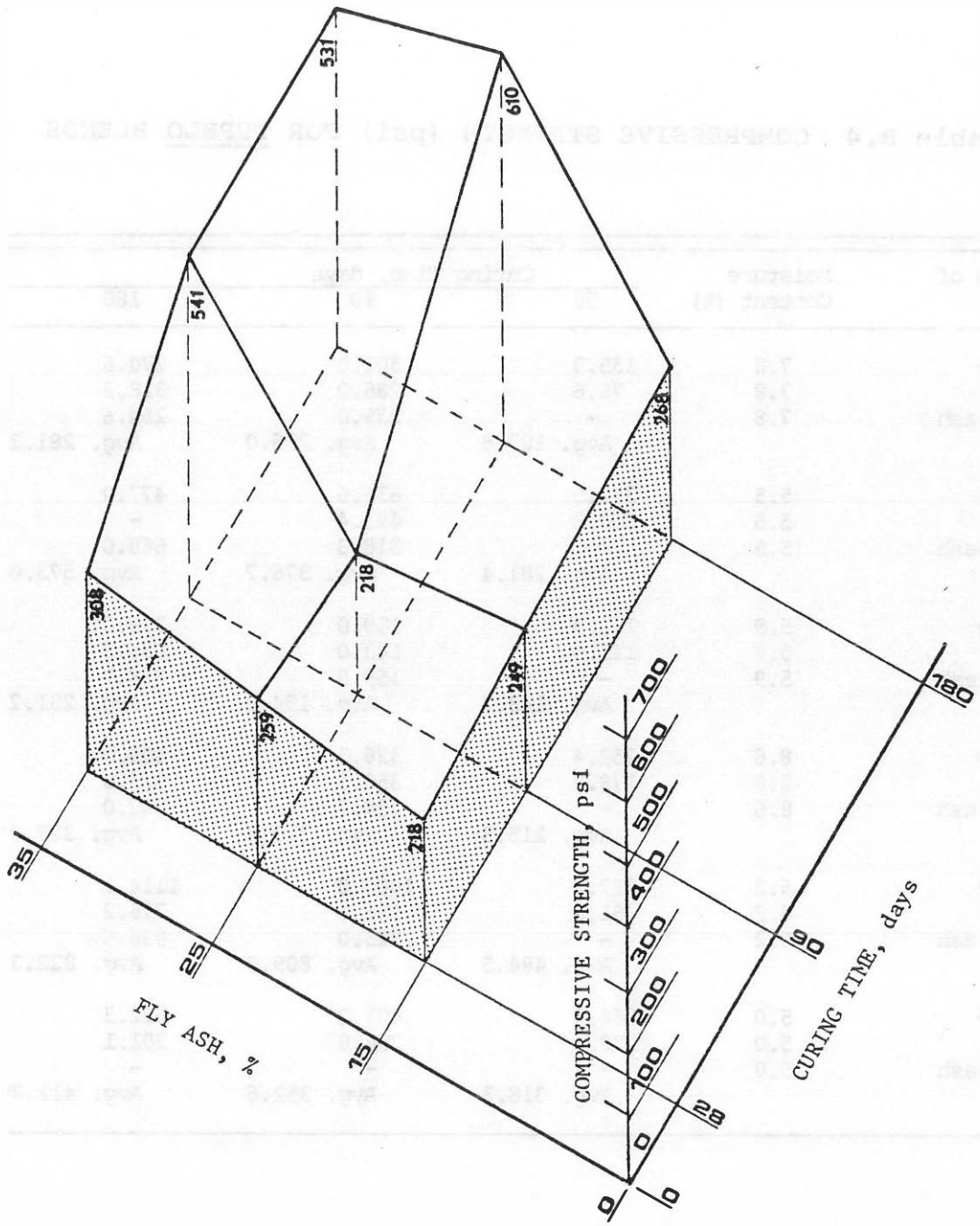

Figure B.5 Compressive strength of Coweta CAB mixes

Table B.4 COMPRESSIVE STRENGTH (psi) FOR TUPELO BLENDS

Type of Mix	Moisture Content (%)	Curing Time, days 28	90	180
FAB+	7.8	135.3	302.0	270.6
15%	7.8	79.6	286.0	318.3
fly ash	7.8	-	239.0	254.6
		Avg. 107.5	Avg. 276.0	Avg. 281.2
FAB+	5.5	312.5	636.6	477.0
25%	5.5	250.3	493.4	-
fly ash	5.5	-	318.3	668.0
		Avg. 281.4	Avg. 376.7	Avg. 573.0
FAB+	5.9	161.9	159.0	318.3
35%	5.9	125.5	143.0	286.5
fly ash	5.9	-	159.0	238.7
		Avg. 143.7	Avg. 154.0	Avg. 281.2
CAB+	8.6	252.4	326.3	406.0
15%	8.6	178.2	350.1	374.0
fly ash	8.6	-	254.7	382.0
		Avg. 215.3	Avg. 310.4	Avg. 387.0
CAB+	6.2	517.2	1066.0	1114.1
25%	6.2	451.8	836.0	716.2
fly ash	6.2	-	525.0	636.6
		Avg. 484.5	Avg. 809.0	Avg. 822.3
CAB+	5.0	364.2	407.2	522.3
35%	5.0	272.4	298.0	301.1
fly ash	5.0	-	-	-
		Avg. 318.3	Avg. 352.6	Avg. 411.7

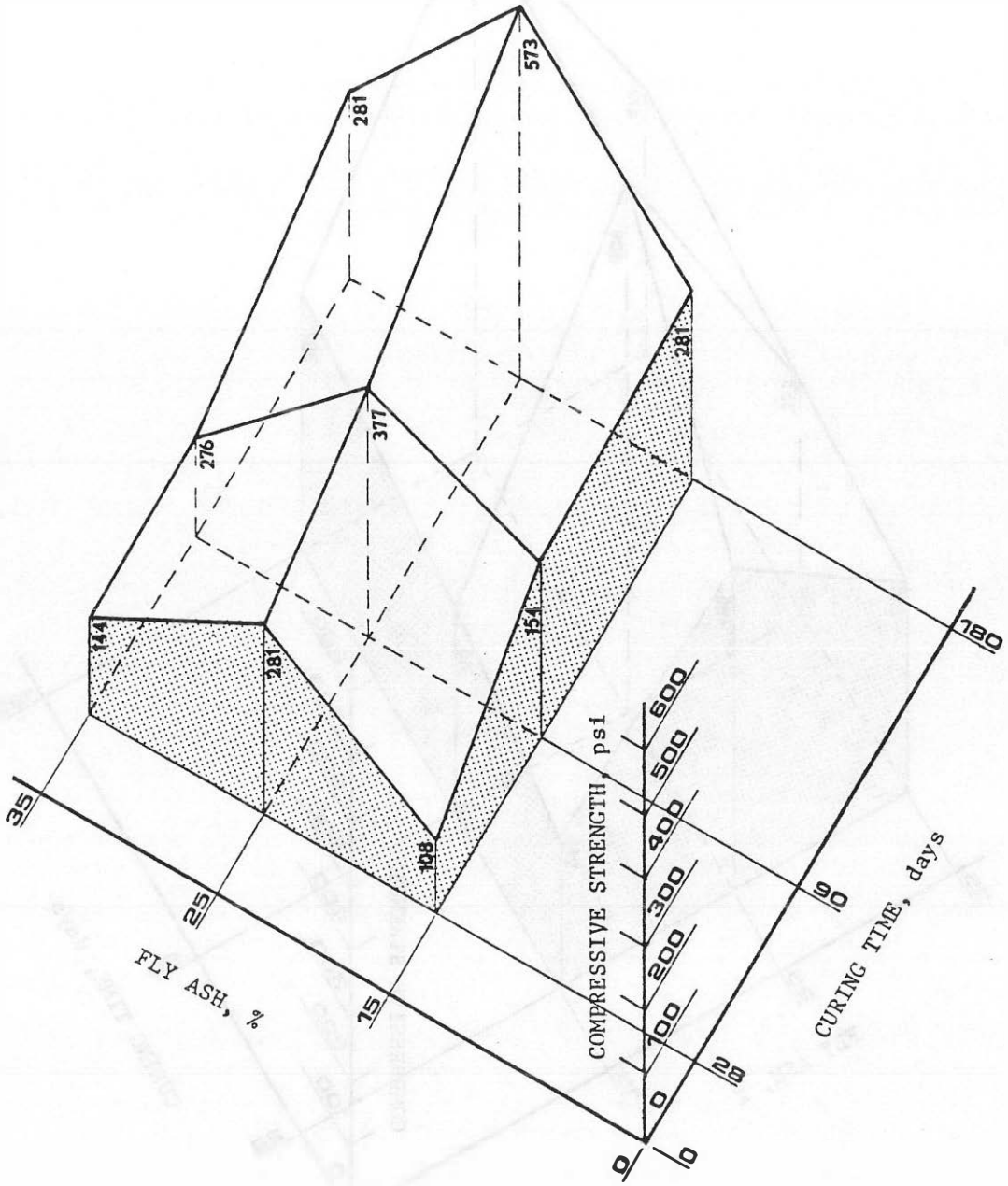

Figure B.3 Compressive strength of Tupelo FAB mixes

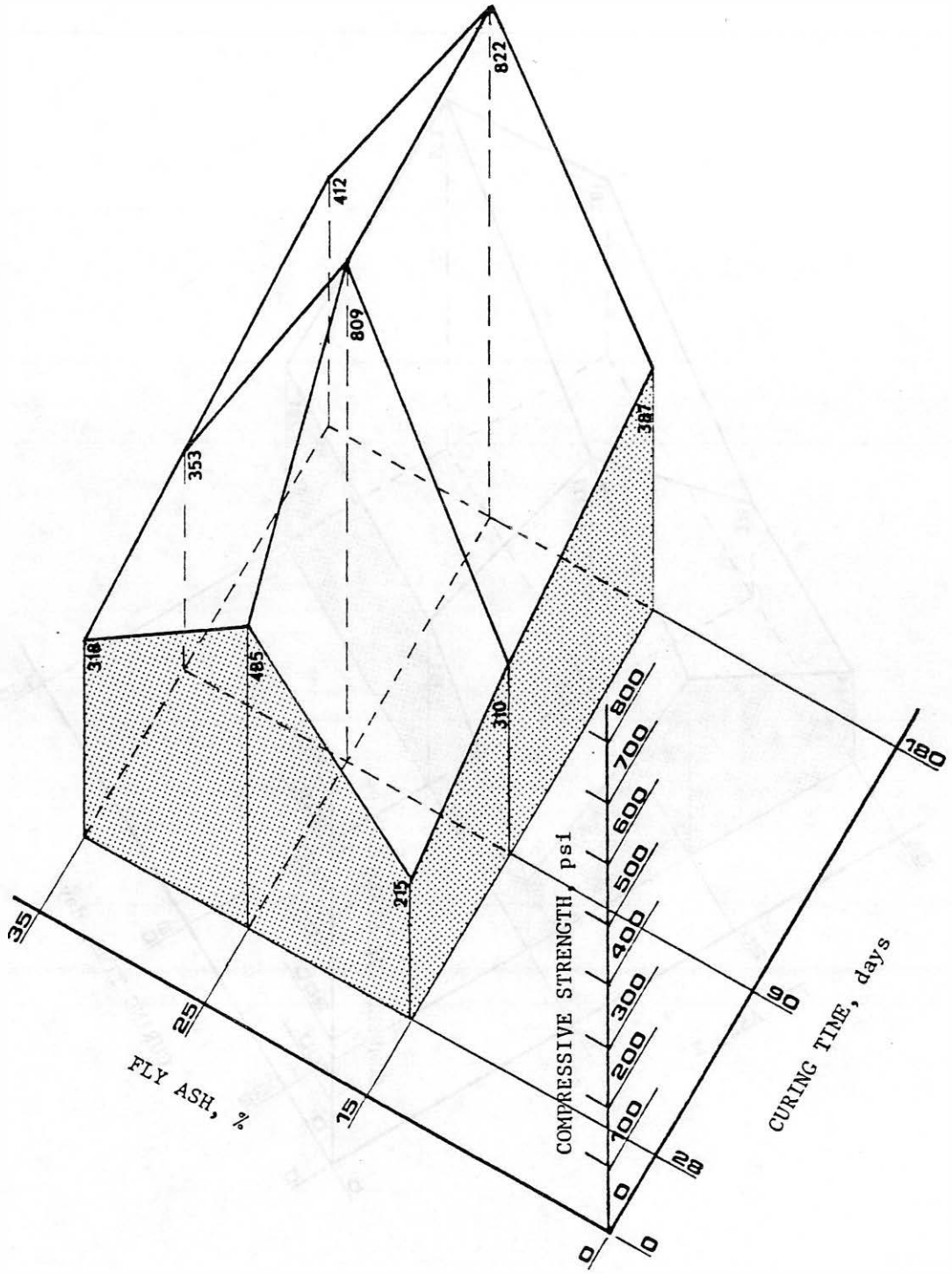

Figure B.8 Compressive strength of Tupelo CAB mixes

Table B.5 COMPRESSIVE STRENGTH (psi) FOR FT. GIBSON BLENDS

Type of Mix	Moisture Content (%)	Curing Time, days		
		28	90	180
FAB+	9.9	159.2	159.2	238.7
15%	9.9	159.2	159.2	238.7
fly ash	9.9	159.2	119.2	198.9
		Avg. 159.2	Avg. 145.9	Avg. 225.4
FAB+	5.3	318.3	596.8	954.9
25%	5.3	381.9	477.5	716.2
fly ash	5.3	302.4	557.1	477.5
		Avg. 334.2	Avg. 543.8	Avg. 716.2
FAB+	5.4	366.0	636.6	795.8
35%	5.4	302.4	557.1	1114.1
fly ash	5.4	254.6	636.6	954.9
		Avg. 307.7	Avg. 610.1	Avg. 954.9
CAB+	6.0	366.1	477.5	915.1
15%	6.0	366.1	716.2	477.5
fly ash	6.0	-	-	795.8
		Avg. 366.1	Avg. 596.9	Avg. 729.5
CAB+	5.2	1480.0	557.1	1273.2
25%	5.2	1082.0	557.1	557.1
fly ash	5.2	-	1432.4	1671.1
		Avg.1281.0	Avg. 848.9	Avg.1167.1
CAB+	5.8	875.0	716.2	1432.4
35%	5.8	446.0	875.4	397.9
fly ash	5.8	796.0	397.9	1114.1
		Avg. 706.0	Avg. 663.2	Avg. 981.5

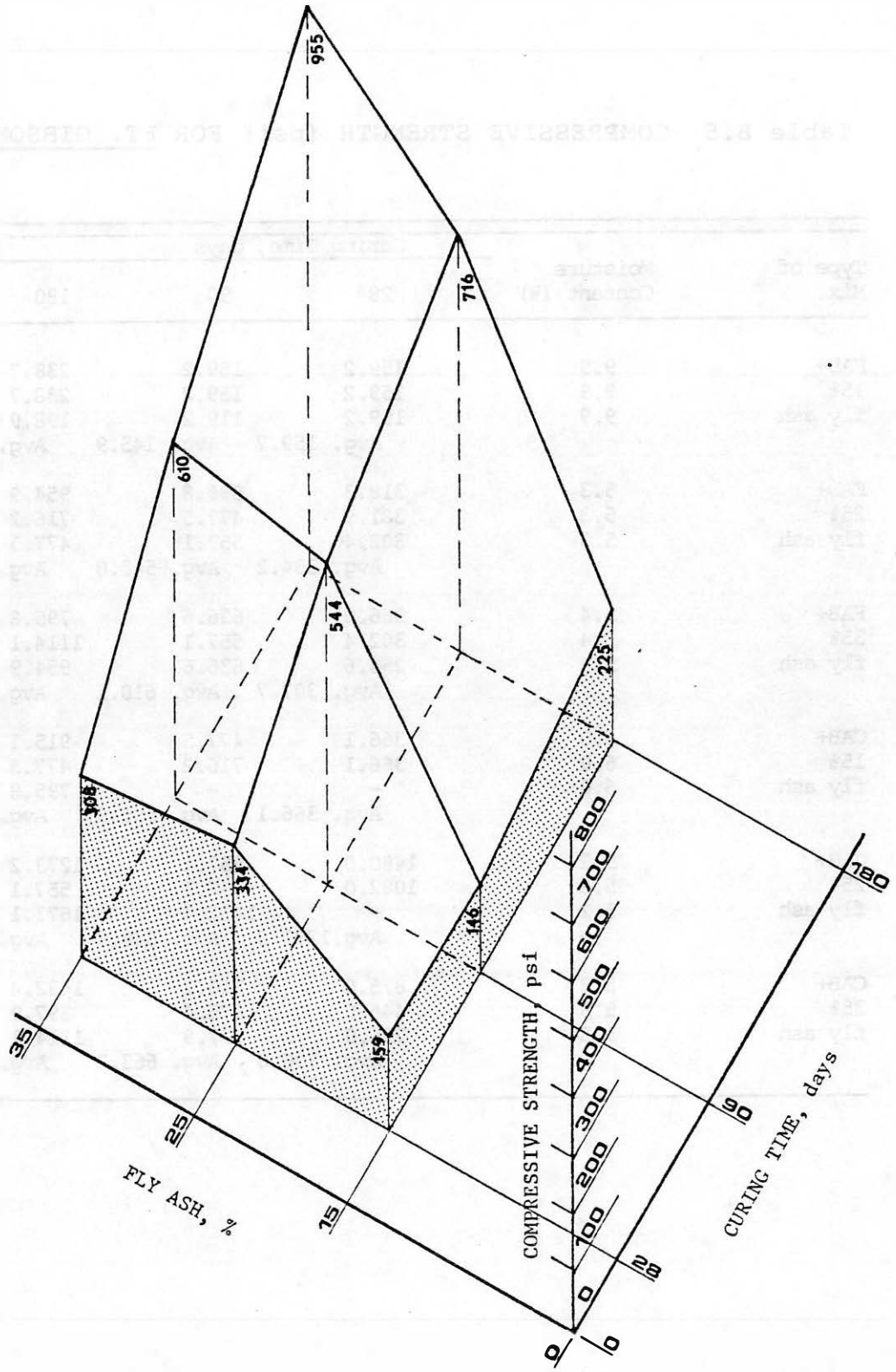

Figure B.9 Compressive strength of Ft. Gibson FAB mixes

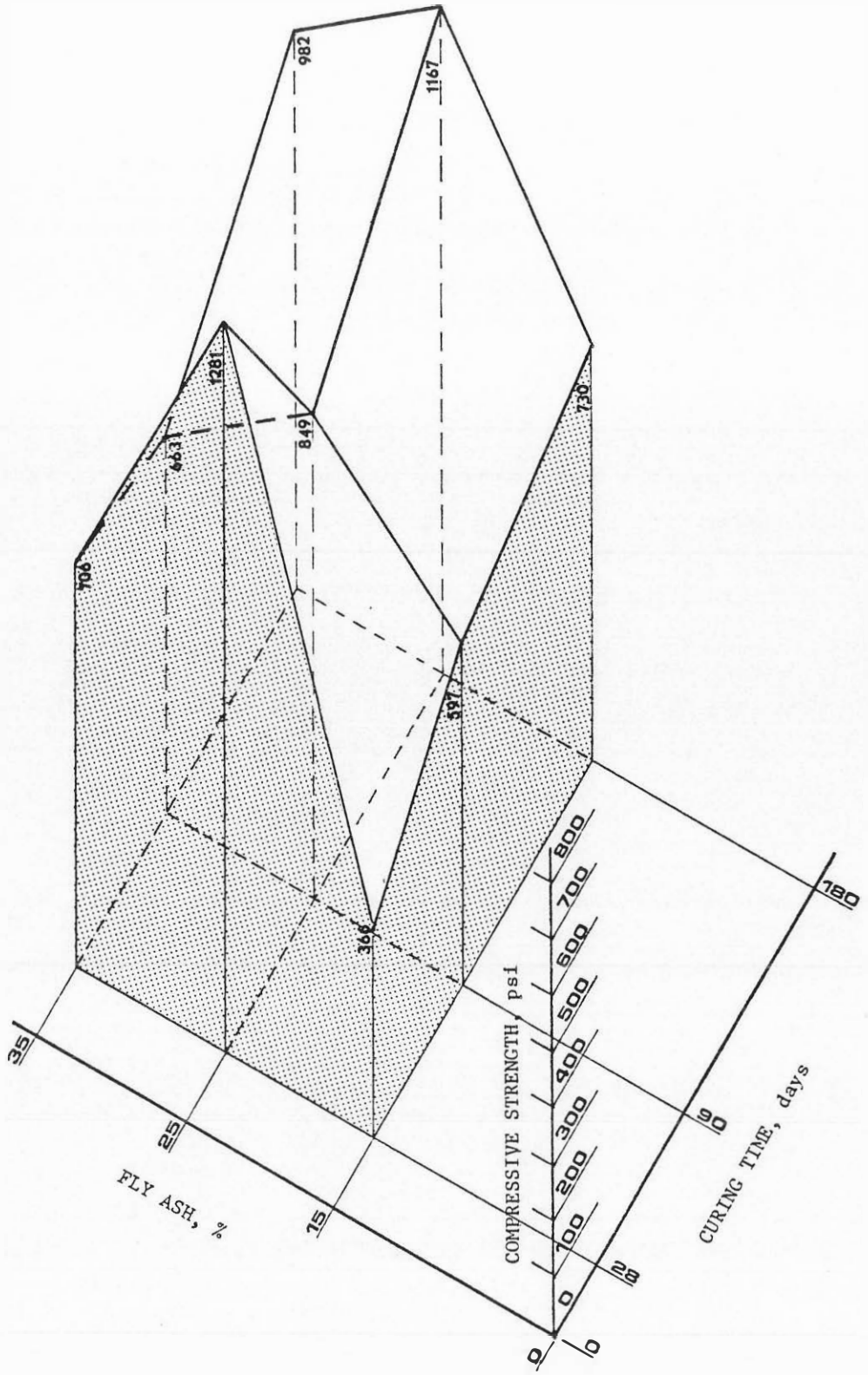

Figure B.10 Compressive strength of Ft. Gibson CAB mixes

APPENDIX C

LOAD-DEFLECTION CURVES FOR BEAMS CURED FOR 90 DAYS

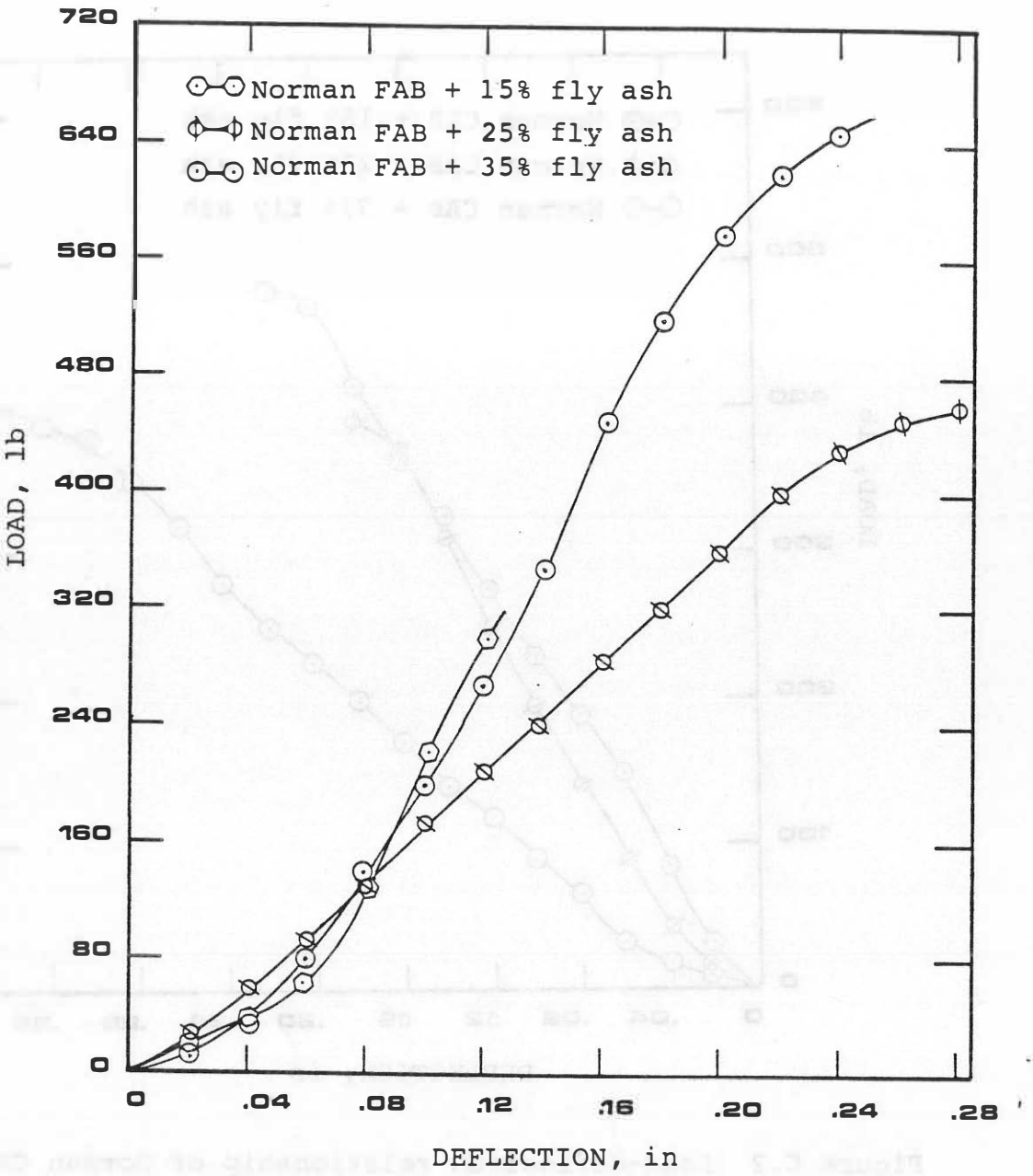

Figure C.3 Load-deflection relationship of Norman FAB

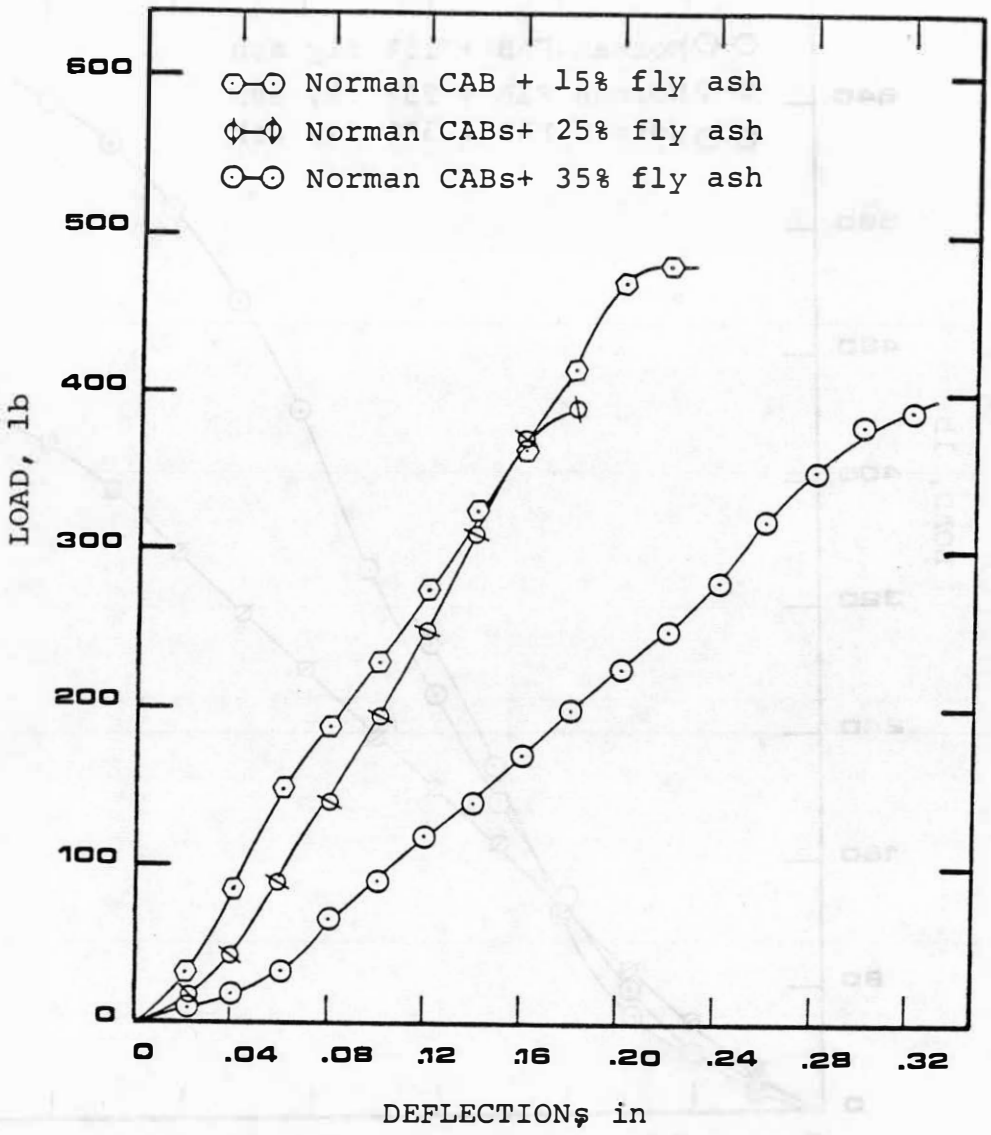

Figure C.2 Load-deflection relationship of Norman CAB

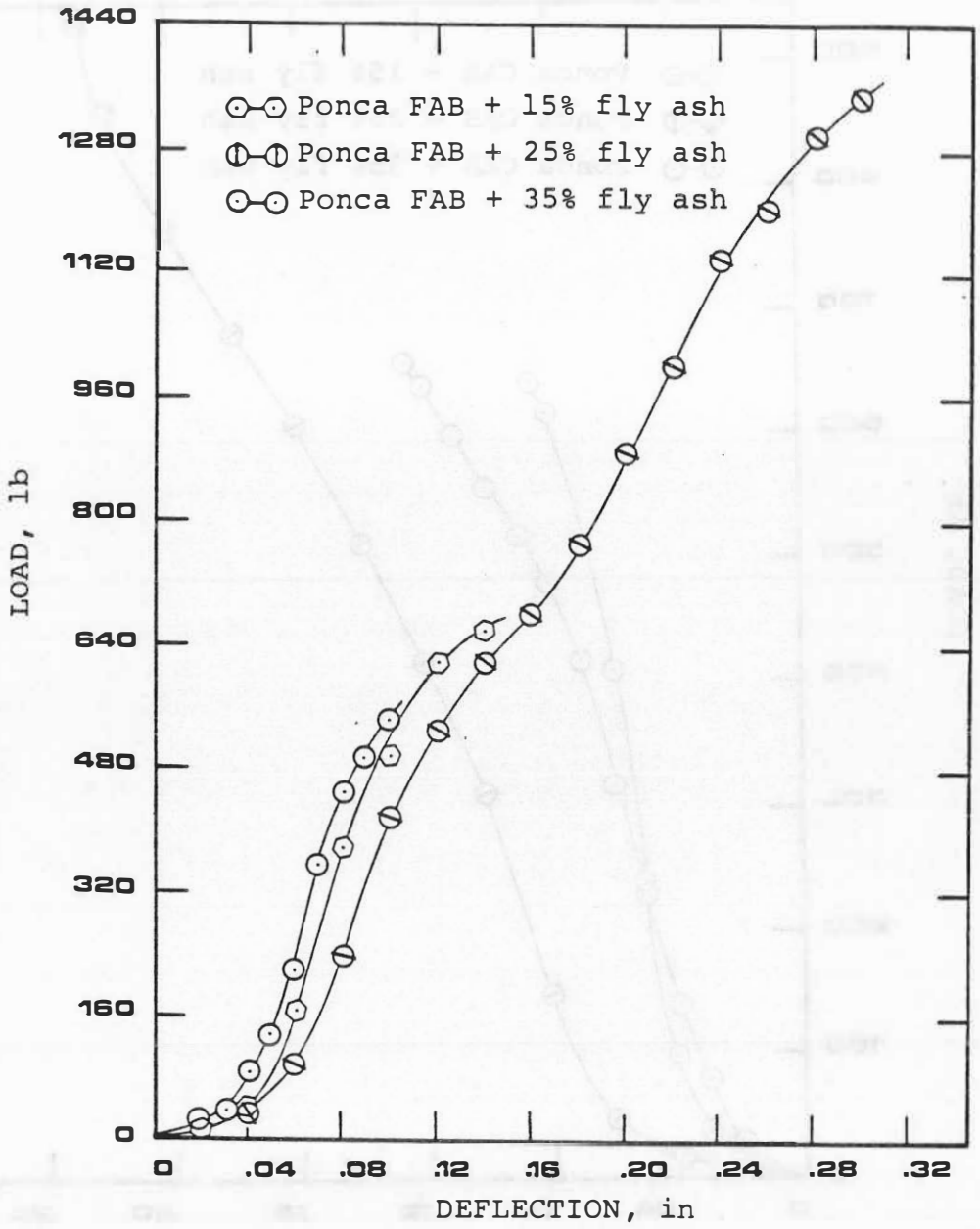

Figure C.3 Load-deflection relationship of Ponca City FAB

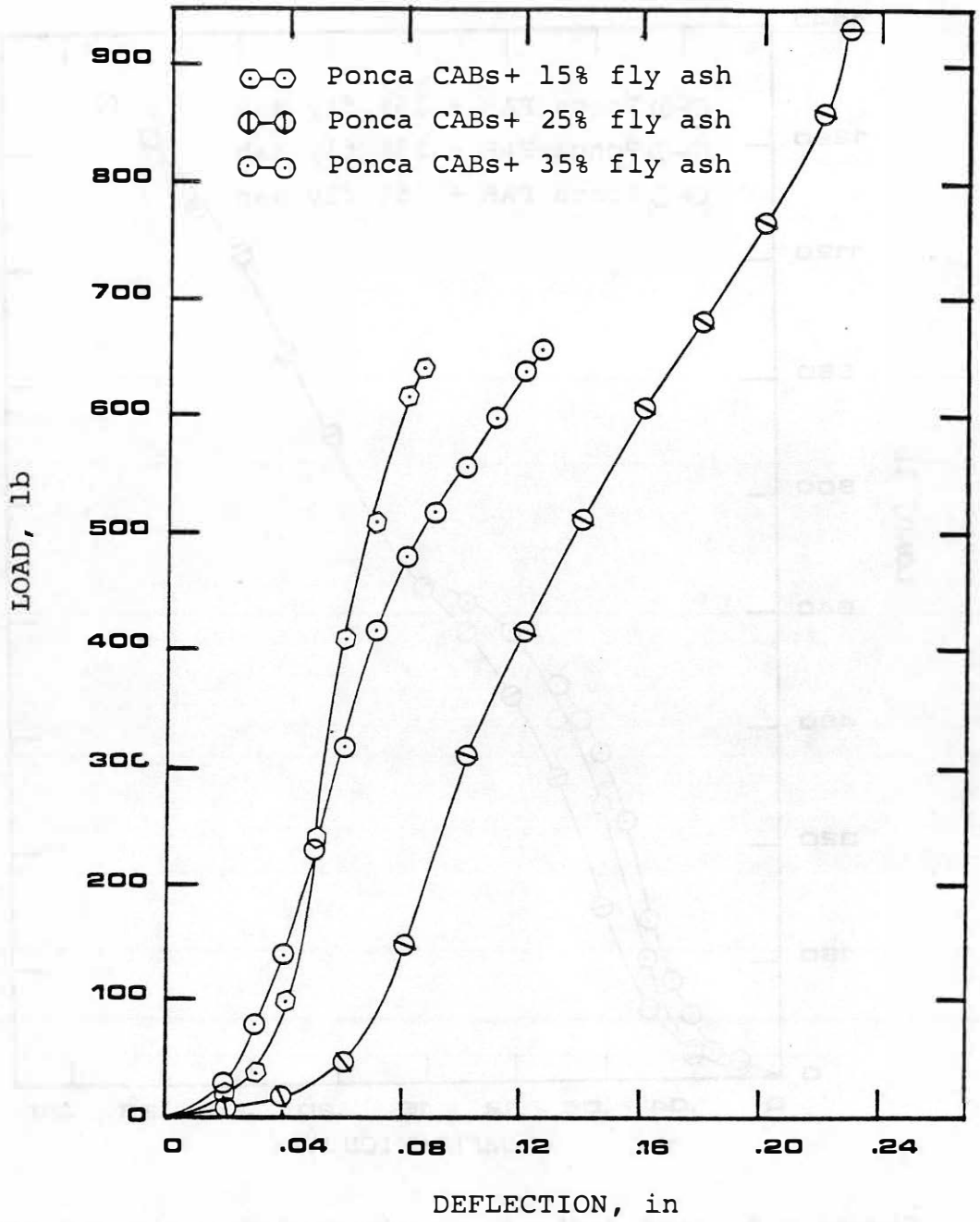

Figure C.4 Load-deflection relationship of Ponca City CAB

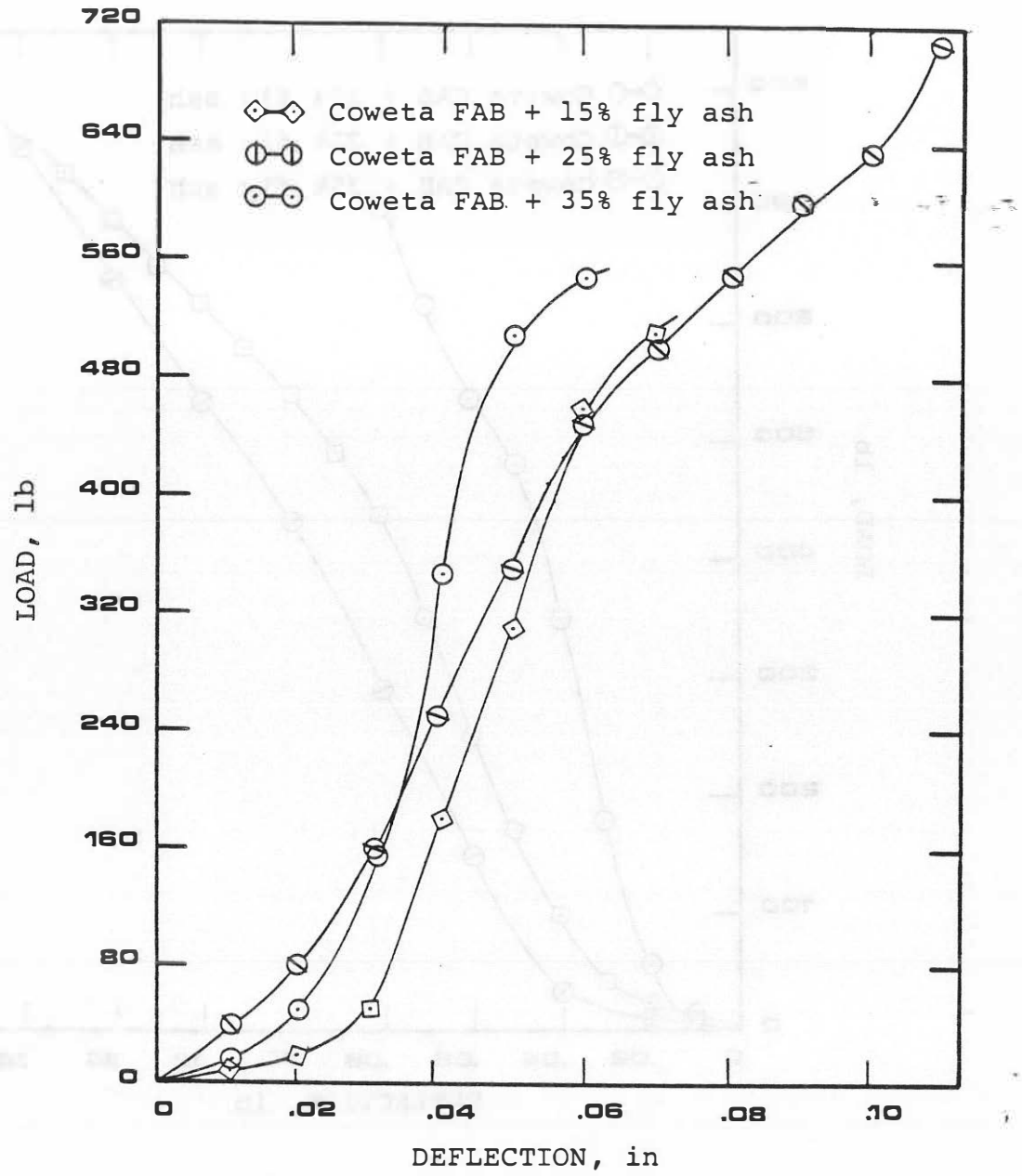

Figure C.5 Load-deflection relationship of Coweta FAB

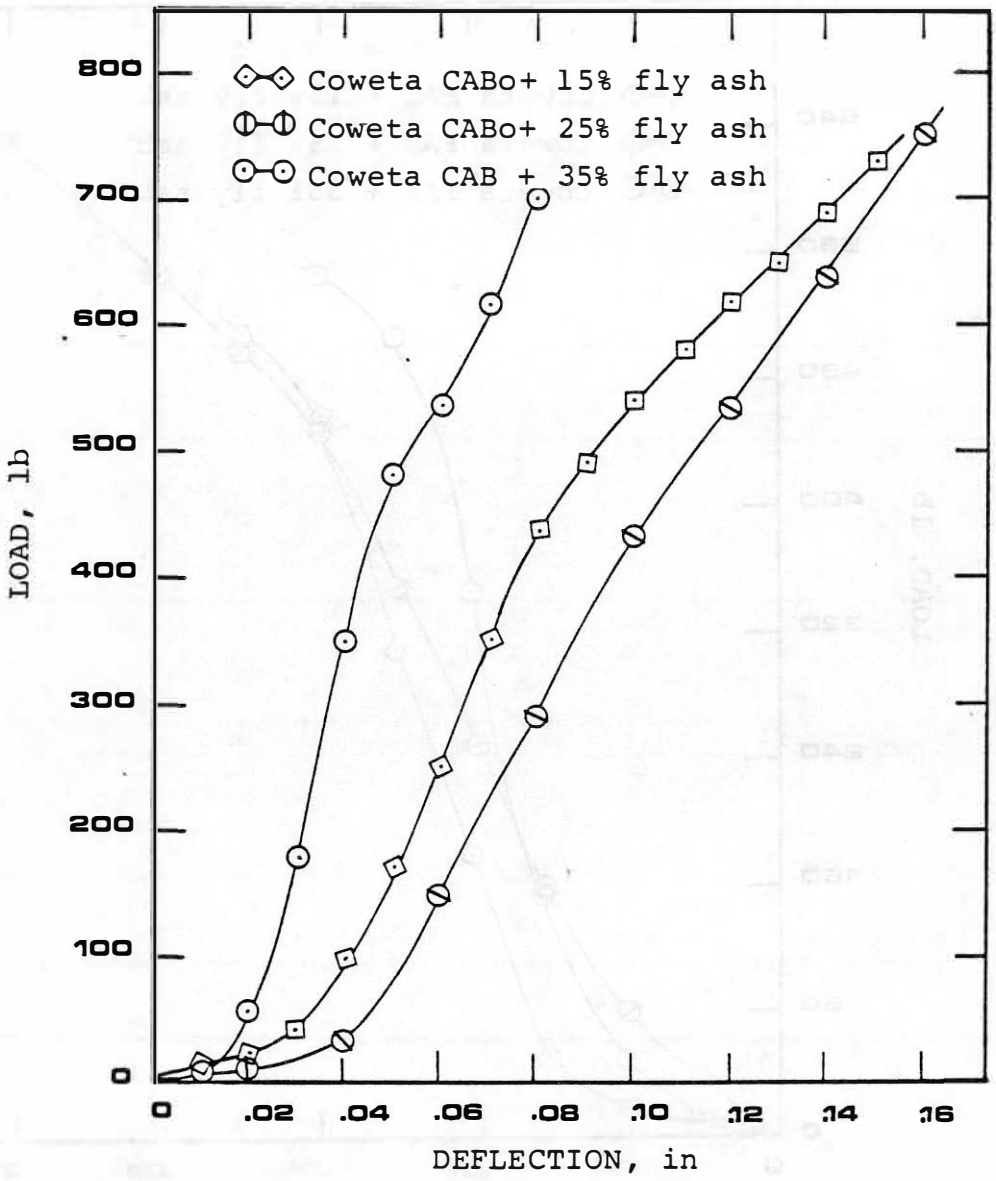

Figure C.6 Load-deflection relationship of Coweta CAB

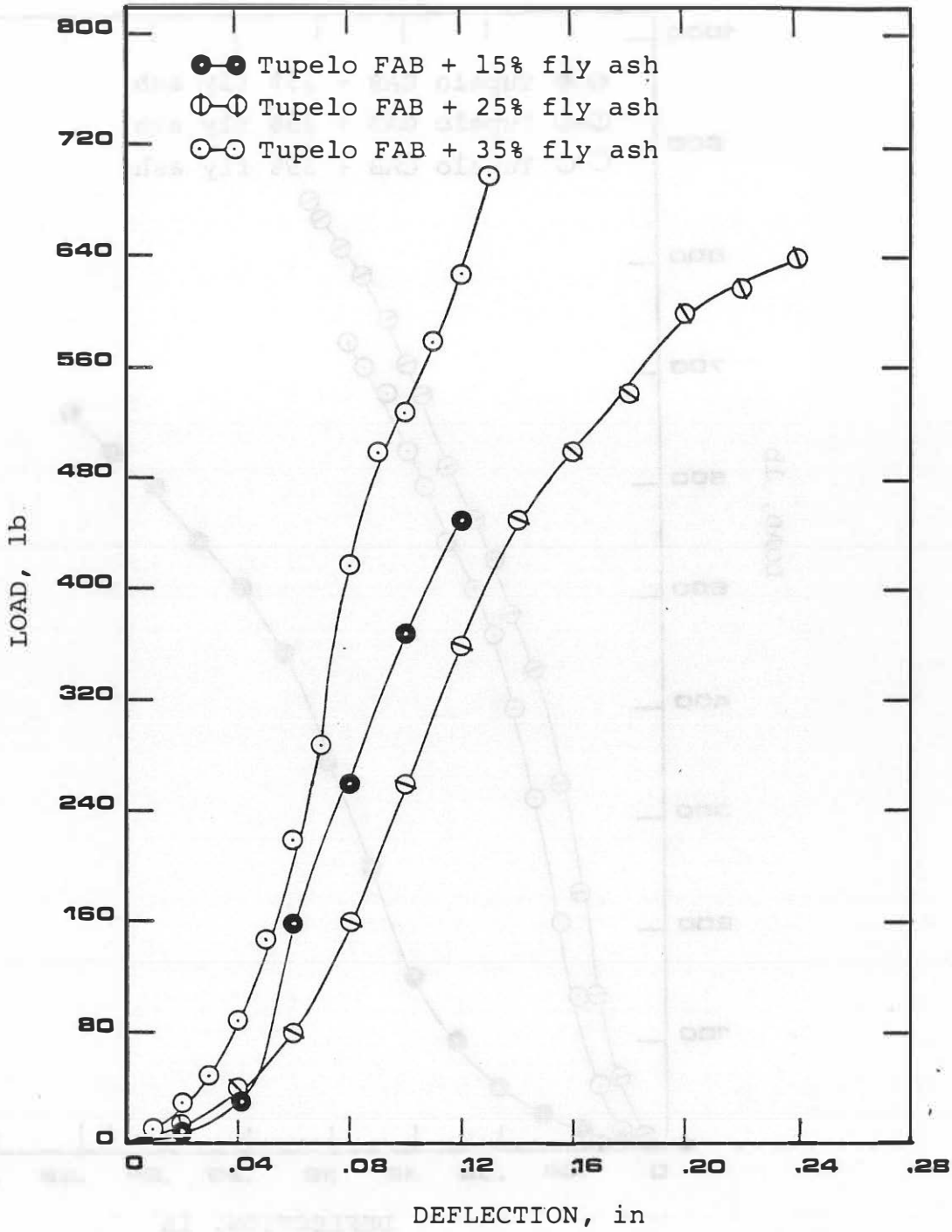

Figure C.37 Load-deflection relationship of Tupelo FAB

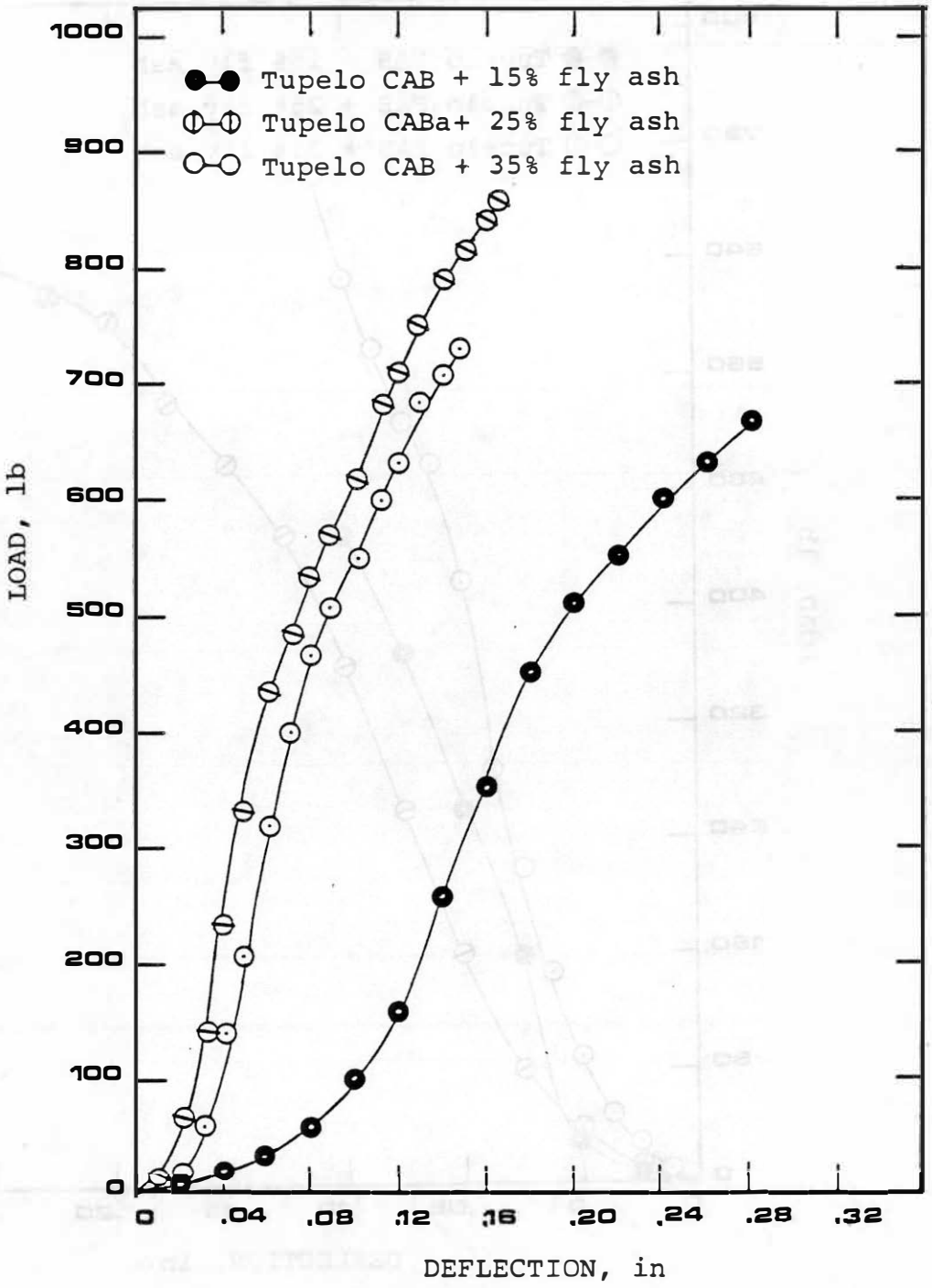

Figure C.8 Load-deflection relationship of Tupelo CAB

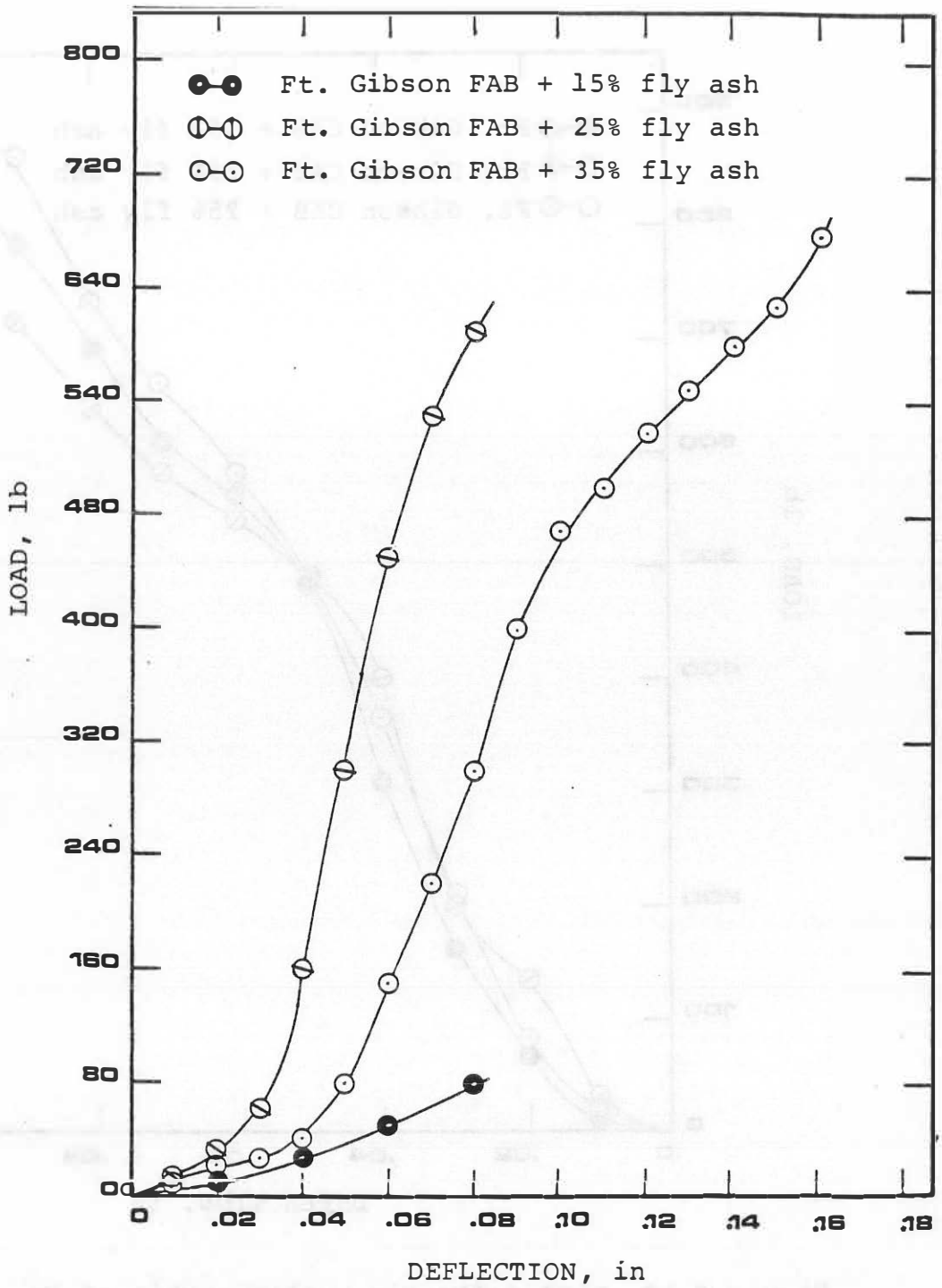

Figure C.9 Load-deflection relationship of Ft. Gibson FAB

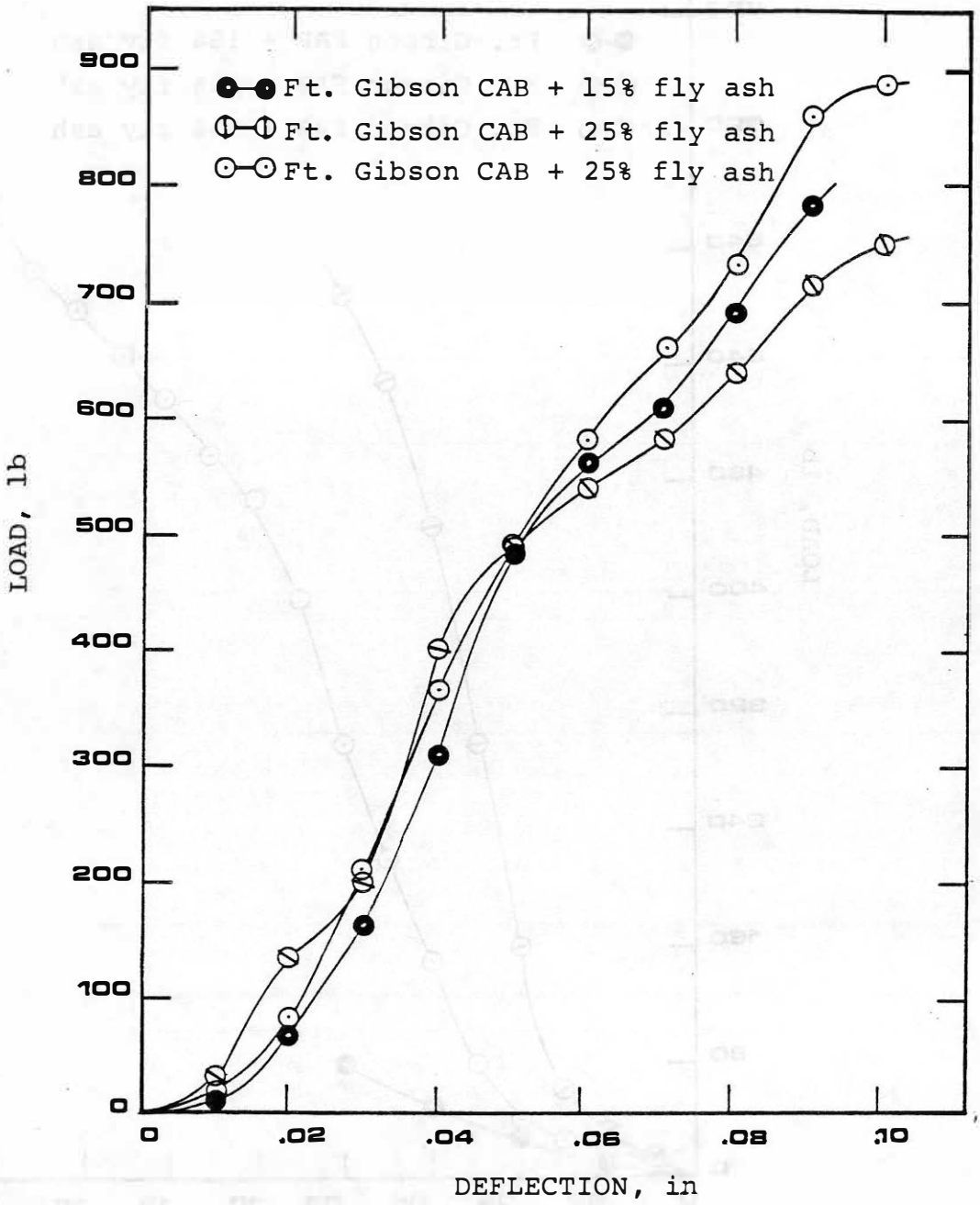

Figure C.10 Load-deflection relationship of Ft. Gibson CAB

APPENDIX D

FLEXURAL ANALYSIS DATA

NOTATION

Adj. = deflection adjustment, in

P_P = proportional load, lb.

ΔL_P = adjusted deflection at proportional load, in

E = modulus of elasticity, psi

P_F = failure load, psi

ΔL_F = adjusted deflection at failure load, in

P = a+b ln (ΔL)s equation of the load-deflection curve in the plastic range.

R^2 = regression coefficient

S_2 = $\frac{a}{1-e^{-a/b}}$: slope of the linearized logarithmic curve with respect to the P-ΔL coordinate system, lb/in

$E_{P/E}$ = ratio of moduli of plasticity to elasticity

E_P = modulus of plasticity, psi

Relationss $E = 3.255 \frac{P_P}{\Delta L_P}$

$$\frac{E_P}{E} = \frac{\Delta L_P}{P_P} \cdot \frac{a}{1-e^{-a/b}}$$

Table D.1 FLEXURAL DATA FOR NORMAN 90-DAY MIXES

Mix Type	Adj. (in)	$P_{p0}/\Delta I_p$ (lb/in)	E (psi)	$P_F/\Delta 10_p$ (lb/in)	Plastic Range P=a+b ln (ΔL)	R^2	$\frac{a}{1-e^{-a/b}}$ (lb/in)	$E_{P/E}$	E_p (psi)
FAB + 15% f.a.	0.05	260/0.06	14,105	310/0.075	-	-	-	-	-
FAB + 25% f.a.	0.01	400/0.21	6,200	460/0.27	P=779.30+240.52 ln (ΔL)	0.97	811.1	0.43	2,640
FAB + 35% f.a.	0.04	300/0.09	10,850	650/0.20	P=1364.37+434.46 ln (ΔL)	0.99	1426.1	0.43	4,642
CAB + 15% f.a.	0.005	470/0.195	7,845	480/0.215	-	-	-	-	-
CAB + 25% f.a.	0.02	250/0.10	8,138	390/0.16	P=974.29+312.86 ln (ΔL)	0.97	1019.6	0.41	3,319
CAB + 35% f.a.	0.04	250/0.18	4,520	390/0.28	P=824.75+335.21 ln (ΔL)	0.99	901.8	0.65	2,935

Table D.2 FLEXURAL DATA FOR PONCA CITY 90-DAY MIXES

Mix Type	Adj. (in)	$P_p/\Delta L_p$ (lb/in)	E (psi)	$P_F/\Delta L_F$ (lb/in)	Plastic Range P=a+b ln (ΔL)	R^2	$\frac{a}{1-e^{-a/b}}$ (lb/in)	$E_{P/E}$	E_p (psi)
FAB + 15% f.a.	0.045	380/0.035	35,340	660/0.095	P=1342.93+287.73 ln (ΔL)	0.99	1355.7	0.13	4,413
FAB + 25% f.a.	0.05	440/0.053	27,023	1350/0.25	P=2110.93+606.69 ln (ΔL)	0.95	2178.1	0.26	7,090
FAB + 35% f.a.	0.037	360/0.023	50,948	540/0.063	P=1038.03+181.61 ln (ΔL)	0.97	1041.5	0.07	3,390
CAB + 15% f.a.	0.035	410/0.025	53,382	640/0.055	P=1650.06+336.95 ln (ΔL)	0.99	1662.5	0.10	5,411
CAB + 25% f.a.	0.06	315/0.04	25,633	930/0.17	P=1600.90+415.72 ln (ΔL)	0.96	1635.7	0.21	5,324
CAB + 35% f.a.	0.023	320/0.037	28,151	660/0.102	P=1374.56+316.27 ln (ΔL)	1.00	1392.6	0.16	4,504

Table D.3 FLEXURAL DATA FOR COWETA 90-DAY MIXES

Mix Type	Adj. (in)	$P_{p0}/\Delta L_P$ (lb/in)	E (psi)	$P_F/\Delta L_F$ (lb/in)	Plastic Range P=a+b ln (ΔL)	R^2	$\frac{a}{1-e^{-a/b}}$ (lb/in)	$E_{P/E}$	E_P (psi)0
FAB + 15% f.a.	0.0275	460/0.0325	46,071	510/0.0425	-	-	-	-	-
FAB + 25% f.a.	0.013	450/0.047	31,165	710/0.097	P=1480.66+341.01 ln (ΔL)	0.97	1500.2	0.16	4,883
FAB + 35% f.a.	0.023	440/0.109	23,158	550/0.037	P=1100.50+165.70 ln (ΔL)	0.98	1101.9	0.27	6,322
CAB + 15% f.a.	0.03	400/0.045	28,933	730/0.12	P=1410.74+327.29 ln (ΔL)	1.00	1429.9	0.16	3,850
CAB + 25% f.a.	0.04	430/0.06	23,328	750/0.12	P=1692.15+453.66 ln (ΔL)	0.98	1733.7	0.24	5,644
CAB + 35% f.a.	0.02	400/0.024	54,250	700/0.06	P=1566.42+313.08 ln (ΔL)	0.99	1577.0	0.10	5,133

Table D.4 FLEXURAL DATA FOR TUPELO 90-DAY MIXES

Mix Type	Adj. (in)	$P_p/\Delta L_p$ (lb/in)	E (psi)	$P_F/\Delta L_F$ (lb/in)	Plastic Range P=a+b ln (ΔL)	R^2	$\frac{a}{1-e^{-a/b}}$ (lb/in)	$E_{P/E}$	E_P (psi)
FAB + 15% f.a.	0.03	370/0.07	17,205	450/0.09	-	-	-	-	-
FAB + 25% f.a.	0.05	360/0.07	16,740	640/0.19	P=1120.32+282.17 ln (ΔL)	0.99	1141.9	0.22	3,718
FAB + 35% f.a.	0.035	420/0.045	30,380	700/0.095	P=1503.43+350.63 ln (ΔL)	0.98	1524.4	0.16	4,861
CAB + 15% f.a.	0.09	350/0.07	16,275	670/0.19	P=1185.46+309.89 ln (ΔL)	0.99	1211.9	0.24	3,946
CAB + 25% f.a.	0.02	330/0.03	35,805	860/0.145	P=1467.47+311.410ln (ΔL)	0.97	1480.8	0.14	4,820
CAB + 35% f.a.	0.024	320/0.036	28,933	730/0.126	P=1414.14+327.66 ln (ΔL)	1.00	1433.3	0.16	4,665

Table D.5 FLEXURAL DATA FOR FT. GIBSON 90-DAY MIXES

Mix Type	Adj. (in)	$P_P/\Delta L_P$ (lb/in)	E (psi)	$P_F/\Delta L_F$ (lb/in)	Plastic Range P=a+b ln (ΔL)	R^2	$\frac{a}{1-e^{-a/b}}$ (lb/in)	$E_{P/E}$	E_P (psi)
FAB + 15% f.a.	0.02	80/0.06	4,340	80/0.06	-	-	-	-	-
FAB + 25% f.a.	0.03	450/0.03	48,825	550/0.05	P=1556.87+314.84 ln (ΔL)	1.00	1568.0	0.11	5,104
FAB + 35% f.a.	0.04	300/0.04	24,412	680/0.12	P=1342.44+317.92 ln (ΔL)	0.99	1362.4	0.18	4,435
CAB + 15% f.a.	0.02	485/0.03	52,623	780/0.07	P=1622.33+326.89 ln (ΔL)	0.96	1633.8	0.10	5,318
CAB + 25% f.a.	0.02	400/0.02	65,000	750/0.08	P=1365.83+251.86 ln (ΔL)	0.97	1371.9	0.07	4,466
CAB + 35% f.a.	0.015	485/0.035	45,105	885/0.085	P=2049.21+470.51 ln (ΔL)	0.98	2075.9	0.15	6,057

APPENDIX E

X-RAY DIFFRACTOGRAMS AND CRYSTALLINE DATA

XRD NOTATION

Mineral Name	Chemical Formula	Symbol
Dicalcium Silicate (C_2S)	$2CaO.SiO_2$	D
Tricalcium Aluminate (C_3A)	$3CaO.Al_2O_3$	T
Calcite (Calcium Carbonate)	$CaCO_3$	C
Portlandite (Calcium Hydroxide)	$Ca(OH)_2$	Pt
Ettringite ($C_3A.3C\bar{S}.H_{32}$)	$3CaO.Al_2O_3.3CaSO_4.32H_2O$	E
Monosulfoaluminate ($C_3A.C\bar{S}.H_{13}$)	$3CaO.Al_2O_3.CaSO_4.13H_2O$	Ms
Quartz	SiO_2	Q
Periclase	MgO	P
Anhydrite	$CaSO_4$	A
Lime	CaO	L
Calcium Aluminum Oxide Sulfate ($C_3A_3\bar{S}$)	$3CaO.3Al_2O_3.CaSO_4$	X
Microline	$KAlSi_3O_8$	Mc
Gismondine (CAS_2H_4)	$CaO.2SiO_2.Al_2O_3.4H_2O$	G
Calcium Aluminate Oxide Hydrate (C_4AH_{19})	$4CaO.Al_2O_3.19H_2O$	Z
Straetlingite (C_2ASH_8)	$2CaO.SiO_2.Al_2O_3.8H_2O$	S
Dolomite	$(MgCaFe)\ CO_3$	Dm

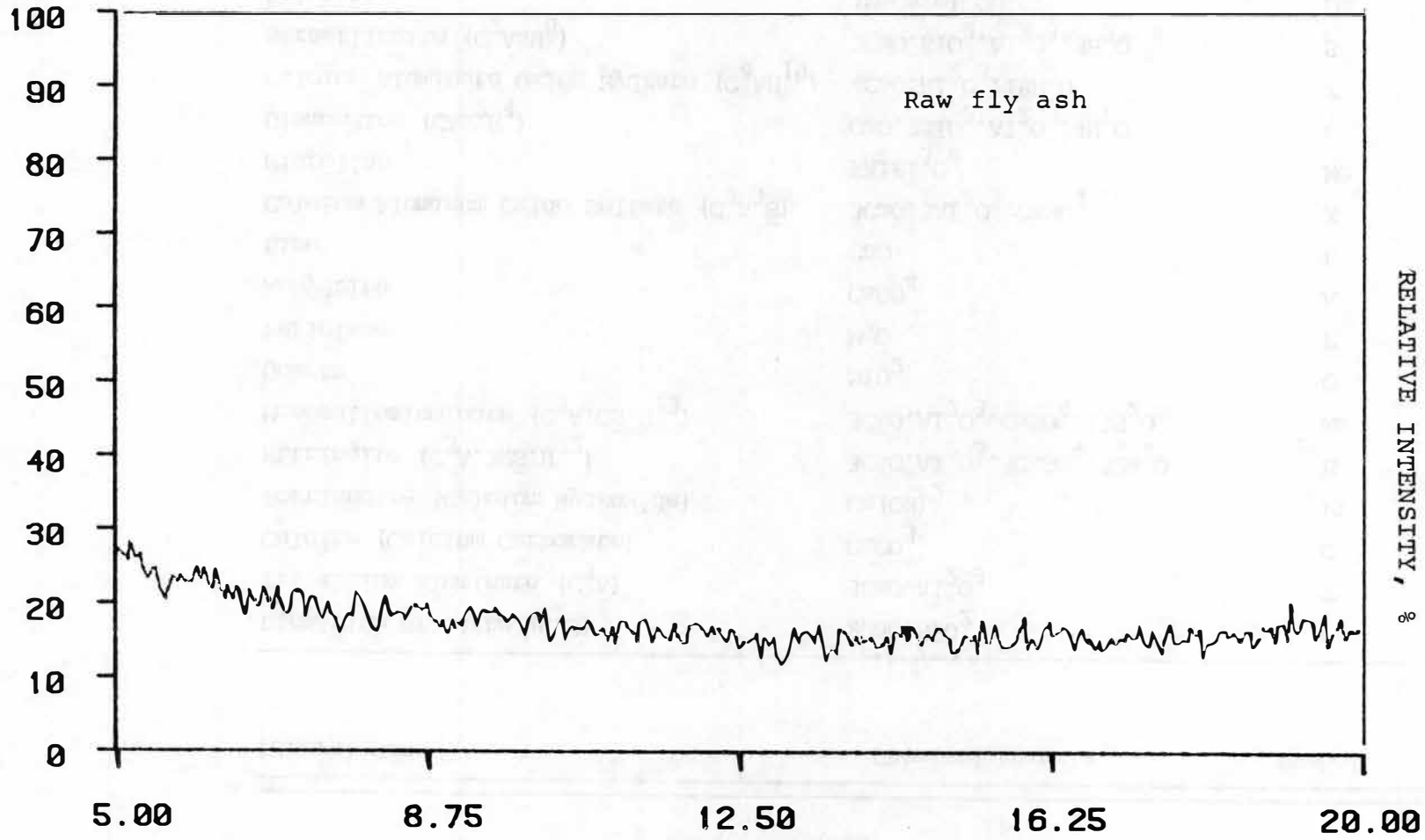

Figure E.1 Raw Fly Ash

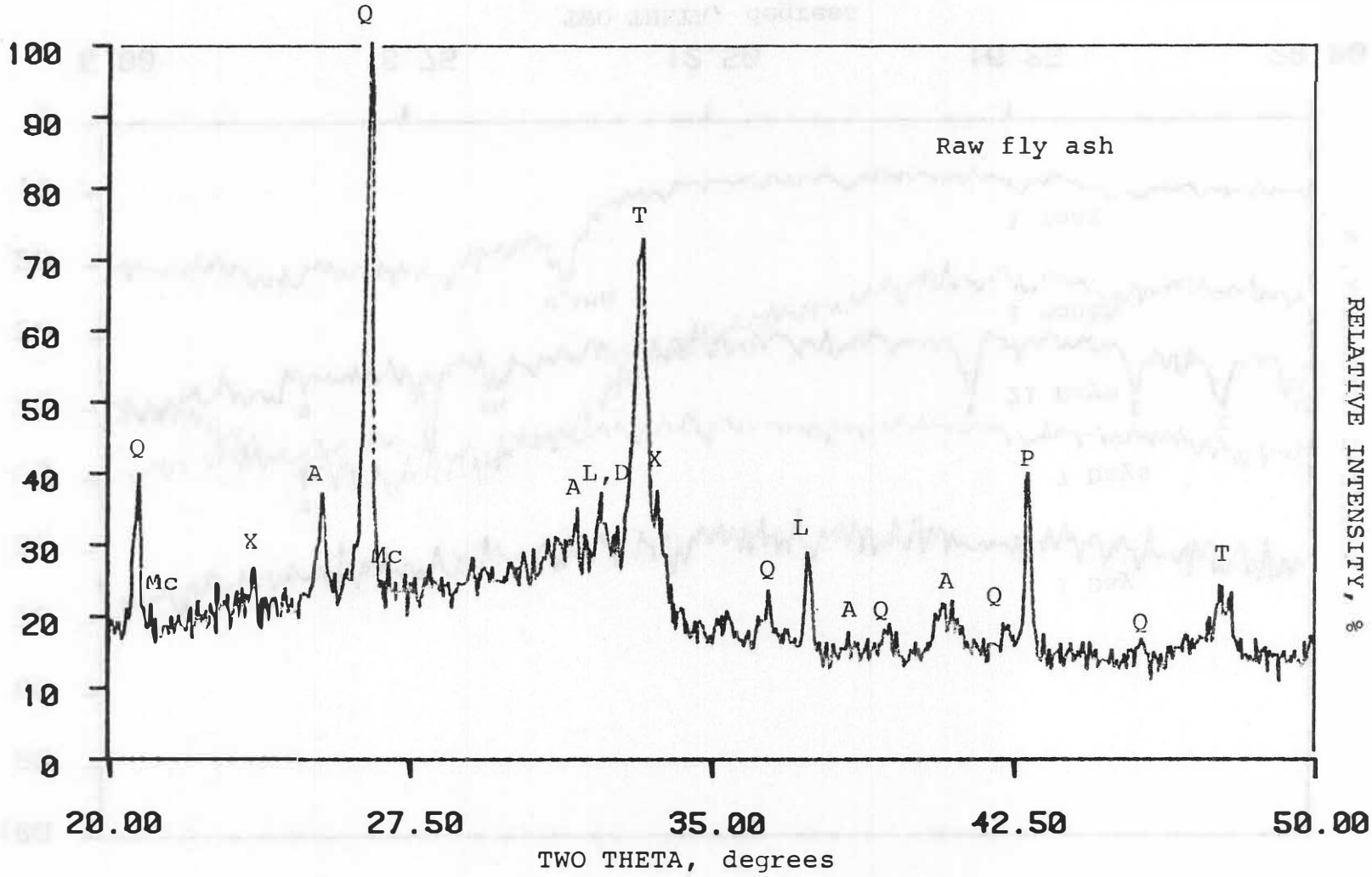

Figure E.2 Raw Fly Ash

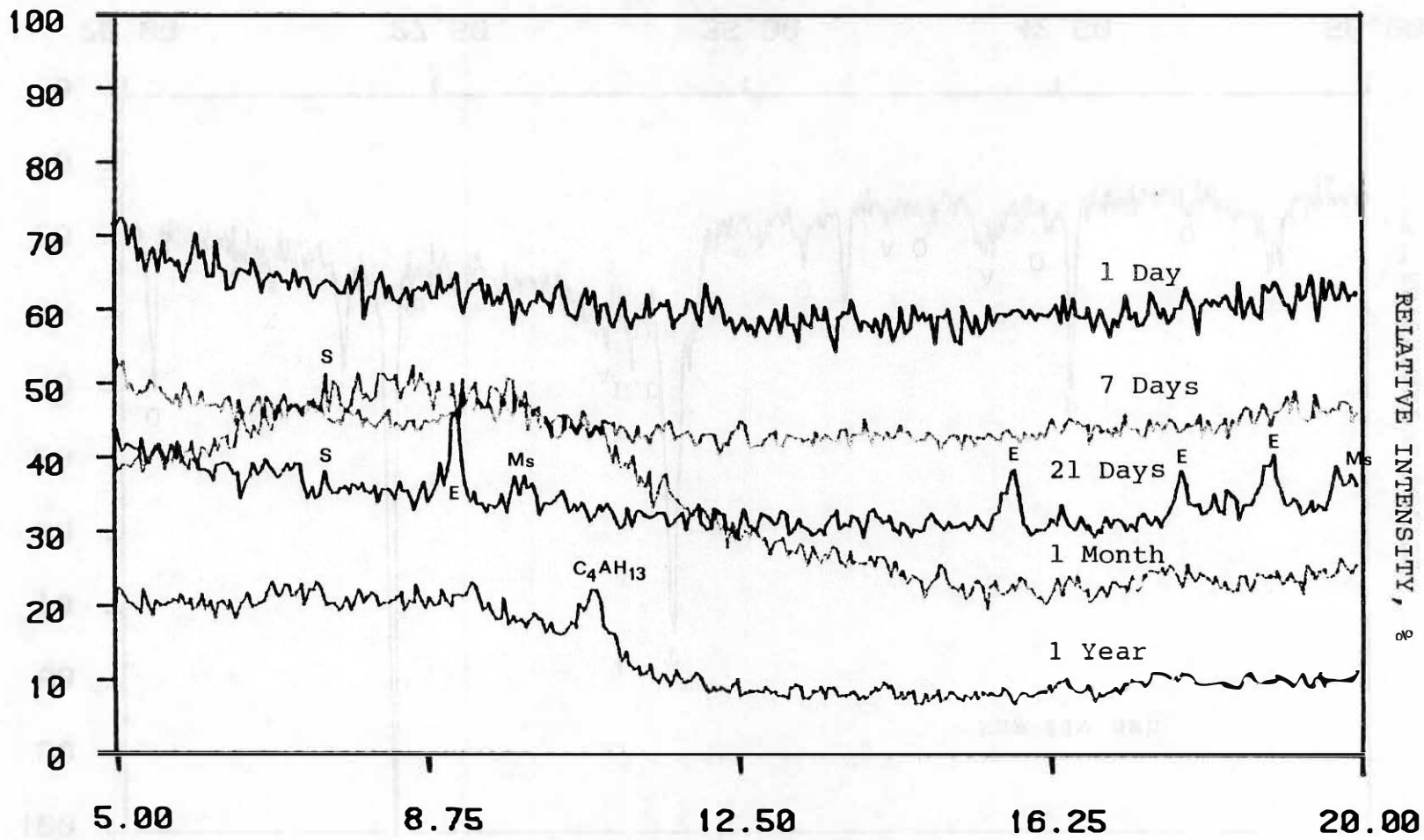

Figure E.3 Fly Ash Pastes

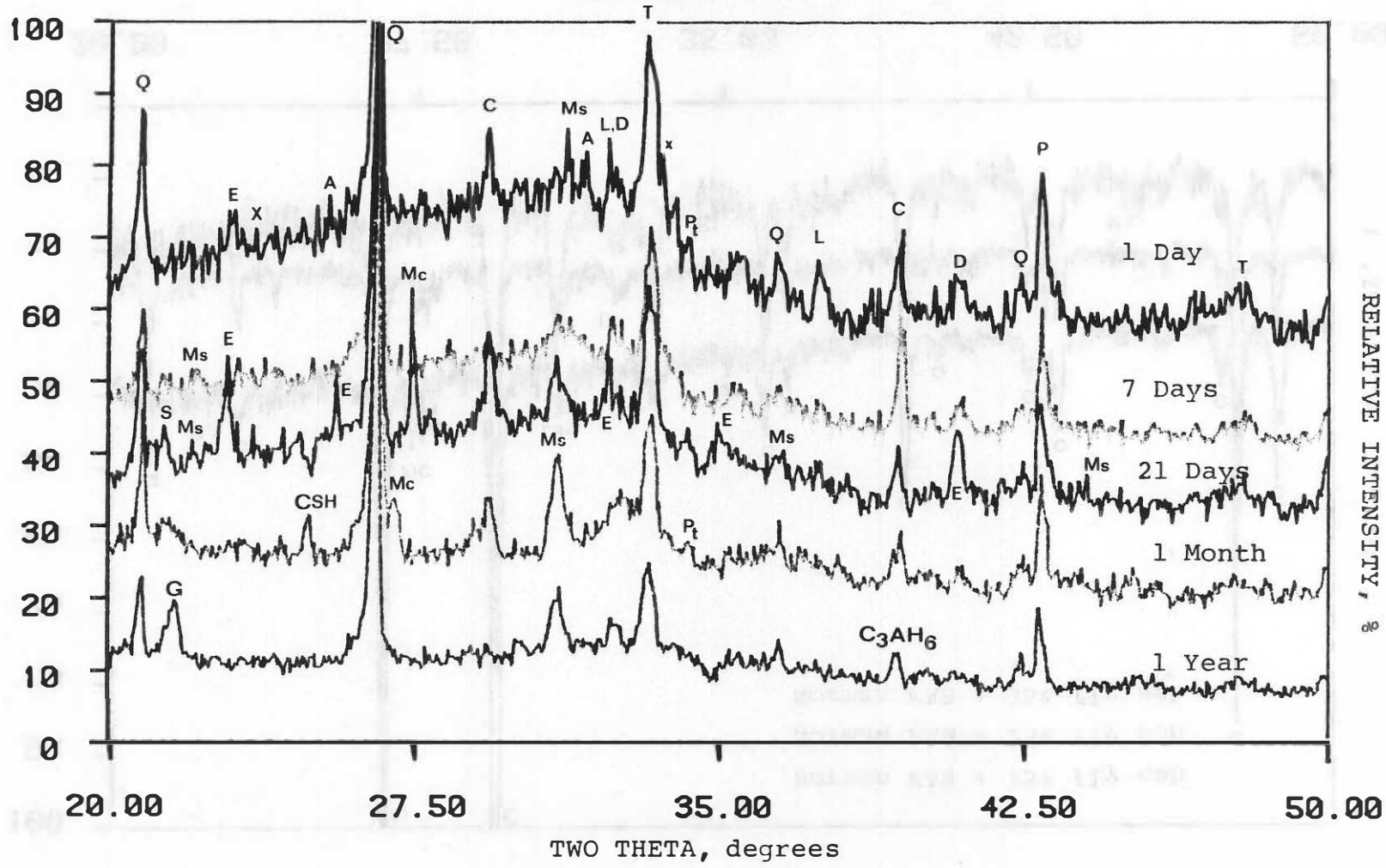

Figure E.4 Fly Ash Pastes

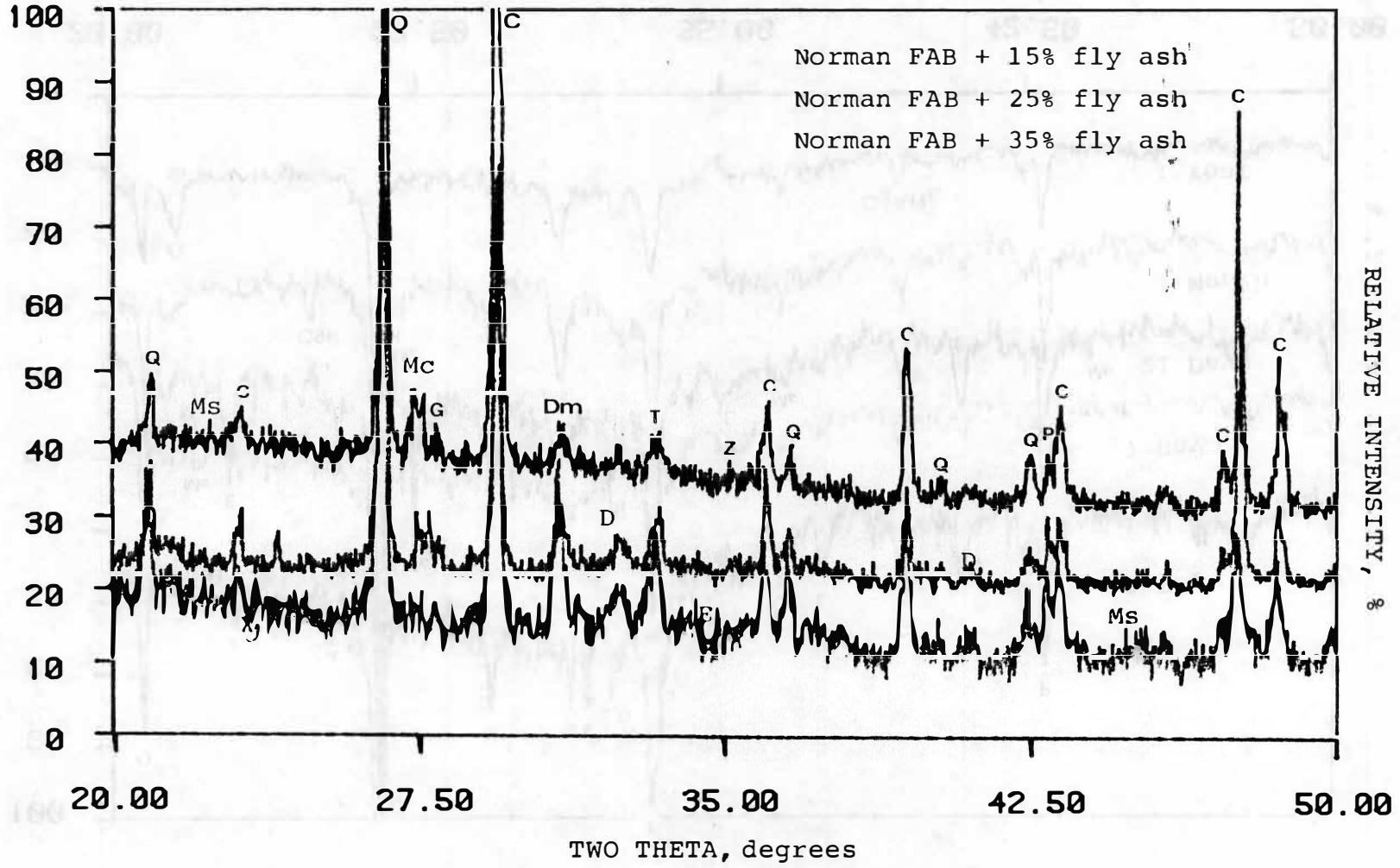

Figure E.5 Norman FABs, 28 days

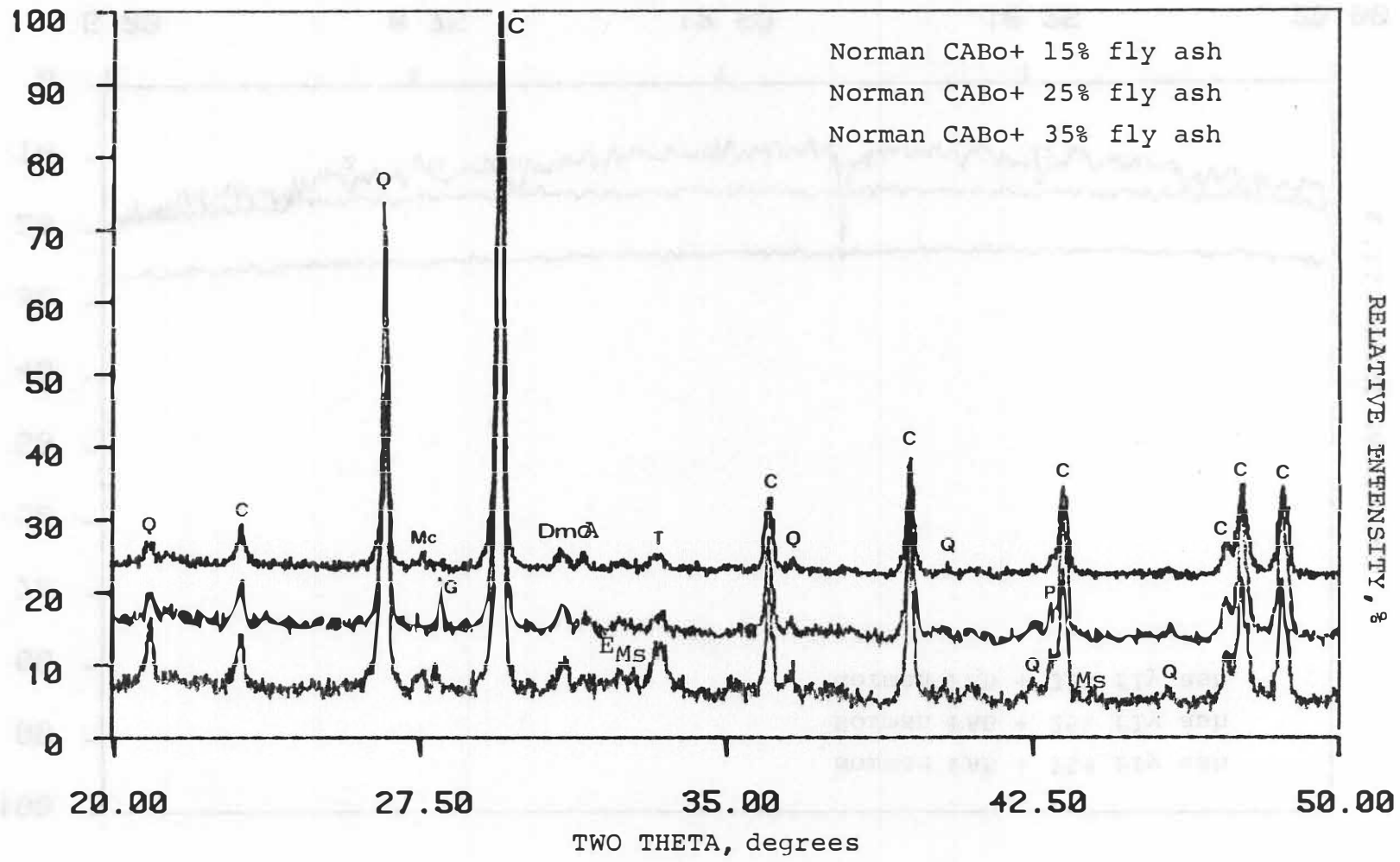

FigureoE.6 Norman CAB, 28 days

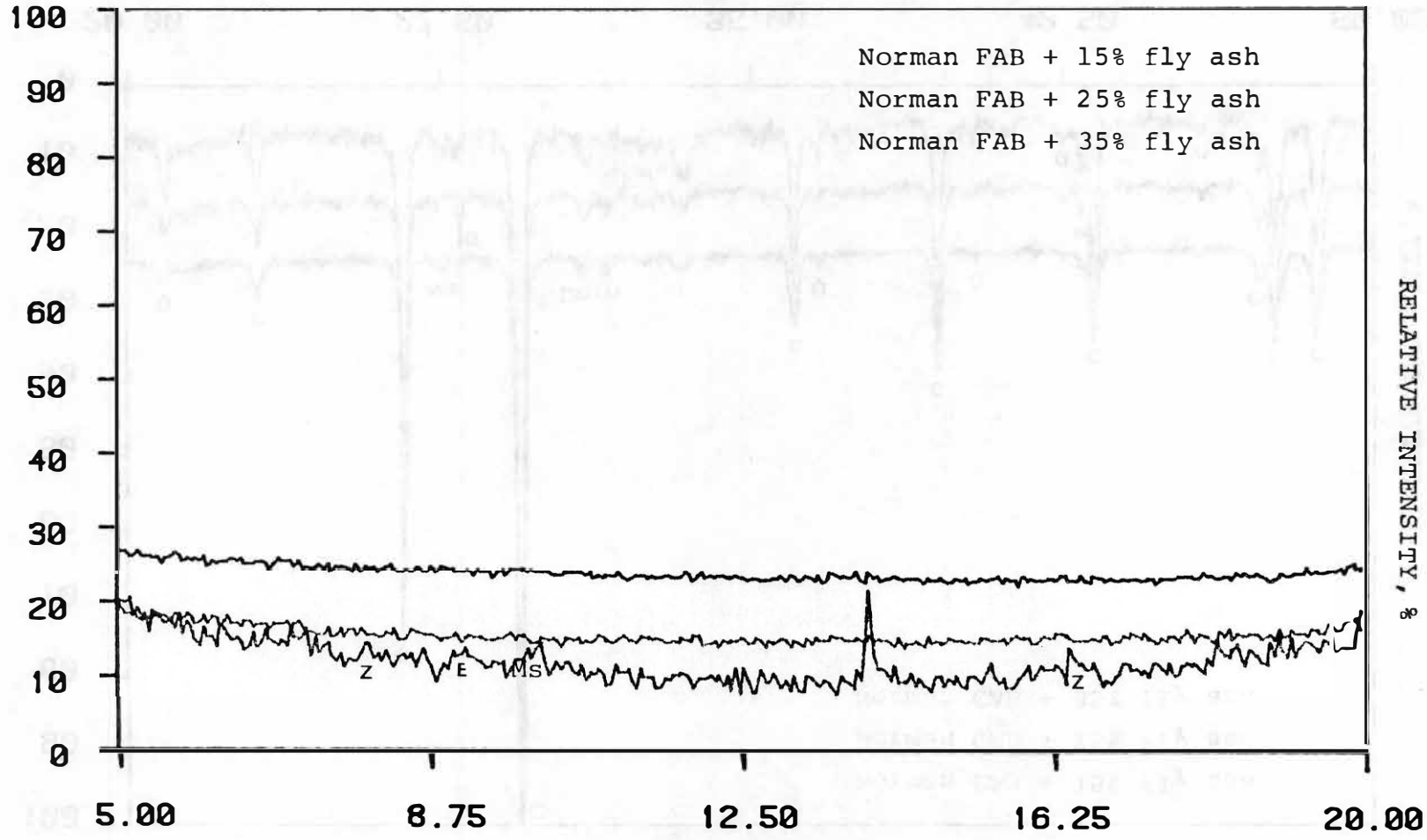

Figure E.3 Norman FAB, 90 days

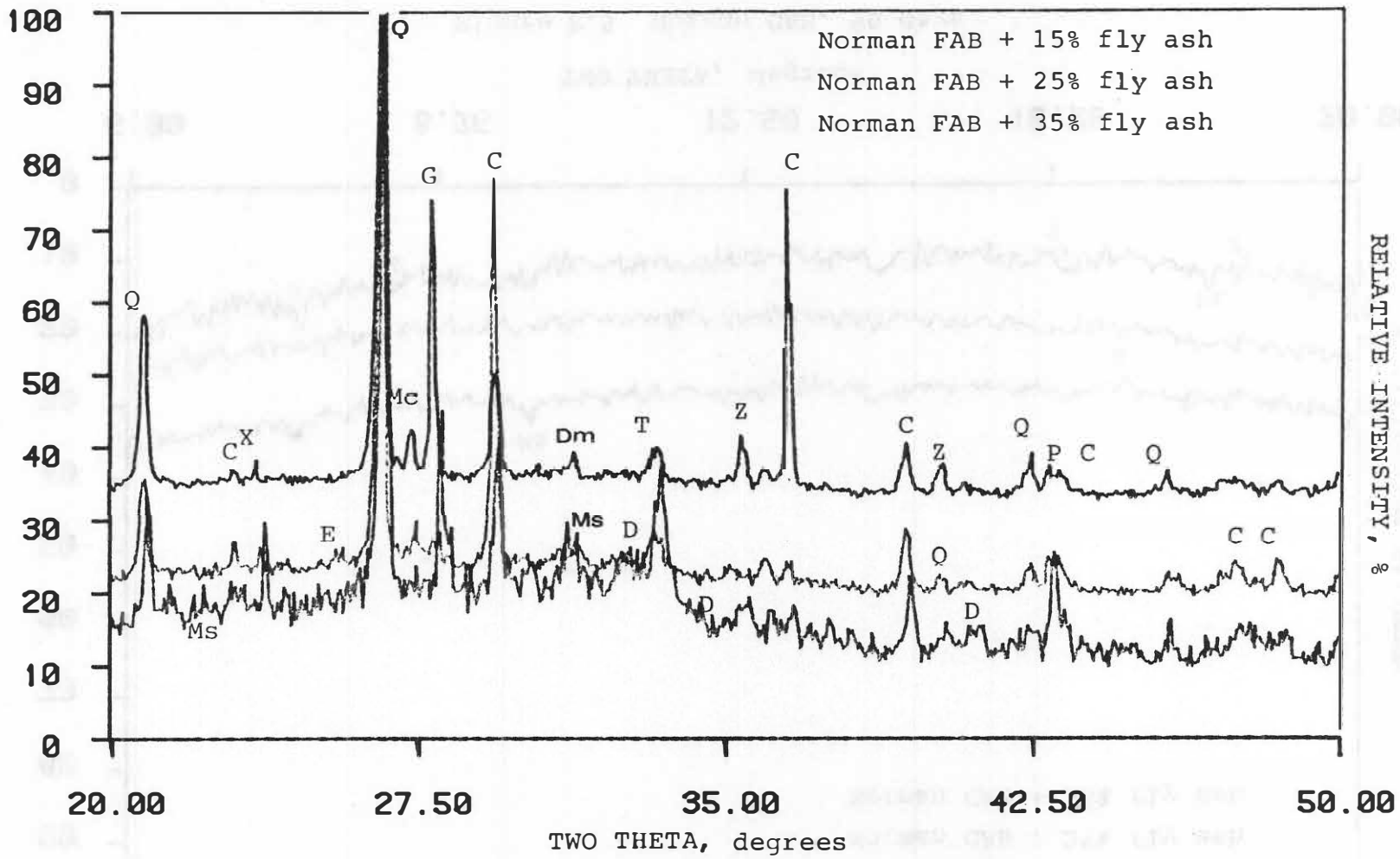

Figure E.8 Norman FAB, 90 days

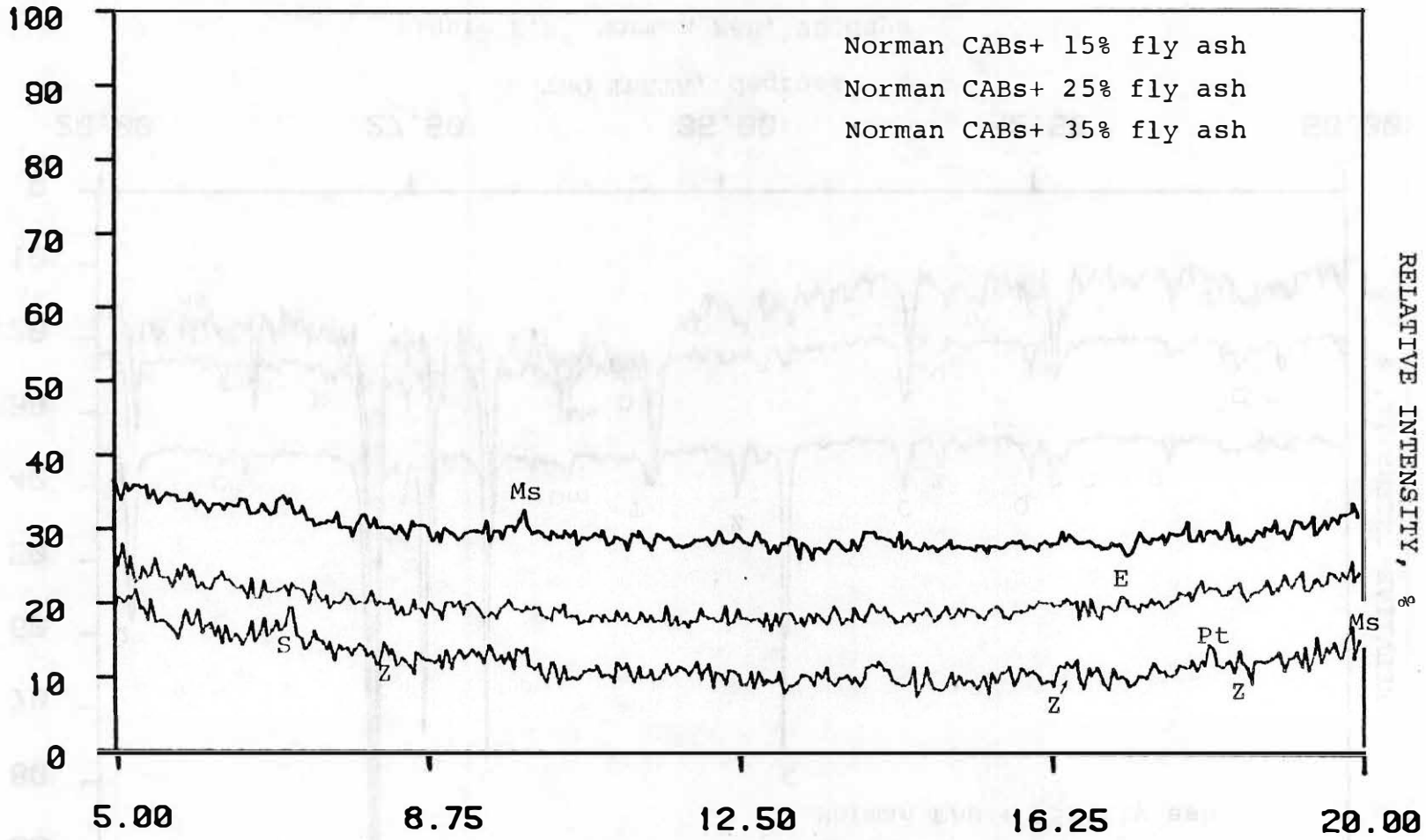

Figure E.9 Norman CAB, 90 days

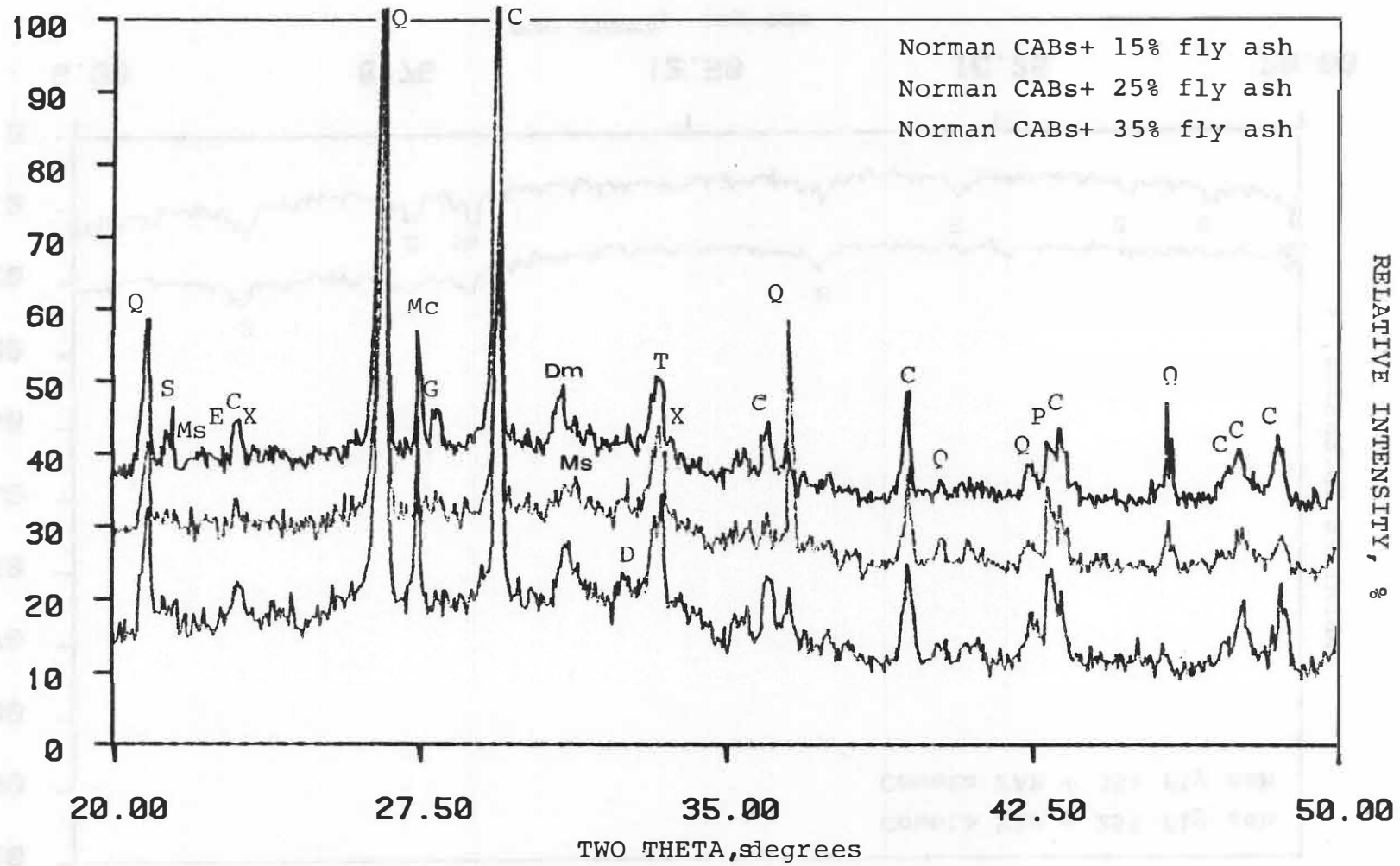

Figure E.10 Norman CAB, 90 days

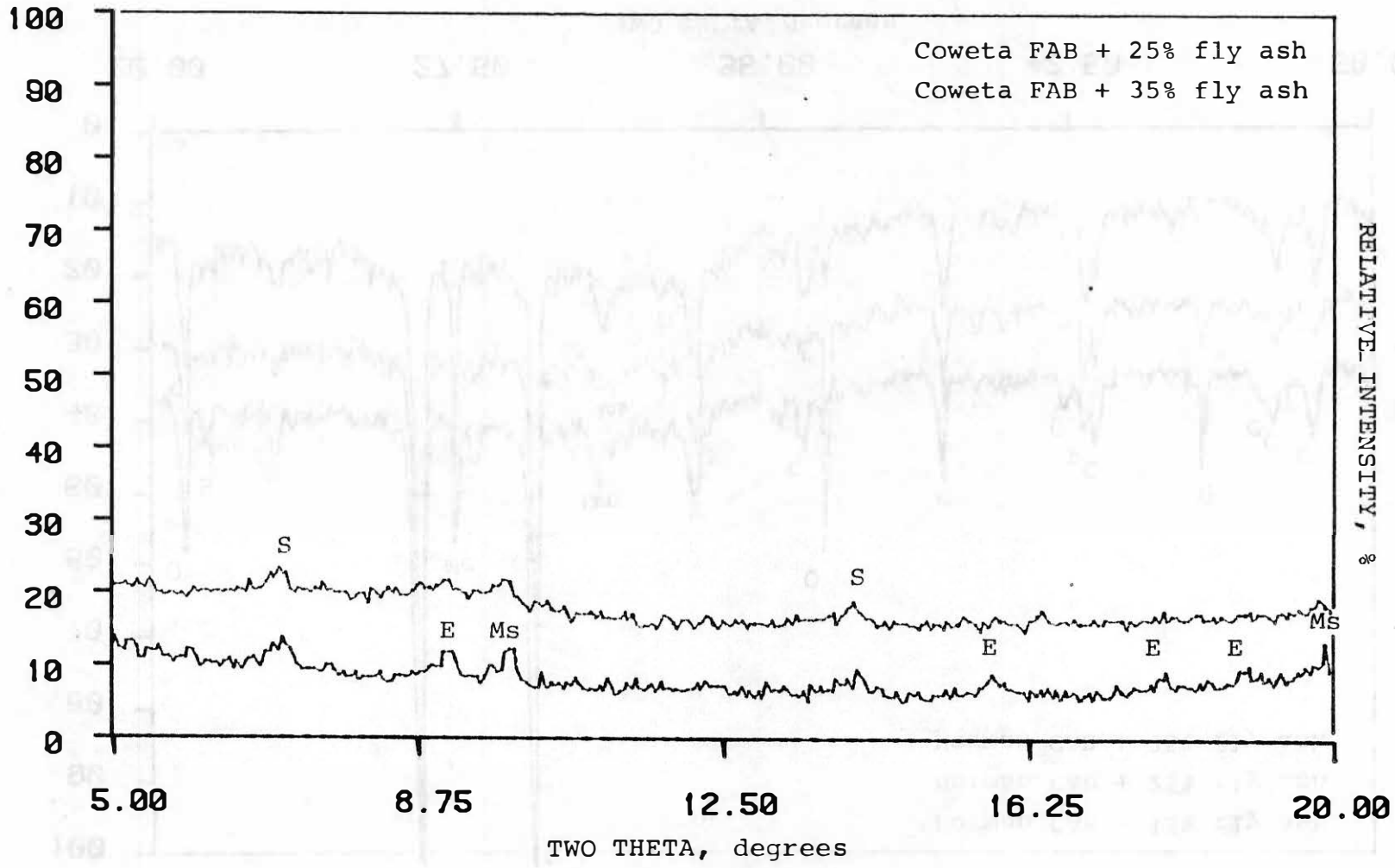

Figure E.11 Coweta FAB, 28 days

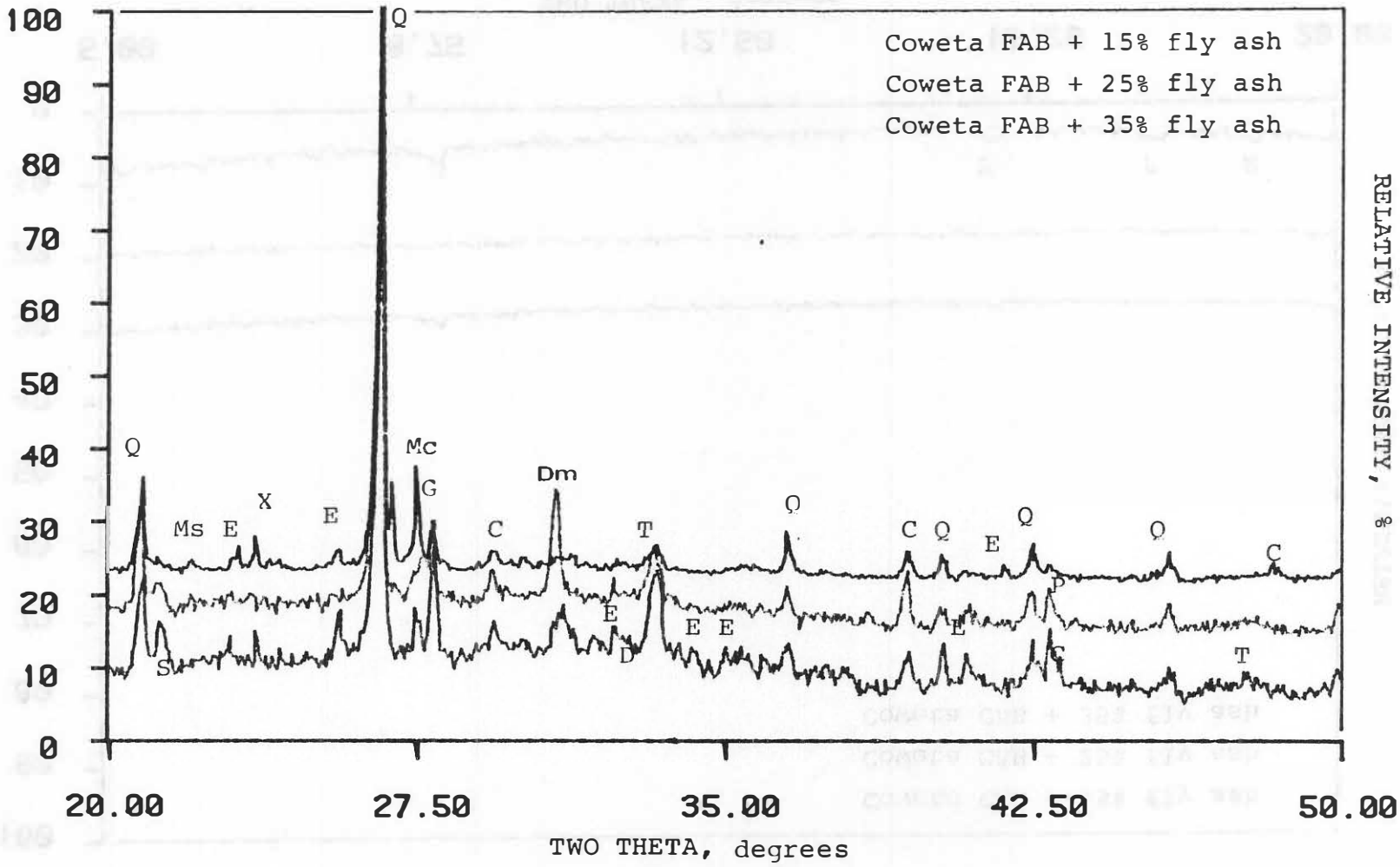

Figure E.12 Coweta FAB, 28 days

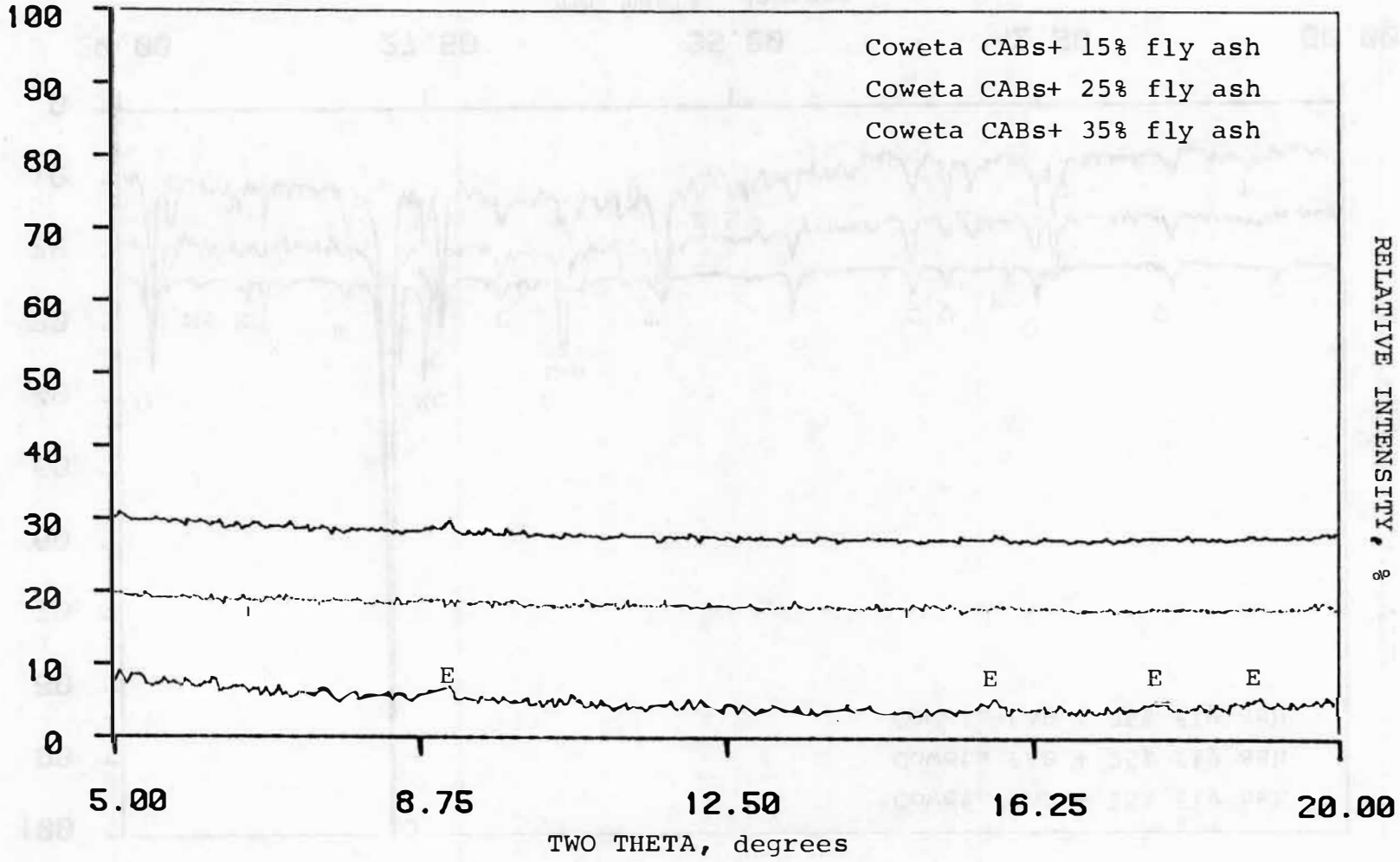

Figure E.13 Coweta CAB, 28 days

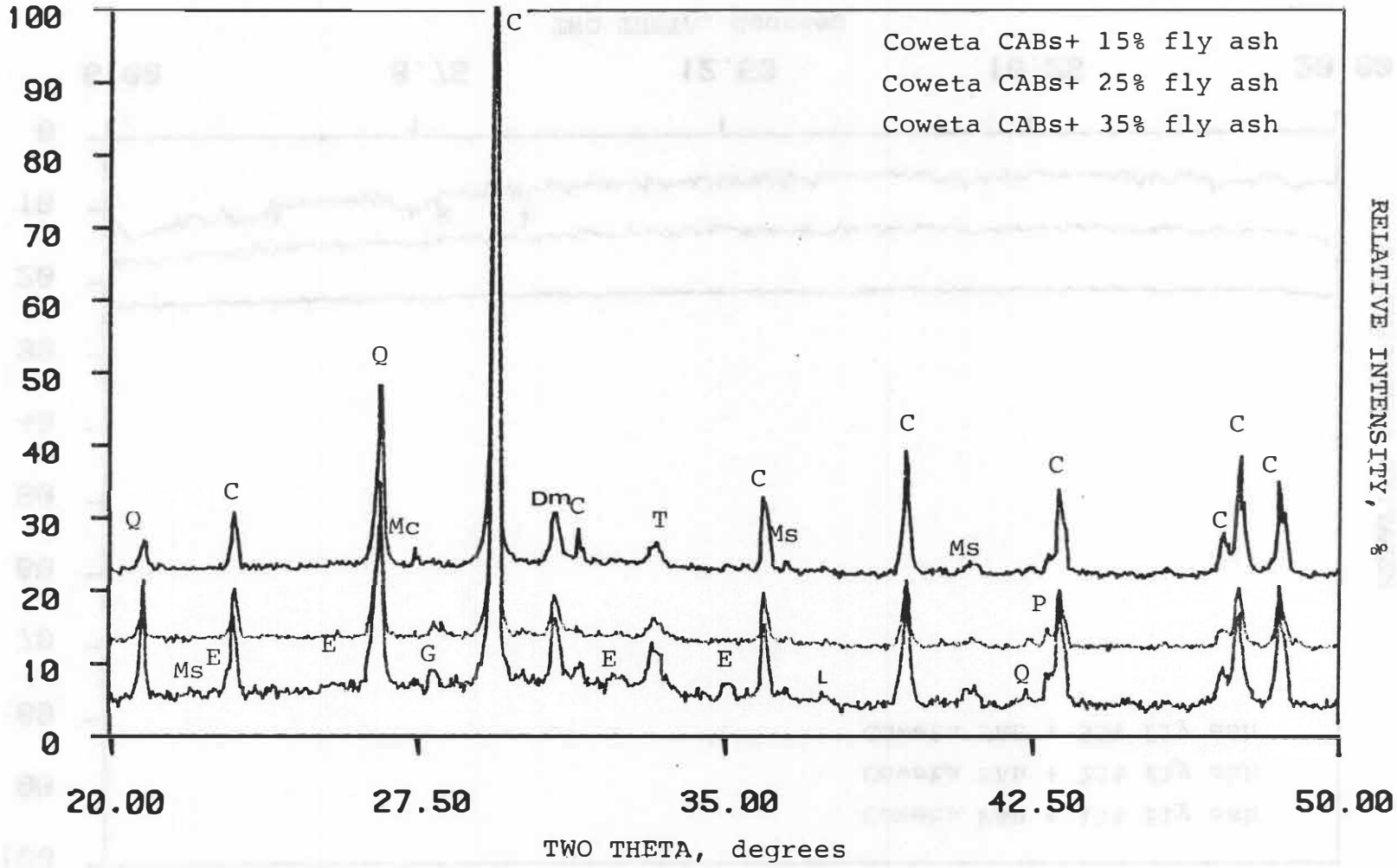

Figure E.14 Coweta CAB, 28 days

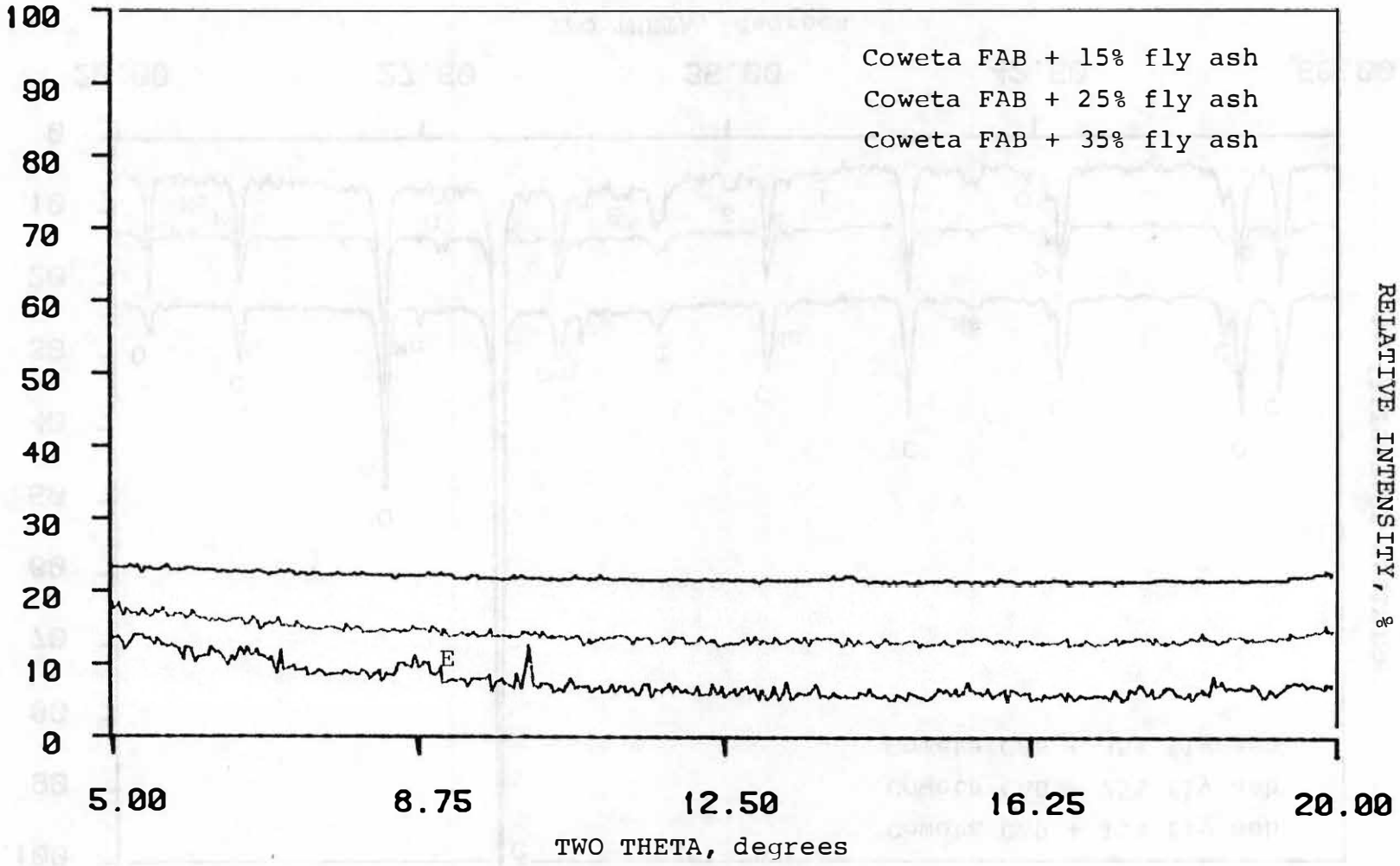

Figure E.15 Coweta FAB, 90 days

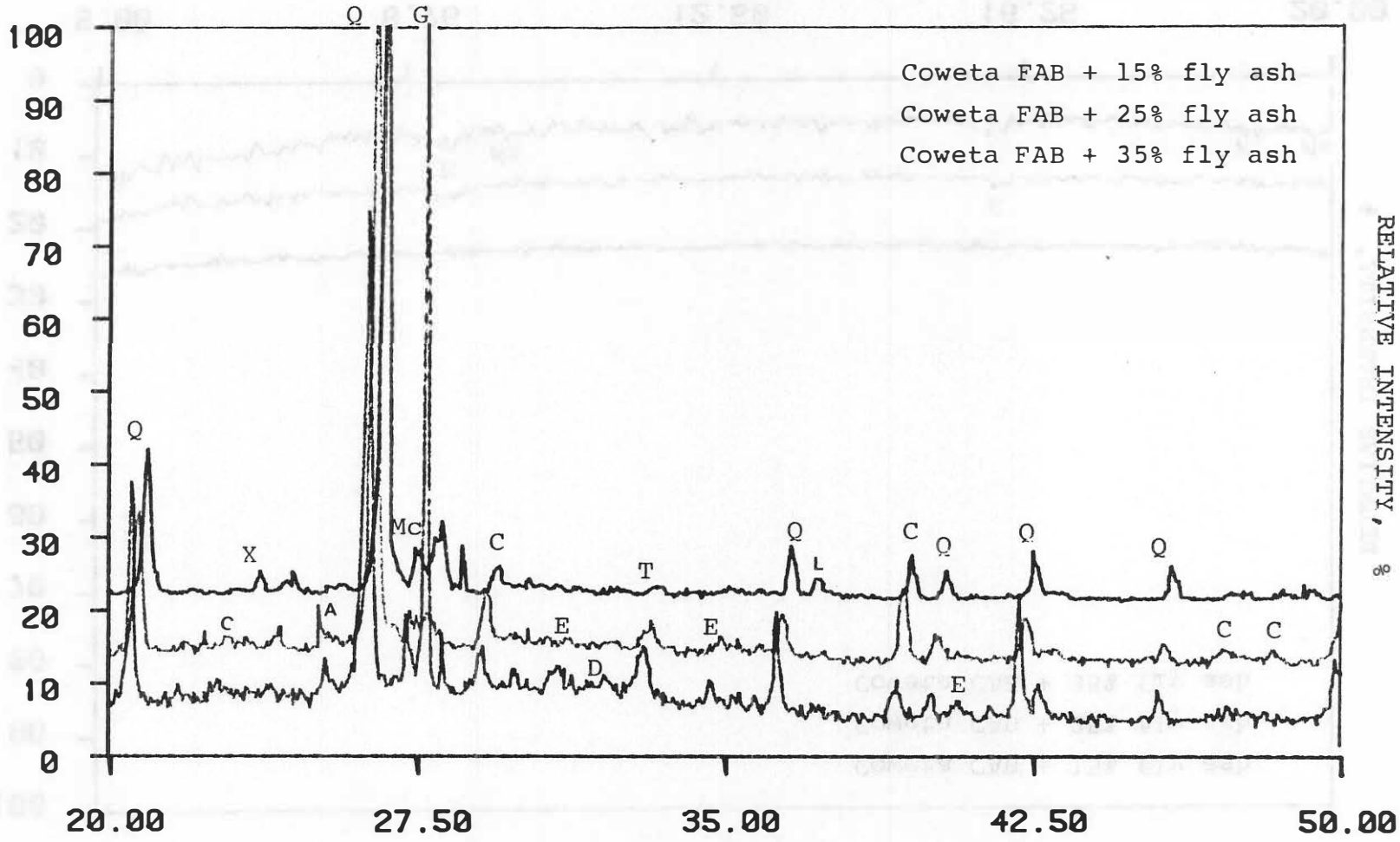

Figure E.16 Coweta FAB, 90 days

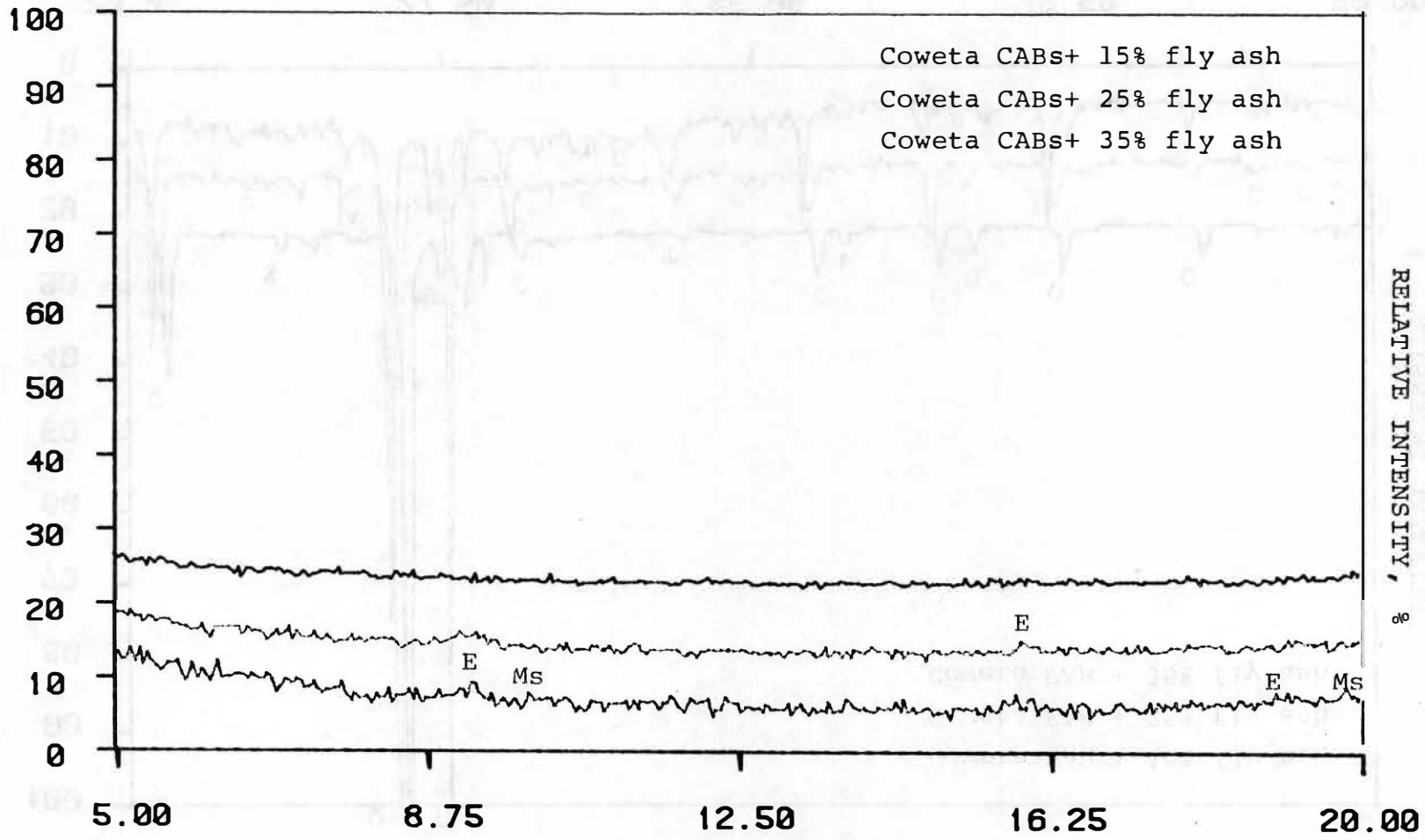

Figure E.17 Coweta CABs, 90 days

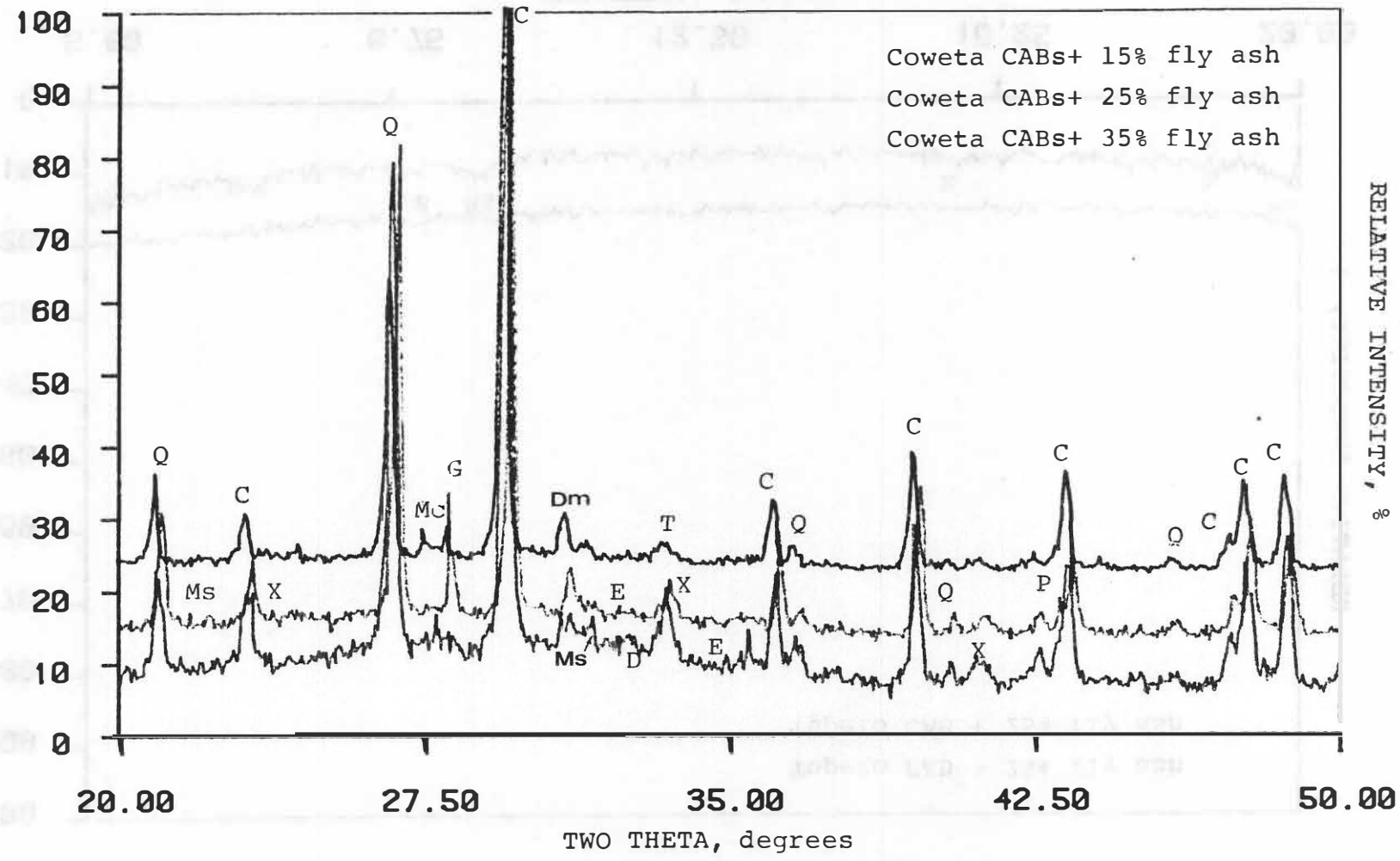

Figure E.18 Coweta CAB, 90 days

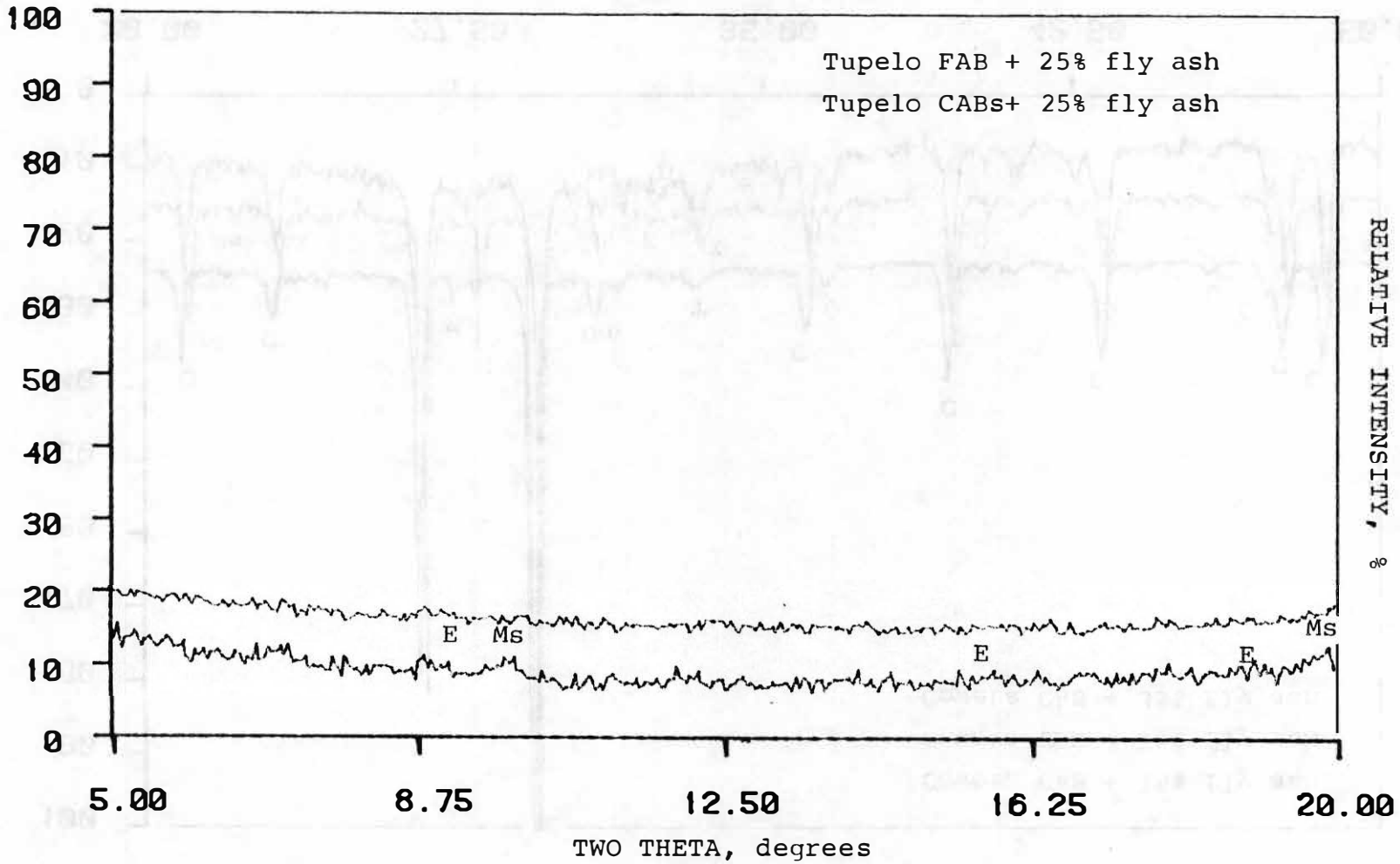

Figure E.19 Tupelo FAB & CAB, 90 days

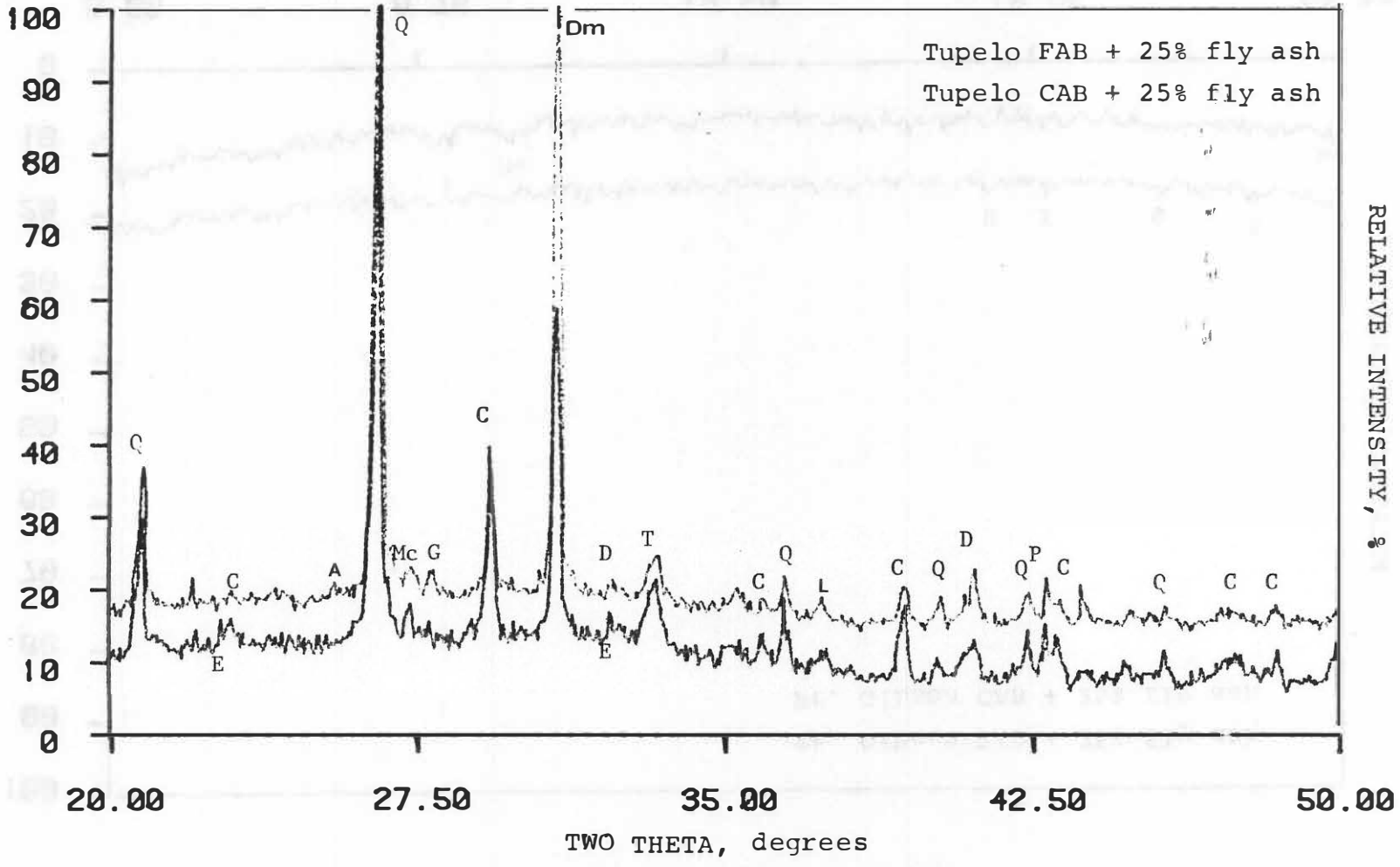

Figure E.20 Tupelo FAB & CABs 90 days

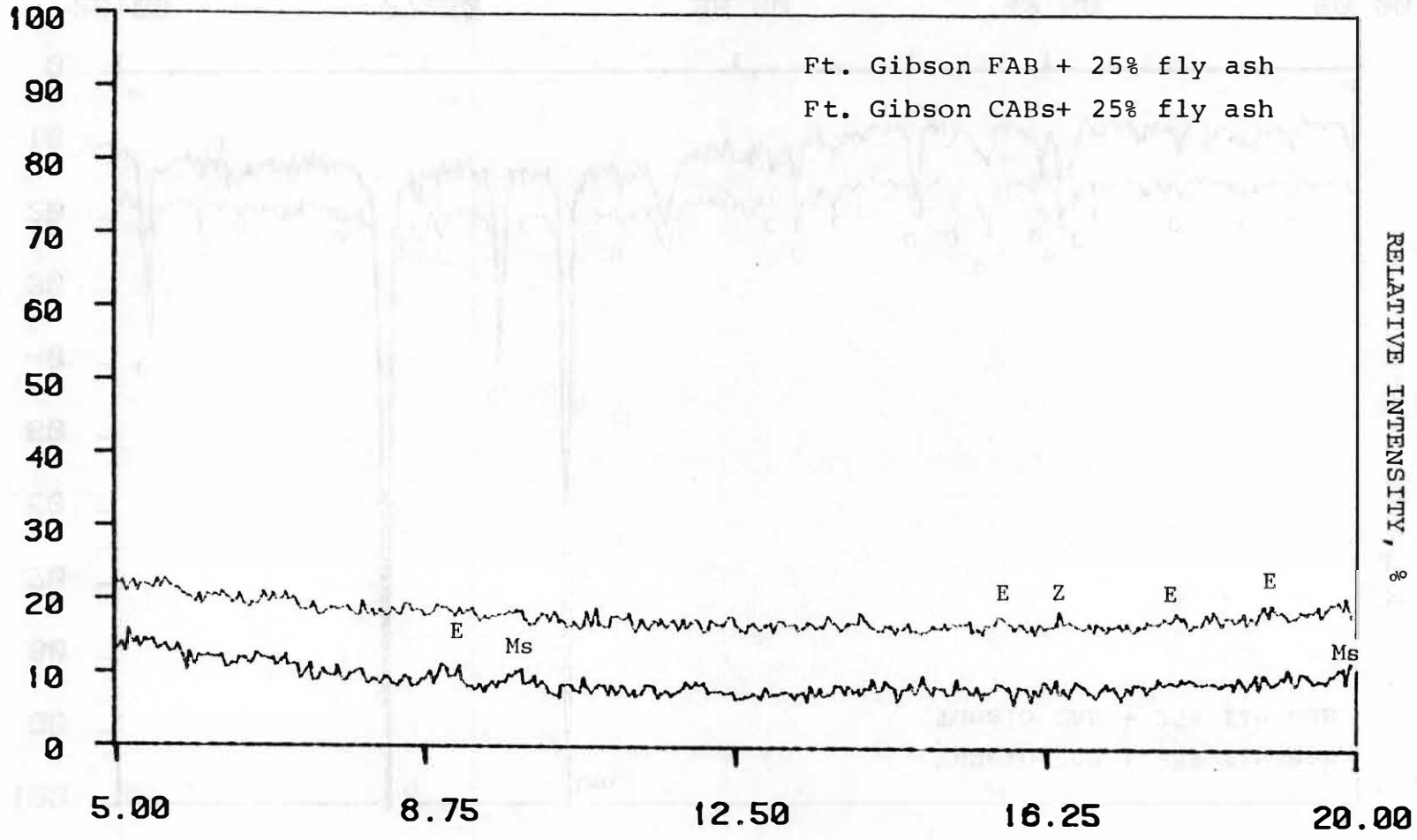

Figure E.21 Ft. Gibson FAB & CABs 90 days

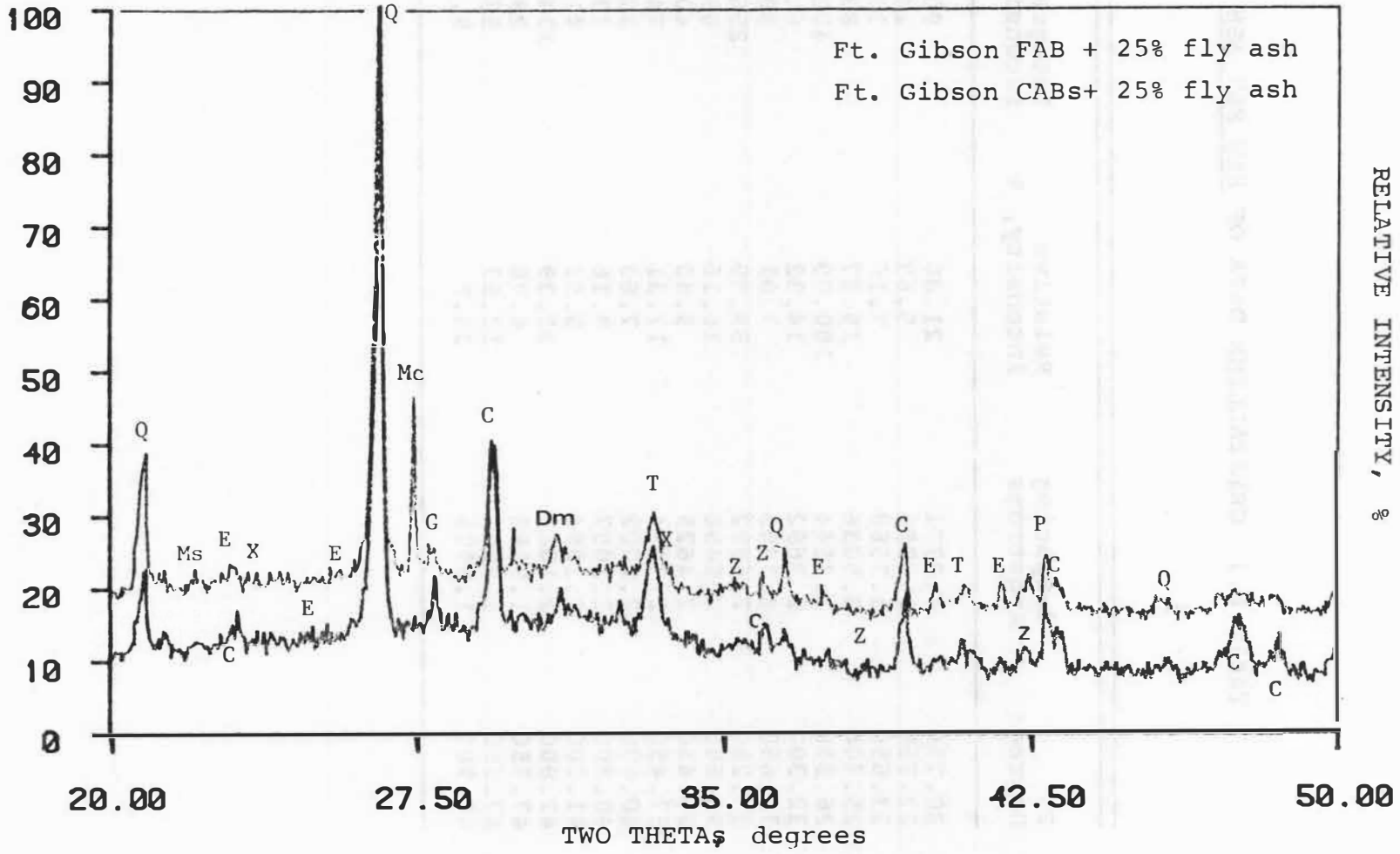

Figure E.22 Ft. Gibson FAB & CAB, 90 days

Table E.1 CRYSTALLINE DATA OF RAW FLY ASH

2θ Degrees	d-Spacing Angstroms	Relative intensity, %	Integrated intensity, cps
20.750	4.2771	21.00	90.5
22.750	3.9054	5.69	24.5
23.650	3.7588	7.16	30.9
25.400	3.5036	19.37	83.5
26.550	3.3544	100.00	431.0
32.300	2.7692	14.32	61.7
32.650	2.7403	7.01	30.2
33.250	2.6922	59.59	256.8
33.800	2.6496	16.16	69.6
36.450	2.4629	9.40	40.5
37.450	2.3994	17.31	74.6
40.600	2.2202	7.63	32.9
40.800	2.2097	9.16	39.5
41.000	2.1994	9.55	41.2
42.900	2.1063	32.39	139.6
47.350	1.9182	6.76	29.1
47.650	1.9068	13.57	58.5
47.900	1.8975	38.8	9.00

Table E.2 CRYSTALLINE DATA OF FLY ASH PASTES, 1-DAY CURING

2θ Degrees	d-Spacing Angstroms	Relative intensity, %	Integrated intensity, cps
20.800	4.2669	34.25	107.8
25.900	3.4371	7.48	23.5
26.200	3.3984	5.94	18.7
26.600	3.3482	100.00	314.6
29.350	3.0405	13.30	41.8
31.300	2.8553	13.19	41.5
32.350	2.7650	12.65	39.8
32.600	2.7444	5.53	17.4
33.350	2.6844	33.62	105.8
33.650	2.6611	16.61	52.3
33.950	2.6383	7.74	24.3
35.500	2.5266	6.47	20.4
33.650	2.5163	6.11	19.2
36.550	2.4563	7.95	25.0
37.450	2.3994	5.30	16.7
39.450	2.2822	12.06	37.9
41.900	2.1994	7.47	23.5
42.450	2.1276	9.44	29.7
46.650	1.9454	5.70	17.9
47.500	1.9125	7.64	24.0
47.750	1.9031	8.06	25.4
48.000	1.8937	9.76	30.7
49.950	1.8243	7.38	23.2
50.150	1.8175	14.14	44.5
54.150	1.6923	7.45	23.4
59.400	1.5546	7.38	23.2
59.650	1.5487	7.40	23.3
60.000	1.5405	7.12	22.4
62.300	1.4890	13.72	43.2

Table E.3 CRYSTALLINE DATA OF FLY ASH PASTE, 7-DAY CURING

2θ Degrees	d-Spacing Angstroms	Relative intensity, %	Integrated intensity, cps
20.850	4.2568	18.14	82.1
23.200	3.8306	6.36	28.8
25.950	3.4306	7.17	32.4
26.150	3.4048	9.02	40.8
26.600	3.3482	100.00	452.4
31.050	2.8777	7.91	35.8
32.400	2.7609	8.33	37.7
32.650	2.7403	8.98	40.6
33.300	2.6883	21.41	96.8
33.800	2.6496	5.22	23.6
39.500	2.2794	40.45	183.0
40.950	2.2020	5.87	26.6
42.950	2.1040	26.94	121.9

Table E.4 CRYSTALLINE DATA OF FLY ASH PASTE, 21-DAY CURING

2θ Degrees	d-Spacing Angstroms	Relative intensity, %	Integrated intensity, cps
9.150	9.6567	17.60	71.8
9.950	8.8820	5.38	22.0
15.800	5.6041	11.29	46.1
17.850	4.9649	9.35	38.1
18.900	4.6913	7.04	28.7
20.800	4.2669	22.45	91.6
21.400	4.1486	6.85	28.0
22.950	3.8718	19.47	79.5
25.650	3.4700	12.57	51.3
26.600	3.3482	100.00	408.1
27.500	3.2406	27.75	13.3
29.400	3.0354	17.29	70.6
31.000	2.8823	8.00	32.6
31.250	2.8598	5.39	22.0
32.350	2.7650	11.35	46.3
32.650	2.7403	7.90	32.3
33.350	2.6844	29.63	21.2
39.450	2.2822	9.29	37.9
40.950	2.2020	12.76	52.1
42.500	2.1252	8.30	33.9
42.900	2.1063	18.77	6.6
43.200	2.0924	8.59	35.1
47.900	1.8975	5.13	20.9
49.900	1.8260	5.52	22.5

Table E.5 CRYSTALLINE DATA OF FLY ASH PASTE, 1-MONTH CURING

2θ Degrees	d-Spacing Angstroms	Relative intensity, %	Integrated intensity, cps
20.850	4.2568	21.90	49.7
24.950	3.5658	6.31	43.1
26.050	3.4176	5.04	34.4
26.650	3.3420	100.00	683.7
27.100	3.2876	9.34	63.8
29.050	3.0712	5.55	38.0
29.400	3.0354	8.37	57.2
31.100	2.8732	15.20	103.9
32.650	2.7403	10.24	70.0
33.350	2.6844	21.60	147.6
36.550	2.4563	7.49	51.2
39.550	2.2767	5.51	37.7
42.500	2.1252	6.74	46.1
43.000	2.1016	15.53	106.2

Table E.6 CRYSTALLINE DATA OF FLY ASH PASTES, 1-YEAR CURING

2θ Degrees	d-Spacing Angstroms	Relative intensity, %	Integrated intensity, cps
10.750	8.2227	8.94	93.0
20.800	4.2669	13.78	143.4
21.650	4.1012	10.05	104.5
26.600	3.3482	100.00	1040.3
31.050	2.8777	5.62	58.5
33.300	2.6883	9.67	100.6
36.500	2.4596	5.70	59.3
42.900	2.1063	11.53	120.0

Table E.7 CRYSTALLINE DATA OF COWETA FAB + 25% FLY ASH, 28-DAYS CURING

2θ Degrees	d-Spacing Angstroms	Relative intensity, %	Integrated intensity, cps
20.800	4.2669	16.19	228.1
26.600	3.3482	100.00	1408.9
27.650	3.2234	5.39	76.0
27.900	3.1951	11.37	160.2
29.350	3.0404	6.16	86.8
30.900	2.8914	17.14	241.5
33.350	2.6844	7.52	106.0
39.400	2.2850	6.86	96.6
42.450	2.1276	5.24	73.8

Table E.8 CRYSTALLINE DATA OF COWETA CABs+ 25% FLY ASH, 28-DAYS CURING

2θ Degrees	d-Spacing Angstroms	Relative intensity, %	Integrated intensity, cps
23.100	3.8470	7.01	231.4
26.600	3.3482	17.31	571.5
29.450	3.0304	100.00	3301.8
36.000	2.4926	6.86	226.7
39.450	2.2822	9.53	314.6
43.200	2.0924	7.97	263.2
47.600	1.9087	5.95	196.5
48.550	1.8736	8.72	287.8

Table E.9 CRYSTALLINE DATA OF COWETA FAB + 15% FLY ASH, 90-DAYS CURING

2θ Degrees	d-Spacing Angstroms	Relative intensity, %	Integrated intensity, cps
20.950	4.2367	20.78	631.7
23.750	3.7431	3.81	115.9
26.750	3.3298	100.00	3040.1
27.550	3.2349	6.50	197.7
27.950	3.1895	5.51	167.4
28.020	3.1618	11.45	348.0
28.650	3.1131	7.38	224.2
36.650	2.4499	8.62	262.0
39.550	2.2726	5.96	181.3
42.550	2.1228	8.57	260.4
45.900	1.9754	5.76	175.0

Table E.10 CRYSTALLINE DATA OF COWETA FAB + 25% FLY ASH, 90-DAYS CURING

2θ Degrees	d-Spacing Angstroms	Relative intensity, %	Integrated intensity, cps
20.700	4.2873	18.53	353.3
25.150	3.5379	6.42	122.5
26.500	3.3606	100.00	1906.9
20.200	3.0557	7.53	143.6
36.400	2.4668	5.52	105.3
39.350	2.2878	9.99	190.4
42.350	2.1324	6.02	114.8

Table E.11 CRYSTALLINE DATA OF COWETA FAB + 35% FLY ASH, 90-DAYS CURING

2θ Degrees	d-Spacing Angstroms	Relative intensity, %	Integrated intensity, cps
20.550	4.3182	34.35	349.6
26.350	3.3794	72.72	740.2
27.300	3.2639	7.39	75.2
27.750	3.2120	100.00	1017.8
33.050	2.7080	8.30	85.4
36.300	2.4727	15.39	156.7
42.150	2.1420	18.72	190.6
42.650	2.1181	5.42	55.2
49.850	1.8277	9.34	95.0

Table E.12 CRYSTALLINE DATA OF COWETA CABs+ 15% FLY ASH, 90-DAYS CURING

2θ Degrees	d-Spacing Angstroms	Relative intensity, %	Integrated intensity, cps
20.900	4.2467	13.44	210.1
23.150	3.8388	8.28	129.3
26.700	3.3359	50.36	786.9
29.500	3.0253	100.00	1562.6
30.950	2.8868	7.53	117.6
36.100	2.4859	11.84	185.1
39.550	2.2767	21.12	330.0
43.300	2.0878	18.18	284.0
47.250	1.9220	5.76	90.1
47.650	1.9068	14.85	232.1
48.650	1.8700	17.22	269.1

Table E.13 CRYSTALLINE DATA OF COWETA CABs+ 25% FLY ASH, 90-DAYS CURING

2θ Degrees	d-Spacing Angstroms	Relative intensity, %	Integrated intensity, cps
21.050	4.2168	16.91	200.3
23.300	3.8144	8.76	103.8
26.900	3.3115	69.02	817.6
28.150	3.1673	17.45	206.8
29.650	3.0104	100.00	1184.7
31.100	2.8732	6.82	80.8
36.250	2.4760	14.63	173.4
39.700	2.2684	21.73	257.4
43.150	2.0947	5.20	61.6
43.450	2.0809	13.91	164.8
47.400	1.9163	5.40	63.9
47.800	1.9012	14.66	173.7
48.800	1.8646	14.95	177.1

Table E.14 CRYSTALLINE DATA OF COWETA CABs+ 35% FLY ASH, 90-DAYS CURING

2θ Degrees	d-Spacing Angstroms	Relative intensity, %	Integrated intensity, cps
21.000	4.2276	14.89	114.3
23.150	3.8388	10.99	84.4
26.700	3.3359	67.72	520.0
29.550	3.0203	100.00	767.9
31.100	2.8732	6.05	46.4
31.650	2.8246	5.56	42.7
33.500	2.6727	6.26	48.1
35.500	2.5266	6.97	53.5
36.150	2.4826	15.72	120.7
39.550	2.2767	26.37	202.5
41.100	2.1943	5.64	43.3
43.000	2.1016	5.05	38.7
43.350	2.0855	18.16	139.4
47.250	1.9220	7.33	56.3
47.700	1.9050	18.18	139.6
48.700	1.8681	23.21	178.2

APPENDIX F

MINERAL DISTRIBUTION IN MIXES AS DETECTED BY X-RAY DIFFRACTION

Table F.1 MINERAL DISTRIBUTION - FLY ASH POWDER AND PASTES

Mineral Name	Chemical Formula	Symbol	Intensity, cps (Relative Intensity, %)					
			Raw Fly Ash	Paste 1-D	Paste 7-D	Paste 21-D	Paste 1-Mo.	Paste 1-Yr.
Dicalcium Silicate (C_2S)	$2CaO.SiO_2$	D	61.7 (14)	39.8 (13)	40.6 (9)	46.3 (11)	70.0 (10)	x
Tricalcium Aluminate (C_3A)	$3CaO.Al_2O_3$	T	256.8 (60)	105.8 (34)	96.8 (21)	121.2 (30)	147.6 (22)	100.6 (10)
Calcite (Calcium Carbonate)	$CaCO_3$	C	-	41.8 (13)	67.8 (15)	70.6 (17)	57.2 (8)	38.6 (4)
Portlandite (Calcium Hydroxide)	$Ca(OH)_2$	Pt	-	24.3 (8)	23.6 (5)	x	26.2 (4)	-
Ettringite ($C_3A.3\bar{C}S.H_{32}$)	$3CaO.Al_2O_3.3CaSO_4.32H_2O$	E	-	9.3 (3)	28.8 (6)	79.5 (19)	x	-
Monosulfoaluminate ($C_3A.\bar{C}S.H_{13}$)	$3CaO.Al_2O_3.CaSO_4.13H_2O$	Ms	-	-	35.8 (8)	32.6 (8)	103.9 (15)	58.5 (6)
Quartz	SiO_2	Q	431.0 (100)	314.6 (100)	452.4 (100)	408.1 (100)	683.7 (100)	1040.3 (100)
Periclase	MgO	P	139.6 (32)	29.7 (9)	121.9 (27)	76.6 (19)	106.2 (16)	120.0 (12)
Anhydrite	$CaSO_4$	A	83.5 (19)	41.5 (13)	15.2 (4)	-	-	-
Lime	CaO	L	74.6 (17)	16.7 (5)	-	-	-	-
Calcium Aluminum Oxide Sulfate ($C_4A_3\bar{S}$)	$3CaO.3Al_2O_3.CaSO_4$	X	69.6 (16)	52.3 (17)	15.9 (4)	-	-	-
Microline	$KAlSi_3O_8$	Mc	x	-	-	113.3 (28)	20.3 (3)	31.2 (3)
Gismondine (CAS_2H_4)	$CaO.2SiO_2.Al_2O_3.4H_2O$	G	-	-	-	-	-	143.4 (14)
Calcium Aluminate Oxide Hydrate (C_4AH_{19})	$4CaO.Al_2O_3.19H_2O$	Z	-	-	-	-	-	20.4 (2)
Straetlingite (C_2ASH_8)	$2CaO.SiO_2.Al_2O_3.8H_2O$	S	-	-	-	15.7 (4)	15.5 (2)	26.7 (3)
Dolomite	$(MgCaFe)CO_3$	Dm	-	-	-	-	-	-

x = trace

Table F.2 MINERAL DISTRIBUTION - NORMAN 28-DAY MIXES

Mineral Name	Chemical Formula	Symbol	Intensity, cps (Relative Intensity, %)					
			FAB + 15	FAB + 25	FAB + 35	CAB + 15	CAB + 25	CAB + 35
Dicalcium Silicate (C_2S)	$2CaO.SiO_2$	D	- -	39.2 (3)	37.0 (6)	-	-	-
Tricalcium Aluminate (C_3A)	$3CaO.Al_2O_3$	T	70.6 (7)	102.1 (9)	80.1 (13)	56.9 (2)	38.1 (2)	55.8 (2)
Calcite (Calcium Carbonate)	$CaCO_3$	C	1007.2 (100)	699.7 (61)	423.9 (68)	2972.2 (100)	1829.6 (100)	2349.3(100)
Portlandite (Calcium Hydroxide)	$Ca(OH)_2$	Pt	-	-	-	-	-	-
Ettringite ($C_3A.3C\bar{S}.H_{32}$)	$3CaO.Al_2O_3.3CaSO_4.32H_2O$	E	-	x	x	-	x	x
Monosulfoaluminate ($C_3A.C\bar{S}.H_{13}$)	$3CaO.Al_2O_3.CaSO_4.13H_2O$	Ms	-	-	x	45.0 (2)	x	x
Quartz	SiO_2	Q	963.9 (96)	1150.6 (100)	624.8 (100)	644.2 (22)	697.5 (38)	715.9 (31)
Periclase	MgO	P	59.2 (6)	124.3 (11)	82.1 (13)	48.0 (2)	93.2 (11)	83.8 (4)
Anhydrite	$CaSO_4$	A	-	-	26.2 (4)	-	-	70.6 (3)
Lime	CaO	L	-	-	-	-	-	-
Calcium Aluminum Oxide Sulfate ($C_4A_3\bar{S}$)	$3CaO.3Al_2O_3.CaSO_4$	X	-	-	15.1 (2)	-	-	19.4 (1)
Microline	$KAlSi_3O_8$	Mc	-	x	x	-	-	-
Gismondine (CAS_2H_4)	$CaO.2SiO_2.Al_2O_3.4H_2O$	G	93.0 (9)	107.0 (9)	x	58.4 (2)	x	x^+
Calcium Aluminate Oxide Hydrate (C_4AH_{19})	$4CaO.Al_2O_3.19H_2O$	Z	28.9 (3)	40.4 (4)	x	-	141.5 (8)	x^+
Straetlingite (C_2ASH_8)	$2CaO.SiO_2.Al_2O_3.8H_2O$	S	-	41.3 (4)	27.9 (4)	28.8 (1)	-	23.8 (1)
Dolomite	$(MgCaFe)CO_3$	Dm	44.9 (5)	62.2 (5)	178.4 (29)	57.0 (2)	68.9 (4)	73.8 (3)

x = trace

x^+ = present, not recorded

Table F.3 MINERAL DISTRIBUTION - NORMAN 90-DAY MIXES

Mineral Name	Chemical Formula	Symbol	Intensity, cps (Relative Intensity, %)					
			FAB + 15	FAB + 25*	FAB + 35	CAB + 15	CAB + 25	CAB + 35
Dicalcium Silicate (C_2S)	$2CaO.SiO_2$	D	- -	35.2 (3)	31.2 (7)	17.5 (3)	30.3 (5)	-
Tricalcium Aluminate (C_3A)	$3CaO.Al_2O_3$	T	92.2 (5)	82.7 (8)	118.9 (28)	93.7 (15)	91.0 (14)	93.0 (18)
Calcite (Calcium Carbonate)	$CaCO_3$	C	269.2 (15)	814.3 (75)	119.6 (28)	543.7 (84)	201.1 (30)	344.3 (66)
Portlandite (Calcium Hydroxide)	$Ca(OH)_2$	Pt	-	-	-	-	-	-
Ettringite ($C_3A.3C\bar{S}.H_{32}$)	$3CaO.Al_2O_3.3CaSO_4.32H_2O$	E	x	21.8 (2)	16.5 (4)	-	-	x
Monosulfoaluminate ($C_3A.C\bar{S}.H_{13}$)	$3CaO.Al_2O_3.CaSO_4.13H_2O$	Ms	63.1 (3)	18.8 (2)	33.8 (8)	27.7 (4)	25.6 (4)	53.6 (10)
Quartz	SiO_2	Q	1812.1 (100)	1079.4 (100)	421.5 (100)	646.0 (100)	660.2 (100)	523.8(100)
Periclase	MgO	P	55.5 (3)	73.8 (7)	87.4 (21)	62.6 (10)	90.6 (14)	73.4 (14)
Anhydrite	$CaSO_4$	A	-	32.0 (3)	33.8 (8)	33.0 (5)	37.0 (6)	35.1 (7)
Lime	CaO	L	-	-	17.6 (4)	x	-	15.3 (3)
Calcium Aluminum Oxide Sulfate ($C_4A_3\bar{S}$)	$3CaO.3Al_2O_3.CaSO_4$	X	60.0 (3)	47.0 (4)	70.9 (17)	24.5 (4)	23.2 (4)	-
Microline	$KAlSi_3O_8$	Mc	44.8 (2)	25.2 (2)	19.1 (5)	29.9 (5)	-	-
Gismondine (CAS_2H_4)	$CaO.2SiO_2.Al_2O_3.4H_2O$	G	123.3 (7)	87.1 (8)	x	130.8 (20)	x	160.2 (31)
Calcium Aluminate Oxide Hydrate (C_4AH_{19})	$4CaO.Al_2O_3.19H_2O$	Z	788.8 (44)	39.2 (4)	137.8 (33)	26.4 (4)	x	-
Straetlingite (C_2ASH_8)	$2CaO.SiO_2.Al_2O_3.8H_2O$	S	19.0 (1)	-	77.9 (19)	19.7 (3)	14.4 (2)	33.0 (6)
Dolomite	$(MgCaFe)CO_3$	Dm	-	34.5 (3)	16.5 (4)	56.1 (9)	-	-

x = trace

* cured for 9 months

Table F.4 MINERAL DISTRIBUTION - COWETA 28-DAY MIXES

Mineral Name	Chemical Formula	Symbol	Intensity, cps (Relative Intensity, %)					
			FAB + 15	FAB + 25	FAB + 35	CAB + 15	CAB + 25	CAB + 35
Dicalcium Silicate (C_2S)	$2CaO.SiO_2$	D	20.2 (1)	39.6 (3)	36.3 (4)	-	-	-
Tricalcium Aluminate (C_3A)	$3CaO.Al_2O_3$	T	108.8 (3)	106.0 (8)	120.2 (12)	71.3 (3)	99.9 (3)	78.2 (5)
Calcite (Calcium Carbonate)	$CaCO_3$	C	120.3 (3)	86.8 (6)	49.2 (5)	2701.9 (100)	3301.8 (100)	1497.0 (100)
Portlandite (Calcium Hydroxide)	$Ca(OH)_2$	Pt	-	-	-	-	-	-
Ettringite ($C_3A.3\bar{C}S.H_{32}$)	$3CaO.Al_2O_3.3CaSO_4.32H_2O$	E	32.1 (1)	34.0 (2)	67.4 (7)	42.1 (2)	x	32.5 (2)
Monosulfoaluminate ($C_3A.\bar{C}S.H_{13}$)	$3CaO.Al_2O_3.CaSO_4.13H_2O$	Ms	43.7 (1)	45.1 (3)	60.8 (7)	x	-	-
Quartz	SiO_2	Q	3587.7 (100)	1408.9 (100)	966.5 (100)	683.4 (25)	571.5 (17)	351.6 (23)
Periclase	MgO	P	95.3 (3)	62.2 (4)	94.6 (10)	52.4 (2)	83.1 (3)	67.8 (5)
Anhydrite	$CaSO_4$	A	-	-	-	-	-	-
Lime	CaO	L	-	-	-	-	-	-
Calcium Aluminum Oxide Sulfate ($C_4A_3\bar{S}$)	$3CaO.3Al_2O_3.CaSO_4$	X	30.1 (1)	19.7 (1)	51.0 (5)	-	-	-
Microline	$KAlSi_3O_8$	Mc	-	-	-	-	-	-
Gismondine (CAS_2H_4)	$CaO.2SiO_2.Al_2O_3.4H_2O$	G	455.5 (13)	26.7 (2)	68.6 (7)	57.8 (2)	-	-
Calcium Aluminate Oxide Hydrate (C_4AH_{19})	$4CaO.Al_2O_3.19H_2O$	Z	304.8 (9)	160.2 (11)	150.5 (16)	-	63.7 (2)	28.7 (2)
Straetlingite (C_2ASH_8)	$2CaO.SiO_2.Al_2O_3.8H_2O$	S	46.6 (1)	54.8 (4)	70.5 (7)	-	-	-
Dolomite	$(MgCaFe)CO_3$	Dm	44.0 (1)	241.5 (17)	25.3 (3)	198.3 (7)	143.9 (4)	147.3 (10)

x = trace

Table F.5 MINERAL DISTRIBUTION - COWETA 90-DAY MIXES

Mineral Name	Chemical Formula	Symbol	Intensity, cps (Relative Intensity, %)					
			FAB + 15	FAB + 25	FAB + 35	CAB + 15	CAB + 25	CAB + 35
Dicalcium Silicate (C_2S)	$2CaO.SiO_2$	D	25.7 (1)	21.9 (1)	-	-	-	-
Tricalcium Aluminate (C_3A)	$3CaO.Al_2O_3$	T	32.8 (1)	75.5 (4)	85.4 (8)	42.4 (3)	40.2 (3)	48.1 (6)
Calcite (Calcium Carbonate)	$CaCO_3$	C	120.2 (4)	143.6 (8)	36.2 (4)	1562.6 (100)	1184.7 (100)	767.9 (100)
Portlandite (Calcium Hydroxide)	$Ca(OH)_2$	Pt	-	-	-	-	-	-
Ettringite ($C_3A.3C\bar{S}.H_{32}$)	$3CaO.Al_2O_3.3CaSO_4.32H_2O$	E	15.5 (1)	24.2 (1)	22.9 (2)	-	16.7 (1)	19.5 (3)
Monosulfoaluminate ($C_3A.C\bar{S}.H_{13}$)	$3CaO.Al_2O_3.CaSO_4.13H_2O$	Ms	-	-	47.8 (5)	x	80.8 (7)	46.4 (6)
Quartz	SiO_2	Q	3040.1 (100)	1906.9 (100)	740.2 (73)	786.9 (50)	817.6 (69)	520.0 (68)
Periclase	MgO	P	35.3 (1)	19.1 (1)	55.2 (5)	37.1 (2)	19.4 (2)	38.7 (5)
Anhydrite	$CaSO_4$	A	39.4 (1)	-	63.0 (6)	35.7 (2)	26.6 (2)	42.7 (6)
Lime	CaO	L	-	-	-	-	-	-
Calcium Aluminum Oxide Sulfate ($C_4A_3\bar{S}$)	$3CaO.3Al_2O_3.CaSO_4$	X	115.9 (4)	59.4 (3)	14.5 (1)	22.1 (1)	7.4 (1)	-
Microline	$KAlSi_3O_8$	Mc	21.2 (1)	23.2 (1)	33.5 (3)	-	-	-
Gismondine (CAS_2H_4)	$CaO.2SiO_2.Al_2O_3.4H_2O$	G	197.7 (7)	44.5 (2)	1017.8 (100)	74.0 (5)	-	-
Calcium Aluminate Oxide Hydrate (C_4AH_{19})	$4CaO.Al_2O_3.19H_2O$	Z	167.4 (6)	78.6 (4)	75.2 (7)	77.9 (5)	206.8 (17)	x
Straetlingite (C_2ASH_8)	$2CaO.SiO_2.Al_2O_3.8H_2O$	S	20.3 (1)	-	-	-	12.3 (1)	17.7 (2)
Dolomite	$(MgCaFe)CO_3$	Dm	49.8 (2)	13.9 (1)	38.5 (4)	117.6 (8)	29.2 (2)	19.5 (3)

x = trace

Table F.6 MINERAL DISTRIBUTION - TUPELO 90-DAY AND FT. GIBSON 90-DAY MIXES

Mineral Name	Chemical Formula	Symbol	Intensity, cps (Relative Intensity, %)			
			FAB + 25	CAB + 25	FAB + 25	CAB + 25
Dicalcium Silicate (C_2S)	$2CaO.SiO_2$	D	33.9 (3)	-	30.6 (3)	36.1 (5)
Tricalcium Aluminate (C_3A)	$3CaO.Al_2O_3$	T	63.4 (5)	75.6 (9)	107.9 (11)	98.6 (13)
Calcite (Calcium Carbonate)	$CaCO_3$	C	220.6 (17)	261.0 (30)	212.0 (21)	211.3 (29)
Portlandite (Calcium Hydroxide)	$Ca(OH)_2$	Pt	-	-	-	-
Ettringite ($C_3A.3C\bar{S}.H_{32}$)	$3CaO.Al_2O_3.3CaSO_4.32H_2O$	E	-	27.3 (3)	21.3 (2)	21.9 (3)
Monosulfoaluminate ($C_3A.C\bar{S}.H_{13}$)	$3CaO.Al_2O_3.CaSO_4.13H_2O$	Ms	-	19.2 (2)	40.5 (4)	19.0 (3)
Quartz	SiO_2	Q	1020.1 (80)	868.2 (100)	989.4 (100)	741.2 (100)
Periclase	MgO	P	90.4 (7)	62.0 (7)	87.3 (9)	66.5 (9)
Anhydrite	$CaSO_4$	A	46.7 (4)	-	23.6 (2)	17.2 (2)
Lime	CaO	L	27.9 (2)	-	-	-
Calcium Aluminum Oxide Sulfate ($C_4A_3\bar{S}$)	$3CaO.3Al_2O_3.CaSO_4$	X	-	-	-	-
Microline	$KAlSi_3O_8$	Mc	31.5 (2)	40.2 (5)	-	26.8 (4)
Gismondine (CAS_2H_4)	$CaO.2SiO_2.Al_2O_3.4H_2O$	G	27.3 (2)	42.7 (5)	282.6 (29)	-
Calcium Aluminate Oxide Hydrate (C_4AH_{19})	$4CaO.Al_2O_3.19H_2O$	Z	34.1 (3)	-	34.8 (4)	61.6 (8)
Straetlingite (C_2ASH_8)	$2CaO.SiO_2.Al_2O_3.8H_2O$	S	-	17.5 (2)	21.1 (2)	21.0 (3)
Dolomite	$(MgCaFe)CO_3$	Dm	1270.4 (100)	440.8 (51)	63.7 (6)	41.3(6)

APPENDIX G

ELECTRON MICROGRAPHS

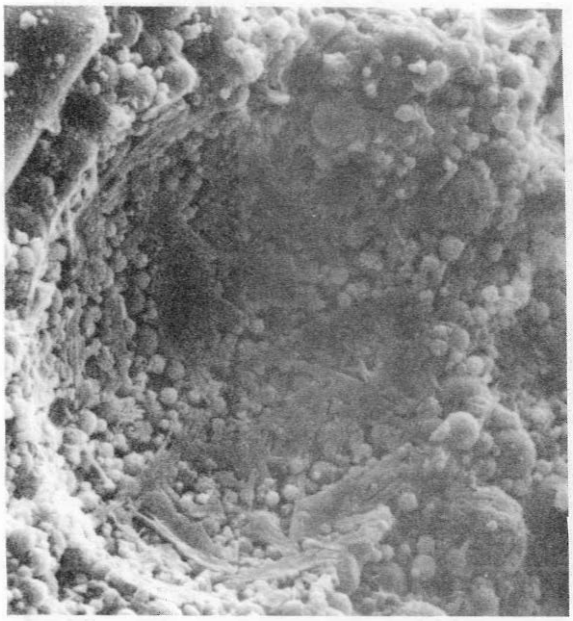

10 µm 1200X (a)

Hydration rim of "pulled out" fly ash particle

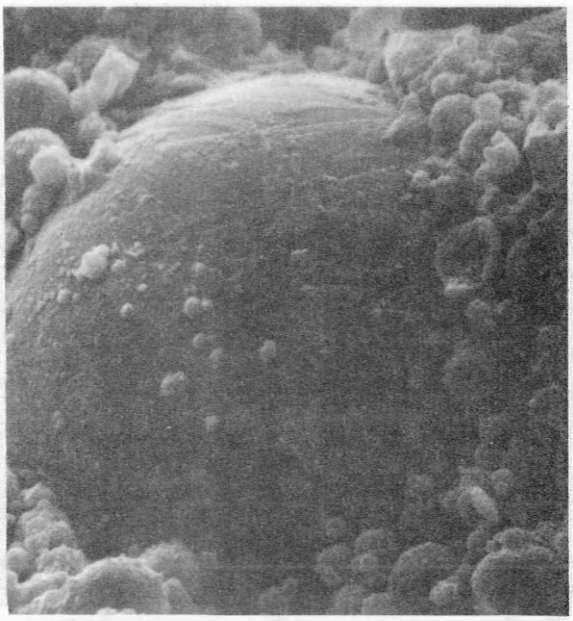

1 µm 3000X (b)

Reacted fly ash particle

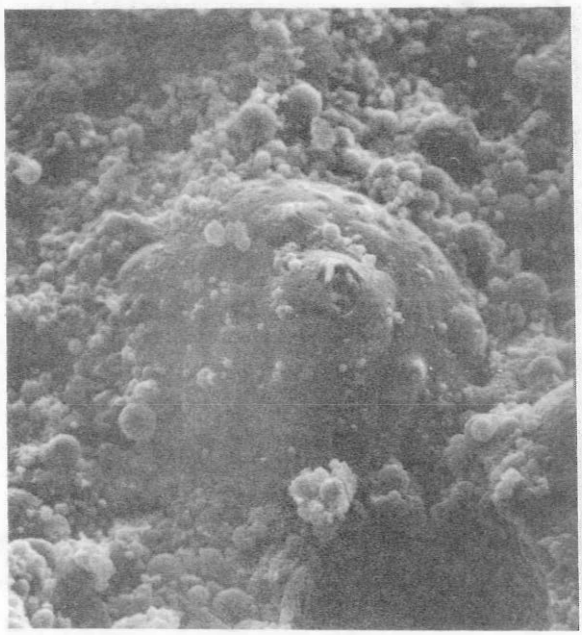

Impregnated plerosphere

10 µm 1000X (c)

Figure G.1 Fly ash paste at 60 days

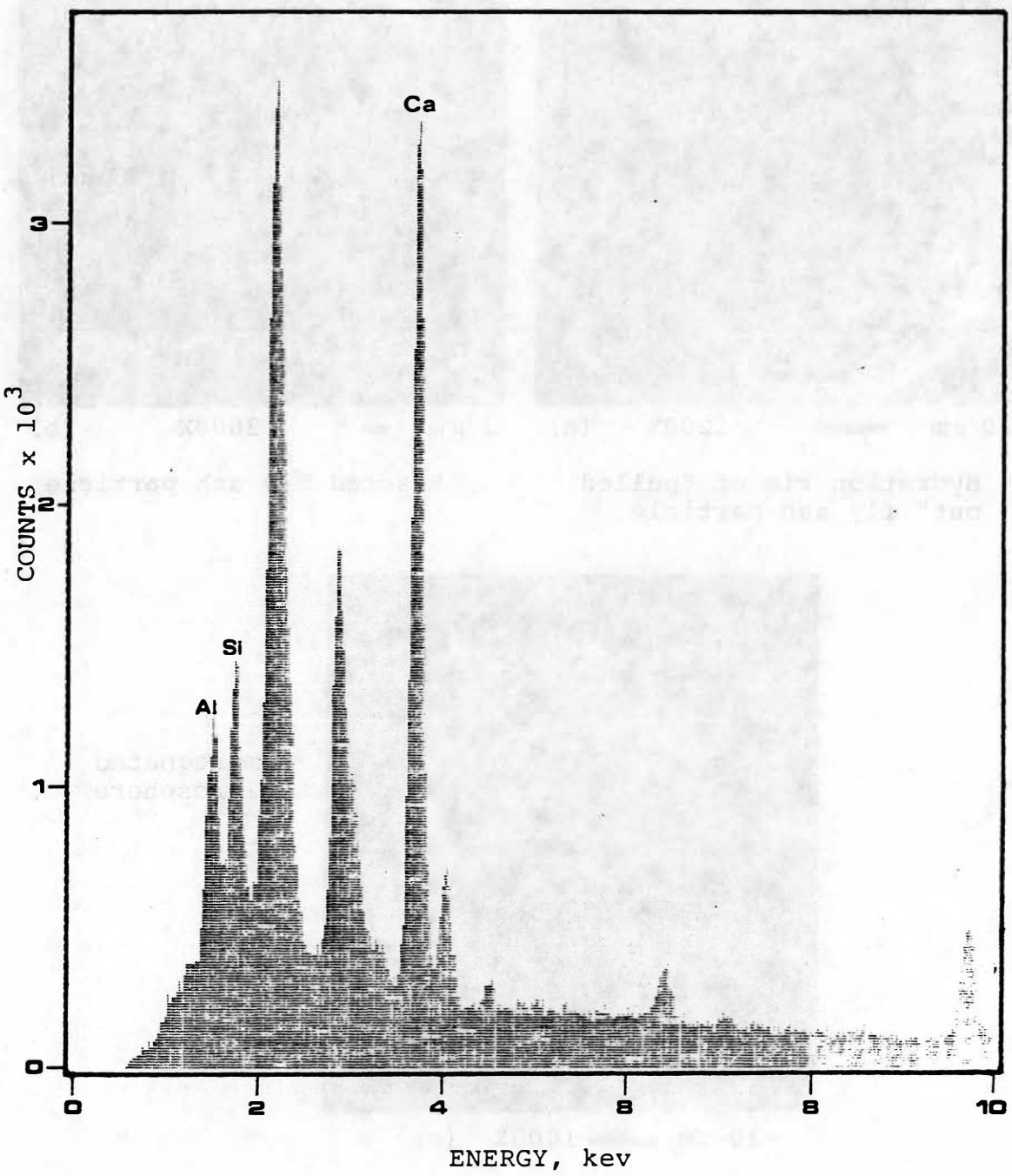

Figure G.2 EDS of the crystals in Figure G.1a

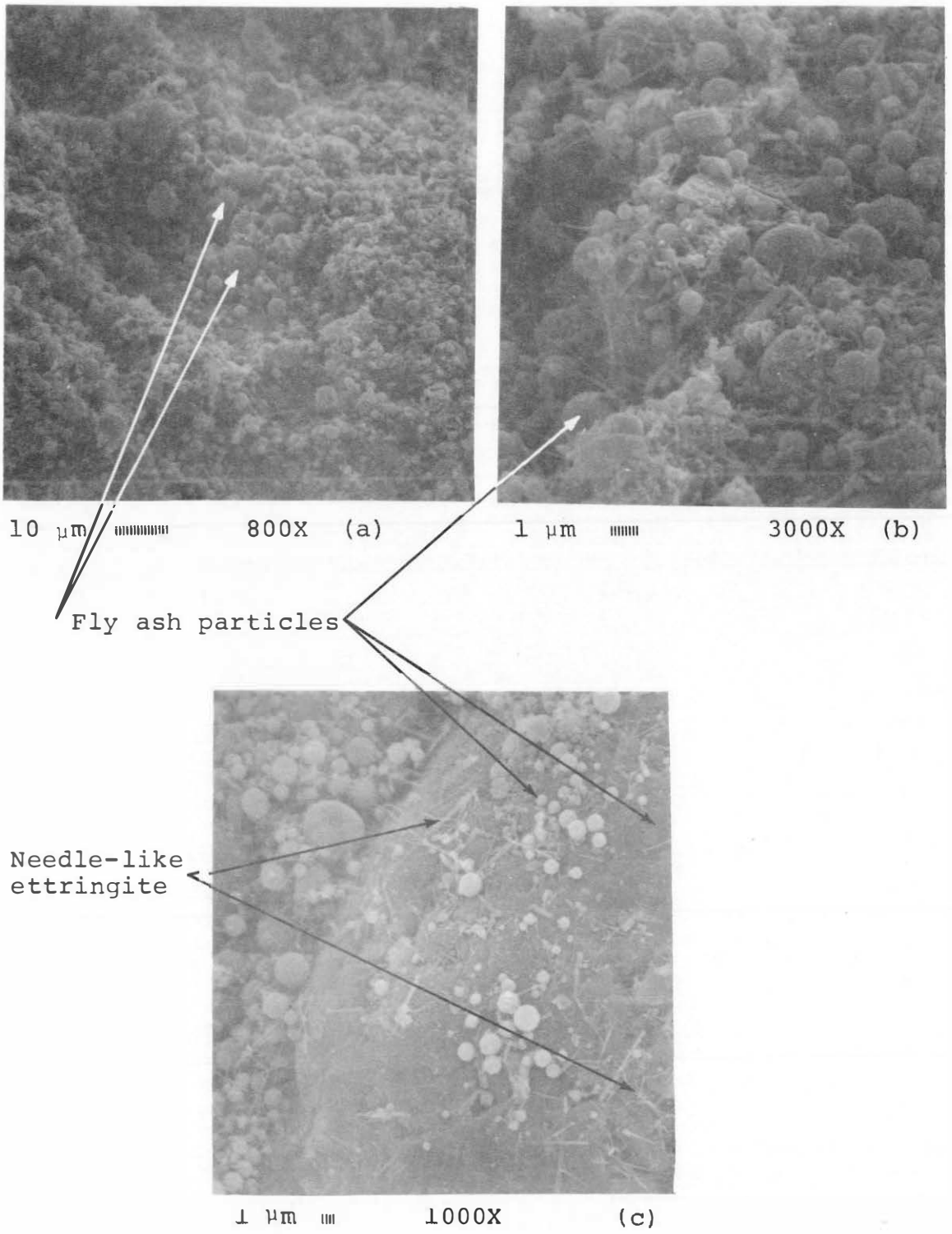

Figure G.3 Norman FAB + 35% fly ash (w/f.a.=0.4) at 1 day

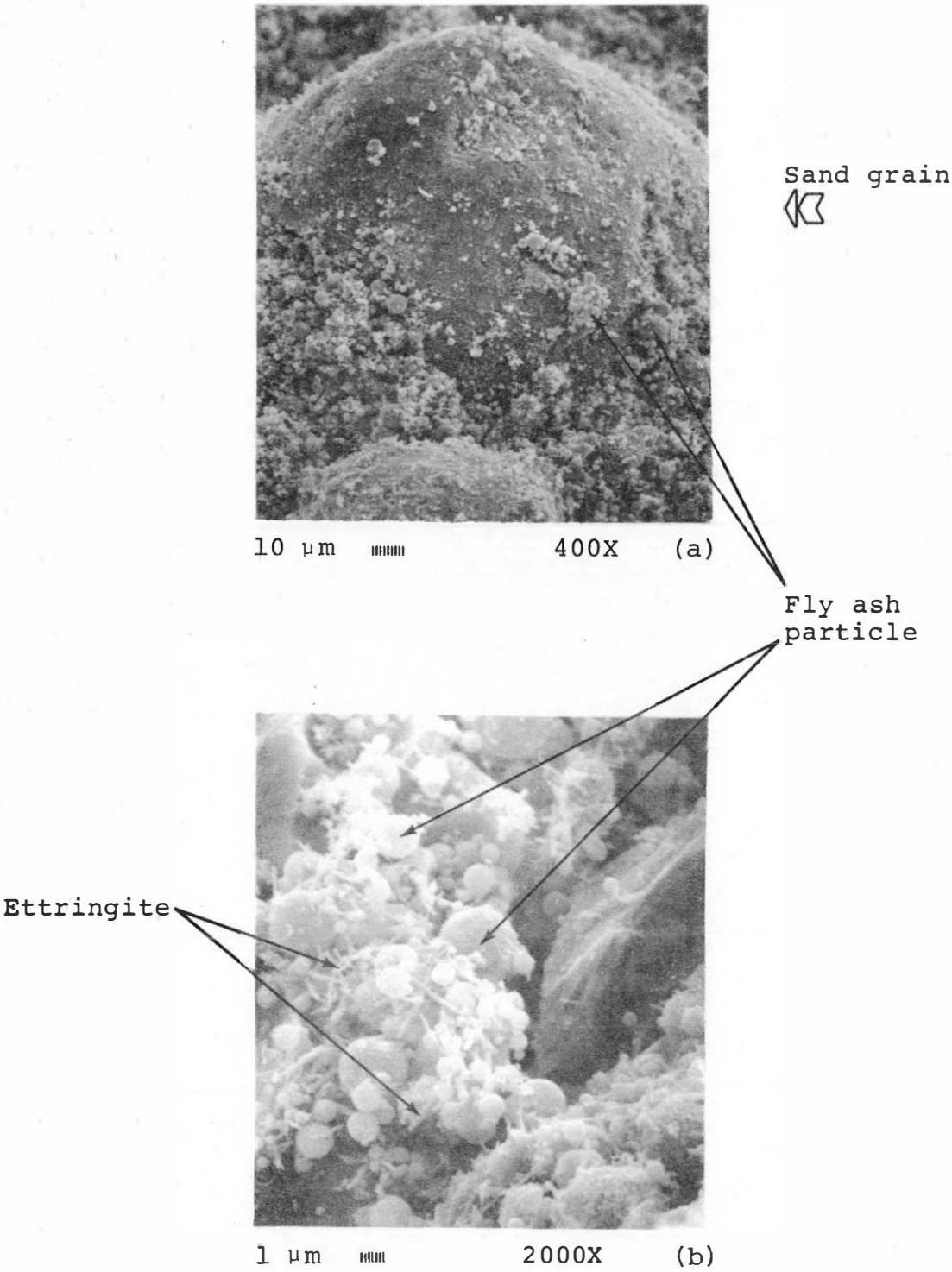

Figure G.4 Norman FAB + 35% fly ash (w/f.a.≈0.4) at 3 days

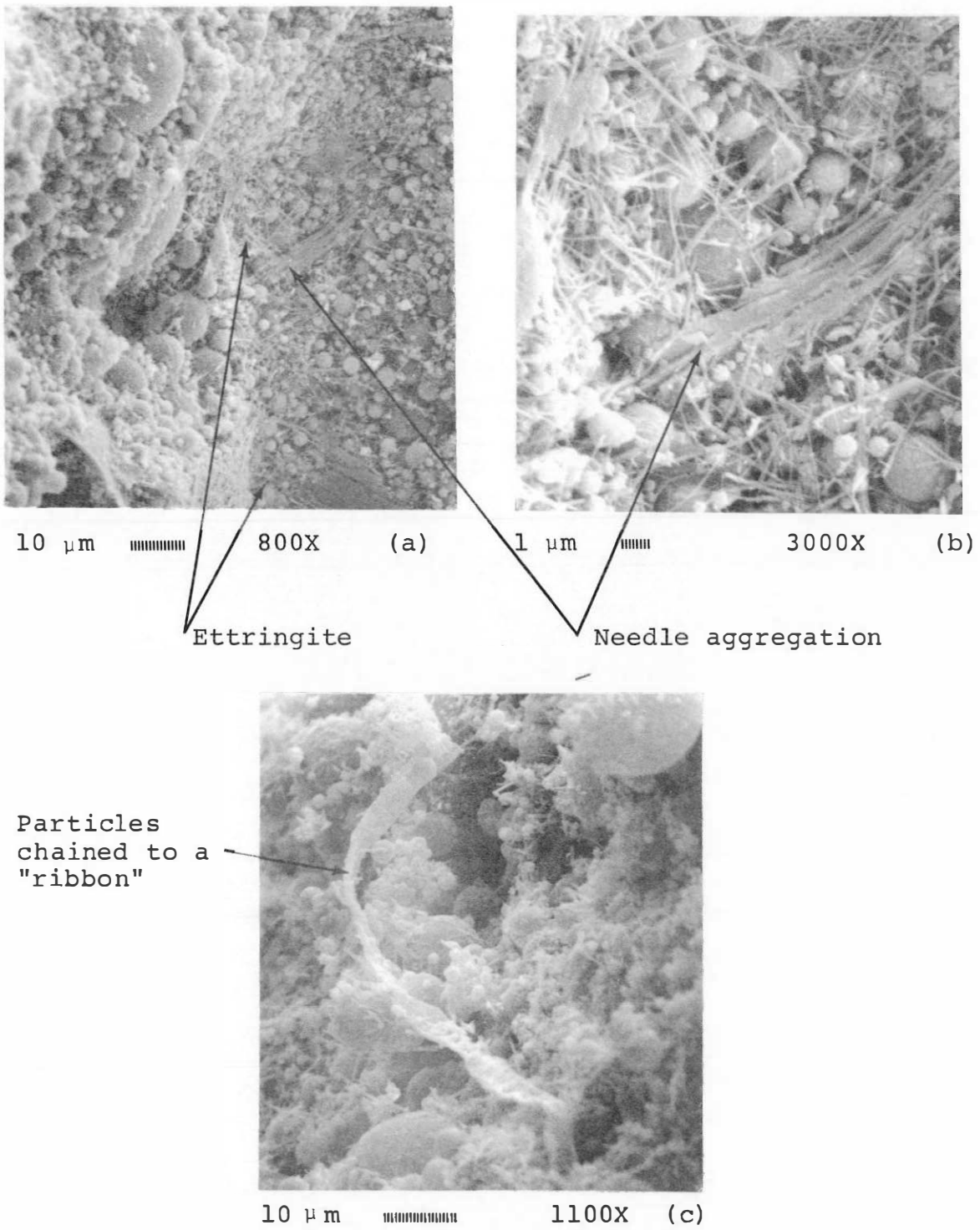

Figure G.5 Norman FAB + 35% fly ash (w/f.a.=0.4) at 7 days

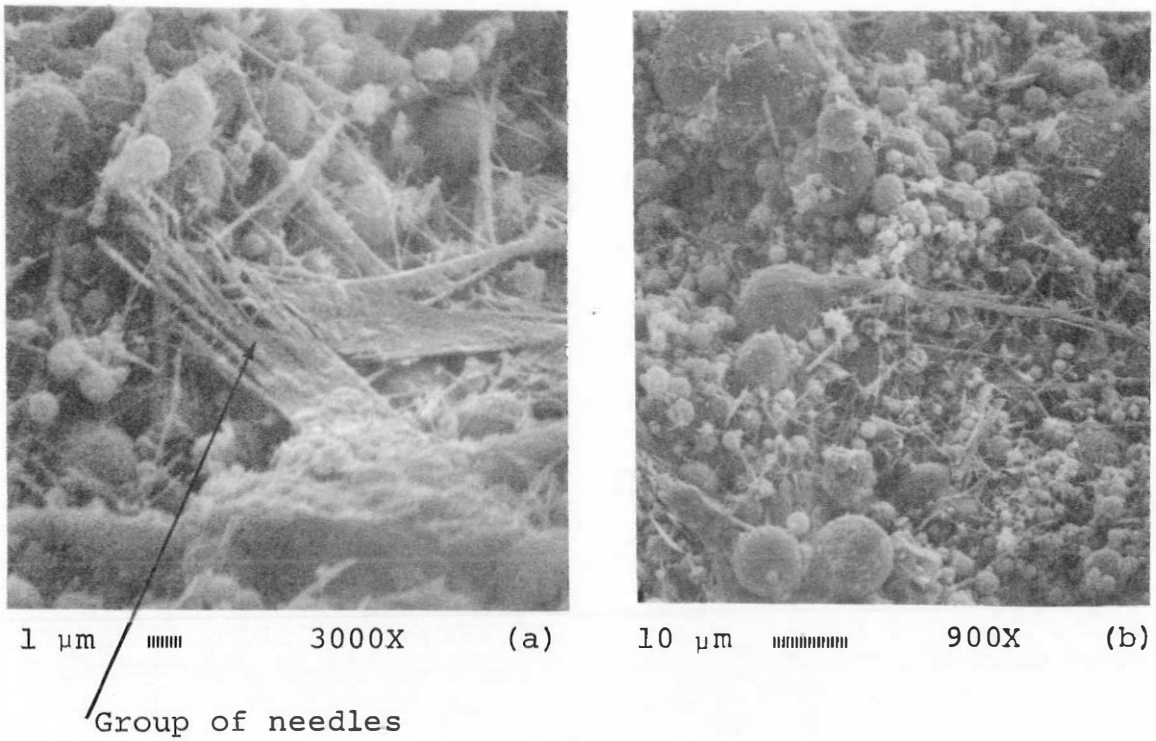

Figure G.6 Norman FAB + 35% fly ash (w/f.a.=0.4) at 28 days

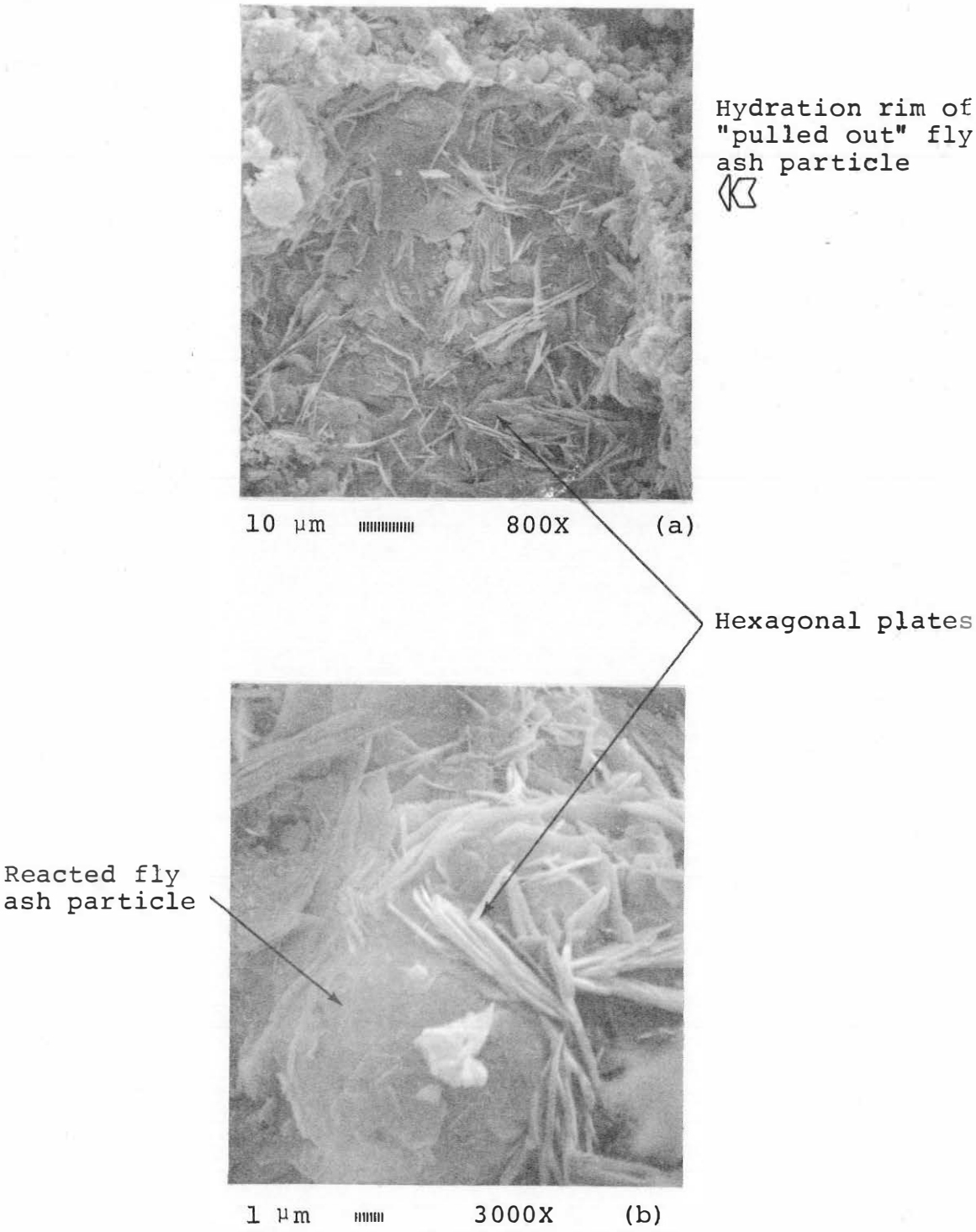

Figure G.7 Norman FAB + 35% fly ash (w/f.a.=0.2) at 28 days

APPENDIX H

A BASE DESIGN PROGRAM

HP 41C, 41CV, 41CX

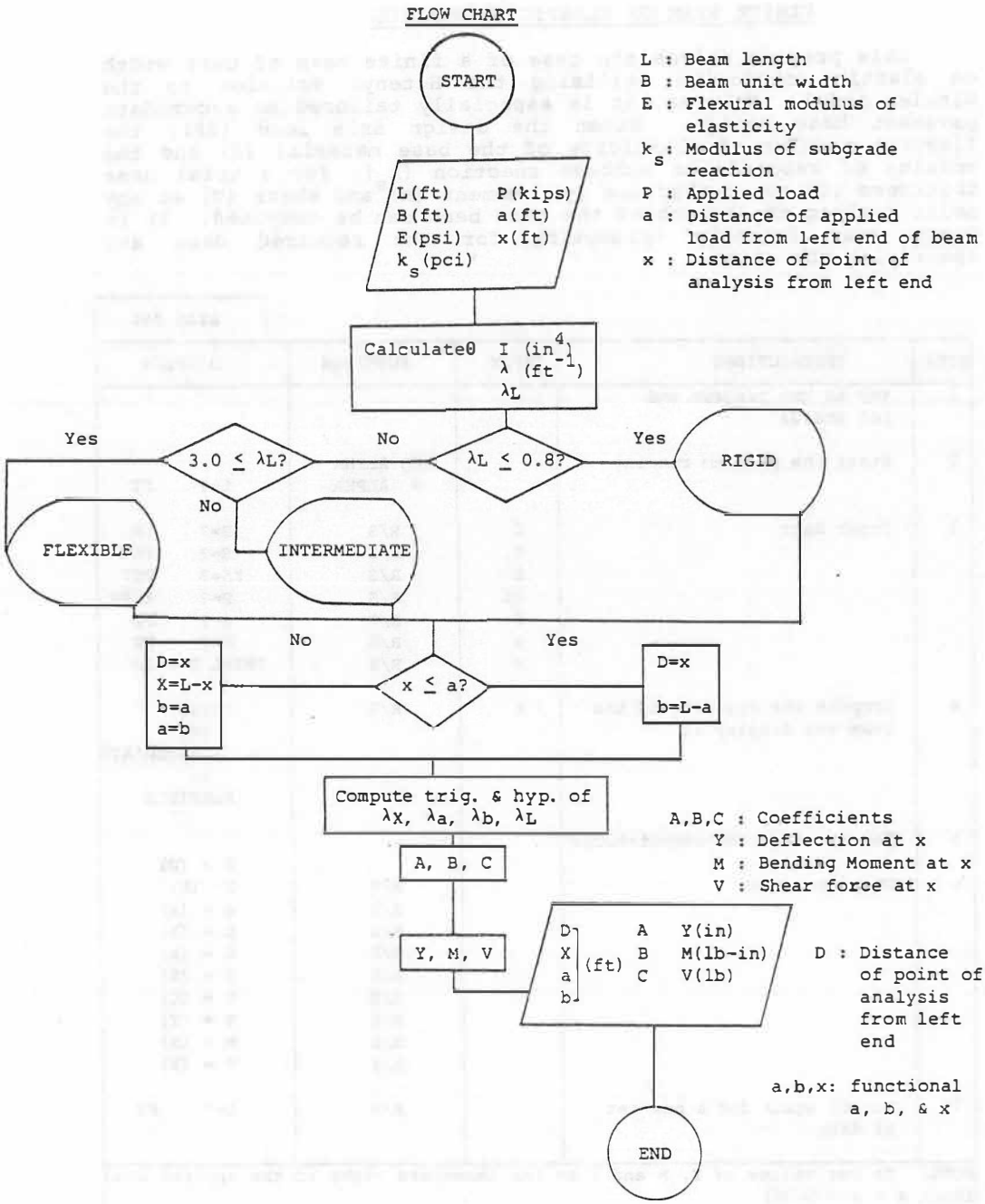
FLOW CHART
START
L(ft) P(kips)
B(ft) a(ft)
E(psi) x(ft)
k_s(pci)
Calculate θ I (in^4)
λ (ft^{-1})
λL
3.0 ≤ λL?
Yes
No
λL ≤ 0.8?
Yes
No
RIGID
FLEXIBLE
INTERMEDIATE
x ≤ a?
No
Yes
D=x
X=L-x
b=a
a=b
D=x
b=L-a
Compute trig. & hyp. of λX, λa, λb, λL
A, B, C
Y, M, V
D
X
a
b
(ft)
A Y(in)
B M(lb-in)
C V(lb)
END
L : Beam length
B : Beam unit width
E : Flexural modulus of elasticity
k_s: Modulus of subgrade reaction
P : Applied load
a : Distance of applied load from left end of beam
x : Distance of point of analysis from left end
A,B,C : Coefficients
Y : Deflection at x
M : Bending Moment at x
V : Shear force at x
D : Distance of point of analysis from left end
a,b,x: functional a, b, & x

FINITE BEAM ON ELASTIC FOUNDATION

This program solves the case of a finite beam of unit width on elastic foundation utilizing the Hetenyi solution to the Winkler model. However, it is especially tailored to accomodate pavement base design. Given the design axle load (2P), the flexural modulus of elasticity of the base material (E) and the modulus of subgrade or subbase reaction (k_s), for a trial base thickness (T) the deflection (y), moment (M) and shear (V) at any point x along the length of the base beam can be computed. It is "very user friendly" prompting for the required data and specifying the units.

SIZE 051

STEP	INSTRUCTIONS	INPUT	FUNCTION	DISPLAY
1	Key in the program and set status			
2	Start the program running		XEQ ALPHA W ALPHA	L=? FT
3	Input data	L	R/S	B=? IN
		B	R/S	E=? PSI
		E	R/S	KS=? PCI
		KS	R/S	P=? KIPS
		P	R/S	a=? FT
		a	R/S	X=? FT
		x	R/S	TRIAL T=? IN
4	Compute the rigidity of the beam and display it	T	R/S	RIGID or INTERMEDIATE or FLEXIBLE
5	Perform required computations			
6	Display output			D = (D)
			R/S	X= (X)
			R/S	a = (a)
			R/S	b = (b)
			R/S	A = (A)
			R/S	B = (B)
			R/S	C = (C)
			R/S	Y = (Y)
			R/S	M = (M)
			R/S	V = (V)
7	Run it again for a new set of data		R/S	L=? FT

NOTE: To get values of Y, M2and V at the immediate right of the applied load input x = a+0.00001

```
01    LBL   "W"
02    "L=?       FT"
03    PROMPT
04    STO  01
05    "B=?       IN"
06    PROMPT
07    STO 02
08    "E=?     PSI"
09    PROMPT
10    STO 03
11    "KS=?    PCI"
12    PROMPT
13    RCL 02
14      *
15    STO 04          → k's
16    "P=?     KIPS"
17    PROMPT
18    STO 05
19    "a=?       FT"
20    PROMPT
21    STO 06
22    "x=?       FT"
23    PROMPT
24    STO 08
25    "TRIAL T=?  IN"
26    PROMPT
27    STO 09
28    FIX 9
29    ENTER
30    3
31    y/x
32    RCL 02
33     *
34    12
35    /
36    STO 10          →I
37    RCL 03
38    *
39    4
40    *
```

Data Entry

Calculates I (in^4)

```
41    1/x
42    RCL 04
43      *
44    ENTER
45    .25
46    Y/X
47    12
48      *
49    STO 11    → λ
50    RCL 01
51      *
52    STO 12    → λL
53    0.8
54    x<>y
55    x<=y?
56    GTO 02
57    3.0
58    RCL 12
59    x<>y
60    x<=y?
61    GTO 01
62    "INTERMEDIATE"
63    BEEP
64    AVIEW
65    PSE
66    GTO 03
67    LBL 01
68    "FLEXIBLE"
69    BEEP
70    AVIEW
71    PSE
72    GTO 03
73    LBL 02
74    "RIGID"
75    BEEP
76    AVIEW
77    PSE
78    LBL 03
79    RCL 08
80    RCL 06
```

Calculates λ (ft^{-1})

Calculates λL

$\lambda L2 \leq 0.8$?

$3.0 \leq \lambda L$?

Depending on value of λL displays if the member is RIGID, INTERMEDIATE, or FLEXIBLE

```
81    x<>y
82    x<=y?
83    GTO 04
84    RCL 01
85    RCL 08                    x>a?
86      -                       if yes a is
87    STO 13    → x             replaced by b
88    RCL 06                    and x is
89    STO 14    → b             measured from
90    CHS                       the right end
91    RCL 01                    of the beam
92      +
93    STO 15    → a
94    GTO 05
95    LBL 04
96    RCL 08
97    STO 13    → X
98    RCL 06
99    STO 15    → a             x ≤ a
100   CHS                       then x,
101   RCL 01                    a,b as are
102     +
103   STO 14    → b
104   LBL 05
105   RCL 11
106   RCL 13
107     *
108   STO 16    → λX            Calculates
109   RCL 11                      λx
110   RCL 15                      λa
111     *                         λb
112   STO 17    → λa
113   RCL 11
114   RCL 14
115     *
116   STO 18    → λb
117   00019.03401               counter for
118   STO 07                    loop of LBL 44
119   RCL 16
120   STO 40

121   XEQ 44                    The values
122   RCL 17                    of λX, λa,
123   STO 40                    λb2and λL
124   XEQ 44                    are placed
125   RCL 18                    in register
126   STO 40                    40 and their
127   XEQ 44                    trig. & hyp.
128   RCL 12                    functions
129   STO 40                    are computed
130   XEQ 44                    (LBL 44)
131   LBL 06
132   RCL 23
133   RCL 30
134     *
135   RCL 24
136   RCL 29
137     *
138     -
139   STO 35
140   RCL 25
141   RCL 28                    Calculates
142     *                           A
143   RCL 26
144   RCL 27
145     *
146     -
147   STO 36
148   RCL 20
149   RCL 21
150     *
151   RCL 19
152   RCL 22
153     *
154     +
155   STO 37
156   RCL 31
157   RCL 26
158     *
159   RCL 28
160     *
```

```
161   RCL 33
162   RCL 24
163    *
164   RCL 30
165    *
166    -
167   STO 38
168   RCL 31
169   x  2
170   RCL 33
171   x / 2
172    -
173   STO 39
174   RCL 35
175   RCL 33
176    *
177   RCL 36
178   RCL 31
179    *
180    +
181   RCL 37
182    *
183   STO 40
184   RCL 38
185   RCL 22
186    *
187   RCL 20
188    *
189    2
190    *
191   RCL 40
192    +
193   RCL 39
194    /
195   STO 41    → A
196   RCL 35
197   RCL 33
198    *
199   RCL 36
200   RCL 31
```

Calculates A

```
201      *
202      +
203   STO 42
204   RCL 20
205   RCL 21
206      *
207   RCL 19
208   RCL 22
209      *
210      -
211   RCL 42
212      *
213   STO 43
214   RCL 38
215   RCL 21
216      *
217   RCL 19
218      *
219      2
220      *
221   RCL 43
222      +
223   RCL 39
224      /
225   STO 44    → B
226   RCL 42
227   RCL 21
228      *
229   RCL 19
230      *
231   STO 45
232   RCL 37
233   RCL 38
234      *
235   RCL 45
236      +
237   RCL 39
238      /
239   STO 50
240   RCL 06
```

Calculates B

Calculates C

```
241   .00001
242    +
243   RCL 08                  Calculates
244   x=y?                        C
245   GTO 43
246   LBL 07
247   RCL 07
248   STO 46      → C
249   RCL 05
250   RCL 11
251    *                      Calculates
252   83.33333333             Deflection
253    *                        Y(in)
254   RCL 04
255    /
256   RCL 41
257    *
258   STO 47      → Y
259   RCL 05
260    2
261    /                      Calculates
262   RCL 11                  Bending Moment
263    /
264   12,000                  M (lb-in)
265    *
266   RCL 44
267    /
268   STO 48      → M
269   RCL 05
270   1,000
271    *                      Calculates
272   RCL 46                  shear
273    *                      V (lbs)
274   STO 49      → V
275   GTO 47
276   LBL 43                  if x=a+0.00001
277   -120                    negates C
278   STO * 50
279   GTO 07
280   LBL 44
```

```
281   RAD
282   RCL 40
283   XEQ 45                  Subroutine
284   STO IND 07              that cal-
285   ISG 07                  culates
286   RCL 40                  the trig.
287   XEQ 46                  & hyp.
288   STO IND 07              functions
289   ISG 07                  of λX,λa,λb,
290   RCL 40                  λb & λL and
291   SIN                     stores them
292   STO IND 07              to registers
293   ISG 07                  19 to 34.
294   RCL 40
295   COS
296   STO IND 07
297   ISG 07
298   RTN
299   GTO 06
300   LBL 45
301   E/X                     Subroutine
302   LAST X                  that
303   CHS                     calculates
304   E/X                     sin h
305    -
306    2
307    /
308   RTN
309   LBL 46
310   E/X
311   LAST X                  Subroutine
312   CHS                     that
313   E/X                     calculates
314    +                      cos h
315    2
316    /
317   RTN
318   LBL 47
319   FIX 4
320   RCL 08
```

```
321   "D="
322   ARCL X
323   AVIEW
324   STOP
325   RCL 13
326   "X="
327   ARCL X
328   AVIEW
329   STOP
330   RCL 15
331   "a="
332   ARCL X
333   AVIEW
334   STOP
335   RCL 14
336   "b="
337   ARCL X
338   AVIEW
339   STOP
340   RCL 41
341   "A="
342   ARCL X
343   AVIEW
344   STOP
345   RCL 44
346   "B="
347   ARCL X
348   AVIEW
349   STOP
350   RCL 46
351   "C="
352   ARCL X
353   AVIEW
354   STOP
355   RCL 47
356   "Y="
357   ARCL X
358   AVIEW
359   STOP
360   RCL 48
361   "M="
362   ARCL X
363   AVIEW
364   STOP
365   RCL 49
366   "V="
367   ARCL X
368   AVIEW
369   STOP
370   BEEP
371   GTO "W"   [Goes to the be-
                ginning of the
                program and ready
                to run for a new
                set of data.]
```

Displays the output:

D : distance of point of analysis from left end, ft.
X : if $x \leq a$, X = D. If $X \neq D$ then X is measured from left end, ft.
a : distance of applied load from left end if $x \leq a$, distance of applied load from right end if $x \geq a$, ft.
b : L - a, ft2
A
B : coefficients
C
Y : deflection, in
M : moment, lb-in
V : shear, lbs

REGISTER ALLOCATION

01	L	11	λ
02	B	12	λL
03	E	13	x functional
04	k_s	14	b functional
05	P	15	a functional
06	a	16	λX
07	counter	17	λa
08	x	18	λb
09	T		
10	I		

	λX	λa	λb	λL
sin h	19	23	27	31
cos h	20	24	28	32
sin	21	25	29	33
cos	22	26	30	34

35		41	A
36		44	B
37	Computational	46	C
38	registers	47	Y
39		48	M
40		49	V
42			
43			
45			
50			

PROGRAM MODIFICATION

The finite beam on elastic foundation program requires the entry of the entire set of data every time it is run. In the case of a base analysis though, where the effect of a single load at various points across the beam is studied, the only variable in the data set is the value of x. In order to avoid the repetitive keying of the same data set, the following addition can be made.

Insert after line 24:

```
"MORE XS?--"
PROMPT
STO 51
X ≠ 0?
XEQ 48
```

Insert after line 317:

```
LBL 48
STO XS, X1-R54
AVIEW
STOP
RCL 51
1000
 /
53.05301
 +
STO 52
RTN
```

Insert after line 370:

```
ISG 52
GTO 49
```

Add after line 371:

```
LBL 49
RCL IND 52
STO 08
GTO 03
```

With this modification after the entry of the first value of x the calculator asks "MORE XS?". At this point the number of additional x's (e.g. 5) must be keyed in before pressing R/S. If no additional x's key in Ø. Then the calculator prompts "STO XS, X1-R54"; store the values of the additional x's starting with register 54 (e.g., 54, 55, 56, 57, 58). Then the program runs for the initial value of x and instead of returning to the start picks the values of x from the specified registers and repeats the computations starting with line 78, thus saving time and effort. After performing the computations for all the input values of x it returns to the start. Depending on the x registers used the SIZE must be increased.

BASE ANALYSIS

L = 12 FT
B = 12 IN
T = 8 IN
E = 27,000 PSI
KS. = 175 PCI
F.S. = .509/y_{max}

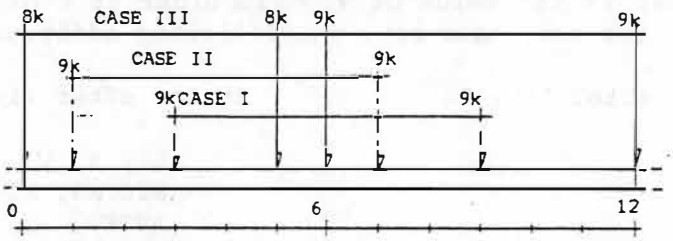

CASE I		x:					
LEFT 9k	Y(in)	-.038	0.170	-.007	.0001	-.0001	
a=3	M(lb-in)	0	28,640	-2,146	141	0	
	V (lb)	0	4,475	-255	12.8	0	
RIGHT 9k	Y	-.0001	.0001	-7.007	0.170	-.038	
a=9	M	0	141	-2,146	28,640	0	
	V	0	12.8	-255	4,475	0	
TOTAL	Y	-.038	.170	-.014	.170	-.038	F.S.
	M	0	28,781	-4,292	28,781	0	2.99
	V	0	4,488	-510	4,488	0	

CASE II		x=0	x=1	x=4	x=7	x=12	
LEFT 9k	Y	.154	.187	-.008	.0002	-.00001	
a=1	M	0	25,860	-2,043	139	0	
	V	0	4,467	-264	14	0	
RIGHT 9k	Y	.0009	.0002	-.006	.168	-0.00001	
a=7	M	0	103	-2,140	28,664	0	
	V	0	15	-254	4,500	0	
TOTAL	Y	.155	.187	-.014	.168	-.00002	F.S.
	M	0	24,963	-4,183	28,803	0	2.72
	V	0	4,482	-518	4,514	0	

CASE III		x=0	x=5	x=6	x=12	
LEFT 6k	Y	.598	-.00001	.002	0	
a=0	M	0	918	211	0	
	V	0	72	39	0	
RIGHT 8k	Y	.00002	.150	.081	.0008	
a=5	M	0	25,479	-2,191	0	
	V	0	4,000	917	0	
TOTAL 8k	Y	.598	.150	.083	.0008	F.S.
	M	0	26,397	-1,980	0	0.85
	V	0	4,072	956	0	
LEFT 9k	Y	.002	.092	.168	.002	
a=6	M	0	-2,462	28,662	0	
	V	0	1,031	4,500	0	
RIGHT 9k	Y	.00002	.0009	.002	.673	
a=12	M	0	-48	237	.00003	
	V	0	8	44	9,000	
TOTAL 9k	Y	.002	.093	.170	.675	F.S.
	M	0	-2,510	28,899	0	0.75
	V	0	1,039	4,544	9,000	
TOTAL 8k	Y	.600	.243	.253	.676	F.S.
& 9k	M	0	23,887	26,919	0	0.75
	V	0	5,111	5,500	9,000	